

# Roller Compaction: Mechanical Properties of Primary Particles, Pre-compacted Body and Ribbon



Riyadh B. Al Asady

Department of Chemical and Biological Engineering

The University of Sheffield

A thesis submitted in partial fulfilment of the  
requirements for the degree of Doctor of Philosophy

August 2016

## Abstract

Roller compaction is a continuous dry granulation process in which the primary powder is compressed at high pressure by two counter rotating rollers to produce a ribbon. It is common that the ribbon is then crushed to produce granules. Although considerable research has been carried out, more understanding of the process is necessary to optimize the efficiency and to improve product quality.

During the compaction process the particles exhibit different behaviours such as rearrangement, elastic and plastic deformation in addition to the fracture. The existence and the limit of each of these behaviours depends mainly on the mechanical properties of the powder and on the applied compaction parameters. The mechanical behaviour of the particles could therefore affect the bonding of the particles to each other.

This study investigates the mechanical properties and specifically the hardness of the material which was measured throughout different stages of the process. The measurements covered different scales of hardness which represents different material properties. Nano-indentation hardness was used to indicate the plastic deformation of the single particle of the primary powder and it was measured for different materials with a wide range of mechanical properties. Then the hardness was linked to the properties of the ribbon. Such a relationship is useful to predict the product quality whilst only using few particles. From the results, the optimum hardness range that produces a good quality ribbon was suggested.

Furthermore, indentation of the pre-compacted body was used as a novel approach to indicate the progress of the compaction process as the powder is grabbed by the two rotating rollers. The hardness was measured for what this study called a “pre-compacted body” which is the powder/compact in the space between the rollers before the minimum gap. This approach was used to determine the nip angle and how different process parameters such as roller speed, roller gap and applied hydraulic pressure affect the nip angle and other ribbon properties including ribbon temperature. The suggested new approach is easy to carry out. The measurement uses the actual data resulting from the process without any assumptions.

Finally, micro indentation hardness of the ribbon was used to indicate the strength of the bonding between the primary particles and it was linked to the granule size distribution resulting from crushing of the ribbon.

The findings from this study can be used by various industries to improve the quality of the product by choosing more appropriate formulation and process parameters. However, some industries need to use specific materials which could be hard to granulate; therefore, they do not have the option to choose the formulation. For these difficult materials, novel roller geometry was designed. The use of the new roller showed a significant improvement in the granulation process and product quality in comparison to the standard roller.

## Acknowledgment

First of all, I would like to thank both my academic supervisors, Prof. Agba D. Salman and Prof. Michael J. Hounslow for their help and support during my PhD. Special thanks to Prof. Salman for his continuous advice and encouragement. His help and the fruitful scientific discussion started even before I started my PhD and I am sure it will continue for the future.

I would like also to thank my colleagues in PPG group. Special thanks go to Syed, your help and care is really appreciated. Thanks to Chalak, William, Mohammed and Menan for being helpful colleagues and great friends. I would like to thanks the current PPG PhD students especially Mingzhe for helping with the last experiments. Thanks to Sushma, Arthi, Qing, Jian Kai, Bilal, Ali, and Osama.

Special thanks to Dr. Ranjit Dhenge for the continuous advice and the help proof reading the papers and the thesis.

I would like to thanks my wife and my daughter for being patients and listened to me talking about my PhD for the last few years. Thanks for your support and encouragement. I could not imagine doing it without your understanding. Finally I would like to thanks my family for their support and care.

## Publications

The following publications are resulted from this thesis

### Journal Papers:

- Al-Asady, R.B, Dhenge, R.M., Hounslow, M.J. and Salman, A.D., 2016. Roller compactor: Determining the nip angle and powder compaction progress by indentation of the pre-compacted body. *Powder Technology*, 300, 107-119.
- Al-Asady, R.B, Osborne, J.D., Hounslow, M.J. and Salman, A.D., 2015. Roller compactor: The effect of mechanical properties of primary particles, *International Journal of Pharmaceutics*, 496, 124-136.

### Conference papers:

- Al-Asady, R.B., Hounslow, M.J. and Salman, A.D., Roller compactor: Mechanical properties of the pre-compacted body, Poster and paper at the 7<sup>th</sup> International Granulation Workshop, Sheffield, UK 1<sup>st</sup>-3<sup>rd</sup> July 2015. Paper number 87.
- Al-Asady, R.B, Hounslow, M.J. and Salman, A.D., Roller compactor: Granule size distribution of roller compaction process: Two parameters Rosin- Rammler equation, Oral presentation and paper at the 7<sup>th</sup> International Granulation Workshop, Sheffield, UK 1<sup>st</sup>-3<sup>rd</sup> July 2015. Paper number 48.
- Al-Asady, R.B., Hounslow, M.J. and Salman, A.D., Modelling of granule size distribution of roller compaction process using two parameters Rosin Rammler equation, Paper and oral presentation at 21<sup>st</sup> International Congress of Chemical and Process Engineering, Prague, Czech republic, 23-27 August, 2014. Paper number 1209.
- Al-Asady, R.B., Hounslow, M.J. and Salman, A.D., Roller compactor: The effect of mechanical properties of primary particles. Oral presentation and paper at the 6<sup>th</sup> International Granulation Workshop, Sheffield, UK. 26-28 June 2013. Paper number 59.

# Table of Contents

<b>Abstract.....</b>	<b>2</b>
<b>Chapter 1 Introduction.....</b>	<b>21</b>
1.1 Agglomeration .....	21
1.2 Dry versus wet granulation .....	21
1.3 Continuous versus batch granulation .....	22
1.4 Roller compaction.....	22
1.4.1 Feeding systems and roller design .....	25
1.5 Overview of the thesis.....	26
<b>Chapter 2 Literature Review.....</b>	<b>27</b>
2.1 Mechanical properties .....	27
2.1.1 Hardness of the material .....	27
2.1.1.1 Mohs scale and static indentation hardness .....	27
2.1.1.2 Depth sensing indentation (Nano- indentation hardness) .....	29
2.1.2 Yield stress of the material.....	32
2.2 Powder behaviour under compaction.....	33
2.3 Mechanical properties of the primary powder and roller compaction process .....	37
2.4 Brittle/ deformation behavior transition.....	39
2.5 Stress applied to the powder during roller compaction process.....	40
2.5.1 Stress distribution at different angular roll position.....	41
2.5.1.1 Johanson’s Theory .....	41
2.5.1.2 Slab method .....	47
2.5.1.3 Finite element analysis.....	49
2.5.2 Stress distribution across the roller width .....	51
2.6 Effect of process parameters of the roller compaction process.....	57
2.6.1 Effect of hydraulic pressure .....	57
2.6.2 Effect of the roll gap .....	59
2.6.3 Effect of roller speed.....	60
2.7 Representing the particle size distribution by mathematical formulas .....	62
2.7.1 Normal Gaussian.....	62
2.7.2 Log-Normal Gaussian .....	63
2.7.3 Rosin- Rammler .....	63
2.7.3.1 Gaudin – Schumann .....	64
2.8 Aim of the research .....	64

---

<b>Chapter 3</b>	<b>Materials and Methods .....</b>	<b>67</b>
3.1	Materials .....	67
3.1.1	Polyvinyl alcohol (PVA).....	67
3.1.2	Starch .....	67
3.1.3	Microcrystalline cellulose (Avicel PH-101) .....	68
3.1.4	Maltodextrin (Glucidex® 6).....	69
3.1.5	Hydroxypropyl methylcellulose (HPMC).....	69
3.1.6	α- lactose monohydrate (Pharmatose 200M) .....	70
3.1.7	Sodium carbonate.....	70
3.1.8	Calcium carbonate (CaCO <sub>3</sub> ).....	71
3.1.9	Powder preparation and conditioning .....	71
3.2	Characterisation of the primary powders .....	72
3.2.1	Measuring the particle size distribution of the primary powder .....	72
3.2.2	Scanning Electron Microscopy .....	72
3.2.3	Determining the flow properties and the compressibility factor of the primary powder .....	72
3.2.3.1	Ring shear cell tester .....	72
3.2.3.2	Determining the repose angle .....	74
3.2.3.3	Determining the compressibility factor of the powder.....	74
3.3	Roller compactor.....	74
3.4	Characterisation of the ribbon.....	76
3.4.1	Measurement of the ribbon strength .....	76
3.4.2	Ribbon surface temperature .....	77
3.4.2.1	Measurement of material emissivity .....	77
3.4.2.2	Measurement of ribbon temperature .....	77
<b>Chapter 4</b>	<b>Measuring the mechanical properties of a single primary particle.</b>	<b>79</b>
4.1	Introduction.....	79
4.1.1	Particle size distribution of the primary powder .....	79
4.1.2	Hardness of the materials.....	82
4.1.3	Investigating the fracture behaviour of the primary powder.....	94
4.1.4	Yield stress of the material.....	97
4.2	Conclusion .....	100
<b>Chapter 5</b>	<b>Mechanical properties of the single primary particle and roller compaction process .....</b>	<b>101</b>
5.1	Introduction.....	101
5.2	Ribbon production .....	101

---

5.3	Results and discussion .....	103
5.3.1	Single particle hardness and ribbon strength .....	103
5.3.2	Single particle hardness and ribbon width .....	121
5.3.3	Amount of fines produced during roller compaction .....	125
5.3.4	Ribbon surface temperature and temperature profile.....	133
5.3.4.1	Measuring the thermal emissivity .....	133
5.3.4.2	Ribbon temperature.....	133
5.3.5	Investigating the behaviour of the low hardness material (PVA and starch). 144	
5.3.5.1	Viscoelasticity experiment.....	145
5.4	Measuring the nano indentation hardness of the ribbon .....	149
5.4.1	Preparing the ribbon to nano indentation test .....	149
5.4.2	Measuring the nano indentation hardness.....	150
5.4.3	Results and discussion .....	150
5.5	Comparing the maximum stress with the yield stress.....	153
5.6	Conclusion .....	154
<b>Chapter 6</b>	<b>Determining the nip angle and powder compaction progress .....</b>	<b>156</b>
6.1	Introduction.....	156
6.2	Material properties of Avicel PH-101.....	156
6.3	Calculation the nip angle by Johanson's theory.....	158
6.4	Production of the pre-compacted body .....	160
6.5	Characterisation of the pre-compacted body and ribbon .....	161
6.5.1	Mechanical properties (Hardness).....	161
6.5.2	Porosity of pre-compacted body and ribbon .....	162
6.6	Results and discussion .....	163
6.6.1	Effect of roll speed.....	163
6.6.2	Effect of hydraulic pressure .....	171
6.6.3	Effect of roller gap .....	177
6.6.4	Other materials.....	183
6.7	Conclusion .....	183
<b>Chapter 7</b>	<b>Stress distribution across roller width .....</b>	<b>185</b>
7.1	Introduction.....	185
7.2	Materials and methods .....	185
7.2.1	Ribbon production.....	185
7.2.2	Determining the pressure profile shape across roller width.....	186
7.2.3	Measuring the porosity of the ribbon centre and side .....	187

---

7.2.4	Measuring the temperature profile across ribbon width.....	187
7.3	Results and discussion .....	187
7.3.1	Flat standard rollers setup .....	187
7.3.1.1	Pressure profile across ribbon width .....	187
7.3.1.2	Temperature profile across ribbon width .....	189
7.3.1.3	Changing the colour of Avicel PH-101 powder after roller compaction ...	191
7.3.2	Design of the new curved roller .....	191
7.3.2.1	Pressure profile across the ribbon width .....	194
7.3.2.2	Temperature profile across ribbon width .....	195
7.3.2.3	Changing the colour of Avicel PH-101 powder after roller compaction ...	197
7.3.3	Comparison of ribbon properties and percentage of fines produced by two types of roller .....	197
7.3.3.1	Ribbon width.....	197
7.3.3.2	Amount of fines .....	198
7.3.3.3	Porosity of the side and centre of the ribbon.....	201
7.3.4	Comparison of ribbon quality of different materials produced by the curved and flat roller.....	203
7.4	Conclusion .....	203
<b>Chapter 8</b>	<b>Mechanical properties and granule size distribution .....</b>	<b>204</b>
8.1	Introduction.....	204
8.2	Materials and methods .....	204
8.2.1	Powder preparation .....	205
8.2.2	Ribbon production.....	205
8.2.3	Ribbon characterization .....	205
8.2.3.1	Ribbon hardness.....	205
8.2.3.2	Ribbon strength.....	207
8.2.4	Crushing of the ribbon .....	207
8.2.5	Measuring the granule size distribution .....	207
8.2.6	Crusher fines .....	208
8.3	Design of the experiments.....	208
8.4	Results and discussions.....	208
8.4.1	Ribbon hardness.....	208
8.4.1.1	Ribbon strength.....	209
8.4.2	Granule size distribution .....	210
8.4.2.1	Effect of roller force.....	210
8.4.3	Effect of crusher speed.....	215



---

8.4.4	Effect of crusher mesh size .....	219
8.4.5	Fitting the granule size distribution to Rosin-Rammler equation .....	223
8.5	Conclusion .....	227
<b>Chapter 9</b>	<b>Conclusion and future work.....</b>	<b>228</b>
9.1	Conclusion .....	228
9.2	Future work.....	229
9.2.1	Measuring the fracture toughness of single primary particle.....	229
9.2.2	Online measuring of the nip angle .....	229
9.2.3	Trying different geometry of the curved roller .....	229
9.2.4	Monitoring the compaction process by measuring the temperature .....	229
9.2.5	Plastic deformation at different temperature and humidity.....	229
<b>References</b>	<b>.....</b>	<b>230</b>
<b>Appendix</b>	<b>.....</b>	<b>243</b>

# List of Figures

Figure 1-1: Wet granulation process .....	22
Figure 1-2: Roller compaction followed by crushing process .....	23
Figure 1-3: Schematic of the roller compactor .....	23
Figure 1-4: Stress distribution in the nip region (Guigon et al., 2007) .....	24
Figure 1-5: Different possible arrangements for the rollers and the feeding system (Guigon et al., 2007) .....	25
Figure 2-1: Force – displacement curve resulted from the nano-indentation test ( $F_{\max}$ : maximum force, $S$ : stiffness of the material, $h_{\max}$ : depth at maximum force, $h_p$ : permanent indentation depth after removing the load) .....	29
Figure 2-2: A schematic diagram shows the indenter in contact with the body during the indentation test ( $h_s$ : sink in depth). (Adapted from Oliver and Pharr (1992)).....	30
Figure 2-3: Compression cycle with possible events .....	34
Figure 2-4: Jenike-Shield yield criterion (Adapted from Johanson (1965)) .....	42
Figure 2-5: Comparison between experimental and predicted pressure profile for different roller gaps (Bindhumadhavan et al., 2005) .....	45
Figure 2-6: Schematic diagram of the slab method (Dec et al., 2003).....	48
Figure 2-7: Roller pressure as a function of angular roll position for different feed stress (Dec et al., 2003) .....	50
Figure 2-8: Relative density distribution across ribbon width for different cases (Miguélez-Morán et al., 2008).....	52
Figure 2-9: Porosity distribution across the ribbon width (red color: low porosity, green color: medium porosity, blue color: high porosity) (Lim et al., 2011).....	53
Figure 2-10: Density distribution across ribbon width (Zhang et al., 2016).....	54
Figure 2-11: Pressure (a) and density (b) distribution across the ribbon width resulted from simulation of the roller compactor process (Cunningham et al., 2010) .....	55
Figure 2-12: Image showing light transmission through a ribbon of sodium chloride (Simon and Guigon, 2003) .....	55
Figure 2-13: (a) Roll fitted with sensors (b) Measured stress profile across roller width (Nesarikar et al., 2012b).....	56
Figure 2-14: The steps to more understanding of the roller compaction process .....	66
Figure 3-1: SEM of the primary particles of PVA.....	67
Figure 3-2: SEM of Starch 1500 primary powder .....	68
Figure 3-3: SEM image of Avicel PH-101 primary particles .....	68
Figure 3-4: SEM image of Glucidex <sup>®</sup> 6 primary powder .....	69
Figure 3-5: SEM image of Tylpor 604 primary powder .....	70

---

Figure 3-6: SEM image of Pharmatose 200M primary particles .....	70
Figure 3-7: SEM image for the sodium carbonate primary powder .....	71
Figure 3-8: SEM image of calcium carbonate primary particles .....	71
Figure 3-9: Ring shear cell tester (Schulze, 2010).....	73
Figure 3-10: Typical yield locus obtained from the ring shear cell test.....	74
Figure 3-11: Image of the Alexanderwerk WP120 Roller Compactor .....	75
Figure 3-12: Roller setup .....	76
Figure 3-13: Schematic of three points bend test setup .....	77
Figure 3-14: Online thermal camera setup.....	78
Figure 4-1: Particle size distribution of different powders .....	80
Figure 4-2: Comparison of particle size distribution of all materials .....	81
Figure 4-3: Block diagram for the setup used for nano-indentation test of a single particle, (Adapted from Hysitron (2006)).....	83
Figure 4-4: Three sided pyramid Berkovich indenter of 142° angle (a) Top view of the used indenter (b) 3-D view (Hysitron, 2016) .....	84
Figure 4-5: Applying, holding and removing the load during nano indentation test versus time .....	85
Figure 4-6: The roundness of the Berkovich tip head.....	85
Figure 4-7: An example of nano indentation curve for viscoelastic material .....	86
Figure 4-8: Force- displacement curve with fracture (Moody et al., 2003) .....	87
Figure 4-9: Force- displacement curves for different materials.....	88
Figure 4-10: AFM image shows 4 indents on calcium carbonate single particle surface.....	89
Figure 4-11: Hardness of calcium carbonate particle as a function of maximum force .....	91
Figure 4-12: Tip slide during the measurement of the hardness by AFM (Lee et al., 2013) ..	91
Figure 4-13: A diagram showing the areas under the curve for plastic and elastic regions.....	92
Figure 4-14: The relation between the work of plastic and Nano indentation hardness for different materials .....	94
Figure 4-15: Single particle compression set up.....	94
Figure 4-16: Force displacement curve resulted from the single particle test .....	96
Figure 4-17: The linearized form of the Hertz equation to find the elastic penetration limit ..	98
Figure 4-18: The plastic region of force displacement curve that fits Eq. 2-8.....	99
Figure 5-1: Split ribbon of Ph.200M produced at hydraulic pressure of 150 and 200 bar.....	102
Figure 5-2: Image shows melting of Glucidex®6 between the two rollers .....	103
Figure 5-3: Ribbon strength for different materials at different hydraulic pressures.....	106

Figure 5-4: Ribbon strength as a function of applied hydraulic pressure for different materials .....	108
Figure 5-5: Comparison of the ribbon strength increase rate as a function of applied hydraulic pressure for different materials .....	109
Figure 5-6: SEM images of primary particles and ribbon surfaces of PVA produced at different hydraulic pressures .....	110
Figure 5-7: SEM image of the internal section across the thickness of the PVA ribbon produced at 230 bar.....	111
Figure 5-8: SEM images of primary particles and ribbon surfaces of starch 1500 produced at different hydraulic pressures .....	112
Figure 5-9: SEM images of primary particles and ribbon surface of Avicel PH-101 at different hydraulic pressures.....	113
Figure 5-10: SEM images of primary particles and ribbon surface of Glucidex <sup>®</sup> 6 produced at different hydraulic pressures .....	115
Figure 5-11: SEM images of primary particles and ribbon surfaces of Tylpor 604 at different hydraulic pressures.....	116
Figure 5-12: SEM images of primary particles and ribbon surfaces of Pharmatose 200M at different hydraulic pressures .....	117
Figure 5-13: SEM images of ribbon surface of sodium carbonate produced at different hydraulic pressures.....	119
Figure 5-14: SEM images of calcium carbonate primary particles and ribbons surface produced at different hydraulic pressures .....	120
Figure 5-15: Image of the roller showing its width.....	121
Figure 5-16: Ribbons produced by different materials at hydraulic pressure of 70 bar.....	121
Figure 5-17: Ribbon width versus nano-indentation hardness of different materials at different applied hydraulic pressures .....	123
Figure 5-18: Ribbon width as a function of hydraulic pressure for different materials.....	124
Figure 5-19: Comparison of ribbon width increase rate as a function of hydraulic pressure for different materials .....	125
Figure 5-20: Fines wt. % as a function of applied hydraulic pressure for different materials	126
Figure 5-21: The amount of fines as a function of ribbon strength for different materials....	130
Figure 5-22: Fines % as a function of applied hydraulic pressure for different materials .....	132
Figure 5-23: Thermal images for ribbon of different materials produced at 100 bar hydraulic pressure .....	134
Figure 5-24: Maximum ribbon surface temperature for different materials at different hydraulic pressures.....	136
Figure 5-25: Comparison of ribbon maximum temperature for different materials at different hydraulic pressures.....	137

Figure 5-26: Temperature profile of different materials at different hydraulic pressures.....	139
Figure 5-27: Temperature profile of different materials at different hydraulic pressures.....	140
Figure 5-28: Scratched cheek plate due to the friction with the ribbon during roller compaction process .....	141
Figure 5-29: Temperature of the ribbon centre for different materials at different hydraulic pressures.....	143
Figure 5-30: Compression of different powders at different strain rates with holding maximum load for 2 hours (■ 100 mm/min. ■ 0.01 mm/min.) .....	146
Figure 5-31: Ribbon mounted and prepared for nano indentation test .....	150
Figure 5-32: Nano- indentation hardness of ribbon produced by different materials at different hydraulic pressures.....	152
Figure 6-1: Particle size distribution of the Avicel PH-101.....	157
Figure 6-2: Pressure density relationship.....	157
Figure 6-3: The pressure gradients at slip and nip zones as a function of angular roll position .....	159
Figure 6-4: Pre-compacted body of Avicel PH-101 and the ribbon .....	160
Figure 6-5: Indentation of the pre-compacted body at different angular roll positions .....	160
Figure 6-6: Cross line laser level .....	161
Figure 6-7: Dimension and shape of Shore A hardness tester tip.....	162
Figure 6-8: X-ray image of one slice of ribbon .....	163
Figure 6-9: Hardness of the pre-compacted body of Avicel PH-101 at different angular roll positions and at different roller speeds .....	164
Figure 6-10: Area under the curve (hardness versus angular roll position) for different roll speed .....	165
Figure 6-11: Determined nip angle as a function of roller speed.....	165
Figure 6-12: Screw speed as a function of roller speed for Avicel PH-101.....	166
Figure 6-13: Three X-ray slices of the pre-compacted body at different angular roll position .....	167
Figure 6-14: Porosity of the pre-compacted body at different angular roll positions and roll speed of 3 rpm.....	167
Figure 6-15: Ribbon width versus roller speed.....	168
Figure 6-16 : Ribbon strength versus roller speed.....	168
Figure 6-17: Ribbon porosity versus roller speed.....	169
Figure 6-18: Percentage of fines versus roller speed .....	170
Figure 6-19: Maximum ribbon temperature for different roller speeds .....	171
Figure 6-20: Shore A hardness for different angular roll position at different hydraulic pressures.....	172

Figure 6-21: Area under the curve (hardness versus angular roll position) for different hydraulic pressures.....	172
Figure 6-22: Determined nip angle for different hydraulic pressure .....	173
Figure 6-23: Screw feeder speed as a function of hydraulic pressure for Avicel PH-101 .....	173
Figure 6-24: Porosity of pre-compacted body at different angular roll positions produced at 100 bar hydraulic pressure .....	174
Figure 6-25: Ribbon width as a function of hydraulic pressure.....	174
Figure 6-26: Ribbon strength as a function of hydraulic pressure .....	175
Figure 6-27: Porosity of the ribbon centre as a function of hydraulic pressure .....	176
Figure 6-28: Percentage of fines versus hydraulic pressure.....	176
Figure 6-29: Ribbon temperature as a function of hydraulic pressure.....	177
Figure 6-30: Shore A hardness at different angular roll position at different roll gap.....	178
Figure 6-31: Area under the curve of the hardness-Angular roll position curves at different gaps .....	178
Figure 6-32: Determined nip angle for different roll gaps .....	179
Figure 6-33: Screw speed as a function of roller gap for Avicel PH-101 .....	180
Figure 6-34: Porosity of pre-compacted body at different angular roll position produced using 2.5 mm roll gap .....	180
Figure 6-35: Width of the ribbon as a function of roller gap .....	181
Figure 6-36: Ribbon strength versus roller gap .....	181
Figure 6-37: Ribbon porosity at different roll gap .....	182
Figure 6-38: Percentage of fines for different roll gap .....	182
Figure 6-39: Maximum ribbon temperature as a function of roller gap.....	183
Figure 7-1: Pressure film (Fuji film).....	186
Figure 7-2: Pressure density chart supplied by Fujifilm (Fujifilm, 2012) .....	186
Figure 7-3: Two flat knurled rollers.....	187
Figure 7-4: Pressure films after passed through the rollers (Left: Calcium carbonate, middle: Pharmatose 200M and right: Avicel PH-101).....	188
Figure 7-5: Image of calcium carbonate ribbon during compaction showing un-compacted ribbon sides compared to the centre.....	188
Figure 7-6: Temperature profile for different materials at different hydraulic pressures .....	190
Figure 7-7 : Avicel PH-101 ribbon produced at 150 bar with dark colour at the centre part of the ribbon .....	191
Figure 7-8: The design of the new roller.....	192
Figure 7-9: Image of the new roller built at the University of Sheffield .....	193

Figure 7-10: Experimental setup showing new curved roller and standard knurled flat roller .....	194
Figure 7-11: Pressure films after passing between the rollers at 100 bar .....	195
Figure 7-12: Temperature profile across the ribbon width of different materials at different hydraulic pressures produced using the new roller (◆ 30 bar,■ 70 bar, ▲ 100 bar) .....	196
Figure 7-13: Avicel PH-101 ribbon produced at 150 bar using the new roller.....	197
Figure 7-14: Comparison of ribbon width produced by the curved and the flat roller (■ flat roller, ◆ Curved new roller) – Ribbons in the images; Bottom: curved roller, top: flat roller .....	198
Figure 7-15: Comparison of the percentage of fines produced from different materials at different pressures using the flat and the curved rollers ( ■ flat roller, ◆ curved new roller).....	200
Figure 7-16: The value of $\Delta\phi$ for different material using the flat roller (■) and the curved new roller (◆) .....	202
Figure 8-1: Particle size distribution of the three primary powders.....	205
Figure 8-2: Sapphire ball that used as indenter to determine the hardness of the ribbon .....	206
Figure 8-3: Typical impression resulted from the indentation of Pharmatose 200M ribbon surface.....	206
Figure 8-4: Crusher system used to crush the ribbons (Alexanderwerk).....	207
Figure 8-5: Illustration of ribbon hardness measurement concept.....	209
Figure 8-6: Illustration of the nano-indentation hardness measurement concept .....	209
Figure 8-7: Granule size distribution of different materials produced at different hydraulic pressures (◆ Calcium carbonate, ■ Ph.200M, ▲ Avicel PH-101) .....	211
Figure 8-8: Crusher fines produced by different materials using different hydraulic pressures .....	213
Figure 8-9: Comparing the granule size distribution of each material at different hydraulic pressures.....	214
Figure 8-10: Granule size distribution of different materials produced at different rotor speeds .....	216
Figure 8-11: Comparing the granule size distribution of each material at different rotor speeds .....	218
Figure 8-12: Crusher fines produced by different materials using different rotor speeds .....	219
Figure 8-13: Granule size distribution of different materials produced at different mesh sizes .....	220
Figure 8-14: Crusher fines produced by different materials using different mesh sizes.....	222
Figure 8-15: Experimental and predicted granule size distribution of different materials produced from crushing ribbons of 100 bar using mesh size of 0.63-1 mm.....	225
Figure 8-16: Relation between the ribbon strength of different materials produced at 100 bar and the two constants of Rosin- Rammler equation.....	226

---

Figure 8-17: Relation between nano- indentation hardness of the single primary particle of different materials and the two constants of Rosin- Rammler equation .....	227
Figure A-1: Image of Starch 1500 ribbon surface produced at 230 bar.....	243
Figure A-2: Image of Avicel PH-101 ribbon surface produced at 230 bar.....	243
Figure A-3: Image of Glucidex®6 produced at 150 bar.....	244
Figure A-4: Image of Tylpor 604 ribbon surface produced at 230 bar.....	244
Figure A-5: Image of Pharmatose 200M ribbon surface produced at 100 bar.....	245
Figure A-6: Image of sodium carbonate ribbon surface produced at 230 bar.....	245
Figure A-7: Image of calcium carbonate ribbon surface produced at 230 bar.....	246
Figure A-8: Shore A hardness of the pre-compacted body produced at 70 bar versus angular roll position for Pharmatose 200M.....	246



## List of Tables

Table 2-1: Commonly used scales to evaluate the static micro hardness of the material (Askeland, 1998).....	28
Table 2-2: Critical size of different pharmaceutical materials (Roberts and Rowe, 1987).....	40
Table 4-1: The main size parameters, $D_{10}$ , $D_{50}$ , and $D_{90}$ for all powders .....	82
Table 4-2: The nano-indentation hardness and the Young's modulus for the single primary particle of different materials (Eq. 2-1 and Eq. 2-5 respectively).....	90
Table 4-3: Work of plastic in nano joule for different materials calculated using nano-indentation fore displacement data .....	93
Table 4-4: Yield stress of three materials .....	100
Table 5-1: Experimental design of roller compaction experiments .....	102
Table 5-2: Flow function coefficient ( <i>ffc</i> ) of different materials .....	127
Table 5-3: Angle of repose for the powders .....	128
Table 5-4: Measured emissivity for different materials .....	133
Table 5-5: The difference between the displacements at maximum load for the two different loading rates .....	147
Table 5-6: Creep of different powders at different loading rates .....	147
Table 5-7: The difference in the height and strength of the compacts produced by different loading rates .....	148
Table 5-8: Maximum normal stress applied to the material at different hydraulic pressure..	153
Table 6-1: Flow properties and compressibility factor of the Avicel PH-101 primary powder .....	158
Table 6-2: The values of the parameters used to calculate the nip angle.....	159
Table 6-3: Experimental design of roller compactor experiments.....	161
Table 7-1: Porosity of the side and the centre of the ribbon for different materials and hydraulic pressures using standard flat roller .....	201
Table 7-2: Porosity of the side and the centre of the ribbon for different materials and hydraulic pressures using curved roller .....	201
Table 8-1: Experimental design of the three different sets .....	208
Table 8-2: Hardness of ribbon centre produced by different materials at different hydraulic pressure .....	208
Table 8-3: Tensile strength of the ribbon of different materials produced at different hydraulic pressures.....	210
Table A-1: Comparison of the ribbon width and amount of fines for different materials using the flat and the curved roller .....	247

## Nomenclature

H	Nano-indentation hardness (GPa)
$F_{\max}$	Maximum force applied during nano-indentation test ( $\mu\text{N}$ )
$A_p (h_c)$	Projected contact area ( $\text{nm}^2$ )
$h_c$	Indenter's contact depth with the tested sample at $F_{\max}$ (nm)
$h_{\max}$	Penetration depth of the tip at maximum load (nm)
$h_s$	Sink in depth (nm)
u	Constant depends on indenter shape (Eq. 2-2)
S	Unloading stiffness of the material ( $\mu\text{N}/\text{nm}$ )
m	constant depends on indenter geometry (Eq. 2-4)
$h_p$	Permanent indentation depth after removing the load (nm)
$E_r$	Reduced Young's modulus (GPa)
$\beta$	factor that depends on the indenter shape (Eq. 2-5)
E	Young's modulus of the material (GPa)
$E_i$	Young's modulus for the indenter (GPa)
$\nu$	Poisson's ratio for the material
$\nu_i$	Poisson's ratio for the indenter
F	Applied force during nano-indentation test ( $\mu\text{N}$ )
r	Radius of the maximum possible contact area between the indenter and the particle (nm)
h	Displacement of the tip during nano-indentation test (nm)
c	Constraint factor (Eq. 2-8)
$P_y$	Yield stress (GPa)
$\varepsilon$	Compact porosity
$D_r$	Relative density of the compact (bulk density over true density of the powder) ( $\text{Kg}/\text{m}^3$ )
N	Heckel coefficient (Eq. 2-9)
J	Constant in the Heckel equation (Eq. 2-9)
P	Pressure applied to the powder bed (GPa)
$V^{\cdot}$	Specific volume of the tablet in Walker equation ( $\text{m}^3/\text{Kg}$ )
$W^{\cdot}$	Walker coefficient which represent the reduction in the volume (Eq. 2-10)
$V^{\cdot}_{sp}$	Specific volume at pressure 1 MPa (Eq. 2-10)
$\sigma_{\theta}$	Normal stress at angular roll position of $\theta$ (GPa)
$\alpha$	Nip angle ( $^{\circ}$ )
$\rho_{\theta}$	Powder density at angular roll position of $\theta$ ( $\text{Kg}/\text{m}^3$ )
$\sigma_{\alpha}$	Normal stress at the nip angle (GPa)
$\rho_{\alpha}$	Powder density at the nip angle (GPa)
$C_k$	Factor indicates the extent of volume reduction (Eq. 2-12)
$a_k$ and $b_k$	Constants (Eq. 2-12)

$\omega$	Natural strain in Adam's equation (Eq. 2-13)
$\tau_o$	Apparent single agglomerate strength (Eq. 2-13)
$\alpha^o$	Quantity related to the pressure coefficient (Eq. 2-13)
$d_{crit}$	Critical size ( $\mu\text{m}$ )
R	Fracture toughness (MPa. $\mu\text{m}$ )
$\theta$	Angular position in roll bite ( $^o$ )
$\delta_E$	Effective angle of the internal friction ( $^o$ )
$\phi_w$	Angle of wall friction ( $^o$ )
D	Roll diameter (m)
G	The gap between the roll (m)
L	Length between two supports (mm) (Three points bend test)
W	Width of the ribbon (mm)
$F_{fr.}$	Force required to break the ribbon (N)
$\sigma_f$	Ribbon flexural stress (MPa)
T	Thickness of the ribbon (mm)
A	Parameter in Johanson's equation
$\nu$	Acute angle between the tangent to the roll surface and the direction of the major principal stress
$\mu$	Parameter in Johanson's equation (Eq. 2-15)
d	Height of the roller indent (m)
K	Compressibility factor (Johanson's theory)
$\rho$	Bulk density of the powder ( $\text{kg/m}^3$ )
$p_{max}$	The maximum stress applied to the powder during roller compactor process (GPa)
$R_f$	Roll force (N)
W	Width of the roller (m)
f	Force factor (Eq. 2-22)
$\sigma_x$	Stress along the x direction (Eq. 2-23)
h	Slab thickness, (Eq. 2-23), (m)
p	Normal pressure acting on the layer, (Eq. 2-23), (GPa)
$\alpha_x$	Instantaneous angle ( $^o$ ), (Eq. 2-23)
$\tau_f$	Frictional stress (Eq. 2-23), (GPa)
$\omega(p)$	Coefficient of friction (Slab's method)
$Y(\rho)$	Effective shear stress (Slab's method) (GPa)
y	Percentage of occurrence in normal Gaussian size distribution
$\sigma$	Standard deviation
$\bar{x}$	Arithmetic mean
$\sigma_g$	Geometric standard deviation
$F_{comp.}$	Force required to break the compact (N)
$D_{comp.}$	Diameter of the compact in mm

---

$H_{\text{comp.}}$	Height of the compact in mm
Y	Cumulative % undersize of size x
n	Uniformity constant (Eq. 2-30)
$x_0$	Size parameter at which 63 % of the particles will pass through ( $\mu\text{m}$ ) (Eq. 2-30)
q	Size parameter in Gaudin – Schumann (Eq. 2-32)
a	Size parameter in Gaudin – Schumann (Eq. 2-32)
$C_0, C_1 \dots C_8$	Constants used to determine the area function between the indenter and the tip for the nano- indentation test
$\Delta\phi$	Absolute value of the difference between the porosity of the side and the centre of the ribbon

# Chapter 1 Introduction

## 1.1 Agglomeration

Agglomeration is a process of size enlargement of solid particles. As a physical process, agglomeration has occurred since solid particles were first found on the earth. Birds built a nest from the mud lined with fine grass using their saliva as a binder. Agglomeration as a science is relatively new. It started in the 1950s with the definition of the bonding mechanism (Pietsch, 2002).

There are many processes which could be carried out to increase the size of solid particles such as sintering, pelletizing, crystallisation and granulation.

Granulation is a process of size enlargement of powder particles where the original particles can still be identified. The increase in the size could be from few micrometres to few millimetres.

It is used in many industries, such as pharmaceutical, food, fertilizer and chemical. Granulation is carried out to improve different properties of the powder such as flowability and bulk density to make them easier to process, mix, handle and transport (Kleinebudde, 2004). It is also used to improve the taste, structure and appearance of the food products.

The good quality of the granulated product makes the granulation a favourite process to many industries among other agglomeration methods. For example, granular fertilizer exhibit less amount of caking compared to the fertilizer produced by other agglomeration processes. This is due to fewer available contact that can develop a solid bridges (Pietsch, 2002).

Recently, many industries are using granulation as a tool to design and produce smart particle that fits their specific application. The definition of the smart particle depends on the industry and their requirement. It could be a particle that dissolves in a specific time, having a specific size or shape, porosity, tabletability...etc.

More understanding of the granulation process will offer more control on the product quality. It will also help in choosing the right formula of the materials and using the right process parameters. This will reduce the need for the trial and error experimentation which is usually used in many granulation processes and reduce product waste that does not pass the required quality standards. It will also improve the quality of the product and consequently the industry will gain more customers.

## 1.2 Dry versus wet granulation

Granulation can be carried out either by a wet or dry process. In the wet granulation, liquid binder used to create viscous bridges and capillary forces to encourage particles to stick to each other and as shown in Figure 1-1. It is followed by a drying process. The common equipment of wet granulation is the twin screw granulator, fluidized bed granulator and high shear mixer. All the wet granulation equipment includes agitation to distribute liquid binder in the powder bed to stick the particles together. In the twin screw granulator, the agitation is

carried out by two rotating screws. In a high shear mixer, it is by a rotating impeller and in the fluidized bed it is by air.

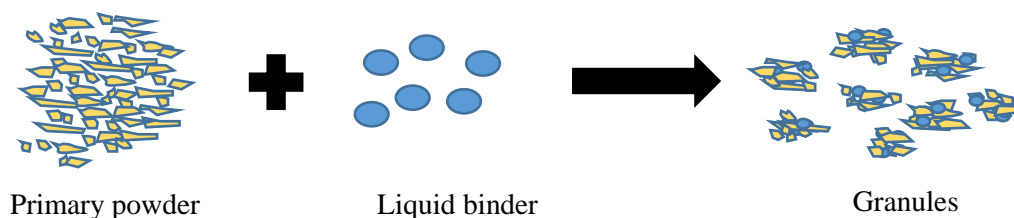


Figure 1-1: Wet granulation process

Dry granulation is a process used to agglomerate powder particles without liquid binder by compressing the powder at high pressure. For this reason, it is suitable to granulate materials that are sensitive to the presence of water or any organic solvents. As there is no liquid used in the process, it is not followed by a drying process so it is also suitable for the materials that are sensitive to the heat (Kleinebudde, 2004). This is especially important in the pharmaceutical industry where the melting point of some material is low. No drying also means reducing the overall cost of the process.

Roller compactor is a common equipment of dry granulation that used to produce ribbon then the ribbon crushed to produce granules. The disadvantage of roller compactor is that not all materials easily produce good ribbon and granules, such as calcium carbonate where the ribbon is too weak (Bacher et al., 2007, Al-Asady et al., 2015). In addition, large amount of fines or un-granulated powder could be produced which is considered as a problem in the industry. Another disadvantage of the roller compactor is reducing the tableability of the powder (Herting and Kleinebudde, 2008, Sun and Kleinebudde, 2016).

### 1.3 Continuous versus batch granulation

Granulation can be carried out by a continuous or batch process, however, the interest in the continuous process is growing due to many advantages. These advantages are applicable to both commercial and pilot scale (research and development) sectors.

In industry, continuous granulation used to avoid scale up problems (Leuenberger, 2001), increase the production capacity by reducing the time and consequently reducing the cost. Offers higher consistency of the product compared to batch process. In the R&D sector, changing of the parameters is fast and easy. Different continuous granulation equipment is commercially available. However commonly used pieces are roller compactor and twin screw granulator as a dry and wet process respectively.

### 1.4 Roller compaction

During roller compaction process, high pressure applied on the powder using two counter rotating rollers to produce a compact or a ribbon as this study will call it. The normal and the shear stresses are both responsible for bonding the particles together. In most of the industries, such as pharmaceutical, the ribbon is crushed into small granules. Figure 1-2 shows a diagram of roller compaction process followed by crushing.

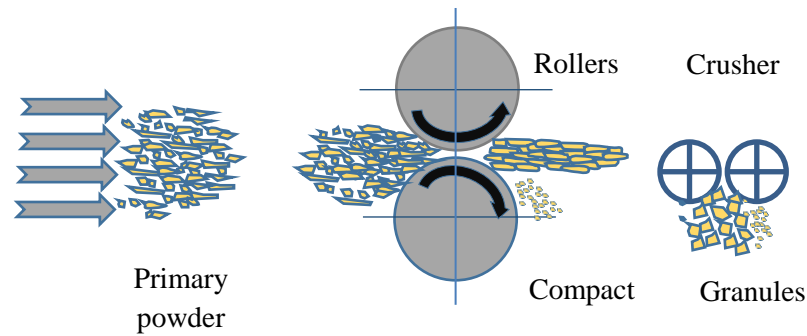


Figure 1-2: Roller compaction followed by crushing process

The roller compaction process was invented in the second half of the 19<sup>th</sup> century. The motive behind the invention was to use an economical method to agglomerate coal screening to produce coal briquettes (Pietsch, 1976). Recently, it has been used in different fields and there is an increasing interest and use of roller compactor in the pharmaceutical industry (Kleinebudde, 2004, Guigon et al., 2007).

In the roller compactor, the powder is grabbed between two counter rotating rollers to produce ribbon by applying high pressure. The pressure can be set by controlling the hydraulic cylinders that apply force to the roller. The required pressure that produce good product depends on the material, process parameters and product specification. The ribbon passes through a crusher. Oscillating crusher is commonly used with roller compactor (Am Ende et al., 2007, Sakwanichol et al., 2012, Yu et al., 2013) where the materials is forced to pass through a sieve of required mesh size. The compaction zone in roller compactor is divided into three zones: slip, nip and release region (Johanson, 1965) as shown in Figure 1-3.

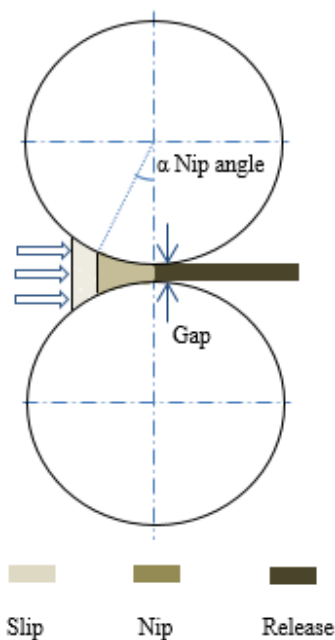


Figure 1-3: Schematic of the roller compactor

The first slip zone is defined by the slipping of the powder on the roller surface because it is moving at a different speed than the roller surface. Within this zone the powder undergoes rearrangement with an insignificant amount of applied stress (Bindhumadhavan et al., 2005). The air trapped between the particles negatively affects the compaction process (Spinov et al., 1967), for this reason, some modern roller compactors use a vacuum system to remove the air from the powder in this zone. The end of the slip and start of the nip zone are defined by the nip angle ( $\alpha$ ). It is the angle at which the powder moves at the same speed as the roller surface (Johanson, 1965). It is also defined as the angle at which the stress applied to the powder starts to increase significantly as the powder being nipped by the rotating rollers (Bindhumadhavan et al., 2005). The nip angle is important because it represents the size of the compaction zone and consequently affects the ribbon density (Yu et al., 2012). As the powder keeps moving towards the minimum gap, the applied stress readily increases due to the decreasing gap until the stress reaches the maximum value. The angle at which the maximum stress occurred is called a neutral angle. It does not necessary to be at the zero angle but could be before that (Bindhumadhavan et al., 2005). The maximum stress applied on the powder and the nip angle are both important factors that affect the product quality. The values of these two terms are depending on the applied process parameters and powder properties.

Figure 1-4 shows the normal stress distribution across different angular roll positions.

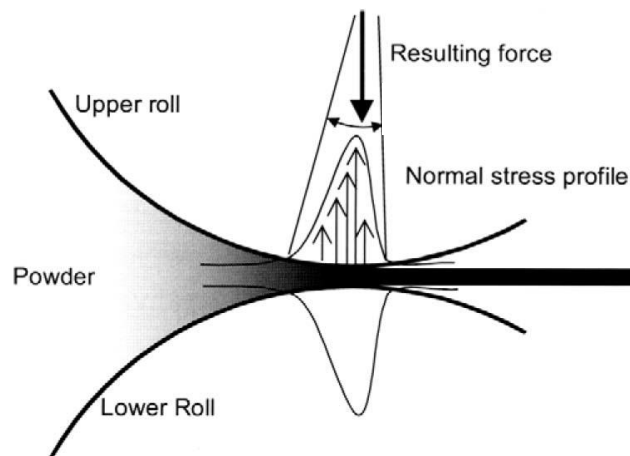


Figure 1-4: Stress distribution in the nip region (Guigon et al., 2007)

The friction between the roller surface- particles and between particles-particles affects the movement of the powder between the two rollers. To build up a pressurized area, two cheek plates are used on the both sides of the rollers to prevent the powder leakage. The inner surface of the cheek plate is made from a low friction material so as not to alter the movement of the powder. In the final region, the release zone, the roller gap begins to increase and the stress is suddenly removed and the compact may elastically recovered.

The product quality of the roller compaction process is controlled by both the applied process parameters and material properties. The important process parameters are the applied pressure, roller gap and roller speed. In term of material properties, the mechanical properties of the material is important however it received limited attention and need to be investigated in details.



### 1.4.1 Feeding systems and roller design

Feeding of the powder is an important issue in the roller compactor system as the poor feeding results in a poor filling of the gap between the rollers which leads to inhomogeneity of the products (Pietsch, 1976). Two feeding systems are commonly used with the roller compactor; gravity and force screw feeders. In the gravity feeder and as indicated by the name, the powder is fed by the gravity using a simple funnel shape hopper. This system is used for free flowing material. If the material is not flowing easily, which is in most of the cases, the force feeder is essential. Many arrangements of the screw feeder are available. Figure 1-5 shows some available arrangements of the screw feeder and rollers. It can be seen from the figure that some of the screws are horizontal, vertical or inclined which followed the design of the rollers. The figure also shows the three main designs of the rollers which are used by roller compactor manufacturers. The horizontal design shown in Figure 1-5 A and I consist of two rollers horizontal to each other and the material flows by gravity from the top. The feeding rate in this design is significantly affected by the flowability of the material. For this reason, the amount of material being fed to the compaction area could differ and the applied pressure on the material will not be the same. Modern roller compactor consists of one movable roller to control the gap and the pressure. In addition, it has automatic gap control which enables changing the speed of the screw feeder to keep the gap and pressure constant during the compaction process. This is considered as an advantage of the screw feeding system.

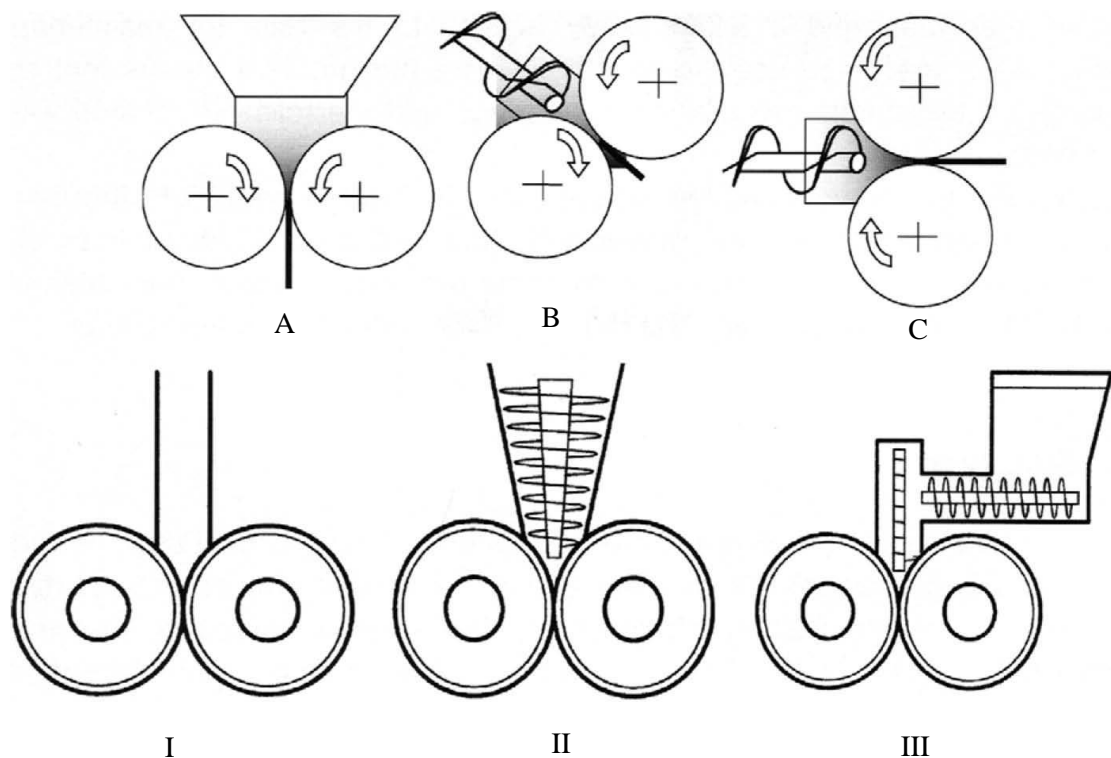


Figure 1-5: Different possible arrangements for the rollers and the feeding system (Guigon et al., 2007)

A and I: gravity feeder, B, C, II and III: different arrangements for screw feeder

## 1.5 Overview of the thesis

The overview of this thesis could be outlined as follows:

**Chapter 2** this chapter is a literature review that covers different subjects. The chapter starts with explanation of the meaning of the mechanical properties of the material with special focus on the hardness and the methods used to measure it. In addition, the survey covers how different roller compaction process studies indicate and refer to the mechanical properties of the powder. The survey also covers the stress distribution across different angular roll positions and across the roller width. The effects of different process parameters of roller compaction process on the product quality are also discussed.

**Chapter 3** presents the materials that used in different experiments of this thesis. The main production and characterisation equipment are described in this chapter. Other specific production and characterisation methods are considered in more details in relevant chapter.

**Chapter 4-8** are experimental chapters that describe the methods and present the results obtained from different studies and as follows:

**Chapter 4** this chapter includes detailed description of the method used to measure the nano indentation hardness of a single primary particle for different powders. In addition to determining and investigating other mechanical properties.

**Chapter 5** this chapter includes an investigation of the link between the nano indentation hardness of single primary particles and different ribbon properties such as ribbon strength, width, temperature and fines. A method to predict the workability of the powder in the roller compaction process is proposed. The study tracks the change in the plastic deformation of the particles after roller compaction process.

**Chapter 6** this chapter investigates the progress of the powder compaction in the pre-compaction area between the two rotating rollers. The effect of different process parameters such as roller speed, roller gap and hydraulic pressure on the compaction behaviour of the powder in this area is also investigated. Novel method is suggested to indicate the progress of the powder compaction and measuring the nip angle. The results are used to explain some changes in the quality of the ribbon upon changing some process parameters of the compaction process.

**Chapter 7** this chapter examines the non-uniformity of the stress applied on the powder along the roller width and how this causes a variation in the ribbon quality. A novel method is suggested to reduce the non-uniformity of the stress and hence improve the quality of the ribbon.

**Chapter 8** this chapter inspects the crushing process of the ribbon produced by different materials into granules. The investigation covers the effect of different process parameters of the roller compaction process and crushers on the granules size distribution. An equation is suggested to represent the granule size distribution. This helps predicting the granule size for different ribbon properties and different crushing process parameters.

**Chapter 9** is the final chapter which summarizes, concludes and highlights the findings and recommends possible future works.

## Chapter 2 Literature Review

### 2.1 Mechanical properties

The mechanical properties of the material describe how it will respond to the applied force.

There are four types of possible responses upon applying and increasing the load to a powder bed. They are rearrangement, reversible elastic deformation, permanent plastic deformation and fracture (Khosravi and Morehead, 1997).

Elastic deformation is a temporary change in the shape of the particle which is recovered after removing the load whereas the plastic deformation is permanent.

#### 2.1.1 Hardness of the material

The plastic deformation of the material can be evaluated by measuring the hardness. The hardness is the ability of the material to resist the indentation or scratching (Tabor, 1951).

Different test methods with different size scales can be used to measure the hardness of the material. The three commonly used hardness measurement methods are Mohs scale, static micro indentation such as Vickers hardness, and depth sensing indentation such as nano-indentation hardness (O'Neill, 1967, Broz et al., 2006).

##### 2.1.1.1 Mohs scale and static indentation hardness

Mohs scale is an easy and quick method to evaluate mechanical properties of a relatively large sample. The test consists of scratching a flat surface of the sample with a standard mineral knife. This scale is ordinal and does not determine an absolute value for the hardness but it evaluates the hardness relative to other materials. During the test, the sample is scratched so the result is affected by the plastic deformation as well as the fracture behaviour of the material (Broz et al., 2006).

Measurement of the static micro indentation hardness consists of applying a specific load for a specific time to a body by an indenter of a known shape and dimension. The area of the resulted impression, after removing the load, is measured by a microscope. Then the hardness is determined by dividing the maximum applied load by the area of the resulted impression. Based on this technique, many methods have been developed to measure the hardness; the main differences between them are the applied force value and the shape and the size of the indenter (Askeland, 1998). Some methods work well with metals for example while they are not applicable for brittle material because of the damage that could happen during applying the load. Table 2-1 summarizes the common scales and the methods that used to measure the static micro hardness of the material with referring to the main features for each scale.

It is not possible to measure any elastic deformation from the static micro hardness test because the impression area is measured after removing the load and after the materials is mostly recovered (Broz et al., 2006). Broz et al. (2006) measured the static micro indentation hardness for different materials and compared it with Mohs hardness. They found that none of the static hardness values increase constantly with Mohs number. They attributed the results to the nature of the Mohs hardness. As it is a measure of the scratch resistance, it is affected by loading and shearing.

Table 2-1: Commonly used scales to evaluate the static micro hardness of the material (Askeland, 1998)

Name	Indenter	Applied load
Brinell test	1-10 mm diameter steel or tungsten carbide ball	Up to 3000 Kg for steel ball
Vickers test	Square based diamond pyramid	1-120 Kg
Knoop test	Rhombic based diamond pyramid	25 g
Rockwell test	Either 1.588 mm diameter steel ball or diamond cone depending on the used scale	10-100 Kg

It can be seen from Table 2-1 that the indenter size and the applied force are relatively big and consequently the size of the resulted impression could be also big. For this reason, these hardness tests could not be used to measure the hardness of a small body such as particle of powder.

Static micro indentation hardness had been used in a few roller compaction studies. Freitag and Kleinebudde (2003) measured the micro indentation hardness of the magnesium carbonate ribbon using a ball indenter with maximum applied force of 1 N. They showed that low roller compaction force produce low hardness ribbon. In addition, low hardness ribbon produced tablet with high strength and the opposite for the high hardness. They also noticed that roller compaction process that produce high hardness ribbon also produce small amount of fines and vice versa. He et al. (2007) measured the dynamic hardness for Avicel PH-102 ribbon produced with and without magnesium stearate using the pendulum impact device that described by Hiestand and Smith (1984). The device consists of a steel ball of 2.54 cm diameter. They stated that the measured hardness is describing the behaviour of the bulk structure rather than the single particle. In addition, they explained the low hardness of the lubricated Avicel PH-102 as the particles slides on each other during the indentation test due to the presence of magnesium stearate which also distracts forming bonds between the MCC particles. This means the tests is not reflecting the plastic deformation of the particles. Miguélez-Morán et al. (2009) measured Vickers hardness for the Avicel PH-101 ribbon using a maximum applied force of about 3 N. They found that the area resulted from the indentation is inversely related to the ribbon density. The ribbon of high density has high hardness as well. They measured the hardness across the ribbon width to determine the density distribution.

In all above studies, the authors found that the hardness is an indication of the ribbon strength rather than the normal indication of plastic deformation. For all discussed studies, the hardness was measured using a big indenter compared to the size of single primary particle and relatively high force. For this reason the indenter landed on an area that includes particles as well as bonds between them. Higher strength of the bonds will increase the resistance to the breakage and consequently increase the hardness. In this thesis, static micro hardness used to indicate the ribbon strength of different materials.

### 2.1.1.2 Depth sensing indentation (Nano-indentation hardness)

During the depth sensing indentation test (DSI), the same procedures of static indentation of applying, holding and removing the load were applied but the force and the penetration depth are measured continuously during the indentation cycle. The result of the test is represented by a force- displacement curve shown in Figure 2-1.

On the nano scale, the applied force and penetration depth could be of order of 1 nano newton and 1 nano meter respectively. For this reason, the optical measurement of the resulting impression area is difficult and time consuming. For this reason, the area of the contact between the indenter and the sample that occurred at the maximum applied load is used to determine the hardness. The contact area is calculated using the area- depth function of the well-defined shape indenter (Fischer-Cripps, 2011).

As the force displacement data are recorded during the DSI test, it can be used to determine the elastic Young's modulus and the stiffness of the material. The unloading part of the force displacement curve is used for this purpose.

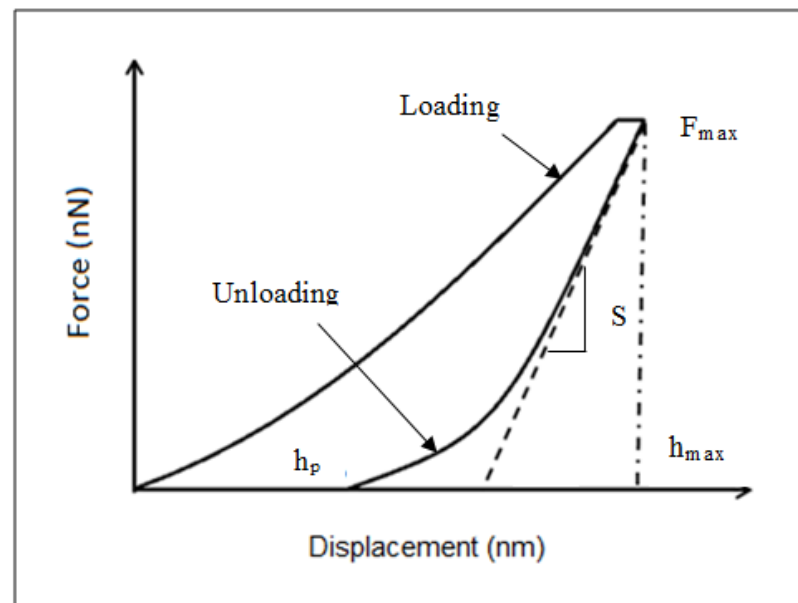


Figure 2-1: Force – displacement curve resulted from the nano-indentation test ( $F_{max}$ : maximum force,  $S$ : stiffness of the material,  $h_{max}$ : depth at maximum force,  $h_p$ : permanent indentation depth after removing the load)

Many interpretations for the load- displacement curve have been developed. According to Fischer-Cripps (2011), the most commonly used approach is that proposed by Oliver and Pharr (1992). By using the data obtained from the DSI experiment and as shown in Figure 2-1, the hardness ( $H$ ) is calculated by the following equation:

$$H = \frac{F_{max}}{A_p(h_c)} \quad \text{Eq. 2-1}$$

Where

$H$  Nano-indentation hardness in GPa

$F_{\max}$  Maximum force in nN as indicated in Figure 2-1

$A_p(h_c)$  Projected contact area in  $\text{nm}^2$

$h_c$  Indenter's contact depth with the tested sample at  $F_{\max}$  in nm

There are three options for the penetration depth value that could be used to determine the contact area (Oliver and Pharr, 1992). They are indenter penetration depth at maximum load ( $h_{\max}$ ) or the penetration after removing the load ( $h_p$ ) or the contact penetration at maximum load ( $h_c$ ). The experiment showed that using the contact depth ( $h_c$ ) determines the area of the indent more accurately than the other two penetrations (Oliver and Pharr, 1992). To determine the real contact depth there is a need to determine the sink in depth ( $h_s$ ) which is shown in Figure 2-2.

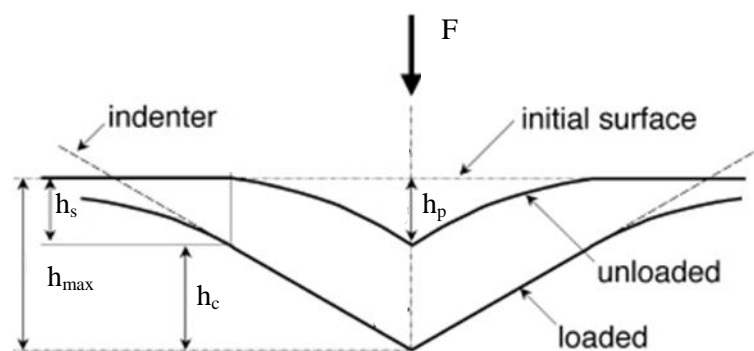


Figure 2-2: A schematic diagram shows the indenter in contact with the body during the indentation test ( $h_s$ : sink in depth). (Adapted from Oliver and Pharr (1992))

The contact depth can be determined using the following equation:

$$h_c = h_{\max} - h_s \quad \text{Eq. 2-2}$$

Where

$h_{\max}$  Penetration depth at maximum load in nm

$h_s$  Sink in depth in nm as shown in Figure 2-2

This equation can be re-written as follows (Pharr and Oliver, 1992):

$$h_c = h_{\max} - u \frac{F_{\max}}{S} \quad \text{Eq. 2-3}$$

Where

$u$  Constant depends on indenter shape (for Berkovich indenter = 0.75)

S Unloading stiffness of the material and can be determined using the upper part of the unloading curve in Figure 2-1 using the following equation:

$$S = \left( \frac{dF}{dh} \right)_{\max} = mF_{\max} (h_{\max} - h_p)^{-1} \quad \text{Eq. 2-4}$$

m constant depends on indenter geometry (1 for flat indenter, 1.5 for spherical and 2 for conical indenter)

$h_p$  Permanent indentation depth after removing the load in nm

The effect of a non-rigid indenter on the load displacement can be effectively measured by using reduced Young's modulus by the following equation:

$$E_r = \frac{\sqrt{\pi}}{2\beta} \frac{S}{\sqrt{A_p(h_c)}} \quad \text{Eq. 2-5}$$

Where

$E_r$  reduced Young's modulus in GPa

$\beta$  A factor that depends on the indenter shape (for Berkovich indenter = 1.034)

The Young's modulus of the material can be then calculated by following equation:

$$\frac{1}{E_r} = \frac{(1 - \nu^2)}{E} + \frac{(1 - \nu_i^2)}{E_i} \quad \text{Eq. 2-6}$$

Where

$E$  Young's modulus of the material in GPa

$E_i$  Young's modulus for the indenter in GPa

$\nu$  Poisson's ratio for the material

$\nu_i$  Poisson's ratio for the indenter

Different kind of indenter tips can be used to indent the sample. However, Berkovich tip of three side pyramid is commonly used due to the well-defined shape which make the determination of the contact area easier (Fischer-Cripps, 2011).

The measurement of nano-indentation hardness requires a small volume of the material. For this reason, it is suitable to measure the mechanical properties of the particles. Nano-indentation test used in this study to determine the plastic and elastic deformation of the single primary particle of different materials. The hardness of a single particle has been measured by the nano indentation technique in different fields. It has been used in the ceramic industry to

predict the milling behaviour of the materials (Meier et al., 2009) and to predict the compressibility of the material (Govedarica et al., 2012). However, it has not been used in the field of granulation.

### 2.1.2 Yield stress of the material

The yield stress ( $P_y$ ) of the material is the stress at which the material starts to deform plastically. It is defined as the stress at which the plastic deformation becomes obvious (Askeland, 1998). It is the limit that separates the elastic from plastic deformation. For one big solid piece of material such as metal, the yield strength is determined directly from the stress-strain curve of either tension or compression (Askeland, 1998). Tabor (1951) proposed a method to determine the yield stress of the material. The method consists of dividing the hardness by approximately three to get the yield stress. This relation is used widely for different materials in spite of the limitations (Lee et al., 2008). To determine the yield stress of a powder in a bed, the case is not that simple. Many approaches have been used in the literature to determine the yield stress of the powder. Uniaxial compression test is used in most of the cases. The test generates an experimental data that correlate the applied pressure to the density of the compact. These data used to extract the yield stress of the powder. The commonly used approach is the Heckel's analysis (Heckel, 1961). More information is given in the next section (Section 2.2).

The elastic and plastic deformation of a particle that is caused by the applied load can be treated and described using contact mechanics (Abdel-Ghani et al., 1991, Ameye et al., 2002). To calculate the yield stress from the loading part of the force displacement curve as shown in Figure 2-1, the elastic region in the curve should be specified. The elastic deformation may be described by Hertz equation (Johnson, 1985, Mangwandi et al., 2007, Mangwandi et al., 2015). The equation describes the relation between the applied force to a sphere particle and the resulted displacement to be as follows:

$$F = \frac{\sqrt{2}}{3} r E_r h^2 \quad \text{Eq. 2-7}$$

Where

F Applied force in nN

r Radius of the maximum possible contact area between the indenter and the particle in nm

$E_r$  Reduced effective Young's modulus in GPa

h Displacement in nm

This equation fits the elastic region of the force displacement curve. For stress greater than the elastic limit, the particle deform plastically and the loading part of the force displacement data shown in Figure 2-1 will be linear and can be described by the following equation (Johnson, 1985)



$$\frac{dF}{dh} = \pi c r P_y \quad \text{Eq. 2-8}$$

Where

$\frac{dF}{dh}$  Slope of the force displacement in the plastic region

$c$  constraint factor and it is equal to 2.8 for full plastic deformation (Johnson, 1985)

$P_y$  Yield stress in GPa

This method used in this study to determine the yield stress of the single particle of some materials using the force-displacement curves resulted from nano-indentation test.

## 2.2 Powder behaviour under compaction

In this section, the behaviour of the powder undergoing compaction is discussed. In addition, some models that used to describe the behaviour of the powder undergoing uniaxial compaction are reviewed. The discussion covers the uniaxial compaction process as it is relevant to the roller compaction and it has been investigated in more details compared to the roller compaction process.

During the compaction of the powder, the particles exhibit different behaviours depending on the mechanical properties of the material and on the applied load. The first response of the powder to the applied load is the rearrangement of the particles. This will bring the particles close to each other. It is expected that the initial powder properties such as surface area, roughness and shape will affect this step (Buckton, 2012). The porosity and the volume of the powder bed will be reduced due to the better rearrangement of the particles. Upon increasing the load to a specific value, there will be no more space for the particle to move. Any further increase in the load will cause change of the particle dimension. This change could be either temporarily elastic deformation or permanent plastic deformation. The particle dimension could also change by fracture into smaller particles. The new small particles undergo further rearrangement followed by elastic, plastic deformation and fracture. This means the particles may undergo through this cycle of events several times during the compaction process which results in reducing the size of the particle. The reduction in the size will continue until the particle will reach a critical size limit at which there is no more possible fracture and the material will change from brittle to a plastically deformable. This brittle/ plastic deformation transition is defined by the critical size (Atkins and Mai, 1986, Roberts and Rowe, 1987, Roberts et al., 1989, Franks and Lange, 1999, Larsson and Kristensen, 2000). Finally and after removing the load, the particle shape may recover due to the elastic recovery. Figure 2-3 shows an illustration of the compression stages and all possible responses of the powder to the applied load. In this figure the shape of the primary particles are assumed to be sphere for illustration purposes.

All the mentioned responses of the powder to the applied load may happen at the same time during the compaction process and the overlapping between them is considered the most common case (Holman, 1991). The extent at which each of this response happened is depending on the mechanical properties of the material and on the applied load in addition to the process conditions such as temperature, compression velocity and compression time

(Armstrong, 1989, Antikainen and Yliruusi, 2003). If the deformation of the material is affected by the compression time and compression rate, the material is referred to be a viscoelastic (Armstrong, 1989).

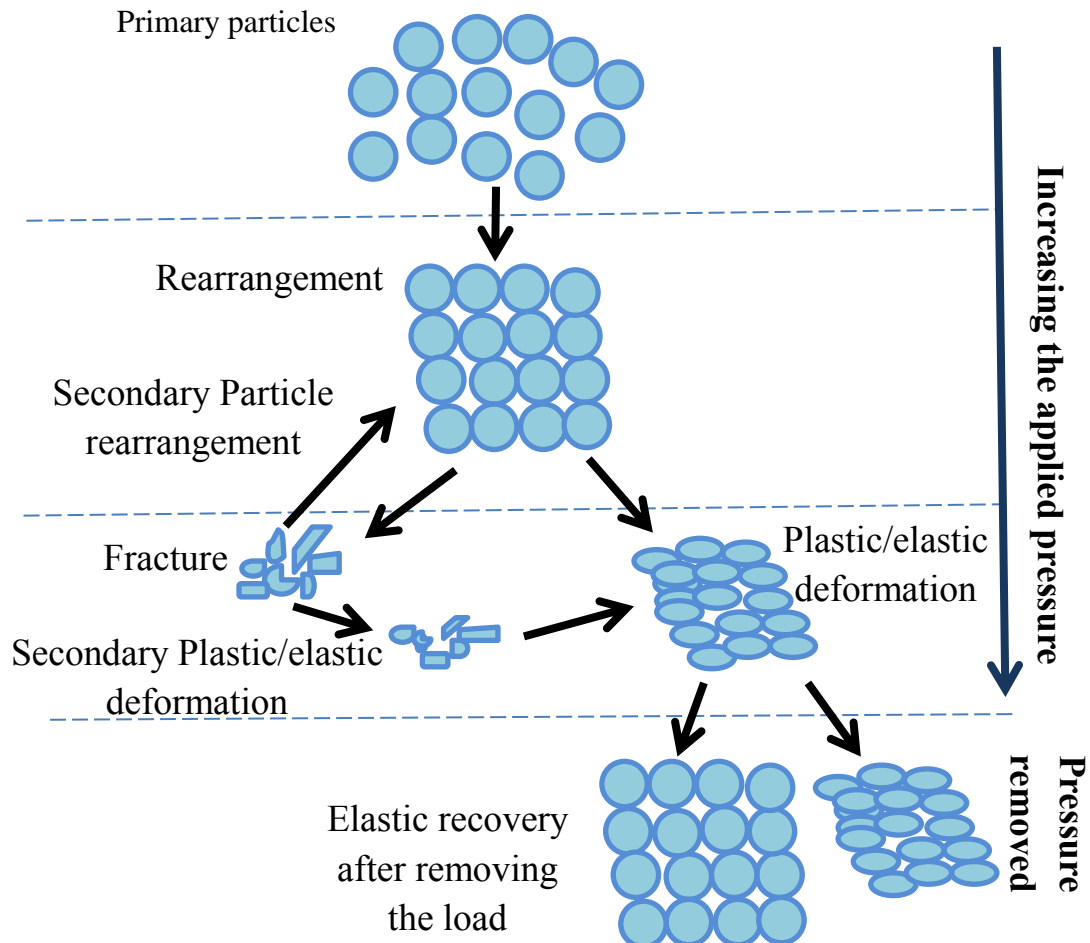


Figure 2-3: Compression cycle with possible events

The word compressibility and compactibility are two terms used in the literatures to describe the behaviour of the powder undergoing uniaxial compaction process. Compressibility is the ability of the powder to reduce the volume under pressure and the compactibility is the ability of the powder to form strong compact such as tablet (Leuenberger, 1982). The two terms are usually presented as a curve or mathematical relation. The compressibility is described by a correlation between the applied pressure and the reduction in the volume of the powder bed which is represented by porosity, relative density and specific volume of the compact. For the compactibility, the curve that correlates the applied pressures with the mechanical properties of the compact represented by compact's crushing strength is used. Several models have been developed and used to evaluate the uniaxial compaction behaviour of the powder bed. Some of the commonly used approaches will be discussed in more details.

Heckel (1961) assumes that the volume reduction of the plastically deforming powder is correlated to the density of the compact by first order kinetic relation. The pores are the

reactant and the density is the product. The equation correlates the porosity of the compact to the applied pressure by the following equation:

$$-\ln\varepsilon = \ln\left(\frac{1}{1-D_r}\right) = N.P + J \quad \text{Eq. 2-9}$$

Where

$\varepsilon$  Compact porosity

$D_r$  Relative density of the compact (bulk density over true density of the powder) at pressure  $P$

$N$  Slope; Heckel coefficient (in the linear region of the curve, yield pressure =  $1/3N$ )

$P$  Applied pressure

$J$  Constant (y- intercept), for the extrapolated linear region it relates to the contribution of rearrangement and fragmentation to the overall volume reduction process.

Another model that describes the behaviour of the powder is Walker model which correlates the specific volume of the compact with the logarithm of the applied compression pressure and as follows (Walker, 1923):

$$V' = W' \cdot \log P + V'_{sp} \quad \text{Eq. 2-10}$$

Where

$V'$  Specific volume of the tablet in  $\text{m}^3/\text{Kg}$

$W'$  Walker coefficient which represent the reduction in the volume

$P$  Applied pressure

$V'_{sp}$  Specific volume at pressure 1 MPa

Another model suggested by Johanson (1965) correlates the pressure applied during roller compaction process to the density of the compact and according to the following equation:

$$\frac{\sigma_\theta}{\sigma_\alpha} = \left(\frac{\rho_\theta}{\rho_\alpha}\right)^k \quad \text{Eq. 2-11}$$

Where

$\sigma_\theta$  and  $\rho_\theta$  normal stress and powder density at angular roll position of  $\theta$

$\sigma_\alpha$  and  $\rho_\alpha$  normal stress and powder density at the nip angle ( $\alpha$ )

$k$  Compressibility factor of the material

Johanson's model describes the reduction in the size of the powder bed and there is no indication of the plastic deformation that the powder could exhibit during roller compaction process.

Kawakita and Lüdde (1971) correlate the reduction in the volume of the powder bed with the applied pressure and as follows:

$$\frac{P}{C_k} = \frac{P}{a_k} + \frac{1}{(a_k)(b_k)} \quad \text{Eq. 2-12}$$

Where

$P$  applied pressure

$C_k$  factor indicates the extent of volume reduction of the powder bed

$a_k$  and  $b_k$  are constants

Adams and McKeown (1996) proposed an equation to correlate the applied pressure to the reduction in the height of the powder bed in confined uniaxial compression and as follows

$$\ln P = \ln\left(\frac{\tau_0}{\alpha^0}\right) + \alpha^0 \omega + \ln\left(1 - e^{(-\alpha^0 \omega)}\right) \quad \text{Eq. 2-13}$$

Where

$P$  applied pressure

$\omega$  natural strain which is given by  $\varepsilon = \ln\left(\frac{h_0}{h}\right)$  where  $h_0$  and  $h$  are the initial and current height of the bed respectively

$\tau_0$  apparent single agglomerate strength (Adams and McKeown, 1996)

$\alpha^0$  quantity related to the pressure coefficient (Adams and McKeown, 1996)

Heckel's model is used in many roller compaction studies to characterize the plasticity of the powder specifically in the studies which investigated the loss of powder compactibility after roller compaction. Freitag and Kleinebudde (2003) compared the tableability of different types of magnesium carbonate as a raw powder with the granules produced by the roller compaction process. They used Heckel approach to determine the mean yield pressure. They stated that Haeckel's plot is extremely sensitive to the small experimental error. He et al. (2007) investigated the decrease in the ability of the MCC and magnesium stearate mixture to produce strong compact after being roller compacted. They used Heckel analysis to determine the mean yield pressure. They stated that mean yield pressure can be used as indication of the plastic deformation of the powder. Bozic et al. (2008) compared the yield pressure, calculated by Heckel plot, of the powder mixture of macrolide antibiotic as active material with other materials such as MCC, talc and magnesium stearate to that of the granules produced by roller compactor. Their results showed that the plasticity is decreased, the yield pressure increased,

after dry granulation process. Patel et al. (2008) used Heckel's plot to determine the yield pressure and they showed that increasing the applied pressure during roller compaction process caused an increase in the yield pressure of the resulted granules. They also mentioned that the yield pressure derived from Heckel plot is affected by particle rearrangement, friction between the particles in addition to the fracture of the particles. That means it is not only an indication of plastic deformation.

According to Sonnergaard (1999) who critically evaluated Heckel's model, the yield pressure that calculated from Heckel's plot is not certainly an indication of the plastic deformation of the material and there is no evidence in the literature that the linear part of the plot represents the plastic deformation. The yield stress of the material is a fundamental property (Askeland, 1998). There is a big conflict in the literatures in the yield pressure values that is determined by Heckel's approach for exactly the same powder (Sonnergaard, 1999). According to the same reference, the yield pressure of the Avicel PH-101 is reported to be 47.6 MPa in one paper and 124 MPa in another one. Due to the some characterisation difficulties and problems, some of the models that are mentioned above are not being used (Rue and Rees, 1978, Sonnergaard, 1999, Bacher et al., 2007).

Despite the considerable number of the models that have been developed to describe the powder behaviour undergoing compaction, none of them evaluate accurately the plastic deformation of the material. The powder bed contains thousands or millions of single particles. During the compaction process the particles will be exposed to a different local stress and according to its location in the bed. For this reason, at any moment of the compaction process, different particles may exhibit different behaviour such as rearrangement, elastic and plastic deformation and fracture. This overlapping in the response make it difficult to distinguish which mechanism caused the reduction in the volume of the powder bed.

In this study, nano-indentation hardness of the single primary particle will be used to indicate the plastic deformation of the materials as a more relevant method.

### **2.3 Mechanical properties of the primary powder and roller compaction process**

In this section, the studies that investigated the roller compaction of the material used in this study as well as some others materials are reviewed. The aim was to examine how different studies refer to the mechanical properties of the material and how it affects the roller compaction process.

Surprisingly, most of the reviewed literatures speculated the mechanical properties of the powder rather than determining them experimentally.

One of the early study of using roller compactor in pharmaceutical industry demonstrated that adding a binder to the lactose and starch mixture decreased the amount of the fines (Kleinebudde, 2004) and produce strong compact. This could be an indication of a bad compactibility of these two materials. Chang et al. (2008) studied the effect of the pregelatinized starch content in the mixture of lactose, talc and magnesium stearate on ribbon porosity and tensile strength. The roller force per unit width of the roller that used to produce the ribbon was small and equal to 7 KN/cm. They reported that increasing the starch content from 0 to 20 % reduced the ribbon tensile strength by 60% and increased the porosity by 10%.

In addition, the granule size distribution resulted from crushing the ribbon is mainly decreased with increasing the starch content in the mixture. These changes have been ascribed to the low compressibility of the pregelatinized starch at low pressure.

Inghelbrecht and Paul Remon (1998) investigated the roller compaction of four types of lactose powder in term of primary particle size, morphology and crystallinity. They stated that lactose is mainly a fragmenting powder. The granule properties resulting from crushing of lactose ribbon changed with changing roll speed. Roll speed controls the dwell time which is the time that the powder stay under pressure between the rollers. The relation between the granule properties and roller speed has been attributed to the partial plasticity of lactose. It was mentioned in the paper that for lactose with 85% crystalline and 15% amorphous content, the consolidation was controlled by the fragmentation of the crystalline lactose whereas the bonding is controlled by the amorphous content of lactose.

Inghelbrecht and Remon (1998b) stated that a wide range of process parameters of roller compactor can be used to produce good ribbon and granules of MCC. However, adding 25, 50 and 75 % of a brittle ibuprofen to many types of plastically deformable microcrystalline cellulose disturbed the bonding and greatly reduced the range of the used process parameters. Their conclusion means that deformable material produces strong ribbon whereas the brittle one does not. Bultmann (2002) investigated the multicomaction of MCC. It was stated in the paper that MCC is plastically deformable material and it is excellent excipient due to its plastic deformability. Gupta et al. (2005) investigated the effect of the moisture content on the roller compaction of MCC powder. They reported that MCC is plastically deformable material and increasing the moisture content improved the roller compaction behavior by improving the compressibility. This has been hypothesized as more moisture caused more deformation of MCC powder. Soh et al. (2008) investigated the roller compaction of different grades of MCC and lactose. The study stated that MCC represents plastically deforming powder while the lactose is brittle. The best compaction was observed for the two MCC grades; Emcocel 90M and Emcocel SCG. On the other hand, the worst compaction behavior was seen for lactose, Pharmatose 200M. Farber et al. (2008) referred to MCC and starch DC as plastically deformable materials.

Bacher et al. (2007) used sorbitol as a binder to granulate different morphological forms of calcium carbonate. Using a binder in roller compactor indicates a low quality ribbon and granules of calcium carbonate.

Skinner et al. (1999) assessed using of Hydroxypropyl cellulose as a binder in roller compaction process. They addressed that it is a good binder due to the excellent plastic flow. The effect of wetting of Hydroxypropyl methylcellulose (HPMC) on the quantity of un-compacted powder, fines, was studied by Inghelbrecht and Remon (1998a). They demonstrated that increasing the moisture content of HPMC powder caused a dramatic decrease in the amount of fines.

Mollan Jr and Çelik (1996) investigated the effect of lubrication with magnesium stearate on the roller compaction of different types of maltodextrin. They referred to two types as plastically deformable material whereas the third one which is granules made by roller compaction as a brittle. Osborne et al. (2013) investigated the effect of the water content on the roller compaction of amorphous maltodextrin. The study showed that the glass transition

temperature decreased upon increasing the water content which caused more plastic deformation of the material and consequently better compaction.

There is a clear conflict in classifying the mechanical attributes of some materials. Inghelbrecht and Remon (1998b) described the ibuprofen as a brittle fragmenting material whereas another study conducted by Patel et al. (2008) described the ibuprofen crystal as deformable material. This happened because both studies did not use a suitable method to characterize the mechanical properties of the material.

From the above review of roller compaction studies, it can be concluded that there is no relevant method being used to measure the plastic deformation of the powder and there is a conflict in the results. Accordingly, there is a need for an adequate method to characterize the mechanical properties of the powder that is able to identify the difference in the mechanical behavior of different materials. In this study, more reliable method to evaluate the plastic deformation was used. The method consists of measuring the nano-indentation hardness of a single primary particle.

## 2.4 Brittle/ deformation behavior transition

The two widely accepted consolidation mechanisms of the powder undergoing compaction are plastic deformation and fracture (Kleinebudde, 2004). As discussed in Section 2.3, some materials have been described as a plastically deformable whereas others described as brittle. Some materials such as specific types of lactose showed both mechanisms. Several studies have shown that the behavior of the material could change from brittle to plastic deformation or vice versa. That depends on many factors such as the temperature (Iveson and Page, 2004), viscosity and the quantity of the liquid in the system (Barsoum and Radovic, 2011). For dry system such as milling and compaction, the main factor that affects the mechanical behavior of the powder is the particle size. Kendall (1978) was the first one to pointed out that below a specific size, it is impossible to crush the particles as the behavior changes from brittle fracture to plastic deformation. This size is called critical size. Above the critical size, the material fractures upon applying a specific load and below this size, the material deforms plastically. The study also proposed an equation to calculate the critical size and as follows

$$d_{\text{crit}} = \frac{32ER}{3P_y^2} \quad \text{Eq. 2-14}$$

Where

$d_{\text{crit}}$  Critical size in  $\mu\text{m}$

$E$  Young's modulus in MPa

$R$  Fracture toughness in MPa.  $\mu\text{m}$

$P_y$  Yield stress in MPa

Roberts and Rowe (1987) investigated the behavior of different pharmaceutical materials undergoing die compaction. They used four materials that represent three different mechanical properties; microcrystalline cellulose as plastically deformable material, crystalline lactose and Propanolamine both represent brittle/plastic materials and finally dolomite, calcium

magnesium carbonate, as a brittle material. They determined the yield pressure of different particle size for different materials using Heckel's approach. They found that as the particle size increased the yield pressure decreased for the materials that showed brittle behavior whereas the yield was independent of the particle size for plastically deformable MCC. The critical size was determined using Kendall's approach. Table 2-2 shows the critical size for different materials. It can be seen from the table that the biggest value is for MCC with 1172  $\mu\text{m}$  whereas it is small for lactose with a value of 27.4  $\mu\text{m}$  and even smaller for calcium carbonate (Calcite).

Table 2-2: Critical size of different pharmaceutical materials (Roberts and Rowe, 1987)

Material	$d_{\text{crit.}} (\mu\text{m})$
Dolomite (calcium magnesium carbonate)	0.11
MCC	1172
Lactose	27.4
Propanolamine derivative	22.1
calcite (Kendall, 1978)	0.8-1

Narayan and Hancock (2003) and Thoorens et al. (2014) stated that the critical size of MCC is bigger than all commercially available grades of diameter less than 200  $\mu\text{m}$ . For this reason, MCC powder is always behave plastically under compression.

Roberts et al. (1989) investigated the behavior of the sodium chloride powder under compaction. They stated that sodium chloride exhibit both brittle fracture and plastic deformation and that depend on the particle size. They found that the critical size of sodium chloride is equal to 33  $\mu\text{m}$ . Larsson and Kristensen (2000) determined the critical size of the Ibuprofen particle from the shape of the force– time curve that recorded during the compression of a single crystal. They compared the critical size that determined experimentally with that determined using Kendall's equation (Kendall, 1978). It was found that the critical size that measured experimentally is much less than that measured using Kendall's approach. The difference is probably because in Kendall's approach, the stress distributed over a bed of particles whereas it was determined experimentally for one single particle only. Balakrishnan et al. (2010) investigated the crushing of the ceramic aggregate. They found that the brittle to plastic transition occur when the particle size decreases below 50 nm. Field et al. (2014) mentioned that it is known in milling that there is a critical size called comminution limit at which the behavior of the material changes from brittle to plastically deformable. The critical size depends on the hardness of the material and fracture toughness. Romeis et al. (2015) investigated the brittle to ductile transition of a glass sphere under compression using a specially made device inside SEM. They found that the critical size is between 500 to 1000 nm.

It can be concluded from the above literatures that even the material that described to be brittle could exhibit plastic deformation if the particle size become less than the critical size. The same could happen to the powder undergoing roller compaction.

## 2.5 Stress applied to the powder during roller compaction process

The stress applied to the material during the roller compaction process is considered to be the most important factor that affects the product quality (Kleinebudde, 2004, Guigon et al., 2007). Therefore, measuring and predicting the stress distribution across the angular roller position and across the roller width is necessary to understand the process and hence control



the product quality. That helps in reducing the trial and error which is being widely used in the roller compactor industry (Kleinebudde, 2004). However, measuring and predicting the stress distribution is not easy due to many existing challenges. The first challenge is the complex design geometry of the compaction area which consist an interaction between the feeding system and the two rotating rollers. The behaviour of the powder in this area is controlled by a big number of parameters which is considered another challenge to control the quality of the product (Reynolds et al., 2010). Powder flowability and the friction between particle- particle and particle- roller surface are crucial parameters to control the compaction of the powder. However to date, these parameters are not fully understood and there is no relevant method to measure them. This is because of the complex area geometry and the value of the stress applied on the powder which could be very small.

### **2.5.1 Stress distribution at different angular roll position**

Stress distribution is considered to be the link between the applied process parameters and the compaction of the powder. It is an important and useful information for the design of roller compactor (Hsu et al., 2010) as it reflects how the roll force being distributed. Many approaches and models have been proposed to describe the densification of the powder undergoing roller compaction and predicting the stress distribution at different angular roll position.

#### **2.5.1.1 Johanson's Theory**

The first model that describe the behaviour of the powder undergoing roller compaction is presented by Johanson (1965). Johanson's approach can be used to answer the question; what is the dimension of the rollers that will apply specific stress on the material? By applying Johanson`s model, the stress distribution across the angular roll position and hence the maximum stress can be calculated taking into consideration the material properties, roller geometry and the gap between the rollers. This is the main advantage of Johanson's model; it requires determining a few powder properties to estimate the stress distribution and the nip angle. Johanson assumes the powder to be compressible, isotropic, cohesive and frictional. Johanson's model was originally based on Jenike yield criteria for hoppers and silos. The roller compaction process is widely accepted as having three different regions through which the powder passes (Guigon et al., 2007). These are known as the slip, nip and release regions and as shown in Figure 1-3. For the plane strain condition between the rollers, the effective yield function can be represented by Figure 2-4.

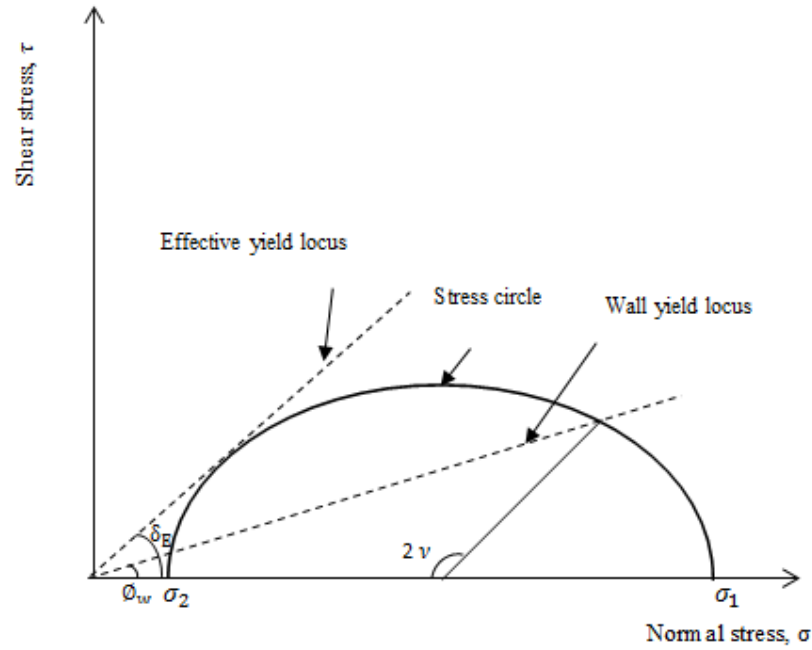


Figure 2-4: Jenike-Shield yield criterion (Adapted from Johanson (1965))

The wall yield locus and the effective yield locus depend on the angle of wall friction ( $\phi_w$ ) which indicates the friction between the particles and the wall, and the effective angle of internal friction ( $\delta_E$ ) which indicates the friction between particle-particle. Both values are measured using the ring shear cell tester.

Johanson presented that the pressure gradient in the slip region, where the roll speed is higher than powder speed, can be described by the following equation:

$$\left(\frac{d\sigma}{dx}\right)_{slip} = \frac{4\sigma_\theta \left(\frac{\pi}{2} - \theta - \nu\right) \tan\delta_E}{\frac{D}{2} \left(1 + \frac{G}{D} - \cos\theta\right) \cot(A - \mu) - \cot(A + \mu)} \quad \text{Eq. 2-15}$$

Where

$\sigma_\theta$  is the mean normal stress at position  $\theta$  in MPa

$\theta$  is the angular position in roll bite, ( $^\circ$ )

$\delta_E$  is the effective angle of the internal friction, ( $^\circ$ ), (related to material flow property)

D is the roll diameter in mm

G is the gap between the roll in mm

Where

A is parameter given by

$$A = \frac{\theta + \nu + \frac{\pi}{2}}{2} \quad \text{Eq. 2-16}$$

$\nu$  is an acute angle between the tangent to the roll surface and the direction of the major principal stress ( $\sigma_1$ ) and it is given by

$$\nu = \frac{1}{2} \left( \pi - \sin^{-1} \frac{\sin \phi_w}{\sin \delta_E} - \phi_w \right) \quad \text{Eq. 2-17}$$

Where

$\phi_w$  Angle of wall friction (°)

$\mu$  can be calculated by the following equation:

$$\mu = \frac{\pi}{4} - \frac{\delta_E}{2}$$

The pressure gradient in the nip region is given by the following equation:

$$\left( \frac{d\sigma}{dx} \right)_{Nip} = \frac{K\sigma_\theta \left( 2\cos\theta - 1 - \frac{G}{D} \right) \tan\theta}{\frac{D}{2} \left[ \frac{d}{D} + \left( 1 + \frac{G}{D} - \cos\theta \right) \cos\theta \right]} \quad \text{Eq. 2-18}$$

Where

$d$  is the height of the roller indent

$K$  is the compressibility factor determined by the following equation:

$$\log \frac{p_1}{p_2} = K \log \frac{\rho_1}{\rho_2} \quad \text{Eq. 2-19}$$

Where

$p$  is the pressure ( $p_1$  and  $p_2$  where two values of pressure)

$\rho$  is the bulk density of the powder ( $\rho_1$  and  $\rho_2$  refer to the bulk density of the powder after applying pressure of  $p_1$  and  $p_2$  respectively)

Johanson suggests that the pressure gradients in the slip and nip regions are equal at the nip angle so the nip angle can be calculated by solving the following equation:

$$\left(\frac{d\sigma}{dx}\right)_{slip} = \left(\frac{d\sigma}{dx}\right)_{nip} \quad \text{Eq. 2-20}$$

After determining the nip angle, the maximum stress applied on the powder ( $p_{max}$ ) between the two rollers can be calculated using the following equation:

$$p_{max} = \frac{2R_f}{W D f} \quad \text{Eq. 2-21}$$

Where

$R_f$  is the roll force in Newton (Supplied by the manufacturer of roller compactor)

$f$  is the force factor which given by the following equation (Johanson, 1965):

$$f = \int_{\theta=0}^{\theta=\alpha} \left[ \frac{G/D}{(1 + G/D - \cos\theta)\cos\theta} \right]^k \cos\theta d\theta \quad \text{Eq. 2-22}$$

Where

$\alpha$  Nip angle (°)

Johanson's theory is the most cited and discussed model that describes the behaviour of the powder undergoing roller compaction. Some studies investigated the validity of the model. Others tried to compare it with different available models and to point out the weakness of the model then tried to improve and modify it. In the following paragraphs, different studies that used Johanson's theory for different purposes are reviewed and discussed. The aim is to understand the weakness and the strength of the model.

Dec et al. (2003) reviewed and compared different existing models that have been proposed to describe the behaviour of the powder undergoing roller compaction with particular focusing on Johanson theory. It has been shown that the results obtained by Johanson's theory are in a good agreement with the experimental results when the powder has high wall friction and low value of compressibility factor. It was stated that the assumptions and the simplifications proposed by Johanson's are the main reason behind the deviation of the theoretical results from the experimental ones.

An experimental validation of Johanson's theory is conducted by Bindhumadhavan et al. (2005). A pressure transducer fitted to the roller has been used as sophisticated method to measure the normal stress distribution at different angular roll position and consequently determine the nip angle and the maximum stress applied to the MCC powder. The effect of different process parameter such as roller gap and roller speed is considered. The study showed that Johanson's model was quite accurate in predicting the maximum stress but the experimentally measured stress profile was not matching the predicted one. The measured stress was increased at a higher rate than that predicted by Johanson's theory as the powder enters the nip area and moving towards the minimum gap and as shown in Figure 2-5.

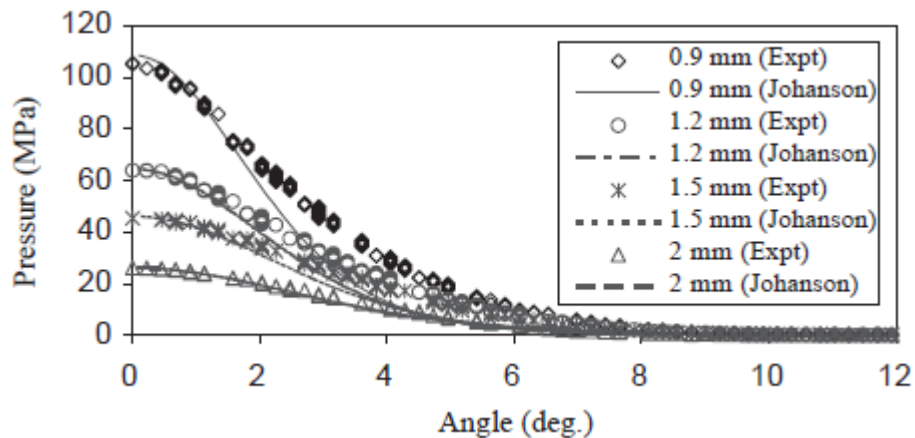


Figure 2-5: Comparison between experimental and predicted pressure profile for different roller gaps (Bindhumadhavan et al., 2005)

They addressed another problem in the model which is the need to experimentally measure the stress at the nip angle to determine the whole stress distribution. This stress could be very low and it is not accurately measured even with the used instrumented roller. In addition, they found that the measured maximum stress is different than the predicted ones at high roll speed of more than 2 rpm. It was found also that the applied stress to the material is decreased upon increasing the roller speed whereas it is constant in Johanson's theory as the roller speed had not been taken into consideration. Patel et al. (2010) investigated the certainty of predicting the stress distribution of roller compaction of Avicel PH-102 using uniaxial compaction data for different roll gaps and roll speeds. They compared the stress distribution measured using a transducer, the same one that used by Bindhumadhavan et al. (2005), with the stress distribution determined by Johanson's theory. More parameters were included in the comparison compared to the study of Bindhumadhavan et al. (2005). They found that the stress distribution predicted using parameters measured by uniaxial compression is different than that measured in the roller compactor and that is due to different reasons. In the roller compactor, the maximum stress applied at the centre of the roller whereas it is less at the edges. This is not the case for the stress applied during uniaxial compression. The other important reason is that in the roller compactor there is shear stress acting on the material due to the difference in the velocity of the powder at different positions. The flow of the powder in the roller compactor is not a plug flow which means the velocity of the powder is not the same everywhere.

Hsu et al. (2010) stated that Johanson's model does not consider the production rate and production time so they modified it to include the time, roll speed and production rate. The input parameters for their design were feeder screw speed, roller speed and roller pressure

whereas the output parameters were ribbon density and thickness. It has been claimed that the improved model is especially useful for the design purposes as it describes the changes during the unsteady state. The model still needs to use the angle of wall friction and internal angle of friction.

Reynolds et al. (2010) introduced the effect of the feeder screw speed in Johanson's model. A method was also presented to determine the compressibility factor "K" using the density and the porosity of the roller compactor compact rather than the classical die powder compaction method. The modified model was used to scale up the roller compaction process using the ribbon density as a product quality target. It has been showed that the model was able to get the targetted ribbon density. Another modification of the Johanson's theory was carried out by Nesarikar et al. (2012a). It has been stated that the weakness of the Johanson model is the need to determine the nip stress in order to determine the stress distribution at different angular roll position. another weakness is the assumption that the angle of wall friction is constant. A modified model has been developed based on the Johanson's theory to eliminate the mentioned weaknesses. They proposed different separated equations to determine the nip angle as a function of roller gap, roller speed and hydraulic pressure. An instrumented roller has been used to determine the nip angle directly from the stress distribution.

Yu et al. (2012) used the stress profile measured by the same instrumented roller that used by Bindhumadhavan et al. (2005), in combination with Johanson's theory to find the nip angle and other parameters such as compressibility factor, effective angle of wall friction and angle of internal friction. A numerical method has been used to find the pressure gradient from the measured profile data. It has been noticed that the pressure gradient curve increased then after arrived to the maximum point starts to decrease. The increasing part of the pressure gradient curve was fitted to the slip pressure gradient equation of Johanson's theory. The decreasing part of the pressure gradient was fitted to the nip pressure gradient equation. Then the nip angle was determined from the intersection of the two pressure gradients that described the slip and the nip region. The angle of wall friction and angle of internal friction were determined as it is the fitting parameters. They claimed that determining the nip angle by this method does not need measuring the angle of wall friction. This is important as such measurement does not simulate the actual situation of the powder undergoing roller compaction. This is because the roller surface geometry and the material of the roller might be different than that used in the shear cell tester. The authors found that the determined angle of wall friction is less than the measured one while the angle of internal friction is larger compared to the measured one. They attributed this difference to the fluctuation in the material feeding where it is neglected in the Johanson's theory. It is also thought that the difference could be because the method did not consider any shear stress acting on the material during the roller compaction process.

Muliadi et al. (2013) used finite element method (FEM) to determine the nip angle, maximum compact density and applied normal stress to the material. The results were compared to that obtained by Johanson's theory. Although the trend was the same for both models, the stress predicted by Johanson's theory is larger than the stress determined by FEM which consequently resulted in larger relative density of the ribbon but the results are in better agreement when the material is more compressible with high angle of wall friction and low internal angle of friction. It was stated that the stress distribution determined by FEM is less affected by the stress at the nip angle compared to Johanson's theory where the stress

distribution significantly affected by the stress at the nip angle. They attributed the inaccuracy of Johanson's theory to the one dimensional velocity gradient assumption.

Bi et al. (2014) examined the accuracy of the maximum stress predicted by Johanson's theory. They used three pharmaceutical formulas in the study. The ribbon density and the maximum stress predicted by Johanson's model for each set of conditions were determined. Then a wafer was produced with same density as the ribbon using uniaxial compression die. It was found that the predicted roller compacted stress is higher than that required to produce the same compact density in the uniaxial die. Their results are opposite to the results of Katashinskii and Vinogradov (1965) and Mal'tsev (1971) who found that the stress in the roller compactor needs to be less than the uniaxial die to produce same density compact. They attributed the difference to the Johanson's assumption of the plug flow. It has been shown by Muliadi et al. (2012) that the velocity of the powder close to the roller surface is higher than the velocity at the centre. In addition, Johanson's model does not consider the difference in the powder flowability across the roller width. This might results in an inadequate amount of powder being fed to the compaction zone. This could be the reason why Johanson's model over predict the value of the stress applied to the material. A new term was introduced to Johanson's model which is the amount of powder at any angular roll position as a fraction from the amount of powder at the previous angular roll position. However they assumed that the maximum stress applied in the roller compactor is equal to the applied stress in the uniaxial to produce same compact density in both cases. It is thought that this assumption is not right as there is a shear stress in the roller compactor in addition to the normal stress applied to the material. Furthermore, the modified model still needs detremining the angle of wall friction, internal angle of friction and the compressibility factor. Similar improvement in the last study has been recently made by Liu and Wassgren (2016). A new term has been added to Johanson's theory that takes into consideration the amount of the material at different positions. They claimed that their modified model reduced the difference in the maximum stress and relative density compared to the FEM model.

As a conclusion from the above studies, Johanson's theory is accurate to determine the maximum stress but not the stress distribution. The sensitivity of the stress distribution to the stress at the nip angle is a problem because to date, it has not been measured accurately. The model requires measurement of angle of wall friction and internal angle of friction by shear cell tester which is not always simulate the powder behaviour during the roller compaction process. In addition, Johanson assumed these two parameters are constant whereas in reality it could change according to the applied stress. This stress is different at different locations between the two rotating rollers. Some other limited assumptions by Johanson are; adequate powder supply and the uniformity of the stress distirbution across the roller width. Another issue of Johanson's model is that the roller speed effect is not considered.

For the above mentioned reasons, Johanson's theory used in this thesis to determine the maximum stress applied to the different materials. To determine the stress distribution and the nip angle, a novel new technique was proposed and tested.

### **2.5.1.2 Slab method**

Katashinskii (1966) presented a method to predict the stress distribution applied on a metallic powder by two counter rotating rollers and it is known as a slab method. The slab model was extensively used to predict the stress distribution in roller compaction of metal powder. It is

similar to Johanson's model however the yield criterion of dense metal powder is used instead of Jenike yield criterion. Later and to improve the model, the yield criterion of metal proposed by Kuhn and Downey (1971) was used (Dec et al., 2003). The area between the two rotating roller is divided into trapezoidal slabs and as shown in Figure 2-6.

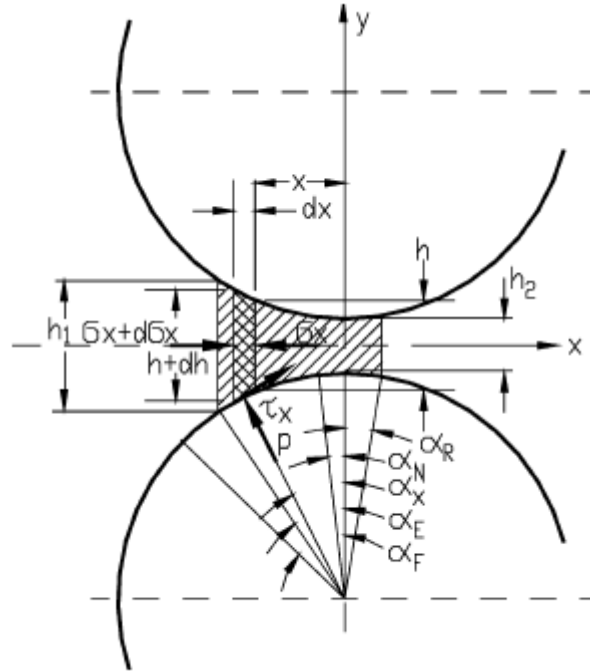


Figure 2-6: Schematic diagram of the slab method (Dec et al., 2003)

The force balance on one slab element along  $x$  direction produced the following equilibrium equation:

$$\frac{d(h\sigma_x)}{dx} + 2(p \tan \alpha_x - \tau_f) = 0 \quad \text{Eq. 2-23}$$

Where

$\sigma_x$  Stress along the  $x$  direction and as shown in Figure 2-6

$h$  Slab thickness

$p$  Normal pressure acting on the layer

$\alpha_x$  Instantaneous angle

$\tau_f$  The frictional stress and could have one of the two following values:

$$\tau_f = Y(\rho) \quad \text{for } \omega(p) p \geq Y(\rho) \quad \text{Eq. 2-24}$$



$$\tau_f = \omega(p) p \quad \text{for } \omega(p) p < Y(\rho) \quad \text{Eq. 2-25}$$

Where

$\omega(p)$  The coefficient of friction as a function of normal pressure and could be determined by the shear cell test (Dec et al., 2003)

$Y(\rho)$  The effective shear stress and can be obtained from the die compression test

The negative side of this model is the need to determine the nip angle experimentally. This is not an easy straight forward task as to date; no easy method can be used to measure the nip angle. The other point that makes this model not being widely used is the need to assume the values for both the initial stress acting on the powder and initial density.

Dec et al. (2003) investigated the validity of the model by comparing the experimentally measured stress profile as a function of angular roll position. An instrumented roller fitted with pressure strain gauge transducer was used to measure the stress applied to the roller surface at different angular roll position. Two materials were used in the investigation; Lignite which is naturally occurring rock and sodium chloride. The nip angle was determined experimentally and the initial density at each position was determined using uniaxial die compression machine using the corresponding measured stress. The stress increased until the compact density was equal to the ribbon density. It was concluded that the stress distribution determined by the model is in agreement with the measured one for lignite but this is not the case for sodium carbonate as the measured profile deviated from the predicted one. This was attributed to the sticking and slipping behavior of this material.

Similar model known as a thin layer model is proposed by Peter et al. (2010) to predict the density and the force during roller compaction process. The model assumes that the plastic deformation that happens during the tableting process is similar to the one happens in the roller compactor so it can be transferred. The area between the rollers was divided into the thin layers with the same width and thickness. It was stated that the pressure applied on each layer could be obtained using tableting or die uniaxial process by achieving the same density. They examined the validity of the model to predict a specific compact density that corresponds to a specific pressure. They compared the predicted density with the real density of the ribbon for different materials. It was shown that the average deviation of the measured density from the measured one is around 6.3%. The main assumption in the model is that the pressure-density relation of the uniaxial die compression could be used to describe the powder behavior during roller compaction. This assumption limit the ability of the model as there is no consideration to any shear stress which obviously exists during roller compaction process.

### 2.5.1.3 Finite element analysis

Computer simulation was used to predict the stress distribution applied to the material during uniaxial die compaction process (Group, 1999). Dec et al. (2003) used two-dimensional finite element analysis method using the available ABAQUS computer code to describe and predict the behavior of the powder during roller compaction process. A pressure dependent yielding plasticity model was used along with linear elasticity to describe the behavior of the powder. The plasticity model was calibrated using an instrumented uniaxial die. Microcrystalline cellulose was used as a model material in the experiment. To simplify the model, the powder

was assumed to be non-cohesive. The yield pressure was estimated from the uniaxial die compression. The use of Drucker-Prager model is considered an improvement over the usage of ellipse yield loci that used in the slab method (Katashinskii and Shtern, 1983b, Katashinskii and Shtern, 1983a). This is because the ellipse yield loci resulted in overestimation of the rolled compact strength when shear stress exists. The computer code was run until the steady state of the set process parameters has been achieved. The aim of the study was to investigate the effect of the friction coefficient and the feed pressure on the roll force, torque, nip angle and neutral angle which is the angle at which the maximum stress applied on the powder. The simulation analysis showed that the friction coefficient and the feed stress affect the compaction process. Figure 2-7 shows the roll pressure as a function of angular roll position with different feed stress.

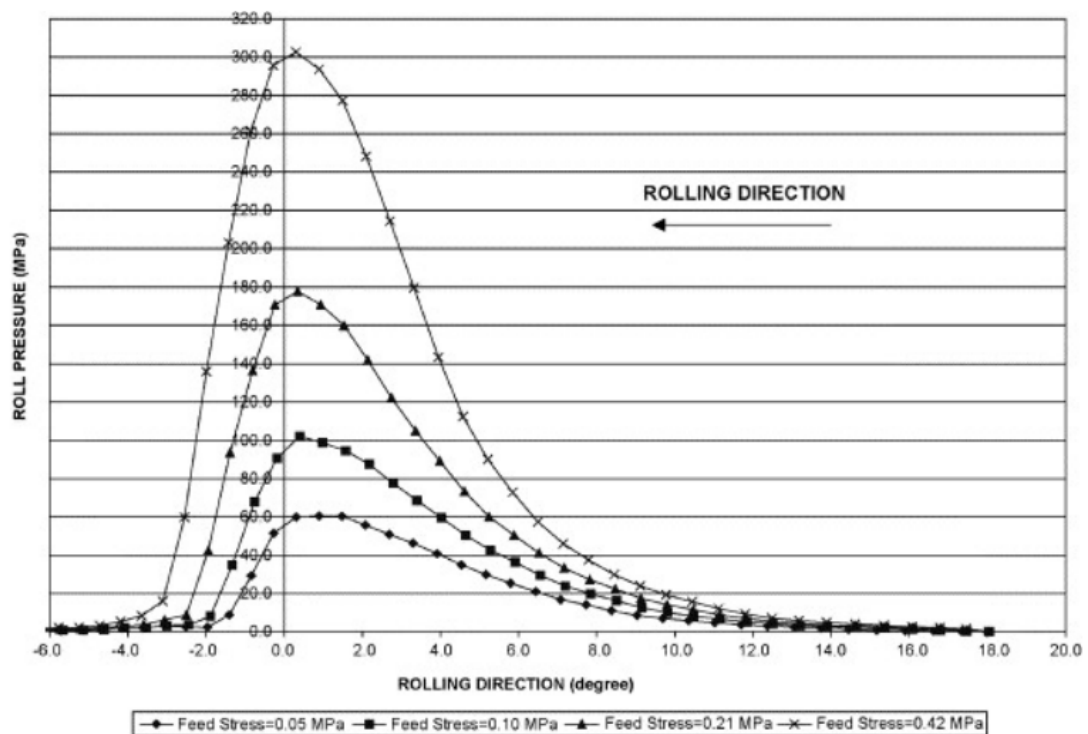


Figure 2-7: Roller pressure as a function of angular roll position for different feed stress (Dec et al., 2003)

Dec et al. (2003) showed that the finite element method (FEM) is useful technique to predict the behavior of the powder undergoing roller compaction such as predicting the relative density of the compact and the stress distribution. The challenge associated with the use of such a model is not coming from the computational side but from the input parameters that need to be defined in order to run the simulation in addition to the model that used to describe the behavior of the powder during roller compaction.

Cunningham et al. (2010) used FEM to simulate the roller compaction process. That enabled them to determine the surface stress distribution and the shear stress at different angular roll positions in addition to the stress distribution transverse the roller width. An instrumented roller compactor was used to get some input parameters.

Muliadi et al. (2013) used 3-D FEM to predict the density of the ribbon. They compared the predicted density to those measured experimentally. They used a feeder piston to feed the powder instead of the screw or gravity feeder. This allowed them to determine the feeding stress by dividing the force that applied inside the piston by the area of a plate at the piston outlet with the same dimension of the piston feeder. Another reason behind using the piston is to reduce the inhomogeneity in the feeding of the powder that could result from using the screw feeder. This is important for their study as they simulated the roller compaction process to predict the density distribution across the ribbon width so there is a need to remove the influence of the screw feeder on the density distribution. They mention that the 3-D FEM can be used to predict the normal and the shear stress applied to the material in addition to the velocity of the powder while it is moving between the two rotating rollers but they focus on the ribbon density distribution. The plastic deformation of the particles was assumed to follow Drucker-Prager model. It was showed that the predicted density distribution across the ribbon width was in a good agreement with the measured one but the model is limited by controlling the roller gap and the elastic behaviour of the material.

From the above review, it can be concluded that the FEM is capable to simulate the behavior of the powder undergoing roller compaction, however, the simulation results depend on the input parameters and the assumptions made to run the simulation. Most existing simulations are assuming the air trapped in the powder does not affect the compaction process which is opposite to the experimental findings. The other backside of the computer modelling is the long time needed to run the simulation to get the results.

There is a need for better understanding of the compaction process and improving the existing models and the methods that used to get the input data for these models.

### **2.5.2 Stress distribution across the roller width**

One of the reported problems associated with the roller compactor process is the inhomogeneity of the density across the ribbon width. The ribbon center is denser than the sides. In this section, the studies that investigated the inhomogeneity of the ribbon density, porosity and stress distribution across the ribbon width were reviewed and discussed. A number of studies have carried out to investigate the ribbon inhomogeneity using a roller compactor with gravity feeder. One of the early investigations of the density distribution across the ribbon width using aluminum powder was carried out by Katashinskii et al. (1975). It was shown that the pressure applied at the middle of the roller is higher than the sides. This led to produce a ribbon with different density across the width. This finding is confirmed by Funakoshi et al. (1977) who estimated the pressure applied at any local position across the ribbon width by determining the force required to drill the ribbon. The study showed that the applied force was higher at the center compared to the sides.

Miguélez-Morán et al. (2008) observed similar results when investigating the effect of lubrication with magnesium stearate on the density distribution of Avicel PH-102 ribbon. The investigation covered three cases; non- lubricated powder and cheek plates, lubricated powder and the third case was lubricated side cheek plates. The results showed that adding a lubricant to the powder reduced the difference in the powder flowability at the centre and the sides due to reducing the friction between the powder and the side cheek plate. This was resulted in almost uniform density distribution across the ribbon width and as shown in Figure 2-8. This is true for different roller speeds of 3 and 5 rpm. It is worth mentioning that a gravity feeder

was used so the quantity of the powder being fed to the area between the rollers is highly influenced by the material flowability.

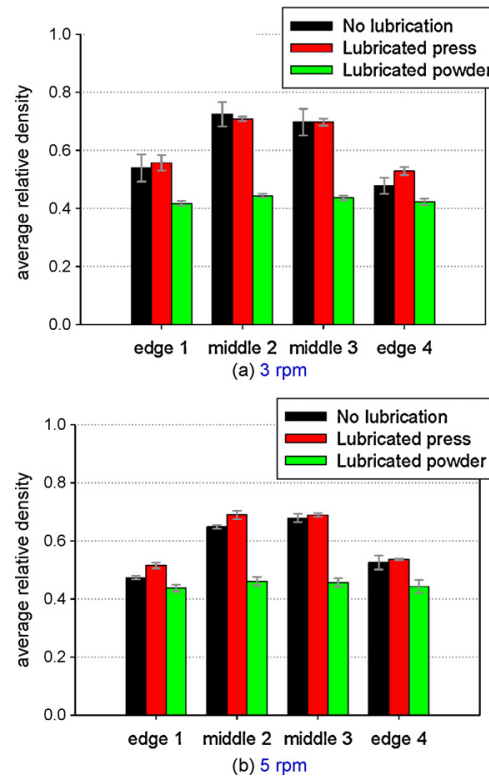


Figure 2-8: Relative density distribution across ribbon width for different cases (Miguélez-Morán et al., 2008)

Another study carried out by the same authors (Miguélez-Morán et al., 2009), investigated the density distribution across the ribbon width of Avicel PH-102 produced in a roller compactor with the gravity feeder. The effect of the roller gap, roller speed and lubrication on the density distribution of the ribbon was also investigated in the study. The results showed that the friction with the side cheek plate is the main reason for the non-uniform density distribution across the ribbon width. Three methods were used to indicate the local ribbon density; sectioning the ribbon then measuring the density of each section, micro indentation at different locations across the ribbon width and X-ray tomography. The study showed that the three methods were able to detect the difference in the density at different locations across ribbon width. In addition, the density distribution determined by the three methods showed that the density at the ribbon centre is always higher than that at the sides. This was attributed to the flowability and to the behavior of the powder during the feeding. Consequently more material was fed to the centre of the roller compared to the edges. The study showed that the sectioning method was simple and fast but with less resolution. In addition, it cannot be used for a very weak ribbon as it might break during the handling. Indentation technique showed better resolution but there is a need for a calibration to find a relation between the hardness and the density of the ribbon. X-ray tomography can be used to get more resolution. Regarding the effect of process parameters, it was found that the density profile across the ribbon width is the same at different process parameters.

Lim et al. (2011) investigated the porosity distribution across the width of Avicel PH-102 ribbon. The porosity was determined using NIR chemical imaging technique with a calibration between the color intensity and ribbon porosity. It was found that the centre of the ribbon is less porous than the edges as shown in Figure 2-9. High porosities at the edges were explained as the side cheek plates allowed the powder to leak so did not exhibit good compaction.

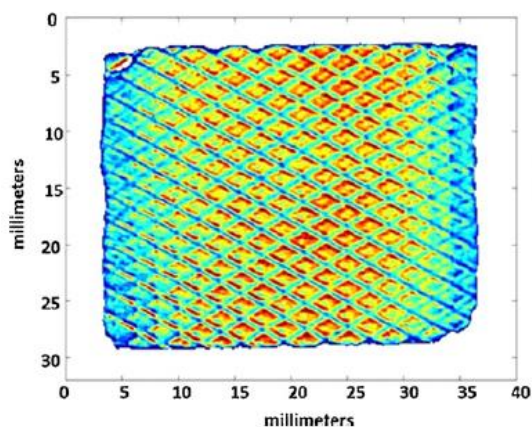


Figure 2-9: Porosity distribution across the ribbon width (red color: low porosity, green color: medium porosity, blue color: high porosity) (Lim et al., 2011)

In recent study carried out by Zhang et al. (2016), a new method using terahertz pulse imaging being used to measure the density distribution across the ribbon width. As the terahertz radiation is capable to pass through most of the material that being used in the pharmaceutical industry, it is able to detect the difference in the density of the material. Terahertz radiation has a wavelength of 0.1-1 mm which makes it penetrate into many materials. The method consists of measuring the time required for the radiation to transmit through the sample which depends on the density. Two MCC grades were used separately to produce ribbon. They used tablets produced from the same material with different densities to do the calibration and to get a relationship between the radiation time and the compact density. Then, the density across the ribbon width was determined using a step of 2 mm. The results showed high density at the centre of the ribbon and it is gradually decreased towards the edge. To validate the results, the density distribution was measured by sectioning the ribbon and measuring the density of each section. The volume of each section was determined by caliper. They showed that the results obtained by the two methods are in a good agreement. They also investigated the effect of different roll speeds and different roll gaps on the ribbon density. They found that the profile of the density distribution still the same upon changing the process parameters but there was a change in the values of the local ribbon density produced at different parameters. Figure 2-10 shows an example of the ribbon density profile.

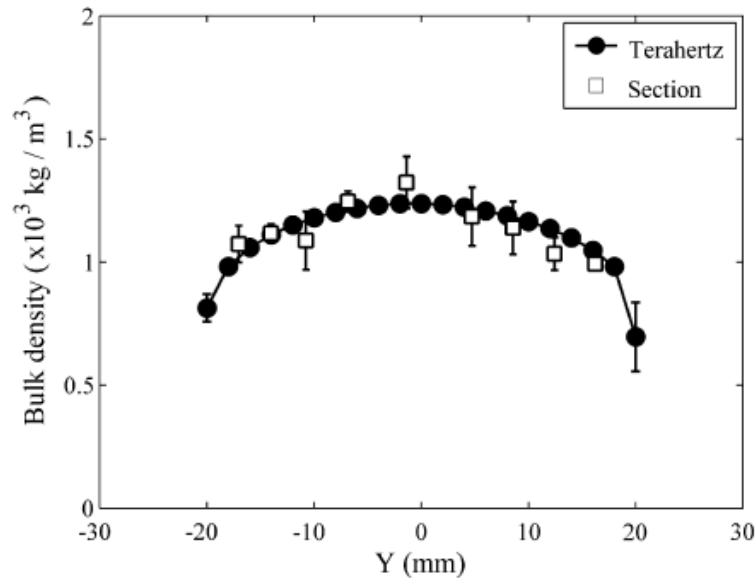


Figure 2-10: Density distribution across ribbon width (Zhang et al., 2016)

All above studies were investigated the density and porosity distribution across the ribbon width using roller compaction with gravity system. In the next paragraphs, other studies that used roller compactor with a screw feeder will be reviewed. Although the screw feeder overcome some problems associated with powder flowability and supply more uniform amount of powder across the roller width, it did not remove the heterogeneity in the ribbon properties such as density distribution across the width.

Funakoshi et al. (1977) and Parrott (1981) stated that the pressure applied on the side of the roller is lower than the centre due the friction of the powder with the cheek plates and the nature of the screw feeder that might supply more material in the centre than the sides. A rim roller was used instead of a side cheek plates. Different angles or different wall slopes of the rim were tested. The results showed that the angle of  $65^\circ$  produced less fines compared to other angles.

Cunningham et al. (2010) investigated the stress distribution across the ribbon width of Avicel PH-102 using a 3-D finite element model. The motive was to examine the reason behind the variation in the ribbon density across the width which consequently caused inconsistency in the granules properties. An instrumented roller compactor with pressure sensors located across the roller width was used. The determined stress showed that the pressure at the centre was higher compared to the edges. This was attributed to the friction between the powder and the side plates. Figure 2-11 shows the results determined using the simulation. It can be seen from the figure that if the friction with the side cheek plate is neglected (uniform inlet feed velocity), the pressure and the density profile across the roller width will be uniform whereas a non-uniform powder inlet velocity caused a variation in the roller pressure and density across the width.

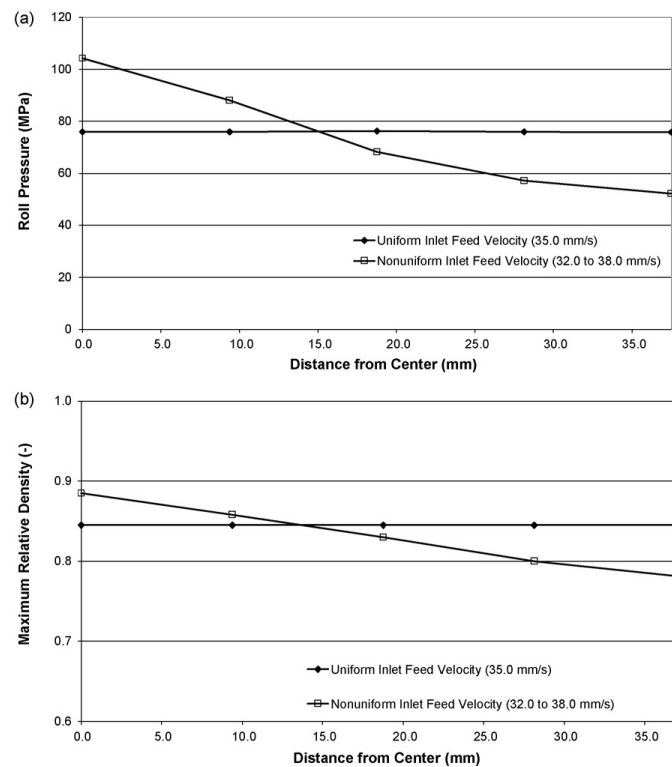


Figure 2-11: Pressure (a) and density (b) distribution across the ribbon width resulted from simulation of the roller compactor process (Cunningham et al., 2010)

Guigon and Simon (2003) and Simon and Guigon (2003) investigated the stress and porosity distribution across ribbon surface of alumina, lactose and sodium chloride. The stress was measured using pressure transducers fitted on the roller surface while the heterogeneity across the ribbon width was measured by light transmission technique. It was found that the pressure and porosity are neither homogeneous across ribbon width nor constant with time. The profile of both maximum stress applied on the powder and lights transmission has the same pattern of the screw feeder and as shown in Figure 2-12. This suggests that the feeding pressure has significant effect on the maximum stress profile that applied on the powder by the rollers. It was shown also that the variation in the maximum stress was more pronounced with alumina and lactose while it is much less for sodium chloride. It was stated that the feeding pressure is related to the packing of the powder in the last flight of the screw feeder.

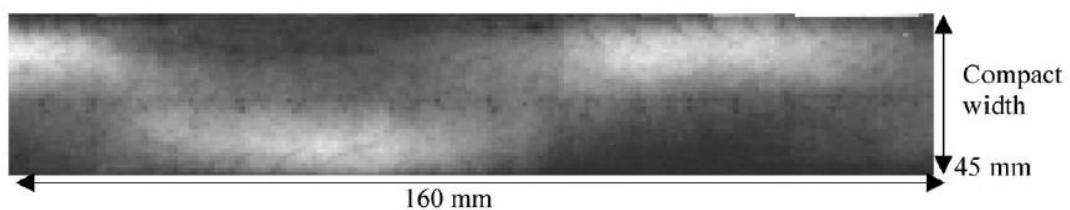
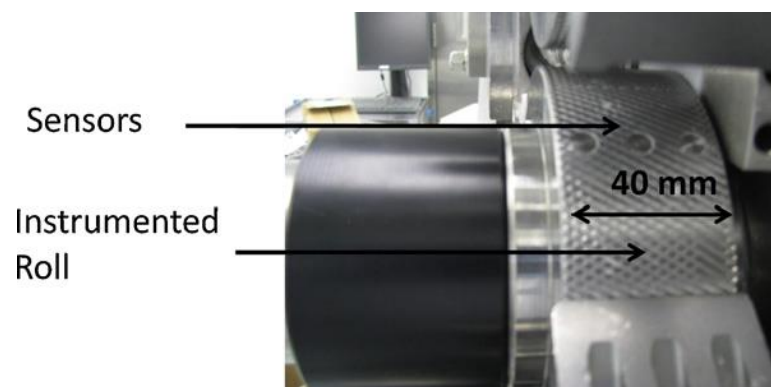


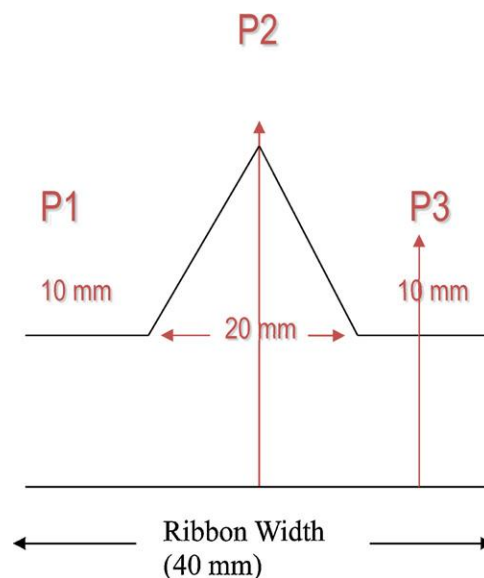
Figure 2-12: Image showing light transmission through a ribbon of sodium chloride (Simon and Guigon, 2003)

Michrafy et al. (2011) investigated the porosity distribution along the width of Avicel PH-102 ribbon. Three methods were used to determine the porosity; light transmission technique, sectioning method along with the mercury porosimetry measurement and finite element simulation. The light transmission principle is simple. The light is passing through the ribbon so some area will be darker than others according to the density or porosity. The roller

compactor system consists of two rotating rollers with two cheek plates on sides and the powder is fed by horizontal screw feeder. The roller instrumented with three strain gauges on the centre and on the sides to measure the normal stress across the ribbon width. Light transmission results showed a pattern of light area with the same shape of the screw feeder. This is in agreement with the results of previous study. Sectioning method with mercury porosimeter showed lower porosity at the centre compared to the sides which indicates higher pressure applied on the centre compared to the sides. Nesarikar et al. (2012b) observed similar results when investigating the profile of the normal stress along the roller width. Alexanderwerk WP120 roller compactor fitted with instrumented rollers with three pressure sensors (Figure 2-13a) was used. The middle sensor measured much higher stress compared to the two on the sides and as shown in Figure 2-13(b). This was attributed to the size and the geometry of the screw feeder which supply more powder to the centre of the roller while supplying less and inconsistent amount to the sides.



(a)



(b)

Figure 2-13: (a) Roll fitted with sensors (b) Measured stress profile across roller width (Nesarikar et al., 2012b)



Muliadi et al. (2013) used the 3-D finite element method to investigate the stress and consequently the density distribution across the roller width using an instrumented roller with pressure transducers. The experimental and numerical results were in agreement with all previous studies which showed higher stress at the centre compared to the sides. Souihi et al. (2015) used the same approach to measure the stress acting on different positions across the width of the roller. The results confirmed the findings in the previous studies as the measured stress acting on the powder at the roller centre is higher than the one acting on the sides.

It can be concluded from the above literatures that the stress and the density distribution across the ribbon width is not uniform. This is considered one of the main problems associated with roller compaction process and the industry is looking for a way to avoid it to improve the product quality. Many methods have been successfully used in the literatures to measure the stress and the density distribution across the ribbon width. However, none of the studies tried to solve the problem of ribbon heterogeneity and none tried to determine the stress profile online during the process.

## **2.6 Effect of process parameters of the roller compaction process**

This section includes a thorough review of the literatures that investigated the effect of different process parameters of the roller compaction process.

### **2.6.1 Effect of hydraulic pressure**

In roller compactor, the primary particles are agglomerated together by applying high pressure using two rotating roller. Different studies have shown that the pressure is the most important parameter which affects the quality of the ribbon and the granules produced from crushing the ribbon. One of the things that indicate the quality of the bonding between the particles is the percentage of fines. The fines is defined as the un-granulated powder after the compaction process has ended. It was shown by different studies that the percentage of fines decreases with increasing the hydraulic pressure. This was noticed for different types of materials regardless of the bonding mechanism. Increasing the pressure caused more plastic deformation and/ or fragmentation and both processes help in bonding the particles to each others. Cohn et al. (1966) in one of the earliest study, optimized the roller compaction process of potassium hydroxide. The study showed that increasing the pressure caused a decrease in the percentage of fines. von Eggelkraut-Gottanka et al. (2002) investigated the effect of different roller compactor process parameters on the roller compaction and tableting of St. John`s Wort dry extract. They reported that the disintegration time of the tablet slightly increase upon decreasing the roller compactor pressure. This was attributed to the increase the amount of fines which formed a layer of gel around the tablet which prevented the water to penetrate inside the tablet. They also showed that the pressure caused an increase in the size of the granules resulted from crushing of the ribbon. They attributed this to the increase in the ribbon strength. Heiman et al. (2015) studied how the percentage of fines and the ribbon density of HPMC are changing with changing the hydraulic pressure. They showed that increasing the pressure caused an increase in the ribbon density and decrease in the amount of fines. In addition to the decreasing the fines and increasing the granule size distribution resulted from milling the ribbons. Omar et al. (2016) confirmed the previous results by showing that the percentage of fines of three types of lactose was decreased upon increasing the hydraulic pressure. Study conducted by Freeman et al. (2016) investigated the effect of the compaction force (3-12 kN/cm) on the granules properties. They demonstrated a clear

relationship between the applied forces during roller compaction with compressibility of the granules. Increasing the force caused a decrease in the compressibility of the granules. The fines is also decreased. Another study conducted by Inghelbrecht and Remon (1998a) showed that increasing the pressure decreased the amount of fines produced from roller compactor but the pressure has no influence on the dissolution rate of the drug in the tablet. Their results contradict the findings of Rambali et al. (2001), who showed that the dissolution profile of the tablets significantly affected by the pressure applied during roller compaction process.

Number of studies has investigated the effect of the pressure on the friability of the granules produced by crushing the ribbon. Inghelbrecht et al. (1997) investigated the effect of different process parameters on the granules quality of deformable maize starch. It was found that the granule friability decreased upon increasing the pressure and that indicates strong bonding between the particles. Inghelbrecht and Paul Remon (1998) confirmed the previous results by showing an opposite relation between the applied pressure and the friability of the granules of different types of lactose. They justified the findings by relating the pressure with the breakage that happened during the compaction process. High pressure caused more breakage which help particle bonding because the mechanism of lactose bonding is fragmentation. It was not mentioned that increasing the pressure could cause an increase in the plastic deformation of the primary particles which is also play an important role in the compaction process (Al-Asady et al., 2015). Weyenberg et al. (2005) investigated the effect of compaction force on the different granules properties of the maize starch such as friability, bulk density, size distribution and flow properties. Higher pressure caused an improvement in the flowability and a decrease in the friability of the granules. In addition, increasing the pressure caused an increase in the granules size distribution and the apparent density. They also showed that the tablets produced from the granules of low compaction pressure are stronger than the tablets made with high pressure granules. This is due to reduction in the tabletability of the powder after the compaction. Other studies showed that increasing the roller compaction pressure reduced the tensile strength of the tablets produced from the granules and vice versa (Bacher et al., 2007). Deformable materials are more sensitive to this behaviour compared to the materials which undergo fragmentation upon compression (Herting and Kleinebudde, 2007).

Another studies investigated the effect of the pressure would have on the ribbon density, strength and porosity. Mansa et al. (2008) proved that ribbon density of different materials such as MCC and DCPA increased with increasing the hydraulic pressure. Miguélez-Morán et al. (2008) confirmed the results by showing that the average ribbon density of the Avicel PH-102 increased with increasing the hydraulic pressure and this is because more pressure caused better bonding of the particles to each other. Lim et al. (2011) investigated the effect of the process parameters on the porosity of Avicel PH-102 ribbon which is measured by the NIR chemical imaging. The porosity decreased upon increasing the pressure which is expected due to the increase of relative density. Nesarikar et al. (2012b) studied how the density of the ribbon produced using placebo formulation of different materials changes with changing the hydraulic pressure (40-70 bar). It was found that the compact porosity decreased with increasing the hydraulic pressure and that because the particle comes close to each other either by fragmentation or by plastic deformation. Osborne et al. (2013) investigated the effect of hydraulic pressure (30-180 bar) on the ribbon strength and temperature of the maltodextrin in addition to the particle size of the granules resulted from crushing the ribbon. They found that the ribbon strength, assessed by three point bend test and by the size of the granules resulted

from milling the ribbon, increased upon increasing the hydraulic pressure. This is due to the increase in the bonding between the particles. As a result of increasing the ribbon strength the granules size resulted from the crushing of the ribbon increased too. Using the granule size as an indication of the strength does not always reflect the difference in the strength because the size depends on the milling parameters. The results showed that increasing the hydraulic pressure caused a decrease in the ribbon porosity and increase of the ribbon temperature which measured by a thermal camera. Omar et al. (2015) investigated the effect of amorphous content and morphology of three different types of lactose. They demonstrated that for all types of lactose, increasing the roller compaction pressure caused an increase in the ribbon strength, width and temperature.

All previous researches have tended to focus on the effect of the pressure on different ribbon and granules properties rather than on understanding the process and material behaviour during the compaction process. This understanding is essential to explain the changes in the product quality. For instance, the effect of the pressure on the powder compaction progress with different angular roll position. In addition, why some materials produce good compact by applying specific pressure while others need different pressure. Another important point is how the plastic deformation of the primary particle changes after being compacted by different hydraulic pressures.

### **2.6.2 Effect of the roll gap**

In roller compactor, the powder is compressed due to increasing the pressure as the powder moves towards the minimum gap between the rollers. The effect of changing the gap on the roller compaction process and on the product quality was reported in different studies.

Johanson's theory (Johanson, 1965) is the first approach to describe the behaviour of the powder undergoing roller compactor. According to Johanson, the effect of the roller gap on the nip angle and on the maximum stress applied on the powder is negligible because the effect of changing the gap on the ratio of roller gap to roller diameter ( $G/D$ ) is very small and as explained in Section 2.5.1.1. Bindhumadhavan et al. (2005) investigated the effect of the roll gap on the nip angle and maximum stress. The study showed that the nip angle increased slightly with increasing the roll gap then decreased with further increase in the gap. The study also showed that increasing the gap caused a decrease in the maximum stress applied over the roller. Yu (2012) looked into the effect of the roller gap on the nip angle and on the maximum stress applied during the compaction of two powders; MCC and DCDP using the same systems of the last study. It was shown that the nip angle of the MCC increased with increasing the roller gap but decreased for DCDP. This was attributed to the bad flowability of the DCDP which caused by a small particle size. This resulted in an insufficient amount of powder fed to the compaction area. The study also showed that the stress applied to the material decreased with increasing the roller gap. Rambali et al. (2001) investigated the effect of changing the roller gap in the range between 0 and 6 mm on the tableability of the granules. The results showed that decreasing the gap caused a small decrease in the tablet strength. This could be an indication of the work of hardening that happening due to the high pressure applied on the powder with using smaller gap which reduce the compactibility of the granules. It was mentioned by Kleinebudde (2004) that the roller gap is important process parameter and could affect ribbon and granules properties and consequently the tablets made out of it.

Guigon and Simon (2003) stated that using a fixed gap with different production rate could be used as a technique to produce same quality ribbon. The same study showed a relation between the roller gap and the maximum normal stress using roller compactor with a screw feeder. Increasing the gap caused an increase in the maximum stress which measured by pressure transducer fitted to the roller. There was no explanation mentioned in the study for this finding. Mansa et al. (2008) investigated the effect of changing the roller gap on the ribbon density of MCC and dicalcium diphosphate anhydrous using a roller compactor with gravity feeder. They found that using smaller gap during roller compaction process caused an increase in the normal stress applied to the powder and consequently increase the ribbon density but the effect is not significant. Nesarikar et al. (2012b) used instrumented roller with pressure sensor to measure the normal stress. They found that the normal stress acted on the roller decreased upon increasing roller gap.

Miguélez-Morán et al. (2009) investigated the effect of changing the roller gap on the ribbon density of Avicel PH-101. It was found that reducing the gap caused an increase in the relative ribbon density and in the ribbon width. They attributed this increase to the increase of the compaction pressure as there is more available powder in the compaction area. Yu (2012) noticed that the fracture energy, which is the energy required to break the ribbon divided by the area of the fracture, and the ribbon bulk density decreased with increasing of the roll gap. The same trend was noticed by Cunningham et al. (2010).

Studying the effect of the roller gap on the maximum ribbon temperature showed that the temperature increase as the roller gap increase (Osborne, 2013). This was attributed to the increase the friction due to increase the screw speed and also producing of thick ribbon which might prevented the heat to dissipate quickly. Same study showed that the strength of maltodextrin ribbon decrease as the gap increase. Srikant et al. (2014) mentioned that the gap is critical parameter which control ribbon properties such as porosities and this is because increasing the gap caused a decrease in the compaction stress.

### **2.6.3 Effect of roller speed**

A number of authors have published work carrying out experimental investigation into the effect of roller speed on the maximum stress applied on the powder and on the ribbon properties.

One of the early investigations of the effect of process parameters on the product quality was carried out by Cohn et al. (1966). They used potassium chloride as a primary powder and speed of 70, 80 and 90 % of the maximum roller speed of 40 rpm. They found increasing the speed caused a slightly decreased in the product quality without mentioning the reason.

Guigon and Simon (2003) mentioned that roller speed is important parameters and there is a range of optimum speed that produced best quality of the compact. If the roller speed is higher than this limit, the ribbon quality will be poor. On the other side, if the roller speed is very low there will be over compaction of the powder.

Bindhumadhavan et al. (2005) measured the maximum stress applied on the Avicel PH-102 for different roller speeds. They showed that the stress decreased as the roller speed increase and consequently there is a decrease in the strength of the compact. They attributed this to the air trapped in the powder bed which negatively affects the compaction process. Yu et al. (2012) in his thesis, confirmed the previous results by showing that the stress applied on the

powder decreased upon increasing the roller speed and there was no ribbon formed when the speed increased to a specific limit. They also showed that the nip angle of MCC and DCPD decreased with increasing roll speed. However the decrease was significant for DCPD due the bad flowability of the powder which caused a reduction in the amount of the powder fed to the compaction zone. It is worth to mention that a gravity feeder was used in the both last studies. Mansa et al. (2008) used artificial intelligent software to predict the effect of the process parameters on the ribbon properties and the nip angle. They used different materials such as MCC, dicalcium phosphate anhydrous and magnesium stearate. They found that the nip angle decreased upon increasing the roller speed which is not good for compaction. Their results are consistence with the results of Miguélez-Morán et al. (2008) which also showed a decrease in the nip angle of Avicel PH-102 with increasing the roller speed.

Nesarikar et al. (2012b) investigated the effect of the roller speed on the normal stress and ribbon density of a mixture of Avicel PH-102 and anhydrous lactose. Four roller speeds of 4, 5, 8 and 12 rpm were used in the study. The results showed that the normal stress that applied on the centre of the roller decreased upon increasing the roller speed. The finding was explained as increasing the roller speed consequently caused an increase in the ratio of screw feeder to roller speed which is the reason that caused a decrease in the normal stress.

Friability of the granules is one of the properties that have been investigated for different roller speeds. A study conducted by Inghelbrecht et al. (1997) to investigate the effect of roller speed (3-13 rpm) on the friability of the plastically deformable maize starch granules. The study showed that increasing the roller speed caused an increase in the granules friability which may indicate a weak bonding between the primary particles. Similar study conducted by Inghelbrecht and Paul Remon (1998) but with four types of lactose of different amorphous content and morphology. They confirmed the results of the previous study; high roll speed resulted in an increase of the granules friability. They explain these findings as changing the roller speed consequently changed the dwell time which affect the compaction of partially deformable lactose. The same results were confirmed by Weyenberg et al. (2005). They showed that the friability of the granules made of formulation mainly contain maize starch increased upon using higher roll speed. Increasing the roller speed caused a decrease in the dwell time which specifically influences plastically deformable material.

Miguélez-Morán et al. (2009) investigated the effect of different roller speeds (3 and 5 rpm) on the density distribution of the ribbon. They mentioned that using high speed caused a decrease in the width of the ribbon. They attributed this to the higher friction between powder particles and the side cheek plates which prevent the powder to be compacted. In addition, using low speed caused an increase in the ribbon average density due to the more air escaping from the powder bed during the compaction. More dwell time results in better arrangement of the particles before arriving to the compaction zone which help the compaction process and allow more time for plastically deformable material to exhibit more deformation. Another study conducted by Lim et al. (2011) examined the effect of different roller speeds on the ribbon porosity of Avicel PH-101. They showed that increasing the roller speed caused an increase in the ribbon porosity and this is because higher roller speed reduced the dwell time and consequently reduced the time available for the particle rearrangement and bonding. Heiman et al. (2015) investigated the same effect of the screw speed to roller speed ratio on the granulation of a mixture of paracetamol as fragmenting material, ibuprofen as plastically deformable material, HPMC and mannitol. They found that the density and the solid fraction of the ribbon increased upon increasing the ratio of screw to roller speed. They attributed this

to the relation between roller speed and the dwell time which is especially important for the compaction of plastically deformable material.

Despite the several investigations in the effect of roller speed on the ribbon and granules properties, there is a need for more understanding of the roller speed effect. For example, how the roller speed affects the progress of the powder compaction at different angular roll position. To date, there is no experimental investigation about the behaviour of the powder in the area between the two rotating rollers.

## 2.7 Representing the particle size distribution by mathematical formulas

Using a mathematical formula is the best way to represent the particle size distribution (PSD). It is better compared the tables or the curves because it offers interpolation, extrapolation. In addition, the parameters of the formula could be related to the parameters of the process.

Many mathematical models are used to represent the PSD including the 3 and 4 parameters equation. Although they may provide high accuracy, their uses are limited due to their mathematical complexity (Djamarani and Clark, 1997).

There are various functions that can describe the particle size distribution. Some examples of the most common mathematical functions are given below;

- 1- Normal Gaussian
- 2- Log- Normal Gaussian
- 3- Rosin- Rammler also called Rosin-Rammler-Sperling-Bennett or Weibull distribution.
- 4- Gaudin-Schuman

The application of any of these functions depends simply on how good to describe the shape of the particle distribution curve (Vesilind, 1980).

### 2.7.1 Normal Gaussian

This equation represents the normal distribution and can be written as follows:

$$y = \frac{1}{\sigma\sqrt{2\pi}} \exp \left[ \frac{-(x - \bar{x})^2}{2\sigma^2} \right] \quad \text{Eq. 2-26}$$

Where  $y$  is the percentage of occurrence ( $df/dx$ ) and could be based on volume, mass, area or number.  $\sigma$  is standard deviation and can be calculated by the following equation:

$$\sigma = \sqrt{\frac{\Sigma(x - \bar{x})^2 \Delta f}{\Sigma \Delta f}} \quad \text{Eq. 2-27}$$

$$\bar{x} \text{ arithmetic mean size} = \frac{\Sigma x \Delta f}{\Sigma \Delta f} \quad \text{Eq. 2-28}$$

Where  $f$  is general term for the frequency (number, length, surface area, volume or weight)

### 2.7.2 Log-Normal Gaussian

A skewed size distribution does not follow the normal distribution function but in many cases follows the log-normal function where the x-axis is log scale (Gupta and Yan, 2006).

This kind of distribution could be used for a powder of natural origin or that obtained by grinding or crushing since many of the powders are logarithmically distributed. The same equation of normal distribution can be used but replacing  $x$  with  $\log x$  and as follows:

$$\frac{df}{d\log x} = \frac{1}{\sqrt{2\pi} \log \sigma_g} \exp \left[ \frac{-(\log x - \log \bar{x}_g)^2}{2 \log^2 \sigma_g} \right] \quad \text{Eq. 2-29}$$

Where

$\sigma_g$       geometric standard deviation

$\bar{x}$       geometric mean of the distribution (the arithmetic mean of the logarithm)

### 2.7.3 Rosin- Rammler

Rosin– Rammler distribution formula, which is known also as Weibull (Peleg, 1996, Patel et al., 1976) was developed in 1933 by Rosin- Rammler. It is widely used in the field of resource recovery because of good fit with the shredded refuse (Vesilind, 1980) and to describe the particle size distribution of the powders produced by crushing and milling (Djamarani and Clark, 1997).

This equation of two parameters was used to represent the sieve analysis of crushed coal. The strength of the equation is that it is suitable to describe the skewed distribution in which significant amounts of powder are either large or small (Allen, 1997). The equation could be written as (Gupta and Yan, 2006, Vesilind, 1980):

$$Y = 1 - \exp \left( \frac{-x}{x_0} \right)^n \quad \text{Eq. 2-30}$$

Where

$Y$       cumulative % undersize of size  $x$

$n$       uniformity constant which is an indication of spreading of particles

$x_0$       the size parameter at which 63 % of the particles will pass through

The linear form of the equation can be derived to be:

$$\log \ln \left[ \frac{1}{1 - Y} \right] = n \log x - n \log x_0 \quad \text{Eq. 2-31}$$

This is the equation of a line.  $x_0$  is defined as the size at which  $\ln \left[ \frac{1}{1-Y} \right] = 1$

Where  $n$  is the slope of the line

Rosin- Rammler equation has been successfully used by Cheong et al. (2004) to predict the fragment size distribution resulting from the fracture of a glass sphere. As shown by Djamarani and Clark (1997), the two parameters of the Rosin-Rammler equation can be determined by using two sieve fractions; coarse and fines only after obtaining some results that correlates these two parameters with coarse + fines % (C+F%) and the ratio of coarse /fines particle.

### 2.7.3.1 Gaudin – Schumann

This equation is an example of a simple power law fit. It usually best fits the middle part of size distributions. It can be written as follows (Gupta and Yan, 2006).

$$Y = 100 \left( \frac{x}{q} \right)^a \quad \text{Eq. 2-32}$$

Where

$Y$  cumulative % undersize of size  $x$

$q$  and  $a$  the size and distribution parameter respectively

By taking the log for both sides, the equation can be written as follows:

$$\log Y = a \log x + \text{constant}$$

This is the equation of a line.  $q$  value can be determined from the plot and corresponds to 100% passing. The parameter  $a$  is the slope of the line. Kafui and Thornton (2000) used this equation to fit the particle size distribution of the fragments produced from impacts of crystalline agglomerates. It is also used to describe the fragment size distribution but according to Cheong et al. (2004) no physical meaning has been given to the parameters of this equation.

## 2.8 Aim of the research

Four responses are possible to happen upon applying a load on the bed of particles during the compaction process: particle rearrangement, elastic and plastic deformation in addition to the fracture. These responses could happen at the same time during the compaction process and it is difficult to distinguish between them. To indicate the plastic deformation of the powder, there is a need to use a reliable method. One of the aims of this study is to evaluate the plastic deformation of the single primary particle by determining the nano-indentation hardness then to understand how this affects the bonding and hence product quality of roller compaction process. Some important ribbon properties that indicate the bonding are ribbon strength, width and the amount of fines. The study aims to suggest a range of hardness that produces ribbon with good quality. This is especially important when the material is expensive or not available in large quantities. This is the case with new pharmaceutical products (Perkins et al., 2007). Confirming such a relationship between ribbon properties and the hardness of the material



will help in choosing the right formula of primary powders to produce required product quality.

Another aim of this study is to investigate the relation between the mechanical properties of the primary powder and the rise in the temperature during roller compaction process.

Furthermore, the study aims to determine the yield strength of the powder using the nano-indentation data. Then suggest a method to predict the workability of the powder for the roller compaction process.

The nip angle and the stress distribution at different angular roll positions are two important parameters that control the compaction process and the quality of the product. Therefore, this study also concentrated on determining the progress of the powder compaction while moving towards the minimum gap. Then determine the nip angle by measuring the Shore A hardness of the pre-compacted body at different angular roll positions. This method takes into consideration the real conditions of the powder compaction process including the shear stress applied on the powder and the roller speed. The ability of the method to detect the changes in the nip angle as a function of different process parameters was investigated and the nip angle values were compared to that determined by Johanson's theory. The results were used to explain some changes in the ribbon properties.

The results of this study showed that some materials were difficult to granulate. In addition, the quality of the ribbon is not uniform across the width. Another aim of this study is to modify the compaction process to improve the compaction of these difficult materials and to reduce the heterogeneity across ribbon width. This was achieved by designing a new roller with new surface geometry.

Crushing the ribbon is the process that usually follows roller compaction process to produce granules. This study investigated how the mechanical properties of the ribbon affect the granule size distribution resulted from the crusher. The investigation covers the effect of different process parameters such as hydraulic pressure applied by the rollers in addition to different crusher parameters such as mesh size and different rotor speed.

Figure 2-14 shows an overall view of how these goals have been achieved.

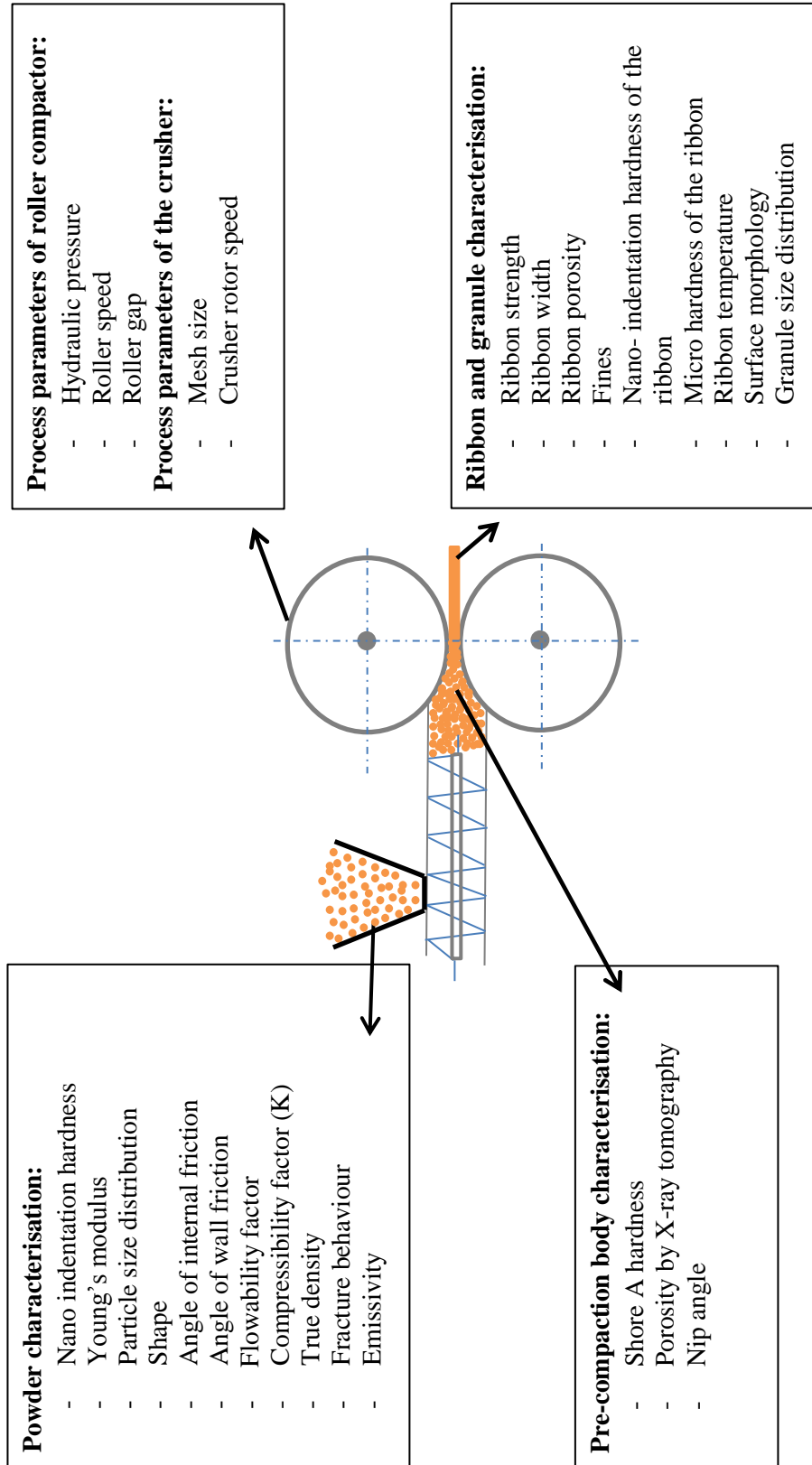


Figure 2-14: The steps to more understanding of the roller compaction process

## Chapter 3 Materials and Methods

This chapter includes description of the materials used in different studies of this thesis along with characterisation methods. In addition, the roller compactor used in the study with some test methods for the ribbon and granules were described. More specific characterisations were described in respective chapter.

### 3.1 Materials

Different powders were used in this study to cover a wide range of mechanical properties. The materials also cover different categories; synthetic and natural polymers, crystalline and amorphous. These materials are used in different industries such as pharmaceutical, food, detergent and ceramic. Furthermore, some preparations such as sieving and conditioning to a specific humidity were carried out. Materials used in particular experiment are mentioned in respective section chapter/ experiment.

#### 3.1.1 Polyvinyl alcohol (PVA)

PVA used in this study was supplied by Japan Vam and Poval Co. Limited. It is a synthetic resin in a white powder form. PVA is used as a binder and as a caking agent due to the good adhesion ability with inorganic substances. It is soluble in water. The solution of PVA in the water is viscous and can be used as a coating agent. The molded products of PVA are used to produce sponge. Figure 3-1 shows SEM image of the PVA primary particles.

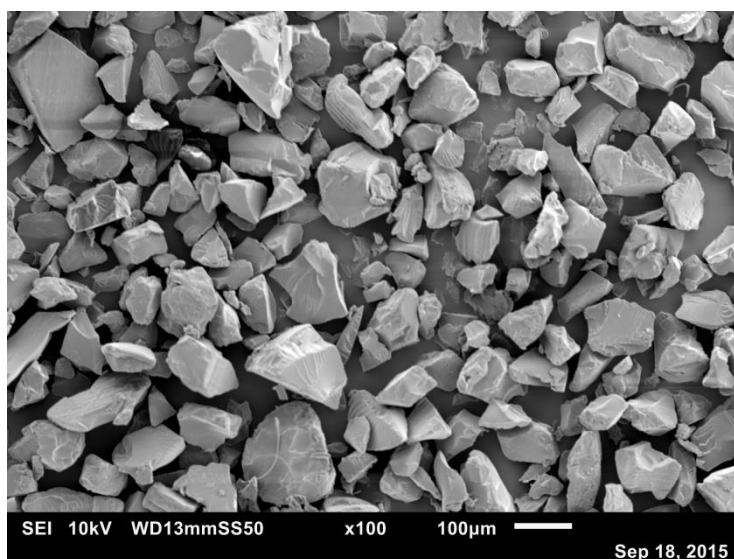


Figure 3-1: SEM of the primary particles of PVA

#### 3.1.2 Starch

Starch 1500, supplied by Colorcon, USA, is a partially pregelatinized maize starch. It is prepared by cooking the starch to make it more soluble in cold water. It is used in pharmaceutical industry as an excipients or disintegrant and in food industry as a thickener. Figure 3-2 shows SEM image of starch particles.

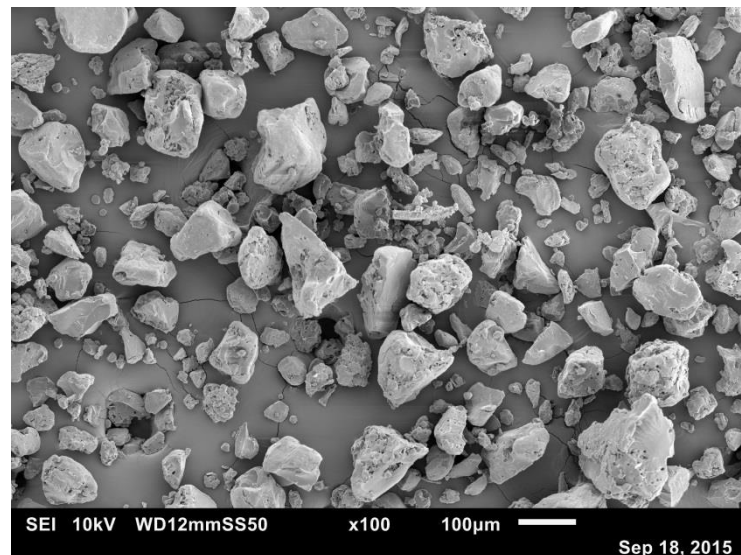


Figure 3-2: SEM of Starch 1500 primary powder

### 3.1.3 Microcrystalline cellulose (Avicel PH-101)

Avicel PH-101 was supplied by FMC Biopolymer (Ireland). It is a white semi-crystalline, plastically deformable and free-flowing powder (Sundar et al., 2011). Microcrystalline cellulose (MCC) is manufactured from wood pulp by hydrolysis process which breaks the cellulose fibres to microcrystalline cellulose. It is widely used in direct compression process (Tableting) as well as in dry and wet granulation. It is a porous material with low density. It is insoluble in water but capable of absorbing water and swelling. MCC is commercially available in different grades with different particle sizes and moisture contents. Figure 3-3 shows an SEM image for primary particles of MCC used in this study. It can be seen from the image that most of the particles have a needle shape.

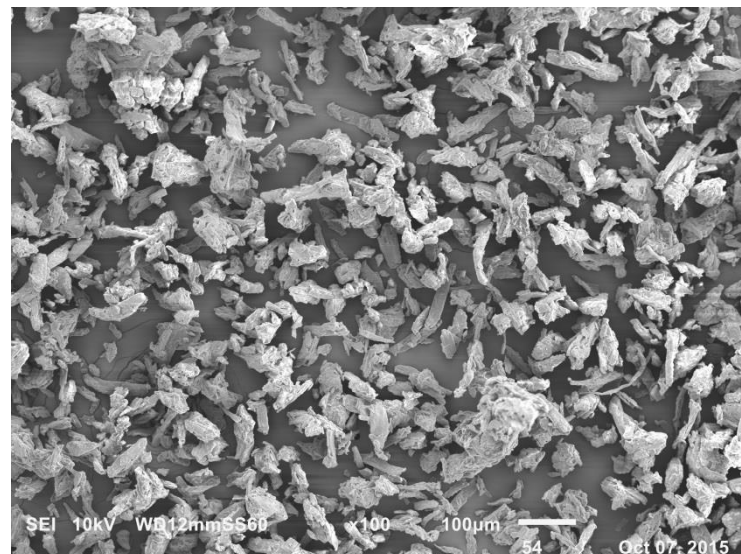
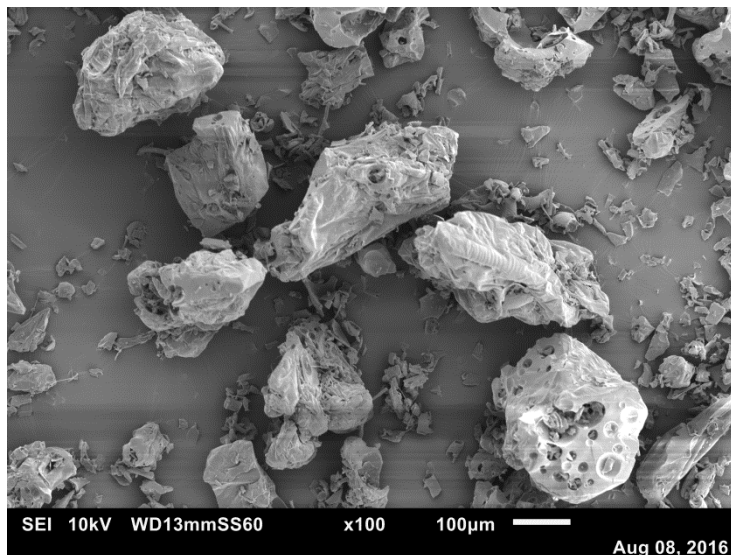


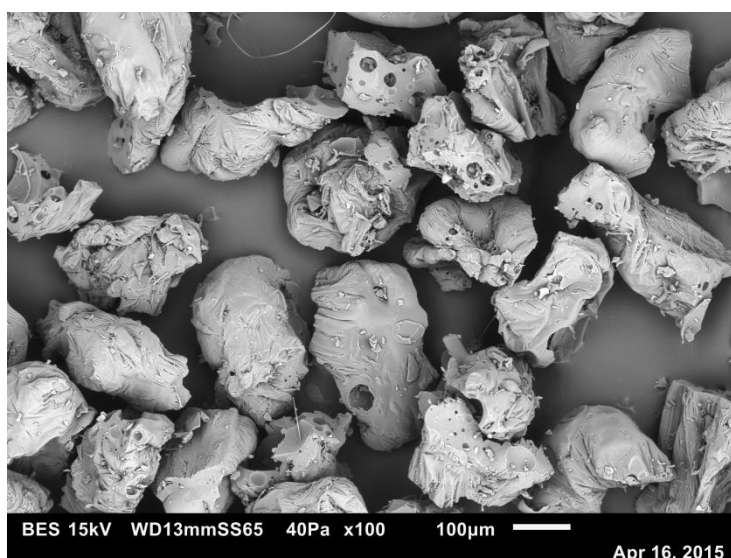
Figure 3-3: SEM image of Avicel PH-101 primary particles

### 3.1.4 Maltodextrin (Glucidex® 6)

Glucidex® 6 supplied by Roquette (France) is a white powder manufactured by hydrolysis of starch. It is widely used in food industry as a source of carbohydrate. Figure 3-4 shows two SEM images of the Glucidex® 6 primary particles. It can be seen from the figure that some particles are hollow with holes on the surface. Image (b) shows clearly that the outer surface of the particle is a thin layer.



(a)



(b)

Figure 3-4: SEM image of Glucidex® 6 primary powder

### 3.1.5 Hydroxypropyl methylcellulose (HPMC)

Tylpor 604 powder (Shin- Etsu, Japan) is an off white powder widely used as a binder and as a coating agent for tablets in pharmaceutical industry due to the nice finish. Figure 3-5 shows an SEM image of Tylpor 604 powder.

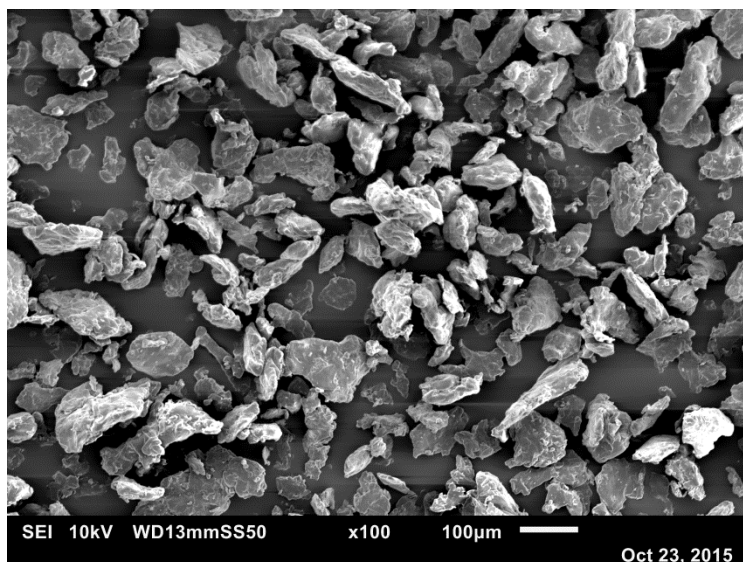


Figure 3-5: SEM image of Tylpor 604 primary powder

### 3.1.6 $\alpha$ -lactose monohydrate (Pharmatose 200M)

Pharmatose 200M used in this study was supplied by DMV-Fonterra Excipients (Netherland). It is white, odourless crystalline form of lactose which is used in many industries, including the pharmaceutical industry, as a well-known excipient or filler to produce tablets and capsules. It is used in both wet and dry granulation processes. Lactose is partially soluble in water and available in different size classes. Figure 3-6 shows SEM image of the primary particles of Pharmatose 200M. It can be seen from the figure that the particles generally have a tomahawk shape.

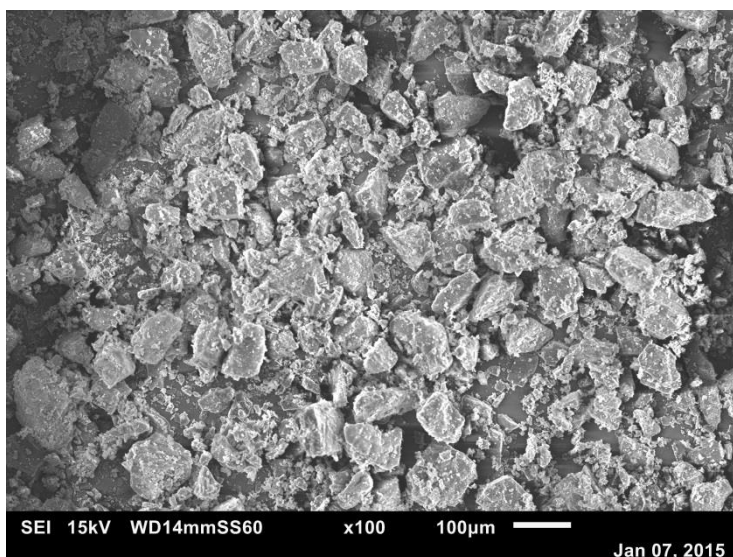


Figure 3-6: SEM image of Pharmatose 200M primary particles

### 3.1.7 Sodium carbonate

Light sodium carbonate or soda ash used in this study was supplied by Tata Chemical Europe. It is white powder mainly used in detergent industry as a water softener. Figure 3-7 shows an SEM image of the sodium carbonate primary powder.

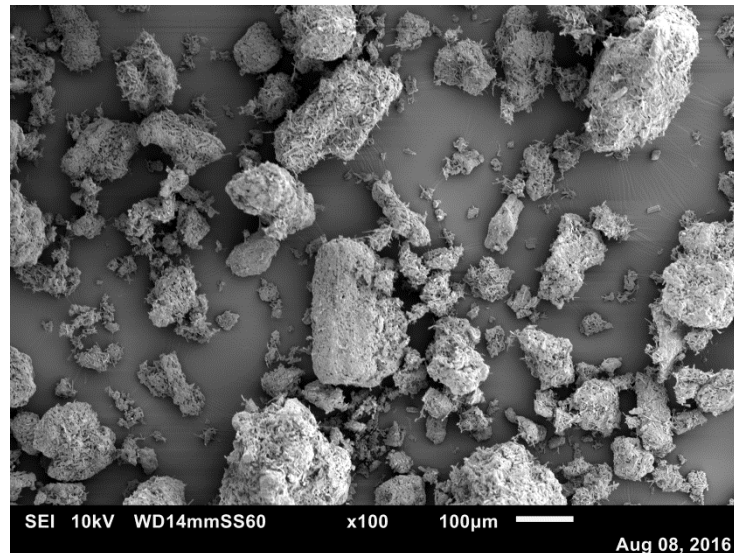


Figure 3-7: SEM image for the sodium carbonate primary powder

### 3.1.8 Calcium carbonate ( $\text{CaCO}_3$ )

Calcium carbonate (Superlon L200) used in this study was supplied by Longcliffe Quarries Ltd., UK. It is fines, dense brown powder produced by crushing of big pieces. It contains at least 98.25% of  $\text{CaCO}_3$ . The major impurities are  $\text{MgCO}_3$ ,  $\text{Al}_2\text{O}_3$  and  $\text{SiO}_2$ . Calcium carbonate is used in different industries, including food, as an inexpensive dietary calcium supply, and pharmaceutical, as inert filler in tablets and carriers for veterinary products. For this reason there are different grades of calcium carbonate. Figure 3-8 shows an SEM image of calcium carbonate particles used in this study. It can be seen from the figures that the particles are agglomerated to each other due to the small particle size.

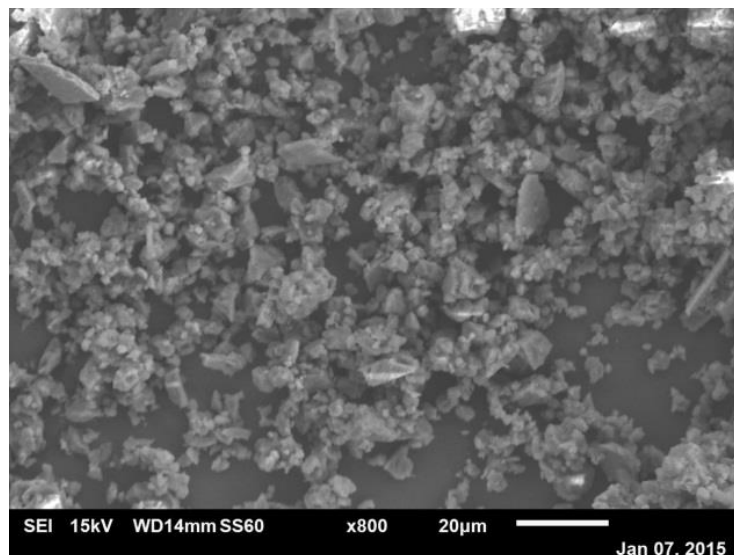


Figure 3-8: SEM image of calcium carbonate primary particles

### 3.1.9 Powder preparation and conditioning

Prior to some experiments (Sections 5.2 and 6.4) and characterisations, the powder of each material was sieved between 63 and 212  $\mu\text{m}$  using a sieve shaker (Retsch Technology,

Germany). Then to condition the powder to a specific relative humidity, the powder was spread as a thin layer in a tray and kept in a humidity chamber (Binder KMF 240 climatic chamber, Binder, UK) at relative humidity of 40% and temperature of 20 °C for three days. The chamber works with a wide range of humidity (10 to 98 % RH) and temperature (-10 to 100 C°). The chamber allows the materials to be conditioned quickly by air circulation. It was shown by a preliminary experiment that this time is sufficient for all materials to be equilibrated to 40% RH.

## **3.2 Characterisation of the primary powders**

### **3.2.1 Measuring the particle size distribution of the primary powder**

Prior to any particle size measurement and to ensure that the measured particle sample is representative for the bulk of the powder, chute splitter sampler was used to get a sample from the powder. It consists of a V-shaped trough. The powder is halved into two parts then one of these parts is halved again. This process is repeated many times until the desired quantity of the sample is obtained.

The particle size distribution of all primary powders used in different experiments were measured using a dynamic image analysis, CAMSIZER<sup>®</sup> XT (Retch Technology, Germany), which is able to measure a particle size from 1 µm to 3 mm. All measurements were carried out using a wet feeding system where the particles dispersed in sunflower oil. The dispersion is especially necessary to avoid sticking of the particles to each other during the measurement.

### **3.2.2 Scanning Electron Microscopy**

Scanning Electron Microscope, SEM (JEOL,UK) was used to capture images of the single particles and ribbon surface. All materials used in this study are not electrically conductive. For this reason, the samples were coated with a thin layer of gold of around 25 nm prior to any imaging.

### **3.2.3 Determining the flow properties and the compressibility factor of the primary powder**

The flowability of the primary powder was determined using two methods namely, ring shear cell and repose angle as explained in the following two sections.

#### **3.2.3.1 Ring shear cell tester**

Determining the flow properties of the powder is important to avoid the problems related to the flowability which could happen during the handling and processing of the powder. In addition, the flowability data could be used to explain the behaviour of the powder in the process. In this study, Schulze ring shear tester RST-XS (Figure 3-9) used to measure the flowability parameters of different powders. Three parameters are determined from the test; effective internal angle of friction ( $\delta_E$ ), angle of wall friction ( $\phi_w$ ) and the flow factor coefficient ( $ffc$ ). The internal angle of friction is an indication of the friction between particle-particle. The test principle is based on measuring the rotational shear stress required to shear one layer of powder against another layer under different normal stress. The test includes two steps; consolidation of the powder in which the powder is loaded by a normal stress then



sheared. The second step is shearing the sample at different normal stress levels. The normal preshear stress is applied on a lid which pushes the powder. Then to shear the sample, the base of the shear cell rotates relative to the lid. More details about the test procedures can be found in Schulze (2008).

To consolidate (preshear) the powder, A normal load of 5000 Pa was used. Then three different normal stress levels of 1500, 2750 and 4000 Pa were used to shear the sample. This load was chosen to avoid significant deformation of the particle which may mislead the measurement results.

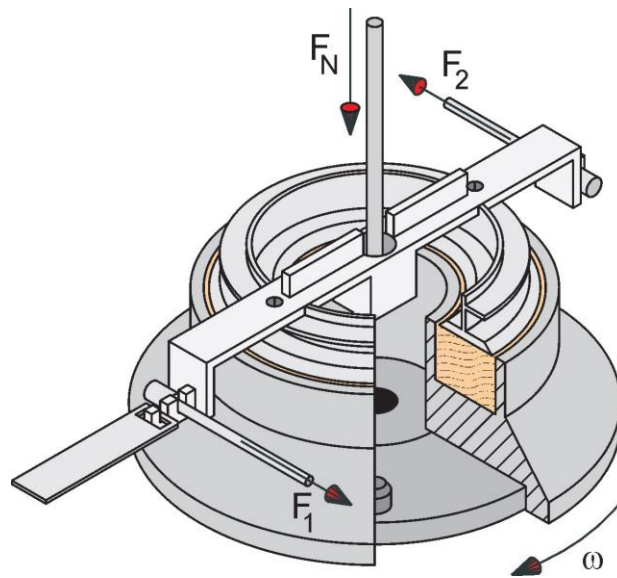


Figure 3-9: Ring shear cell tester (Schulze, 2010)

Figure 3-10 shows typical yield locus obtained from the shear cell tester. The flow factor coefficient was determined using the following equation (Schulze, 2010);

$$ffc = \frac{\sigma_1}{\sigma_c} \quad \text{Eq. 3-1}$$

Where

$ffc$  Flow factor coefficient

$\sigma_1$  Major principal stress (Figure 3-10)

$\sigma_c$  Unconfined yield strength (Figure 3-10)

$\sigma_2$  Minor principal stress (Figure 3-10)

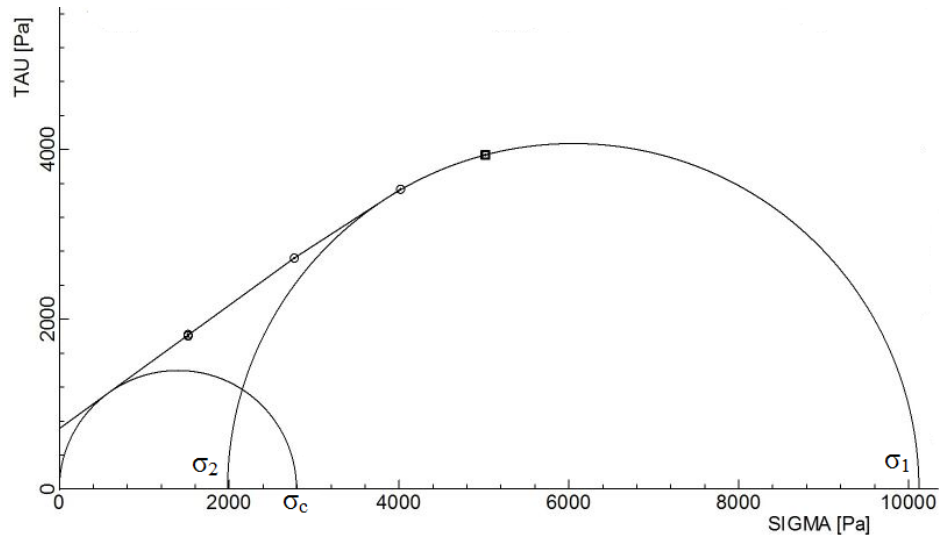


Figure 3-10: Typical yield locus obtained from the ring shear cell test

The angle of the wall friction is an indication of the friction between the powder and metal surface. It is measured by shearing the powder against a metal surface using the same maximum normal load and the same stress levels that used to measure internal angle of friction.

### 3.2.3.2 Determining the repose angle

Another term that indicates the flowability of the material is the angle of repose. The angle of repose for sieved and conditioned powder was measured using Mark 4 AOR device supplied by the Powder Research Ltd, UK. 100 gram of the powder was poured gradually from a fixed height by a vibrator on a flat surface. The angle of the repose is defined as the angle between the heap slope and the horizontal line of the heap base. The height and the length of the heap base were directly measured by using a graduated background surface of the device. The length of the horizontal line was averaged for the minimum and maximum length for each measurement and then used to determine the repose angle using the inverse tangent function. The lower the repose angle, the better the powder flowability and the opposite for the high repose angle (Geldart et al., 2006).

### 3.2.3.3 Determining the compressibility factor of the powder

The compressibility factor (K) was determined by compacting a sample of 0.2 g with a pressure range of 12–180 MPa in a die of D2 tool steel hardened to 40 Rockwell C scale, of 10 mm inner diameter by using a material testing machine (Instron 3367, Germany). The compression speed was 1mm/min. Then the out-die volume of the compact and the weight were measured for each pressure and the compressibility factor (K) was determined from the logarithmic plot of the pressure versus bulk density and according to Eq. 2-19:

$$\log \frac{p_1}{p_2} = K \log \frac{\rho_1}{\rho_2}$$

## 3.3 Roller compactor

The roller compactor used in this study is WP 120 Alexanderwerk, Germany (Figure 3-11). It has a feed hopper which transports the powder downwards towards the screw feeder which

consists of one rotating screw with adjustable speed. The screw feeder is used to transport, pre-compact and feed the material to the compaction area between the two rotating rollers. There is a vacuum de-aerating system which removes the air from the feed screw system in order to improve the transportation and the compaction of the powder. Then, the material enters the gap area between the two rotating rollers. The rollers of 12 cm diameter and 4 cm width with knurled surface (Figure 3-12) are the main part of the equipment and are arranged vertically to each other and press the powder by controlled hydraulic pressure between 18-230 bar (Roll force of 7.5- 95.3 kN). The rollers rotate with a speed range between 3 to 13 rpm (Roll surface speed of 18.8- 81.6 mm/s). The roller gap is controlled by an automated feedback system which keeps the gap constant to a set value by automatically changing the feeder screw speed which changes the feed rate. The ribbon samples were collected at each set of conditions at steady state after achieving the required parameters, hydraulic pressure and gap.

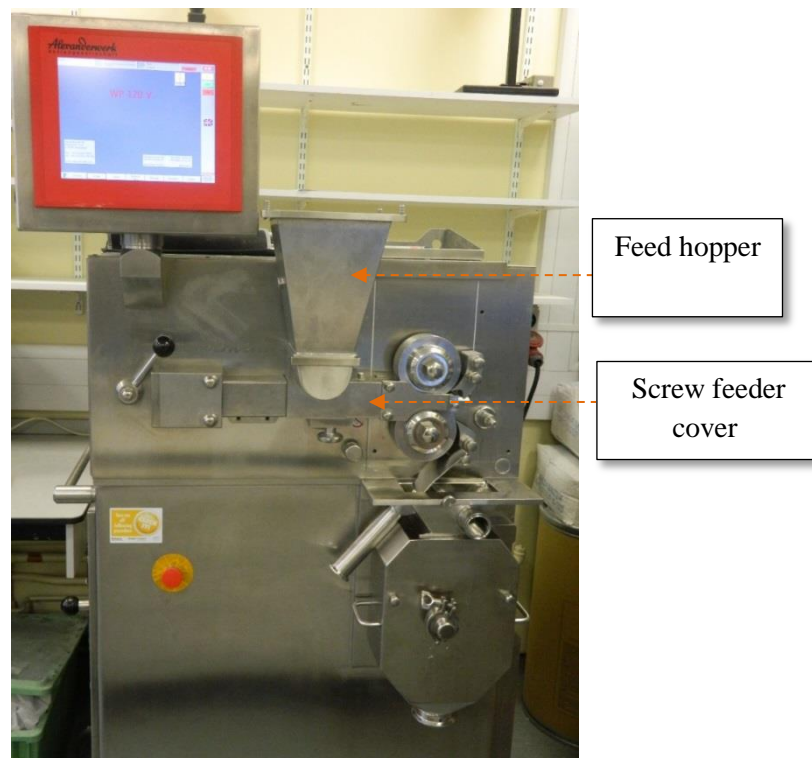


Figure 3-11: Image of the Alexanderwerk WP120 Roller Compactor

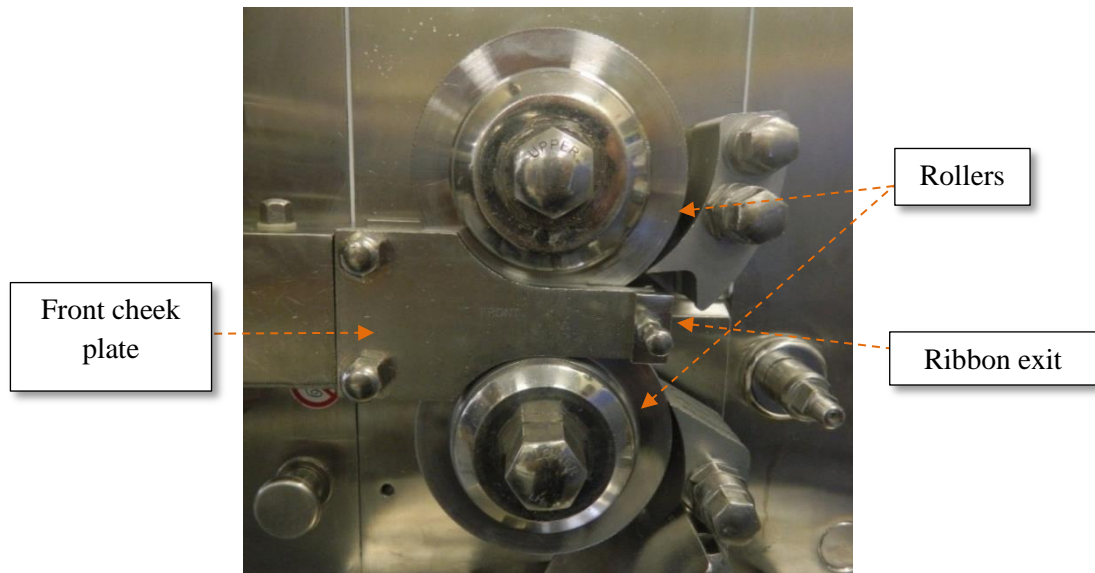


Figure 3-12: Roller setup

To maintain the humidity of the powder during the compaction process, a specially built (in-house) hopper lid was used. The lid was connected to a humidity generator (Gen RH, surface measurement system, UK) by tube. The humidity generator was set to specific humidity and according the requirement of the experiment. The humidity generator is able to supply conditioned air in the range of 0-95 % RH. To control the humidity, part of the dry air is passing through a water container and according to the required humidity. There is a sensor fixed to the end of the humidity generator tube which sends a feedback signal to the system in order to maintain the humidity to the set value.

### 3.4 Characterisation of the ribbon

#### 3.4.1 Measurement of the ribbon strength

Three points bend test (Harirtian and Michael, 2000, Osborne et al., 2013) was used to determine the ribbon strength. A material testing machine (Zwick Roell, Germany) was used to determine the force required to break the ribbon. The ribbons were placed on two supports. Force was then applied at the centre of the ribbon at speed of 1 mm/min. The force increased gradually until the ribbon broke. The measurement was repeated at least five times for each ribbon sample. Figure 3-13 shows the three point bend test setup.

The flexural strength was calculated using the force required to break the ribbon according to the following equation:

$$\sigma_f = \frac{3F_{fr} \cdot L}{2WT^2} \quad \text{Eq. 3-2}$$

Where

$\sigma_f$  Flexural strength in MPa

$F_{fr}$  Force required to break the ribbon in N

- L Length between the two supports in mm
- W Width of the ribbon in mm
- T Thickness of the ribbon in mm

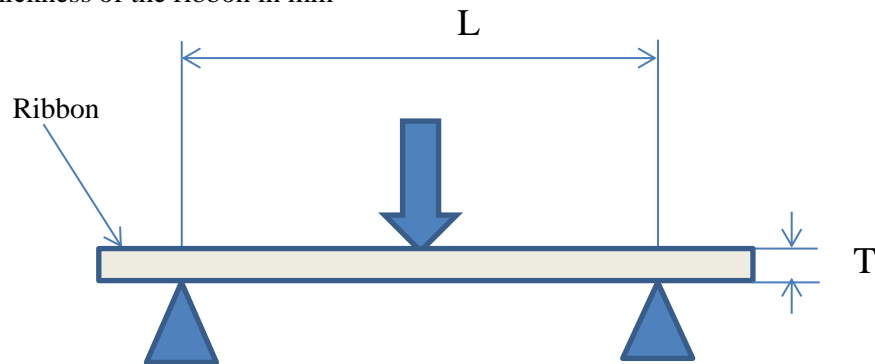


Figure 3-13: Schematic of three points bend test setup

### 3.4.2 Ribbon surface temperature

#### 3.4.2.1 Measurement of material emissivity

The emissivity of the material is a measure of how much heat is emitted from an object compared to a perfect black body. Two methods were used to determine the emissivity.

The powders were heated and kept in the oven at 70 °C for 24 hours then a thermometer was immersed in the powder bed instantaneously to measure the real temperature. The temperature of the powder was compared to that recorded by thermal camera. The two temperature values were used with the Flir R&D software to determine the thermal emissivity of the powder. Another method was also used to determine the emissivity of the ribbons under investigation using a material of known emissivity. Scotch black PVC electrical tape of 0.95 emissivity was used for this purpose. The ribbon was partially covered with the PVC tape and heated evenly to approximately 70 °C in the oven for 24 h. The temperatures of the tape and the ribbon were measured instantaneously using thermal camera. Then the emissivity of the ribbon was determined using Flir R&D software.

#### 3.4.2.2 Measurement of ribbon temperature

The surface temperature of the exiting ribbon (freshly produced ribbon) from the rollers was measured online using thermal image camera, FLIR SC655, with a frame rate of 50 frame/sec. The camera was positioned facing the point between the rollers where the ribbons were produced. Figure 3-14 shows the setup used in the experiment. The temperature of a recently produced ribbon was recorded for 1 minute for each experiment. The recording was started after approximately 30 sec of achieving the steady state of required process parameters, hydraulic pressure and roller gap.

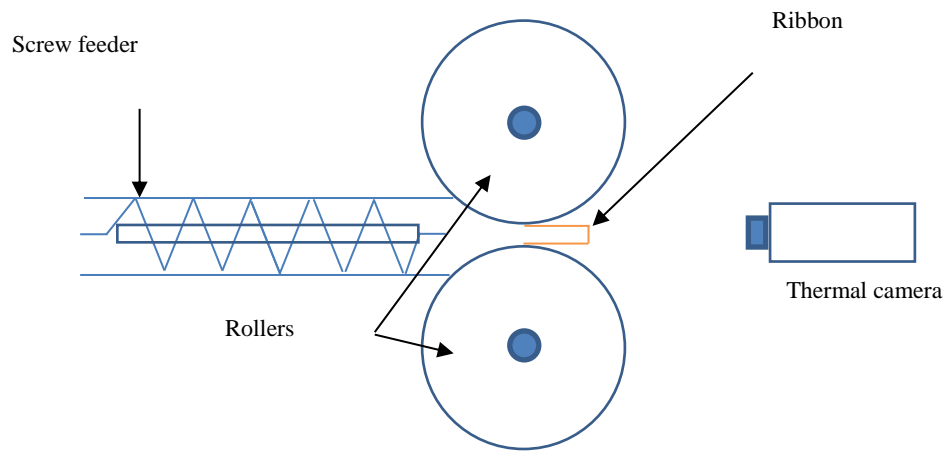


Figure 3-14: Online thermal camera setup

## **Chapter 4 Measuring the mechanical properties of a single primary particle**

### **4.1 Introduction**

Several models have been developed and used to evaluate the compaction behaviour and the mechanical properties of the powder such as yield stress (Heckel, 1961) and as discussed in Section 2.2. All the methods investigate the compaction of the powder as a bed rather than single particle. The powder bed contains thousands or even millions of single particles. During the compaction, the particles will expose to a different local stress depends on its location in the bed. For example, how close the particle is to the position of applying the load. For this reason, at any moment of the compaction process, different particles may exhibit different behaviours such as rearrangement, elastic and plastic deformation in addition to the fracture. This overlapping between different responses makes it difficult to distinguish which response caused the volume reduction of the powder bed. There is a need for more reliable method to determine the mechanical properties of the powder.

The main aim of this study is to evaluate the plastic deformation of the materials by measuring the nano- indentation hardness of the primary single particle for eight different materials and then correlates the hardness with the properties of the ribbon and granules.

#### **4.1.1 Particle size distribution of the primary powder**

Different materials were used to investigate the effect of the hardness of primary single particle; Polyvinyl alcohol (PVA), Starch 1500, Avicel PH-101, Glucidex<sup>®</sup>6, Tylpor 604, Pharmatose 200M, sodium carbonate and calcium carbonate. These materials have been chosen due to the expected wide range of the mechanical properties.

The particle size distributions of the sieved fractions for different powder between 63-212  $\mu\text{m}$  were measured. Figure 4-1 shows the cumulative particle size distribution, based on volume, for each material. The y-axis is the cumulative volume percent and the x- axis is the particle size class in micrometer.

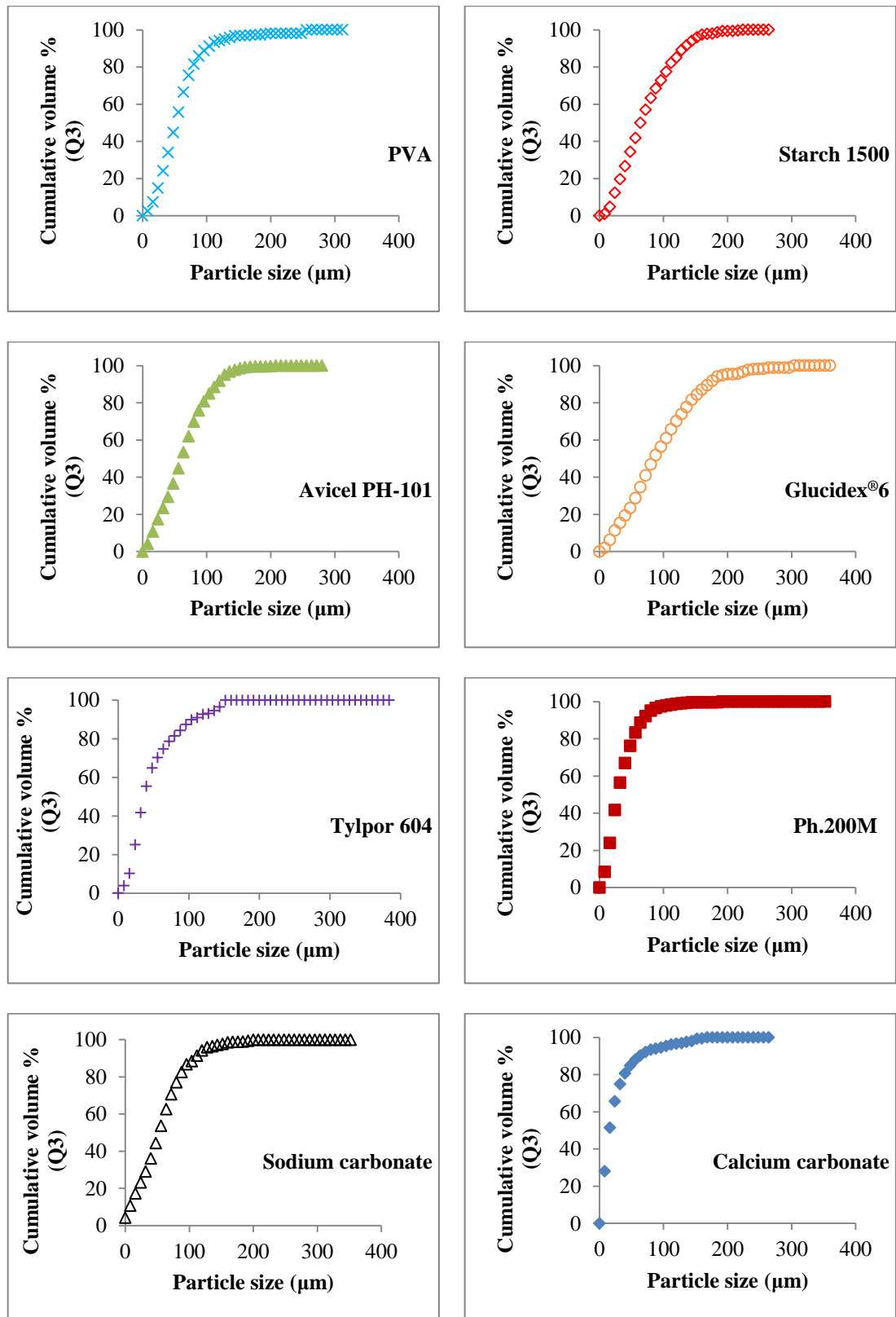


Figure 4-1: Particle size distribution of different powders

Figure 4-2 shows a comparison of the particle size distributions of different types of powder used in this study. It can be seen from Figure 4-2 that calcium carbonate and Pharmatose 200M have the smallest particle size compared to other materials which also mean highest surface area. It can be seen also from the figure that Glucidex®6, Starch 1500 and Avicel PH-



101 have the largest particle size (smaller surface area compared to other materials). This difference in the particle size will be used to support the results in Section 5.3.

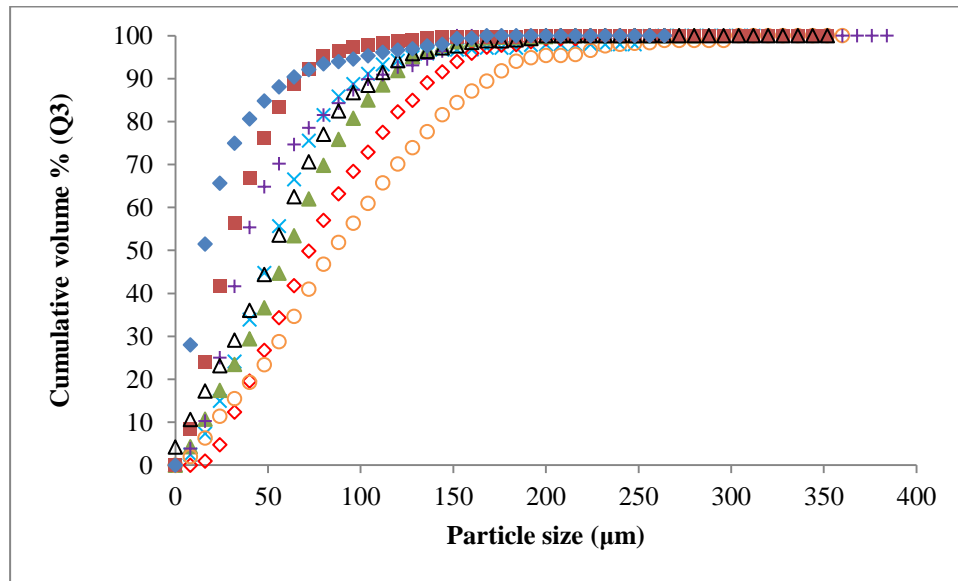


Figure 4-2: Comparison of particle size distribution of all materials

× PVA, ◇ Starch 1500, ▲ Avicel PH-101, ○ Glucidex<sup>®</sup>6, + Tylpor 604, ■ Pharmatose 200M, Δ sodium carbonate, ◆ calcium carbonate

Table 4-1 shows the three size parameters;  $D_{10}$ ,  $D_{50}$  and  $D_{90}$  for all materials. It can be seen from Figure 4-2 and Table 4-1 that calcium carbonate and Pharmatose 200M (Brittle material) have the smallest size parameters while the biggest is for Glucidex<sup>®</sup>6, Starch 1500 and Avicel PH-101 (Deformable materials).

Table 4-1: The main size parameters,  $D_{10}$ ,  $D_{50}$ , and  $D_{90}$  for all powders

Material	$D_{10}$ $\mu\text{m}$	$D_{50}$ $\mu\text{m}$	$D_{90}$ $\mu\text{m}$
Calcium carbonate	4.6	15.3	64.8
Pharmatose 200M	8.77	28	66.7
Tylpor 604	15.8	37	110.4
PVA	19.5	51.5	99.45
Sodium carbonate	15.2	60.7	115.8
Avicel PH-101	15.07	60.87	115
Starch 1500	21.75	64.3	131.7
Glucidex <sup>®</sup> 6	22	85.7	169.7

It can be seen from Figure 3-8 that calcium carbonate particles are agglomerated together due to the small size and it is difficult to distinguish individual single particle. This could be the reason why it did not pass through the sieve of 63  $\mu\text{m}$ . The SEM images for different materials in Section 3.1 confirm the size range of the particle in Figure 4-1 and Table 4-1.

#### 4.1.2 Hardness of the materials

A nano-indenter, Triboscope (TS70) manufactured by Hysitron Inc. (USA), combined with an atomic force microscope, AFM, (Dimension TM 3100, Veeco) was used to indent the particle and ribbon surface using the standard Berkovich tip of a three sided pyramid shape. Berkovich tip is commonly used in the nano indentation test because of the well-defined geometry that makes determining the contact area with the sample as a function of penetration depth more accurate (Fischer-Cripps, 2011). The whole setup is shown in Figure 4-3. The AFM was used to find a good flat surface suitable for the test. Then the load was applied by a tip controlled by transducer. The resolution of the transducer for measuring the load is less than 1 nN and for measuring the displacement is 0.0004 nm (Hysitron, 2013). The shape of the used Berkovich tip is shown in Figure 4-4.

To measure the hardness of a single particle, the particles were spread and glued on a metal sample holder coated with a very thin layer of mixed resin and hardener (Araldite, Bosik Findly Ltd., UK). Some extra particles were removed from the sample under optical microscope.

Prior to the tests, the nano-indenter was calibrated using fused silica which is standard material of known hardness and Young's modulus. The calibration was carried out using load and penetration depth close to that expected to be applied to the samples.

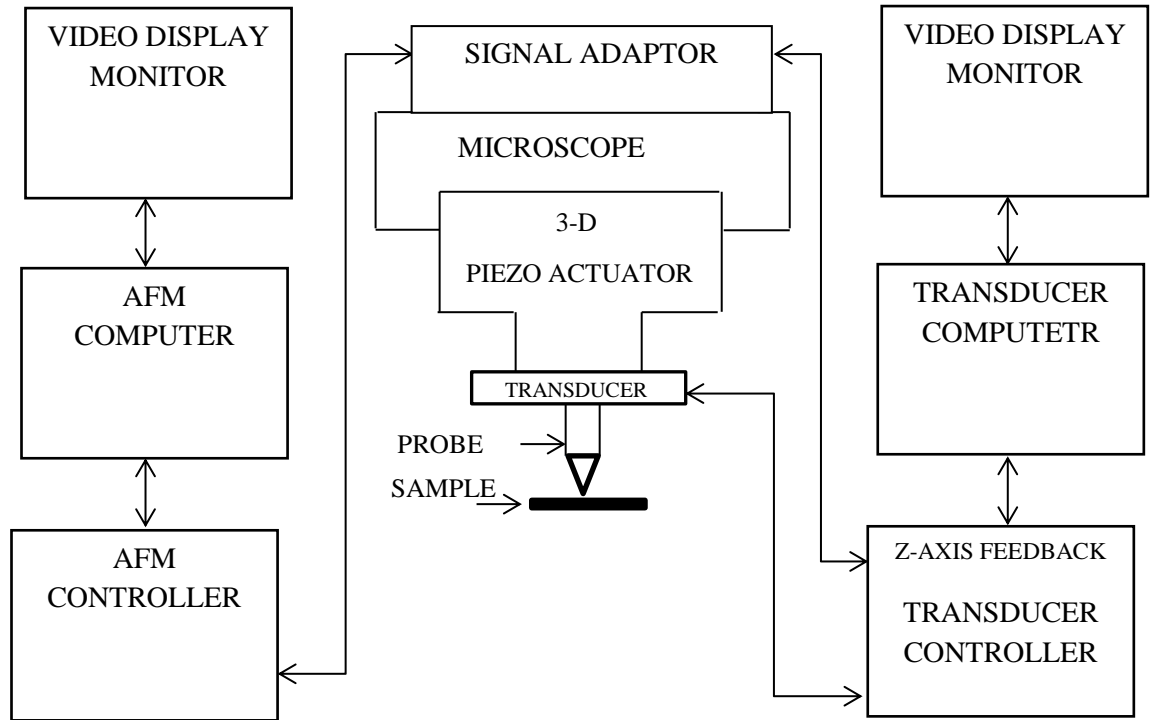
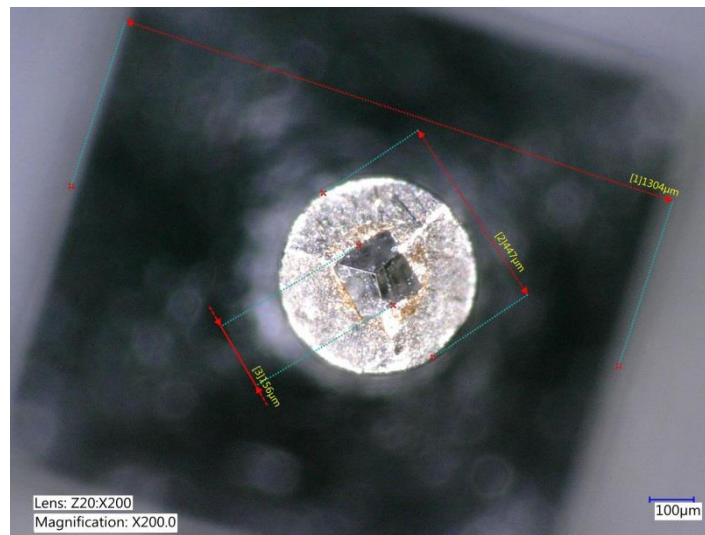
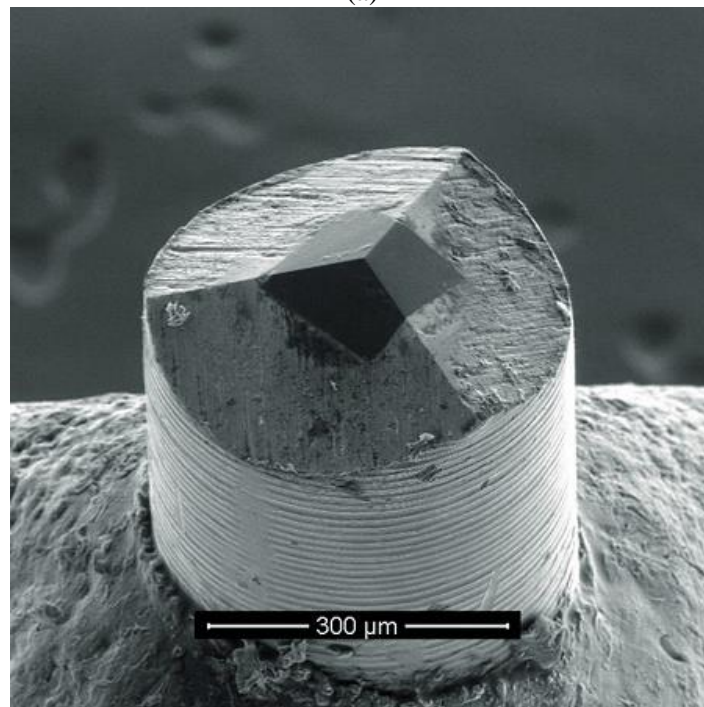


Figure 4-3: Block diagram for the setup used for nano-indentation test of a single particle, (Adapted from Hysitron (2006))



(a)



(b)

Figure 4-4: Three sided pyramid Berkovich indenter of  $142^\circ$  angle (a) Top view of the used indenter (b) 3-D view (Hysitron, 2016)

At least 4 indentation cycles were carried out for each of five particles of each material. That means at least 20 indentation cycles were carried out for each material. The load of  $200 \mu\text{N}$  was applied at a rate of  $40 \mu\text{N}$  per second for five seconds and held for another five seconds, then unloaded for five seconds and as shown in Figure 4-5.

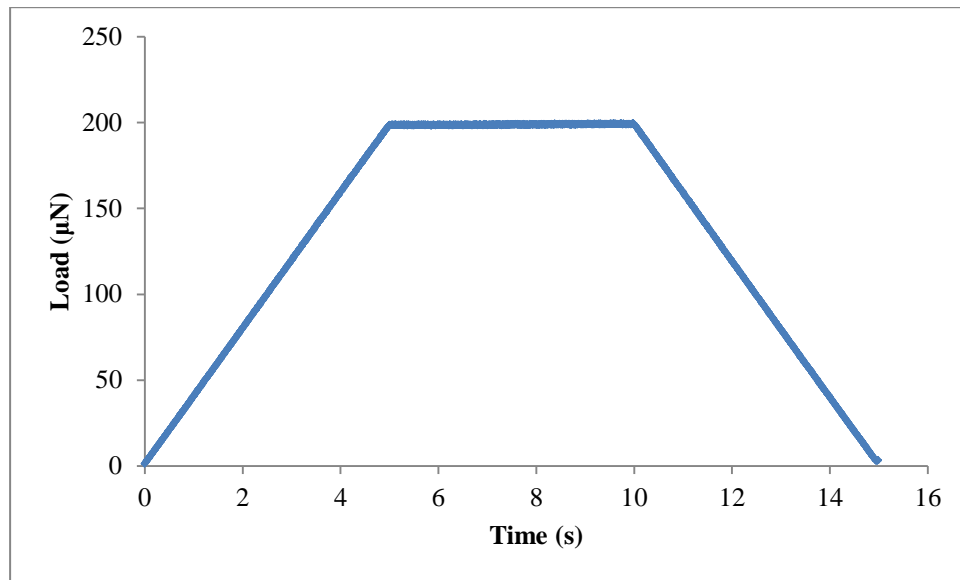


Figure 4-5: Applying, holding and removing the load during nano indentation test versus time

Different loads were initially used to indent the particles of different materials. It was found that 200  $\mu\text{N}$  was suitable load. Low load resulted in inconsistency in the results which could be due to the tip vibration that happens close to the surface which caused a non-solid contact between the tip and the particle surface. This is in agreement with the literature (Taylor et al., 2004). The steady contact is important to obtain an accurate measurement and make the analysis of force-displacement curve easy (Taylor et al., 2004). In addition, most of the commercially available pyramid indenters are not self-symmetrical as it ends with a round cap as shown in Figure 4-6. The area of this round shape is unknown and it might change with the usage. The round shape of the tip head results in error of hardness measurement as the initial contact with the sample will be elastic (Fischer-Cripps, 2011). For this reason, the hardness value will be unstable at low penetration depth then with increasing the penetration depth, it will be constant (Chen et al., 2007). In addition, if the area of the contact between the tip and the sample is small, it will be affected by the tip head roundness. This effect becomes less pronounced as the contact area increased. Berkovich tip is commonly used for small size indentation because it has advantage of the well-defined area function and the three lines of the pyramid meet at a point which resulted in a relatively small round shape (Fischer-Cripps, 2011).

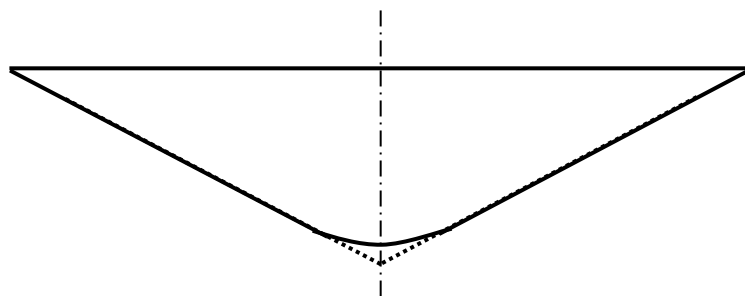


Figure 4-6: The roundness of the Berkovich tip head

The good value of the nano-indentation hardness is the one that does not change with changing the applied force or penetration depth. For this reason the small penetration depth should be avoided (Chen et al., 2007).

Holding the maximum load for a specific time is important because some material exhibit viscoelastic behaviour (slow deformation). This means the material is continuously plastically deformed upon holding the load. An example of this case is shown in Figure 4-7. It can be seen from the figure and specifically in the force holding part that the force has decreased with the holding time. For this reason, the unloading curve looks different than the standard one in Figure 2-1.

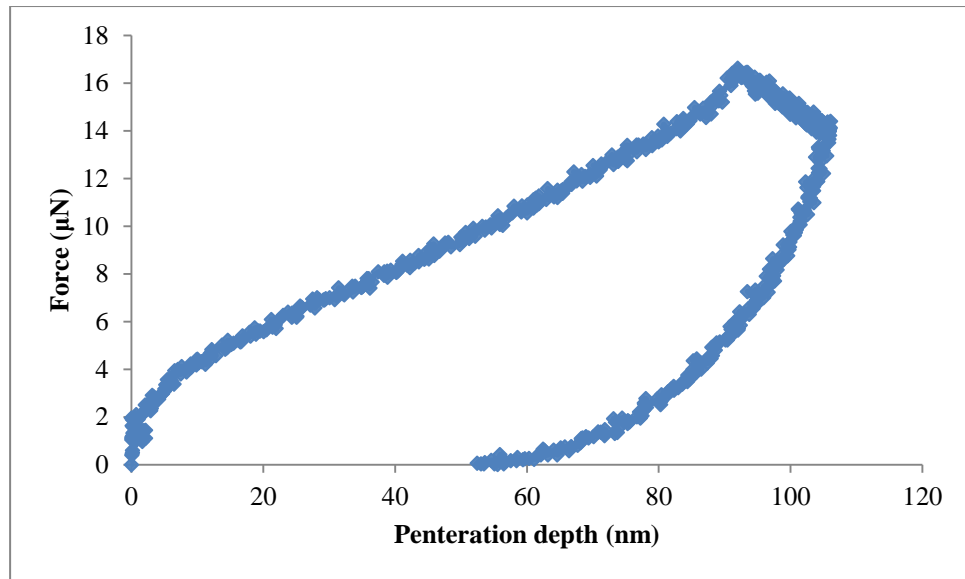


Figure 4-7: An example of nano indentation curve for viscoelastic material

Using high load during the indentation test may cause crack in the sample which results in an incorrect value for the hardness. An example of force- displacement curve with cracks is shown in Figure 4-8. It can be seen from the figure that there is a slip in the loading curve.

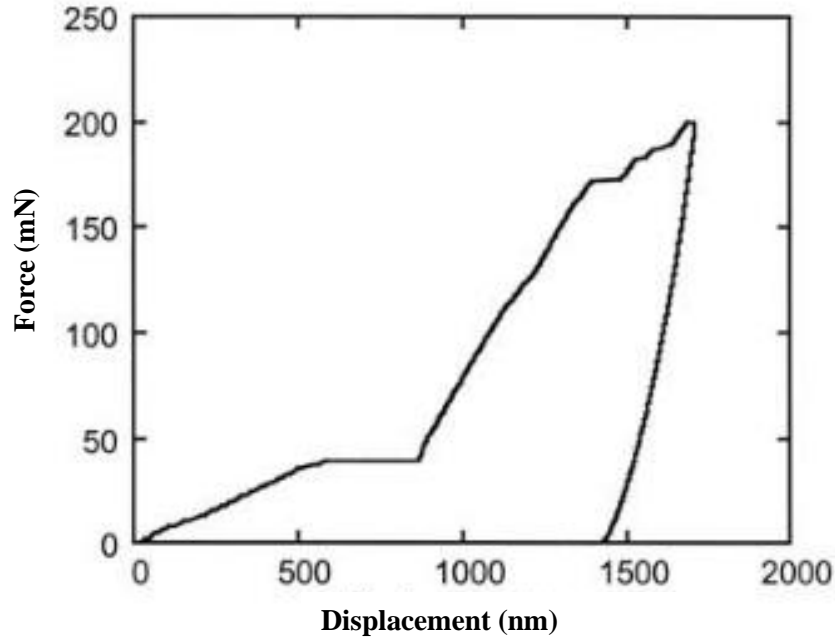


Figure 4-8: Force- displacement curve with fracture (Moody et al., 2003)

The contact area between the tip and the sample was determined using Oliver & Pharr approach (Oliver and Pharr, 2004) which has been explained in more details in Section 2.1.1.2. The hardness was determined using the force displacement data resulted from the nano-indentation test. It is determined by dividing the maximum force by the area of the contact between the tip and the sample at maximum force. The contact area is calculated according to the following equation (Oliver and Pharr, 1992):

$$A(h_c) = C_0 h_c^2 + C_1 h_c + C_2 h_c^{1/2} + C_3 h_c^{1/4} + \dots + C_8 h_c^{1/128} \quad \text{Eq. 4-1}$$

Where

$C_0, C_1 \dots C_8$  are constants

$h_c$  The contact depth between the indenter and the specimen at maximum force (Eq. 2-3)

Figure 4-9 shows the average force displacement data resulted from the nano indentation test for all materials. It can be seen from the curves that the values of the displacement at maximum load and the permanent plastic displacement after removing the load are different for different materials. The highest values are for the PVA whereas the smallest ones are for calcium carbonate. This difference is due to the mechanical properties and specifically the hardness of the material. Large displacement value indicates soft material whereas the small one means hard material. It can be also seen that the force applied to the PVA and starch particles decreased during the period of holding the maximum load. That indicates viscoelastic behaviour of these two materials compared to other materials.

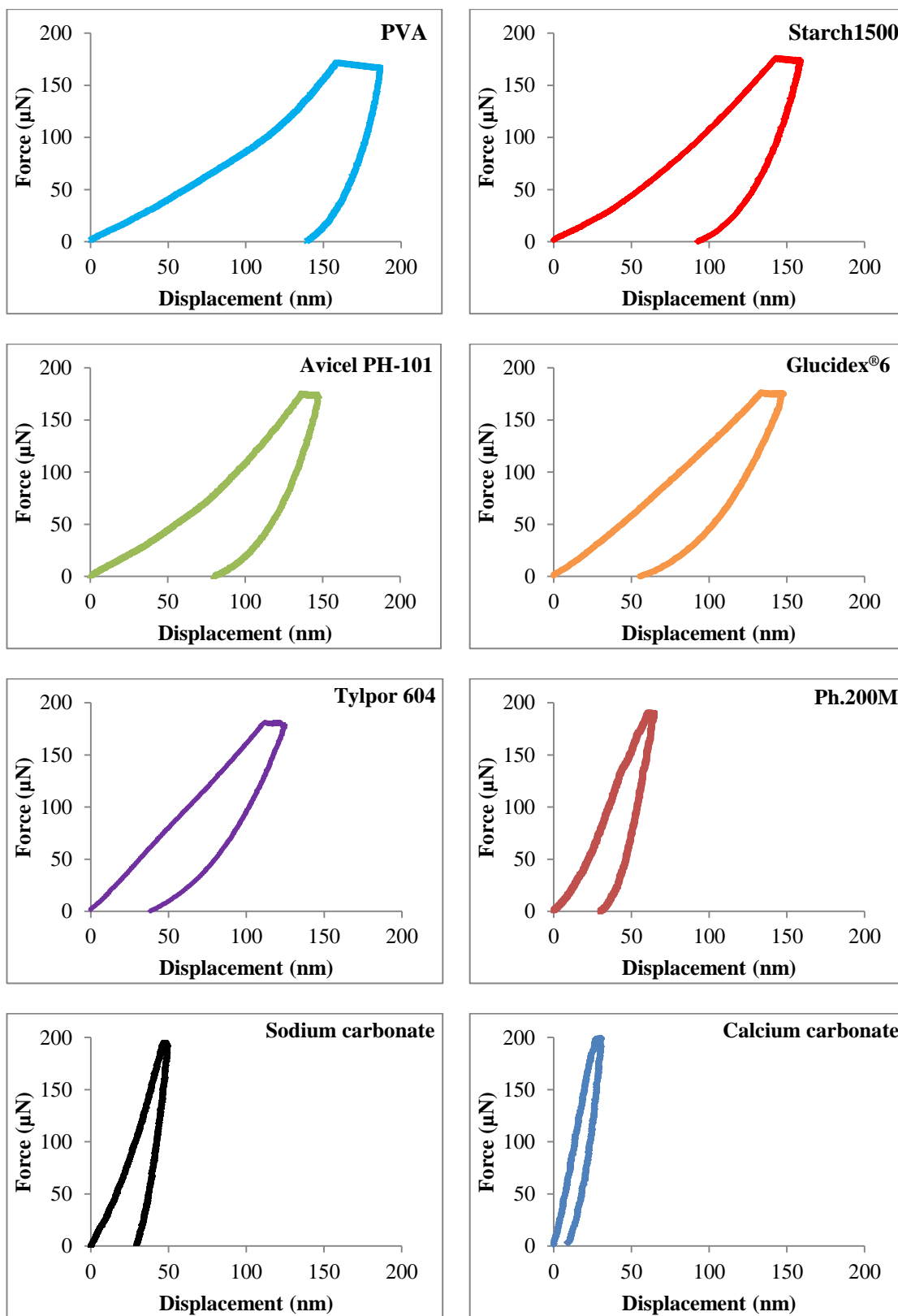


Figure 4-9: Force- displacement curves for different materials



Figure 4-10 shows an AFM image with four indents on a single particle surface of calcium carbonate. The depth is represented by the colour. Darker colour indicates deeper surface. The area of each indent is about  $1 \mu\text{m}^2$ .

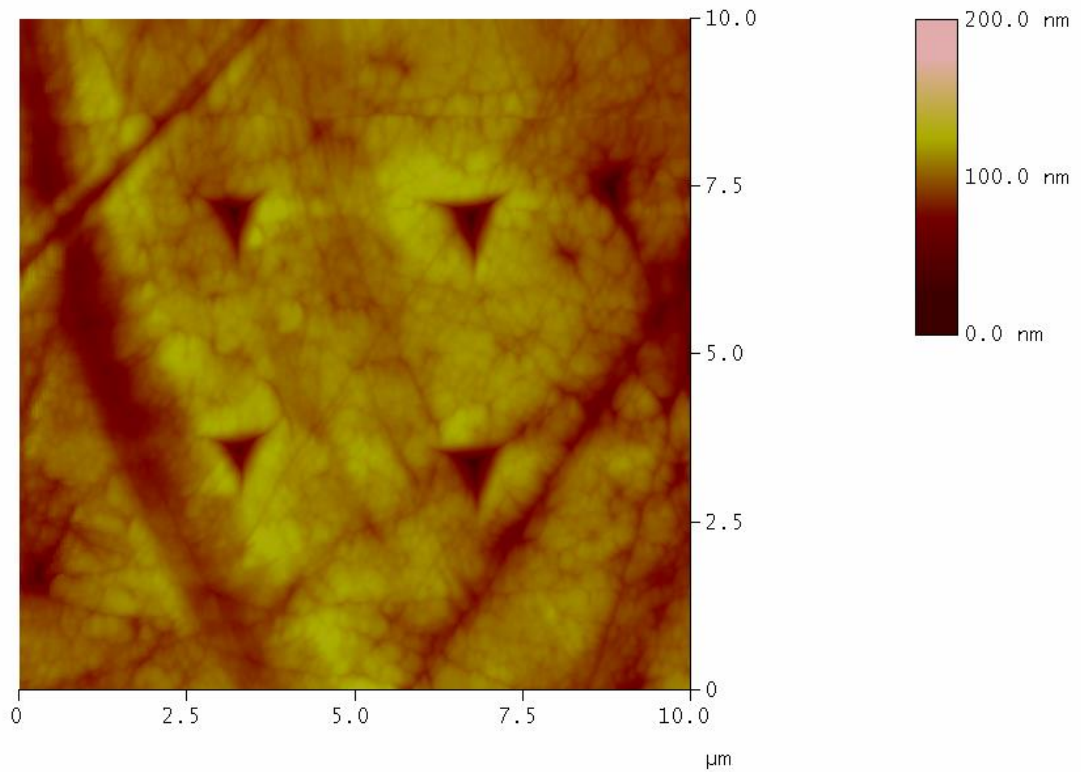


Figure 4-10: AFM image shows 4 indents on calcium carbonate single particle surface

Table 4-2 shows the hardness and reduced Young's modulus for each material determined from the nano-indentation test.

Table 4-2: The nano-indentation hardness and the Young's modulus for the single primary particle of different materials (Eq. 2-1 and Eq. 2-5 respectively)

<b>Material</b>	<b>Nano indentation hardness (GPa)</b>	<b>Reduced Young's Modulus (GPa)</b>
Polyvinyl alcohol (PVA)	0.13±0.05	3.72 ± 0.48
Starch 1500	0.24±0.018	5.48 ± 0.34
Avicel PH-101	0.44±0.09	5.5 ± 1
Glucidex®6	0.58±0.051	5.91 ± 1.3
Tylpor 604	0.7±0.062	6.27 ± 1
Pharmatose 200M	1±0.12	14.21 ± 1.9
Sodium carbonate	1.7±0.15	35.42 ± 2.8
Calcium carbonate	2.55±0.08	45.32 ± 4

It can be seen from Table 4-2 that PVA and starch have the lowest hardness. The hardness of Avicel PH-101, Glucidex®6 and Tylpor 604 are in the middle range from 0.44 to 0.7 GPa. Pharmatose 200M hardness is 1 GPa followed by the sodium carbonate of 1.7 GPa and the hardest material is calcium carbonate with 2.55 GPa. It can be seen from the table that soft material has low Young's modulus and the opposite for the hard material which has large Young's modulus. In another words, for all materials, increasing the hardness are accompanied by increasing the Young's modulus. Low value of Young's modulus indicates high elasticity compared to the high value. The results in Table 4-2 suggest that soft material with low hardness exhibit high elasticity.

In order to investigate whether the hardness value is changing with using different load to indent the particles, different loads were used to indent a single particle of calcium carbonate. Figure 4-11 shows the measured hardness as a function of the applied load. It can be seen from the figure that the hardness value is stable over a wide range of applied load. That indicates a good hardness value which is independent of the load.

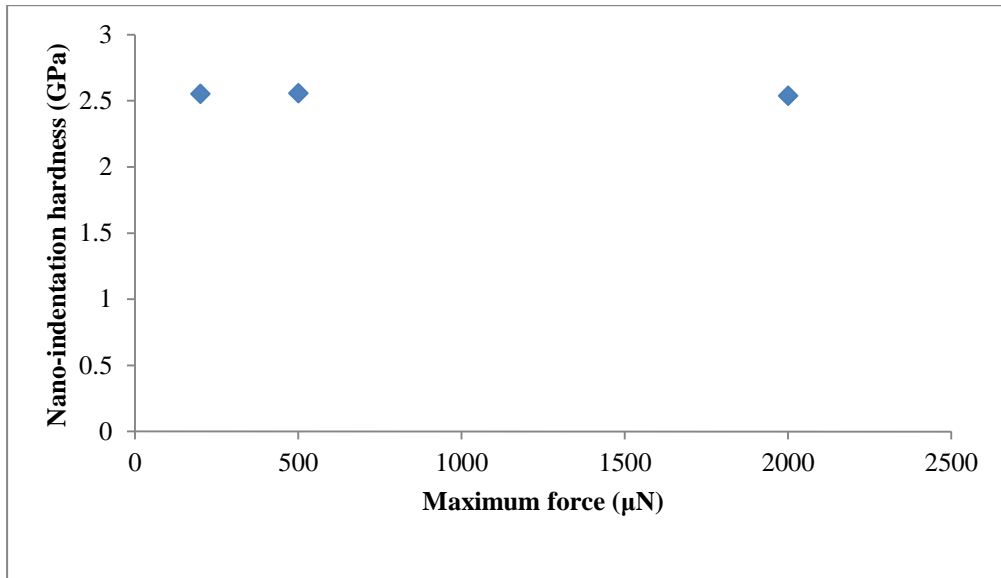


Figure 4-11: Hardness of calcium carbonate particle as a function of maximum force

The mechanical properties of some materials have been measured in different previous studies. The hardness of PVA is measured by Mohsin et al. (2011) and it is equal to 0.13 GPa. The hardness of Avicel PH-101 and corn starch is equal to 0.433 GPa and 0.225 GPa respectively as measured by Govedarica et al. (2012). Broz et al. (2006) measured the hardness of calcite which is a rock consists mainly of calcium carbonate. They found that the hardness is equal to 2.21 GPa. It can be seen from these values that the results listed in Table 4-2 are in a good agreement with literatures. It is worth to mention that all mentioned literatures used nano indenter to measure the hardness and not AFM. There is a significant uncertainty of hardness measured by AFM due to the bending of the cantilever which lead to the slip of the tip and consequently wrong penetration depth measurement and as shown in Figure 4-12 (Lee et al., 2013). For this reason, the results in the literatures that used AFM will not be considered for comparison purposes.

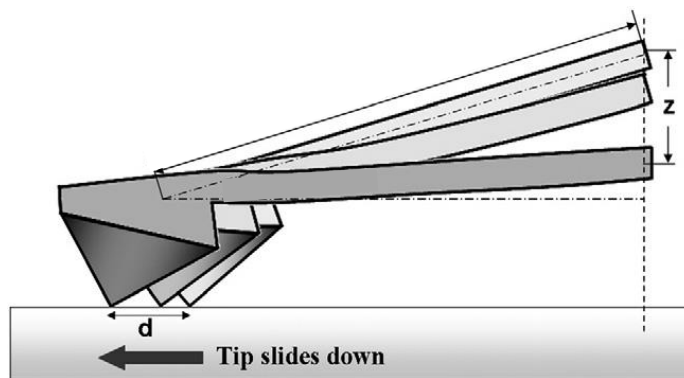


Figure 4-12: Tip slide during the measurement of the hardness by AFM (Lee et al., 2013)

The work applied to the material during the indentation test is consumed into two types; work of elastic which is the amount of work consumed to cause elastic deformation of the material

and work of plastic which is the amount of work that caused plastic deformation. The total work can be determined by following equation:

$$\text{Work}_{\text{total}} = \text{Work}_{\text{elastic}} + \text{Work}_{\text{plastic}} \quad \text{Eq. 4-2}$$

Figure 4-13 shows a force-displacement curve indicating the work of elastic as the area under the unloading curve. The work of plastic is the area between loading and unloading curves which represents the amount of work needed to cause plastic deformation.

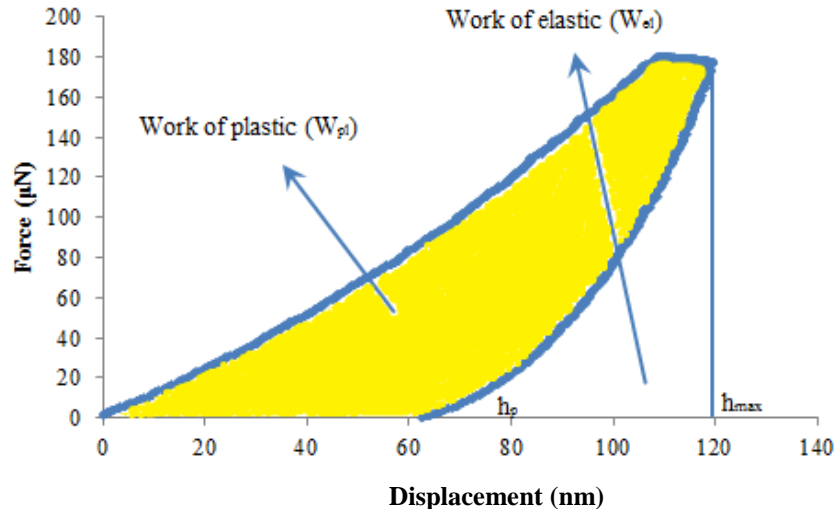


Figure 4-13: A diagram showing the areas under the curve for plastic and elastic regions

Work of plastic can be determined by calculating the area under the curve and according to the following equation:

$$W_{\text{plastic}} = \int_0^{h_p} F dh \quad \text{Eq. 4-3}$$

Where  $h_p$  is the permanent displacement of the sample after removing the load in nm

F is the force in  $\mu\text{N}$

Work of elastic can be calculated according to the following equation:

$$W_{\text{elastic}} = \int_{h_p}^{h_{\text{max}}} F dh \quad \text{Eq. 4-4}$$

Where  $h_{\text{max}}$  is the displacement at maximum load. Table 4-3 shows the determined work of plastic for all eight materials. The area under the curve was determined using trapezium rule which consisting of dividing the area under the curve into small trapeziums. Total area is equal to the summation of all trapeziums.

Table 4-3: Work of plastic in nano joule for different materials calculated using nano-indentation fore displacement data

<b>Materials</b>	<b>Reduced Young's Modulus (GPa)</b>	<b>Hardness (GPa)</b>	<b><math>W_{pl}</math> (<math>10^{-6}</math> nJ)</b>
Polyvinyl alcohol (PVA)	5.5	0.13	12929
Starch 1500	5.48	0.24	9954
Avicel PH-101	6.27	0.44	8439
Glucidex <sup>®</sup> 6	5.91	0.58	7189
Tylpor 604	3.72	0.7	6185
Pharmatose 200M	14.21	1	3552
Sodium carbonate	35.42	1.7	3346
Calcium carbonate	45.32	2.55	2233

By comparing the values of the nano indentation hardness with the work of plastic in Table 4-3, it can be noticed that the plastically deformable materials of low hardness showing more work of plastic and the opposite for hard materials. The results showed that plastically deformable materials consume more energy compared to the less deformable materials.

It can be seen from Table 4-3 that there is a big difference between the work of plastic of Tylpor 604 and Pharmatose 200M. The difference is from 6185 to 3552  $\times 10^{-6}$  nJ. This big difference may indicate different mechanical behaviours of the materials. According to this characterization, PVA, Starch 1500, Avicel PH-101, Glucidex<sup>®</sup>6 and Tylpor 604 are plastically deformable materials compared to Pharmatose 200M which could be considered as partially plastically deformable material. Sodium carbonate behaviour is the same as that of Pharmatose 200M but with less plastic deformation. There is a significant difference between the work of plastic of calcium carbonate compared to other materials. For this reason, this material is hard.

It can be seen that the order of the material plasticity, represented by the hardness, is in a good agreement with work of plastic. That is mean both values could be used as an indication of the plasticity of the materials. Using the work of compression and decompression of the bulk compaction process as an indication of the plasticity of the material was successfully reported by Aburub et al. (2007) and Buckner et al. (2010). They stated that it is valid for medium pressure range as high pressure could cause breakage of the particles and the energy required for breakage could not be separated from that required for the plastic deformation.

Figure 4-14 shows the relationship between the work of plastic and the nano indentation hardness of the materials. The figure confirms the agreement in the order between the two terms for different materials.

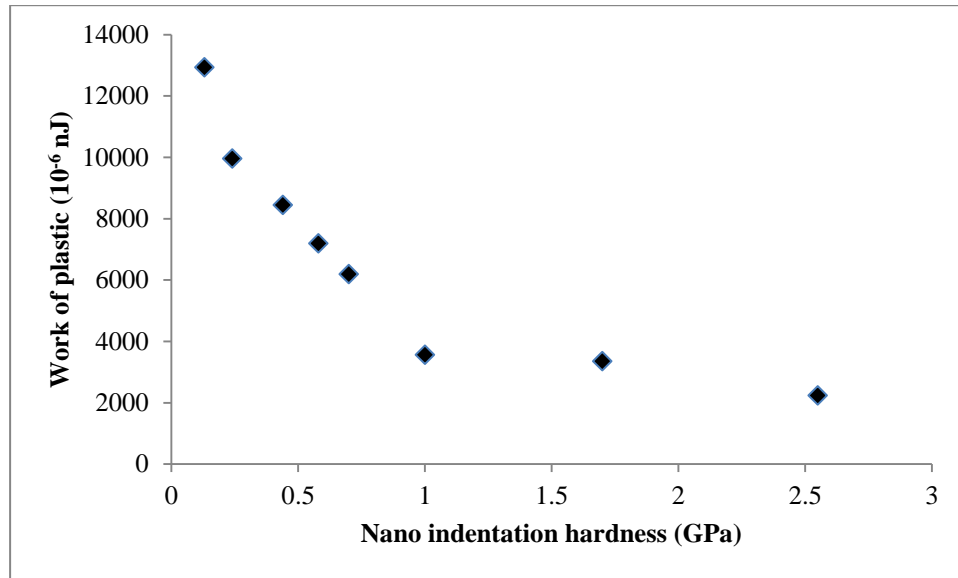


Figure 4-14: The relation between the work of plastic and Nano indentation hardness for different materials

### 4.1.3 Investigating the fracture behaviour of the primary powder

A material testing machine (Zwick Roell, Germany) was used to qualitatively investigate the behaviour of the single particle under compaction and as illustrated in the setup shown in Figure 4-15.

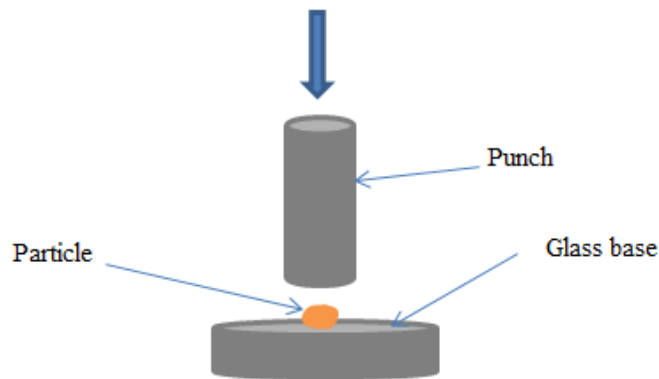


Figure 4-15: Single particle compression set up

Particles with size around  $200\ \mu\text{m}$  were chosen to do the test because of ease of handling. At least five particles of each material were tested. A punch of 10 mm in diameter was used to push the particle against a smooth glass base at speed of 0.01 mm/min. The force displacement data resulted from the test of different materials are presented in Figure 4-16. It can be seen from the figure that there is a continuous increase in the force as the punch moved down for the curves of PVA, Starch, Avicel PH-101, Glucidex and Tylpor. The case is different for the curves of the other three materials; Pharmatose 200M, sodium carbonate and calcium carbonate. For these three materials, it can be noticed that there is a fluctuation in the

measured force as the punch moves down. This is believed to be due to the fracture that happened during the compaction of the particle. The particles fracture caused a non-full solid contact between the punch and the particle which caused reduction in the recorded force.

These results are in agreement with the results of material characterisation based on the nano indentation hardness and work of plastic in Table 4-3. This confirms that using the data resulted from nano-indentation test is good method to characterise the mechanical behaviour of the material.

For the three non- plastically deformable materials in Figure 4-16, it can be noticed that the maximum force for Pharmatose 200M was around 0.8 N whereas it is 0.045 and 1.6 N for sodium carbonate and calcium carbonate respectively. If the particle size of the three materials assumed to be the same, one can conclude that the force required to break the particle of calcium carbonate is the highest among other materials, which means it is hard material, followed by Pharmatose 200M and the most brittle particle is the particle of sodium carbonate.

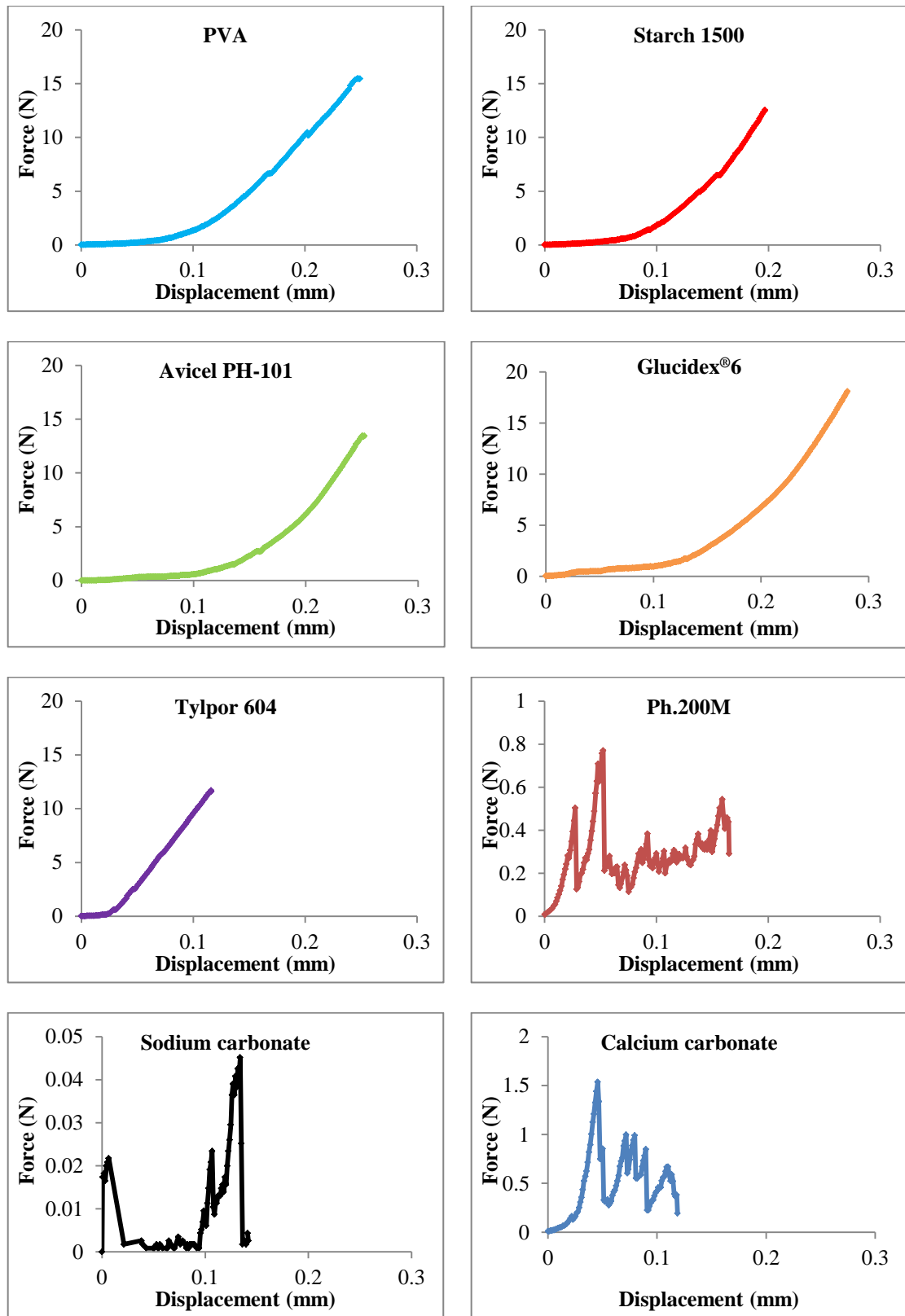


Figure 4-16: Force displacement curve resulted from the single particle test



#### **4.1.4 Yield stress of the material**

The yield stress of three powders, Avicel PH-101, Pharmatose 200M and calcium carbonate were determined using the force displacement data resulted from the nano indentation experiment as described in Section 2.1.2. Within the elastic limit, the force displacement data can be described by Eq. 2-7. The elastic limits were determined by plotting  $F^2$  versus  $h^3$  of the loading curve of the force displacement data resulted from the nano-indentation test and as shown in Figure 4-17. The point that deviates from the linear gradient by two percent is the end point of the elastic region.

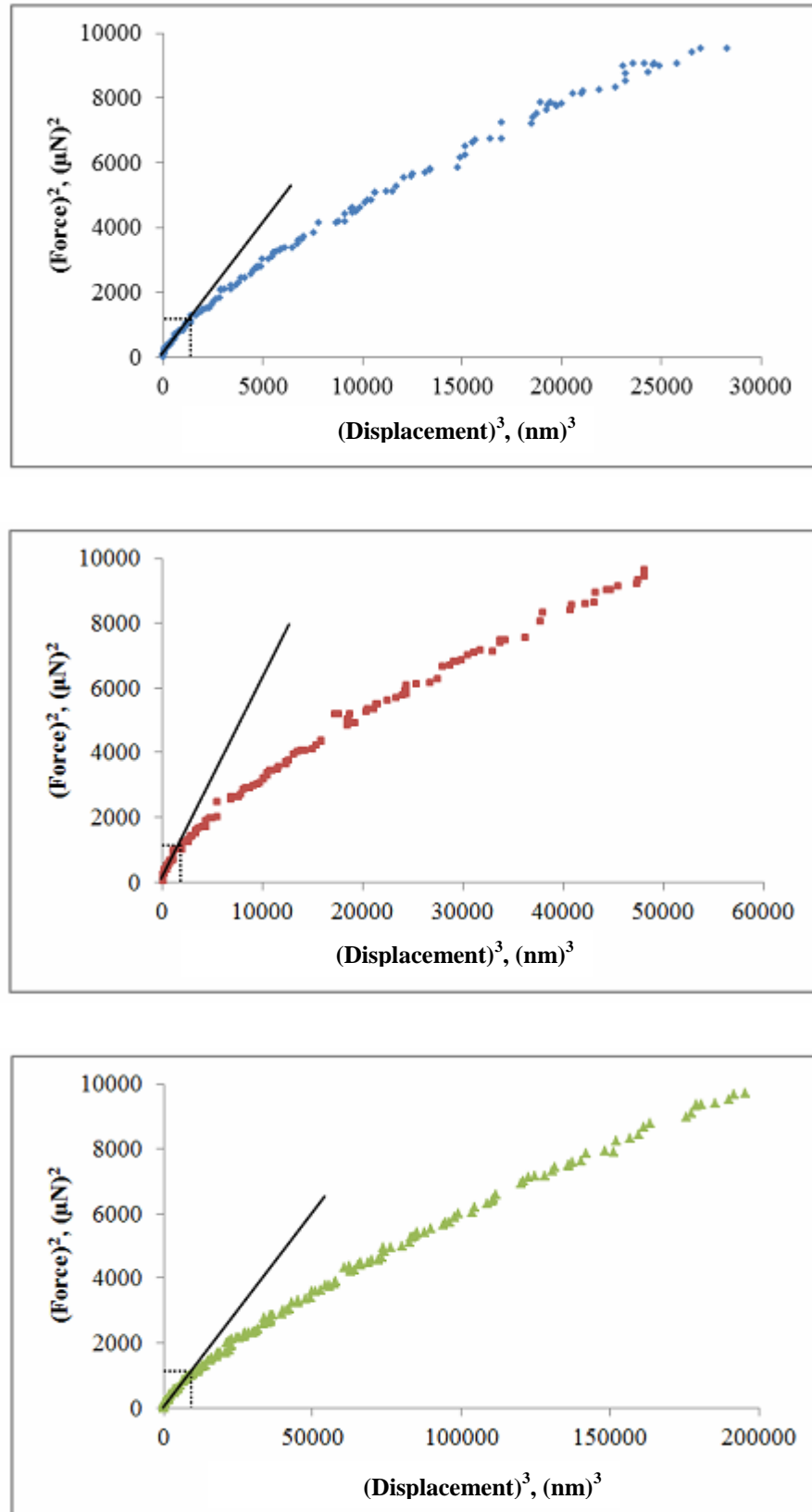


Figure 4-17: The linearized form of the Hertz equation to find the elastic penetration limit

(◆ Calcium carbonate, ■ Pharmatose 200M, ▲ Avicel PH-101)

For the stress larger than the elastic limit, the particle deforms plastically and the force displacement data will be linear and can be described by Eq. 2-8 as shown in Figure 4-18.

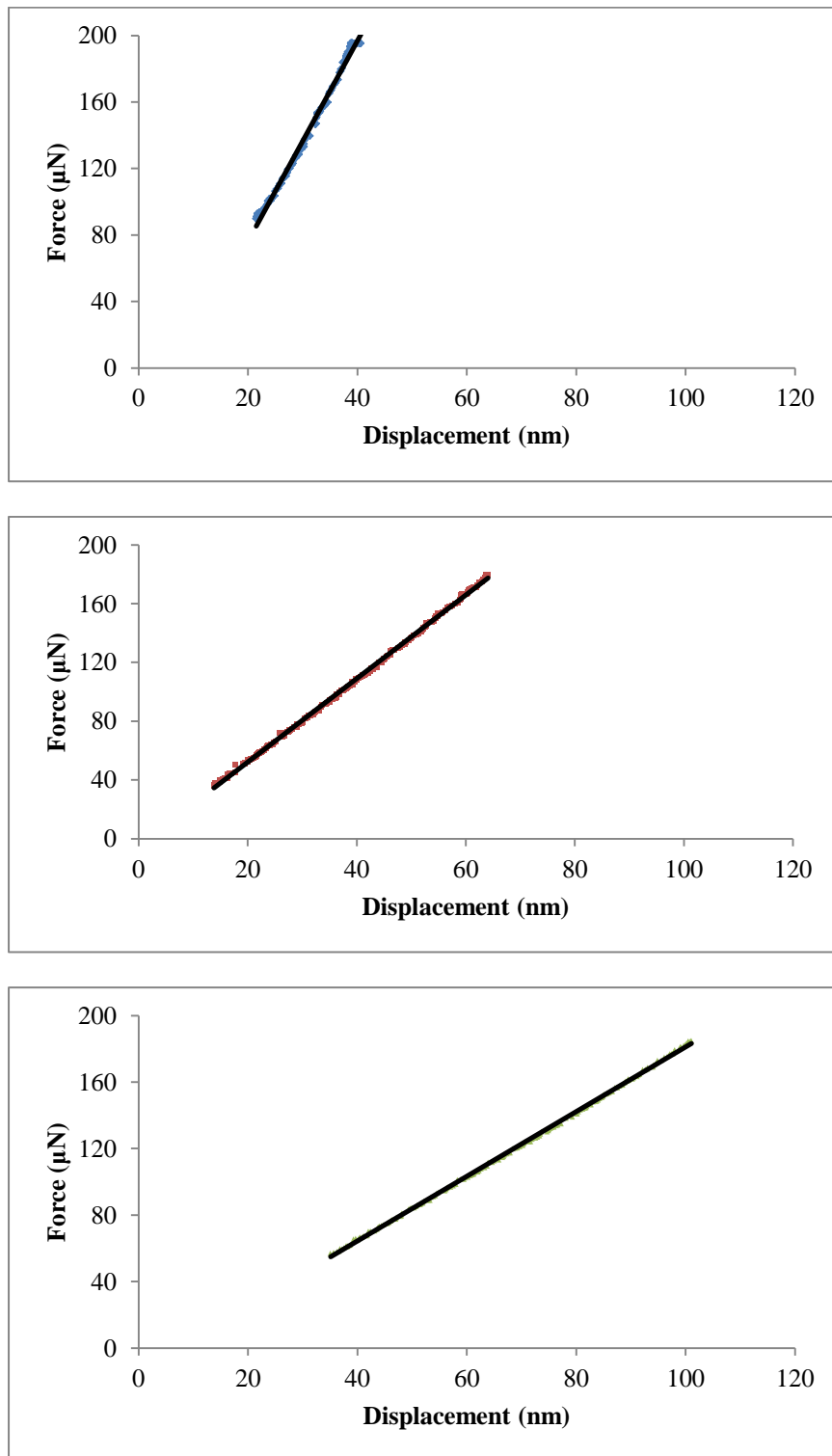


Figure 4-18: The plastic region of force displacement curve that fits Eq. 2-8

(◆ Calcium carbonate, ■ Pharmatose 200M, ▲ Avicel PH-101)

Table 4-4 shows the results of determined yield stress for three different materials.

Table 4-4: Yield stress of three materials

<b>Material</b>	<b>Yield stress (GPa)</b>
Calcium carbonate	0.62
Pharmatose 200M	0.168
Avicel PH-101	0.007

It can be seen from Table 4-4 that the yield stress of Avicel PH-101 is the smallest among the other two materials followed by the Pharmatose 200M and the highest yield stress is for calcium carbonate. The trend of these results is in agreement with the trend of the nano-indentation hardness of the materials as both are an indication of the plastic deformation of the material.

Khomane and Bansal (2013) suggested an experimental method to determine the yield stress of the microcrystalline cellulose by correlating the conductivity with the compaction pressure. They determined the yield stress to be 0.01685 GPa.

## 4.2 Conclusion

In this chapter, the nano indentation hardness and Young's modulus were successfully determined for different materials. The results showed that the used materials have a wide range of mechanical properties.

The concept of work of elastic and work of plastic were used to get more information about the mechanical behaviour of the material. Specifically to determine the material that is showing brittle/plastic behaviour such as lactose. The results of characterising the mechanical behaviour of a single particle, by compression test, are in a good agreement with the characterisation that determined by work of elastic and plastic.

In this chapter the mechanical properties have been characterised for different types of materials. In the next chapter, the effect of different mechanical properties on the product quality and roller compaction process will be investigated.

## **Chapter 5 Mechanical properties of the single primary particle and roller compaction process**

### **5.1 Introduction**

During roller compaction process, the powder exhibit different behaviours as it moves between the two rotating rollers towards the minimum gap. At low stress in the feeding zone, the particles rearrange themselves. As the powder moves forwards, the stress increase and the particles deform or/ and fracture. Understanding the mechanism of the compaction process is useful as it helps choosing the right formula to achieve the required products quality. This can reduce the need for the trial and error experimentations which is recently being practiced in roller compactor industry (Kleinebudde, 2004).

In the roller compactor, different studies showed that different powders produced ribbons and consequently granules with different quality. The study in this chapter aims to investigate whether this difference in the ability of the material to be compacted or agglomerated is correlated to the mechanical properties of a single primary particle, namely nano-indentation hardness, which have been measured for eight different materials (Chapter 4). Using the mechanical properties of a single particle to predict ribbon properties, such as ribbon strength, width, surface temperature or temperature profile along the width of the ribbon in addition to the amount of fines, is important because it requires only a few particles. This is especially important when the material is expensive or not available in large quantities which is generally the case in the pharmaceutical industry (Perkins et al., 2007).

### **5.2 Ribbon production**

Eight different materials that mentioned in Section 4.1.1 were used as primary powder to investigate the effect of the particle hardness during roller compaction process. These materials have been chosen deliberately to cover wide range of mechanical properties. The materials also cover different categories of material; synthetic and natural polymers, crystalline and amorphous. These materials are used in different industries such as pharmaceutical, food, detergent and ceramic. The Particle size distributions of different materials are shown in Figures 4-1. The powder of different materials were sieved and conditioned as described in Section 3.1.9.

Different hydraulic pressures were used to produce ribbons of different materials. Table 5-1 shows the experimental design used in this study. It can be seen from the table that the hydraulic pressure was varied but the roller gap and roller speed were kept constant. It is worth to mention that the automatic feedback system that keeps the roller gap constant was switched on for all experiments.

Table 5-1: Experimental design of roller compaction experiments

Hydraulic pressure (bar)	Roller gap (mm)	Roller speed (rpm)
18, 30, 70, 100, 150, 200 and 230	fixed at 3	fixed at 3

At some process parameters, the ribbons of some materials were not suitable for analysing. The ribbons produced by sodium carbonate and calcium carbonate at hydraulic pressures of 18 and 30 bar were extremely weak and difficult to handle. The ribbons produced by Pharmatose 200M at 150, 200 and 230 bar were not suitable for analysis since they split into two longitudinal parts and as shown in Figure 5-1. This could be due to the partial plasticity of Pharmatose 200M which means that the materials in the inside layers of the ribbon need to recover after removing the stress, whereas the materials on the surface were plastically deformed. This failure or defect could be due to the capping which is known in manufacturing of tablets or due to the lamination (Sonnergaard, 2006, Prigge and Sommer, 2011).

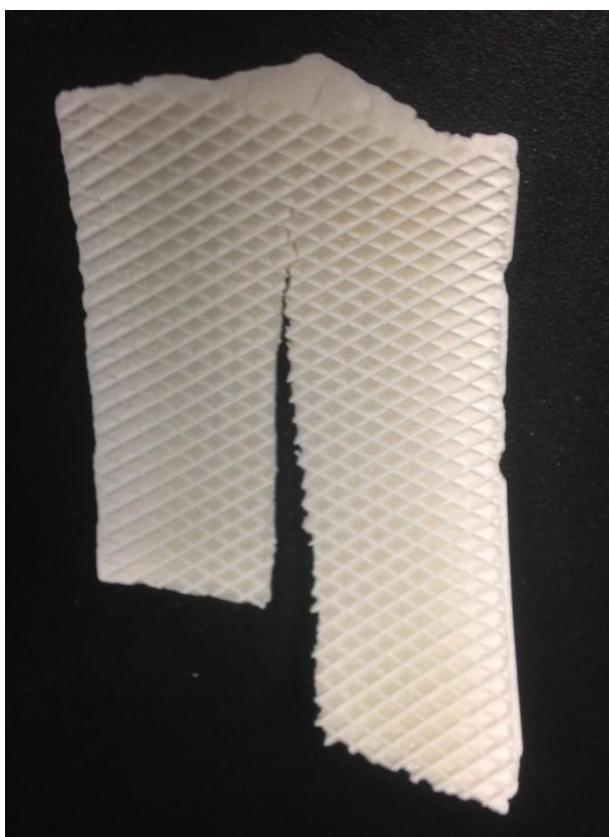


Figure 5-1: Split ribbon of Ph.200M produced at hydraulic pressure of 150 and 200 bar

At high pressures of 200 and 230 bar, there was a problem in the feeding of Glucidex<sup>®</sup>6. The screw feeder struggled to rotate and pushed the powder towards the rollers area. This is believed due to the high applied pressure which increased the temperature and caused melting of the powder as shown in Figure 5-2. Maltodextrin is amorphous material with glass transition temperature between 40- 140 °C depends on the water content (Palzer, 2009).



Figure 5-2: Image shows melting of Glucidex®6 between the two rollers

## 5.3 Results and discussion

### 5.3.1 Single particle hardness and ribbon strength

Ribbon strength is a measure of the strength of bonding between the particles. It can be used to indicate the compaction performance of the powder undergoing roller compaction.

The strength of the ribbons produced at different hydraulic pressures was measured as described in Section 3.4.1. Figure 5-3 shows the strength of the ribbon produced at different hydraulic pressures (Roll forces) using different materials which are represented by their hardness. The x-axis is the nano-indentation hardness of the single primary particle in GPa and the y-axis is the ribbon strength in MPa. At low hydraulic pressures of 18 and 30 bar, almost three categories of ribbon strength can be distinguished; the first category is weak ribbons produced by plastically deformable material with low hardness such as PVA and starch of hardness range between 0.13-0.24 GPa. These two materials exhibit viscoelastic behaviour as mentioned in Section 4.1.2 and it is investigated in more details in separate section of this chapter. The second category is strong and good compacted ribbons produced by plastically deformable materials with medium hardness range between 0.44- 0.7 GPa. These materials are Avicel PH-101, Glucidex®6 and Tylpor 604. The third category is medium ribbon strength produced by partially deformable Pharmatose 200M. At these two hydraulic pressures, there were no ribbons produced by the hard materials such as sodium carbonate and calcium carbonate of hardness equal to 1.7 and 2.55 GPa respectively. The product was small flakes with a large percentage of un-granulated powder (fines). At higher hydraulic pressures, almost the same categories can be identified except that there is an improvement in the ribbon strength of PVA and starch especially at high pressure. In addition, sodium carbonate and calcium carbonate produced ribbons but the ribbons are weak even at high hydraulic pressures of 200 and 230 bar.

For all materials with the hardness range of 0.44 (Avicel PH-101) to 2.44 GPa (Calcium carbonate) in Figure 5-3, and for all hydraulic pressures, the ribbons produced from low hardness powder (within the mentioned range) has higher strength and the opposite for the ribbons produced with high hardness powder which produced weak ribbons. Low hardness means that the material is deformable and under compaction even with low hydraulic pressure it will deform and produce strong ribbon. As the hardness of the material increase, the pressure will be not enough to cause enough plastic deformation to bond the particles together so the ribbon produced were weak.

Although the particle size of brittle material, Pharmatose 200M and calcium carbonate are smaller (higher surface area) compared to the size of the deformable materials, Avicel PH-101, Glucdex<sup>®</sup>6 and starch 1500 and as shown in Figure 4-2 and in Table 4-1, the brittle materials produced weak ribbon compared to the deformable materials. That supports our hypothesis of the relation between the strength of the ribbon and the plastic deformation of the material. In other words, the effect of plastic deformation of the primary powder on the ribbon strength is more important than the effect of the particle size and the surface area.

According to Rumpf (1958) and Celik (2011), the main compaction bonding mechanisms are solid bridges, attraction between solid particles and mechanical interlocking. All these three mechanism required a contact area between the particles. The plastic deformation caused a permanent increase in the contact area between the particles which will improve the bonding (Rubinstein, 1988). In addition the plastic deformation of the powder that happening during the roller compaction of the powder may help the plastic flow and create solid bridge between the particles.

The results of ribbon strength of different materials in Figure 5-3 are in agreement with previous studies (Inghelbrecht and Paul Remon, 1998, Bultmann, 2002, He et al., 2007, Yu et al., 2012) which confirmed that the ribbon produced by MCC are strong with regular shape and this is due to the high plasticity of this material (Thoorens et al., 2014) which caused an increase in the contact area. Skinner et al. (1999) showed that hydroxypropyl methylcellulose can be used as a binder in roller compaction process and that indicates good compactibility. Soh et al. (2008) showed that the lactose produced weak ribbon compared to MCC. Chang et al. (2008) stated that adding starch to the feed mixture reduce the ribbon strength. In addition, starch produce weak tablet at low hydraulic pressure but the tablet strength improves as the pressure increases and this is due to the slow plastic deformation of starch (Bolhuis and Chowhan, 1996). Calcium carbonate needs a binder to produce acceptable ribbon and granule quality (Bacher et al., 2007) and this is an indication of poor compatibility of this material.

Although the fragmentation is another accepted mechanism or behaviour for the powder undergoing roller compaction, the results from this study suggests that the fracture brings the particles close to each other but does not help the bonding too much. In another words, the plastic deformation is more important than the fracture. This is clear especially with sodium carbonate which is extremely brittle material as shown in Section 4.1.3. Despite the significant fracture, the ribbon was too weak and this is because the hardness of this material is high. A study conducted by Bolhuis and Chowhan (1996) support our results. They stated that the fragmentation is responsible for the consolidation of the lactose powder whereas the amorphous part of the lactose is responsible for the bonding (Inghelbrecht and Paul Remon, 1998). It is well known that in food and pharmaceutical industry, the amorphous material is more deformable than the crystalline (Palzer, 2010, Palzer, 2011, Osborne et al., 2013).



Among all other materials, only PVA and starch behaved in an unexpected way at low hydraulic pressures. The nano indentation hardness of these two materials is the lowest among other materials. They are supposed to deform plastically at even low hydraulic pressures and produce good ribbons. The behaviour of these two materials was investigated in Section 5.3.5.

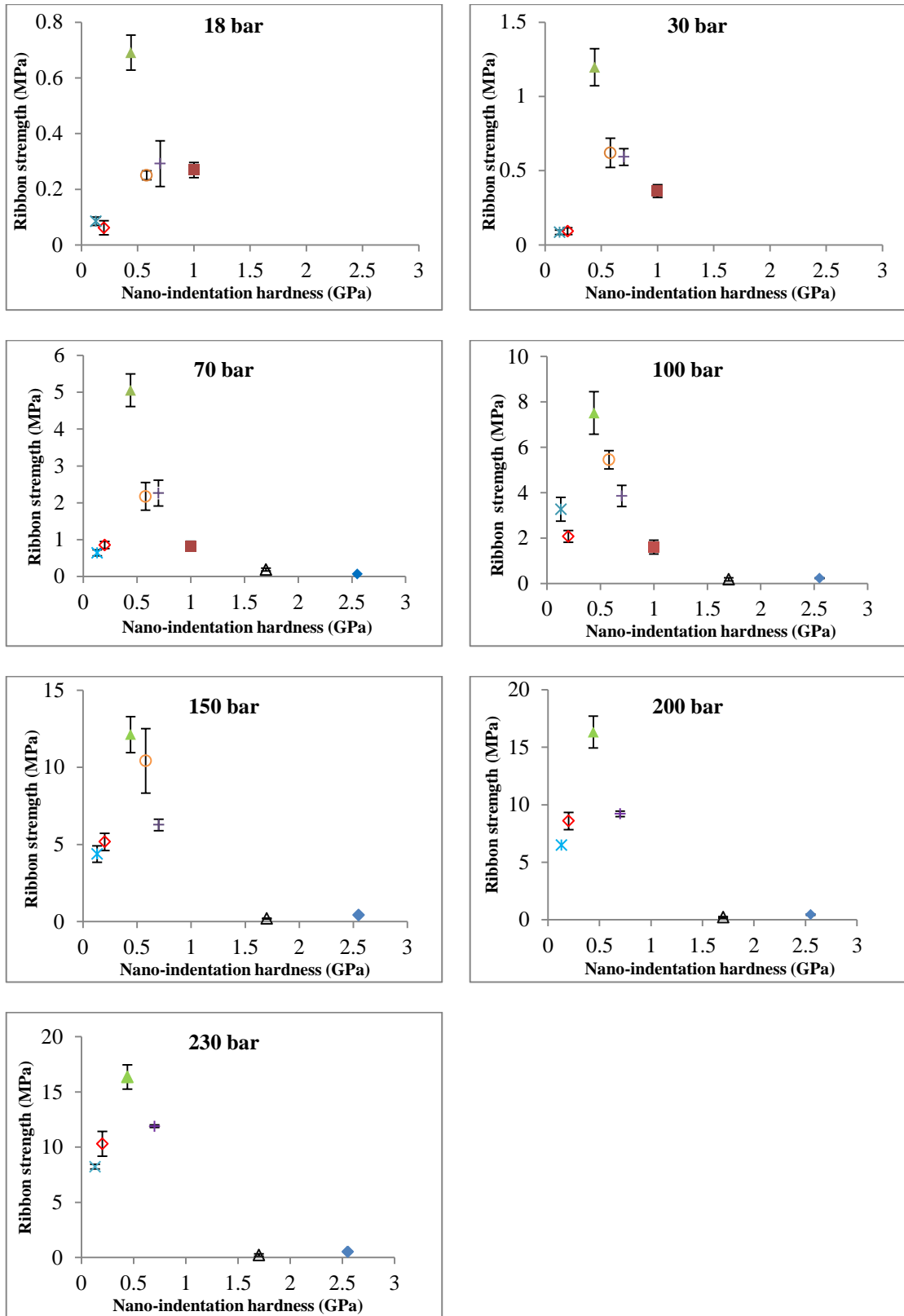


Figure 5-3: Ribbon strength for different materials at different hydraulic pressures

× PVA, ◇ Starch 1500, ▲ Avicel PH-101, ○ Glucidex®6, + Tylpor 604, ■ Pharmatose 200M, △ sodium carbonate, ◆ calcium carbonate

Figure 5-4 shows how the ribbon strength of different materials changes with increasing the hydraulic pressure (Roll force). The lower x-axis is the hydraulic pressure where the upper x-axis is the roll separating force and as supplied by the manufacturer. The roll force is equal to the hydraulic pressure divided by the cross sectional area of the hydraulic cylinders inside the roller compactor machine. For more details see Table 5-8. Hydraulic pressure of 100 bar is equivalent to 41.5 kN roll force and as marked on the figures. It can be seen from the figure that for all materials, increasing the hydraulic pressure caused an increase in the ribbon strength. However, the rate of the increase is different for different materials. It can be seen from the figure that the strength of the plastically deformable materials with low and medium hardness range increased at a higher rate compared to the materials of higher hardness. Avicel PH-101 exhibited the largest rate of increase from 0.69 MPa at 18 bar to 16.35 MPa at 230 bar. The ribbon strength of the partially deformable Lactose (Pharmatose 200M) was increased from 0.27 MPa at 18 bars to 1.6 MPa at 100 bar which is not big as the rate of increase of plastically deformable materials. For hard materials such as sodium carbonate and calcium carbonate, there is no significant increase in the strength of the ribbon as the pressure increases.

Improving the product quality during roller compaction with increasing the hydraulic pressure was reported in many previous studies (Inghelbrecht and Paul Remon, 1998, Rambali et al., 2001, Kleinebudde, 2004, Osborne et al., 2013).

Figure 5-5 shows a comparison of ribbon strength increasing rate for different materials at different hydraulic pressures. The figure shows clearly the difference in the increasing rate of the ribbon strength for different materials.

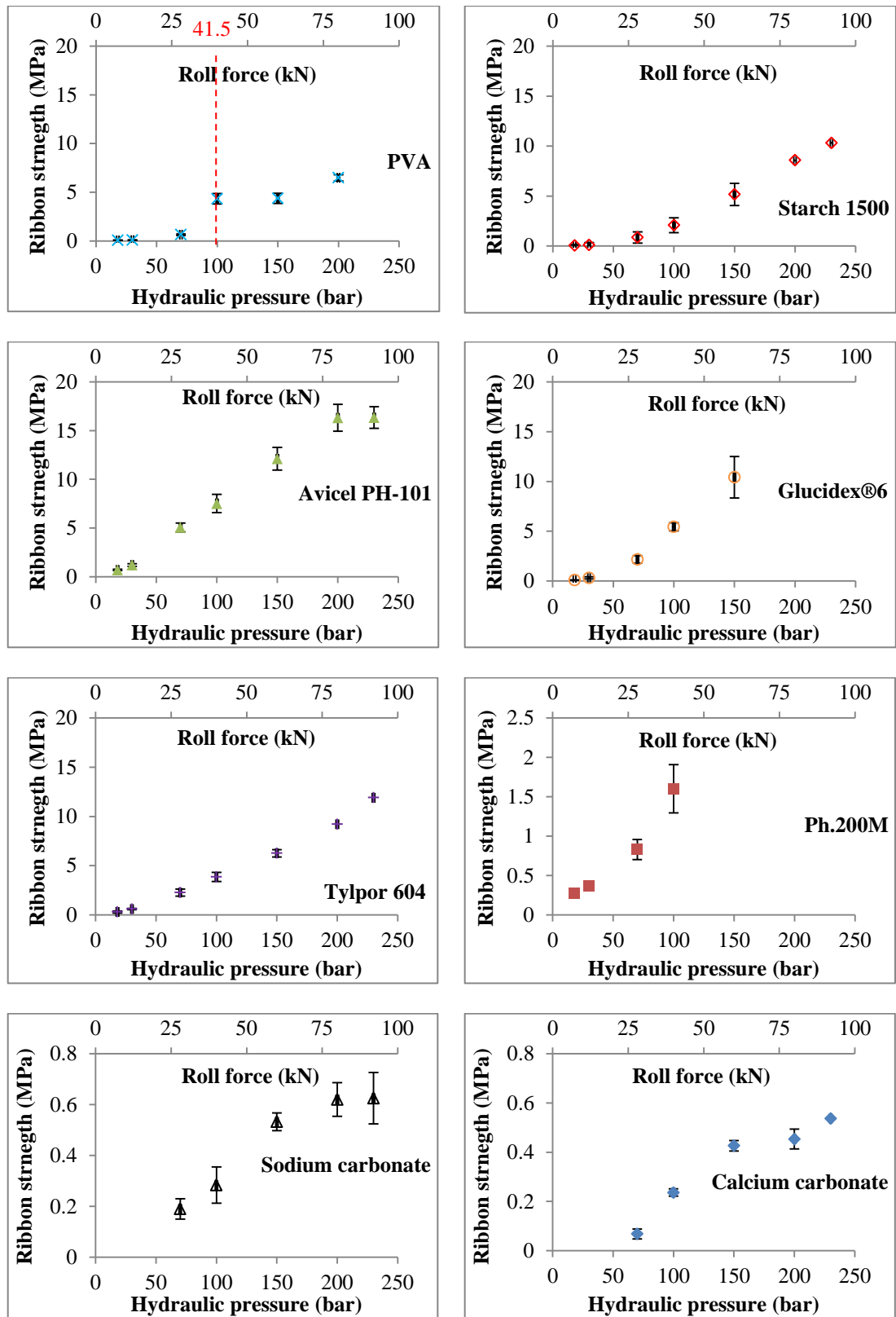


Figure 5-4: Ribbon strength as a function of applied hydraulic pressure for different materials

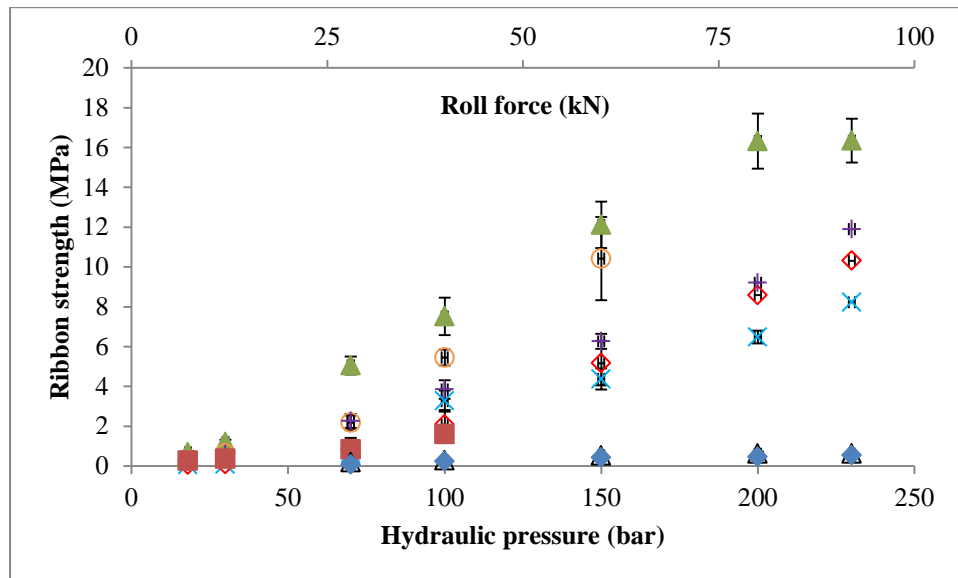


Figure 5-5: Comparison of the ribbon strength increase rate as a function of applied hydraulic pressure for different materials

× PVA, ◇ Starch 1500, ▲ Avicel PH-101, ○ Glucidex®6, + Tylpor 604, ■ Pharmatose 200M, △ sodium carbonate, ◆ calcium carbonate

Figure 5-6 shows the SEM images of primary powders and ribbon surface of PVA produced at different hydraulic pressures. It can be seen from the figure that although the PVA has lowest hardness among the other powders, the compacted particles are still having almost the same shape of the primary particles. This suggests that the particles did not exhibit significant plastic deformation or fracture during the compaction. There are some signs of deformation and compaction, squashed particles, on the surfaces of the ribbon produced at 200 and 230 bar but many particles with original shapes can be still identified. This may explain why the ribbon strength of PVA is not as good as other materials with medium hardness range. To make sure that the particles of PVA did not deform even in the interior section across ribbon thickness and not only on the ribbon surface, a further SEM were carried out for the interior section of the PVA ribbon. This was obtained by breaking the ribbons into halves and doing the SEM for the side section along the ribbon thickness. Figure 5-7 shows SEM images of the interior section of the PVA ribbon produced at 230 bar. It can be seen from the figure that the particles exhibit neither significant deformation nor fracture. This is confirming the previous observation.

For the starch in Figure 5-8, particles with original primary powder shapes can be identified on the surface of the ribbon produced at hydraulic pressures of 18, 30, 70 and 100 bar. At 150 bar there are still some particles that kept their original shapes. For the ribbons produced at 200 and 230 bar, the particles deformed and it was difficult to distinguish any primary particles that kept their original shape on the ribbon surfaces. Figure A- 1 (Appendix A) shows a higher magnification image of starch ribbon produced at 230 bar. It can be seen that the particles are flattened and their projected area increased compared to the area of the original primary particles. This is a sign of plastic deformation of the particles.

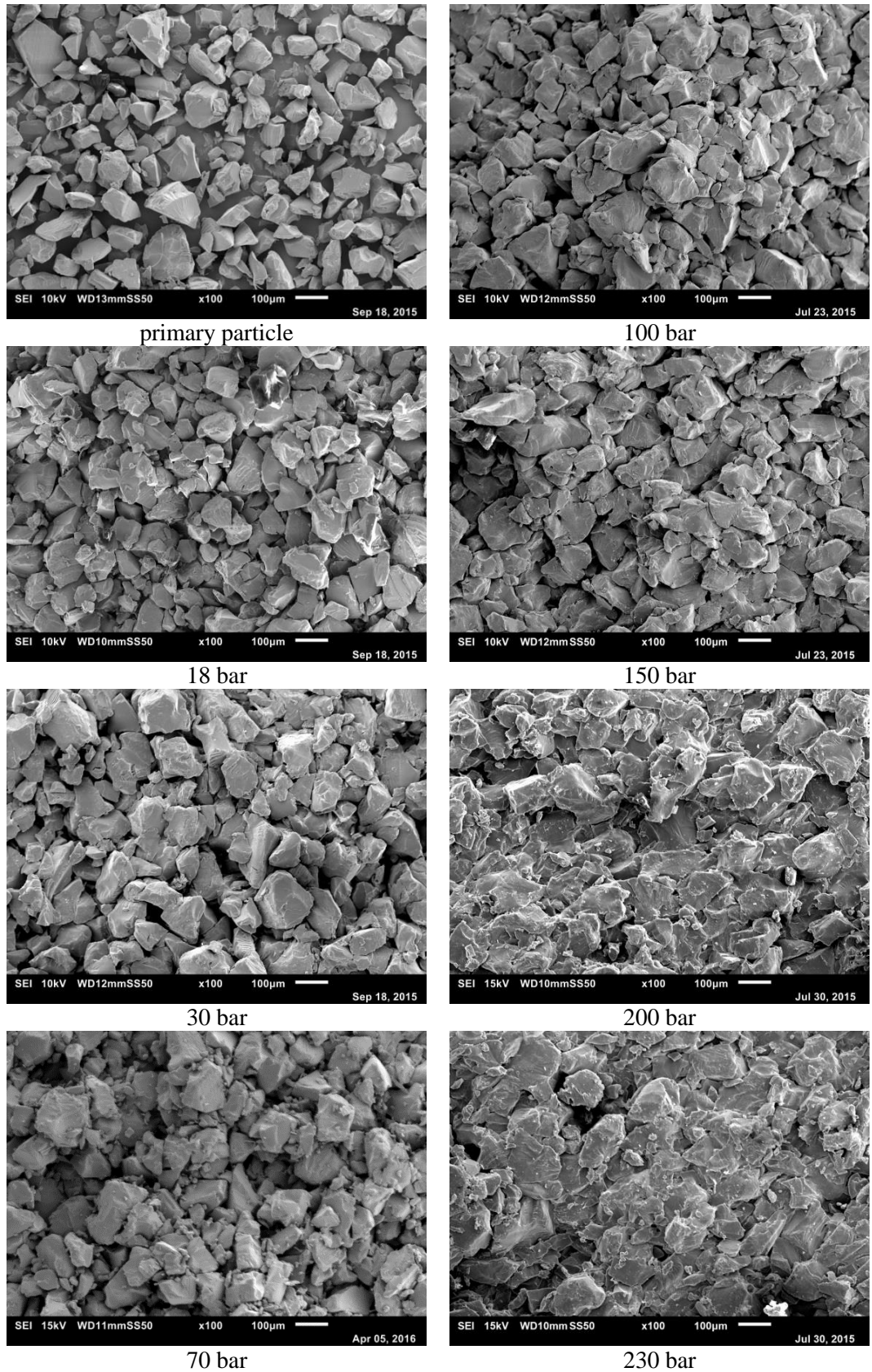


Figure 5-6: SEM images of primary particles and ribbon surfaces of PVA produced at different hydraulic pressures

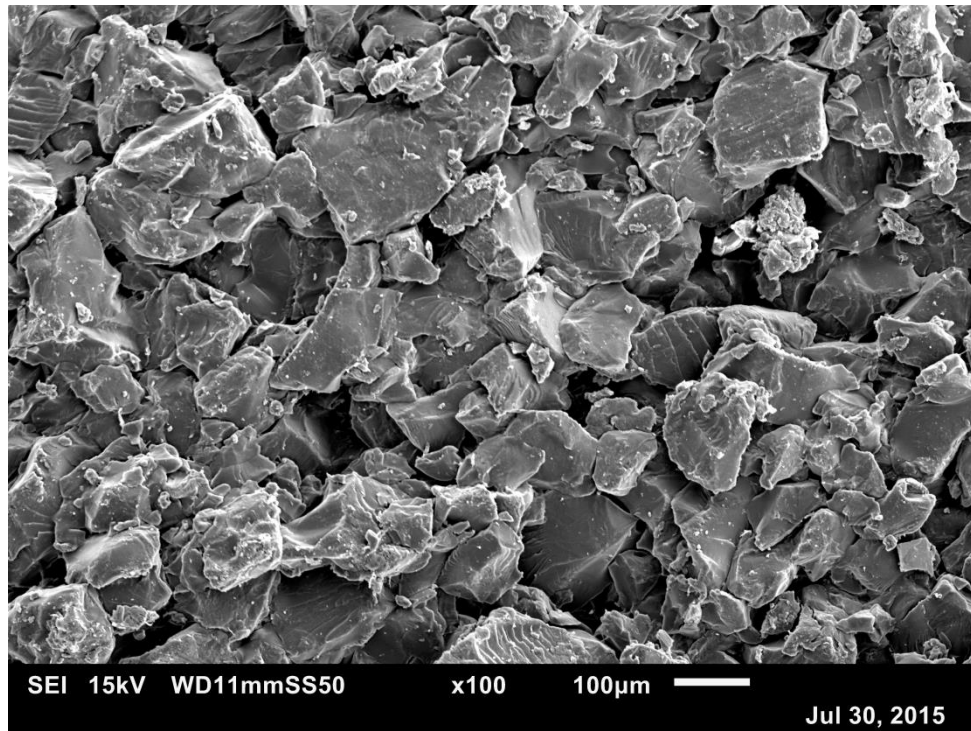


Figure 5-7: SEM image of the internal section across the thickness of the PVA ribbon produced at 230 bar

Figure 5-9 shows the SEM images of the primary powder and ribbon surfaces of Avicel PH-101 produced at different hydraulic pressures. It can be seen that at low pressure, the particles are getting closer to each other without significant change in their shape and the size. In addition, there is no sign of fracture as the original shape of the primary particles can still be identified. At high pressures of 70 bar and above, the images show clear plastic deformation, change of shape, of the primary particles. The deformation increases as the pressure increases which may explain the high rate of increase in the ribbon strength over increasing the pressure.

Figure A- 2 (Appendix A) shows SEM image, at higher magnification, for the surface of the Avicel PH-101 ribbon produced at 230 bar. The image shows clearly a deformation of the particles as the projected area of the particles is bigger than that of the original primary particles due to the flattening.

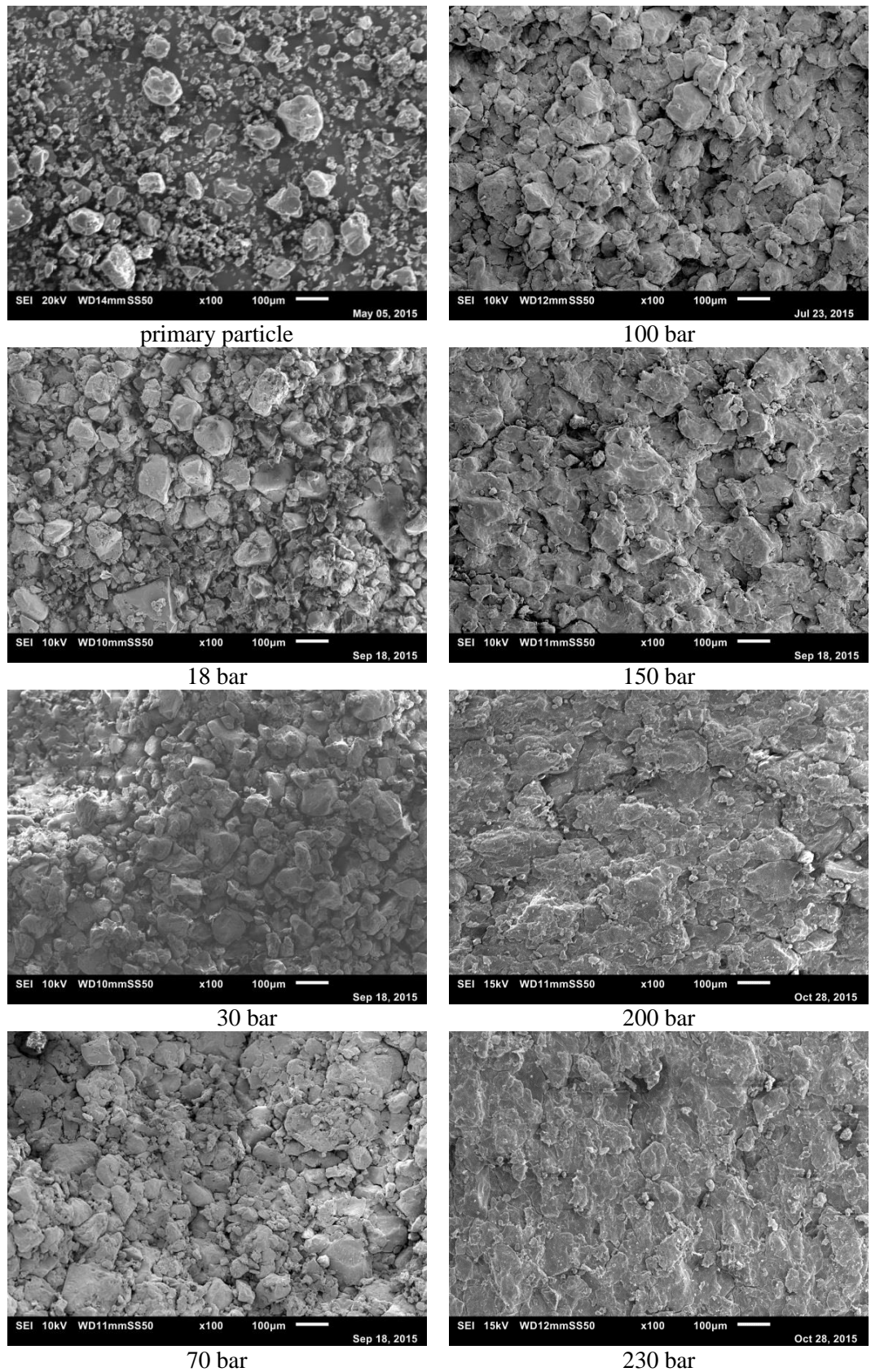


Figure 5-8: SEM images of primary particles and ribbon surfaces of starch 1500 produced at different hydraulic pressures



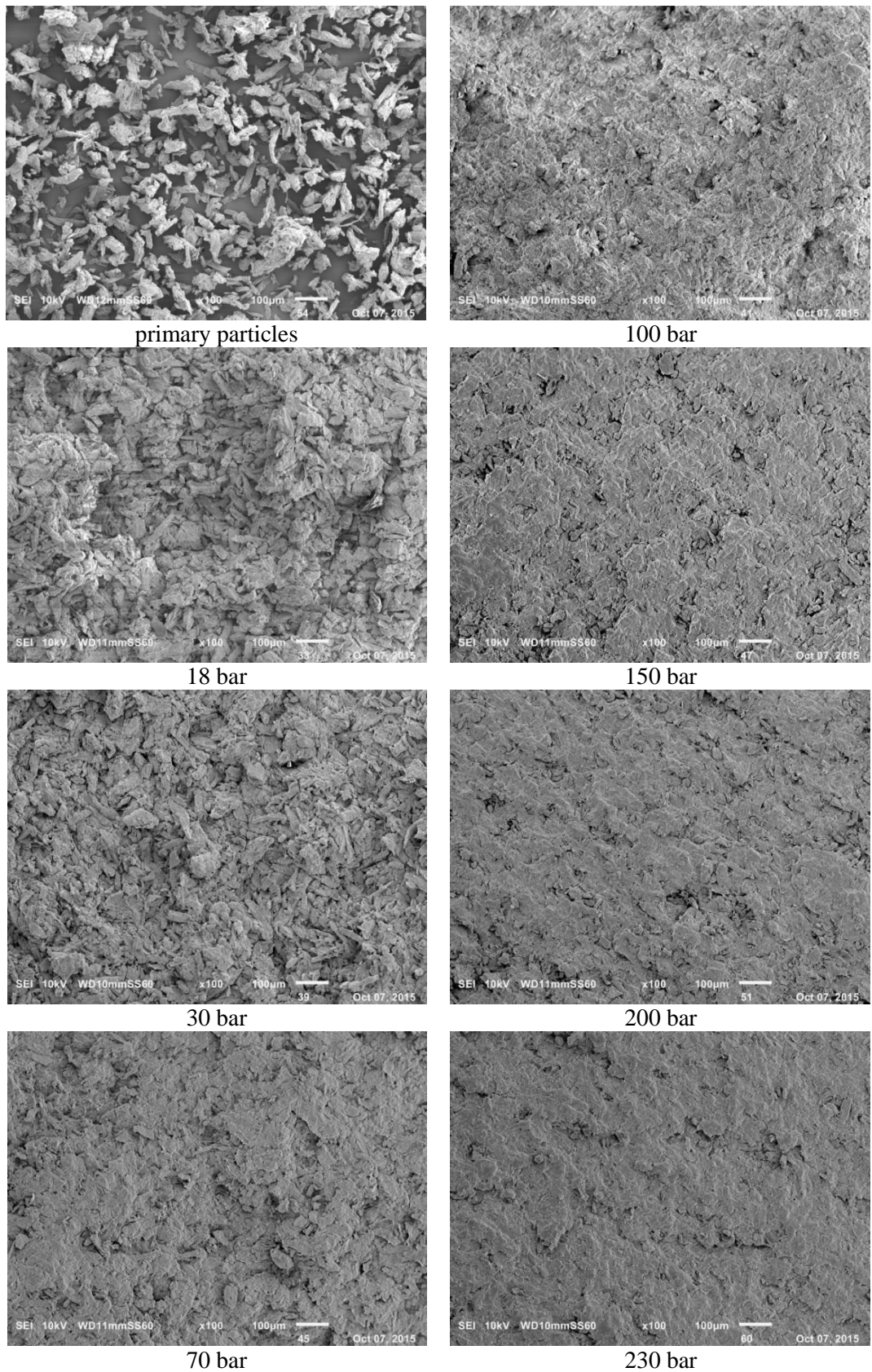


Figure 5-9: SEM images of primary particles and ribbon surface of Avicel PH-101 at different hydraulic pressures

Figure 5-10 shows SEM images of the primary particles and ribbon surfaces of Glucidex<sup>®</sup>6 at different hydraulic pressures. It can be seen from the figure that at low pressures, 18, 30 and 70 bar, the particles are fractured despite the good deformability of this material. This is due to the hollow structure of the primary particles as discussed in Section 3.1.4. In addition, the large size of the particle could be another reason that caused fracture. The relationship between the size and mechanical properties has been explained in more details in Section 2.4. The deformation increased as the pressure increased. At pressure of 100 and 150 bar, the ribbon surfaces look smooth which make it difficult to distinguish any individual particle with original shape and this is a sign of plastic deformation. This is also clear in Figure A- 3 (Appendix A) which is an image of 150 bar ribbon surface but with higher magnification.

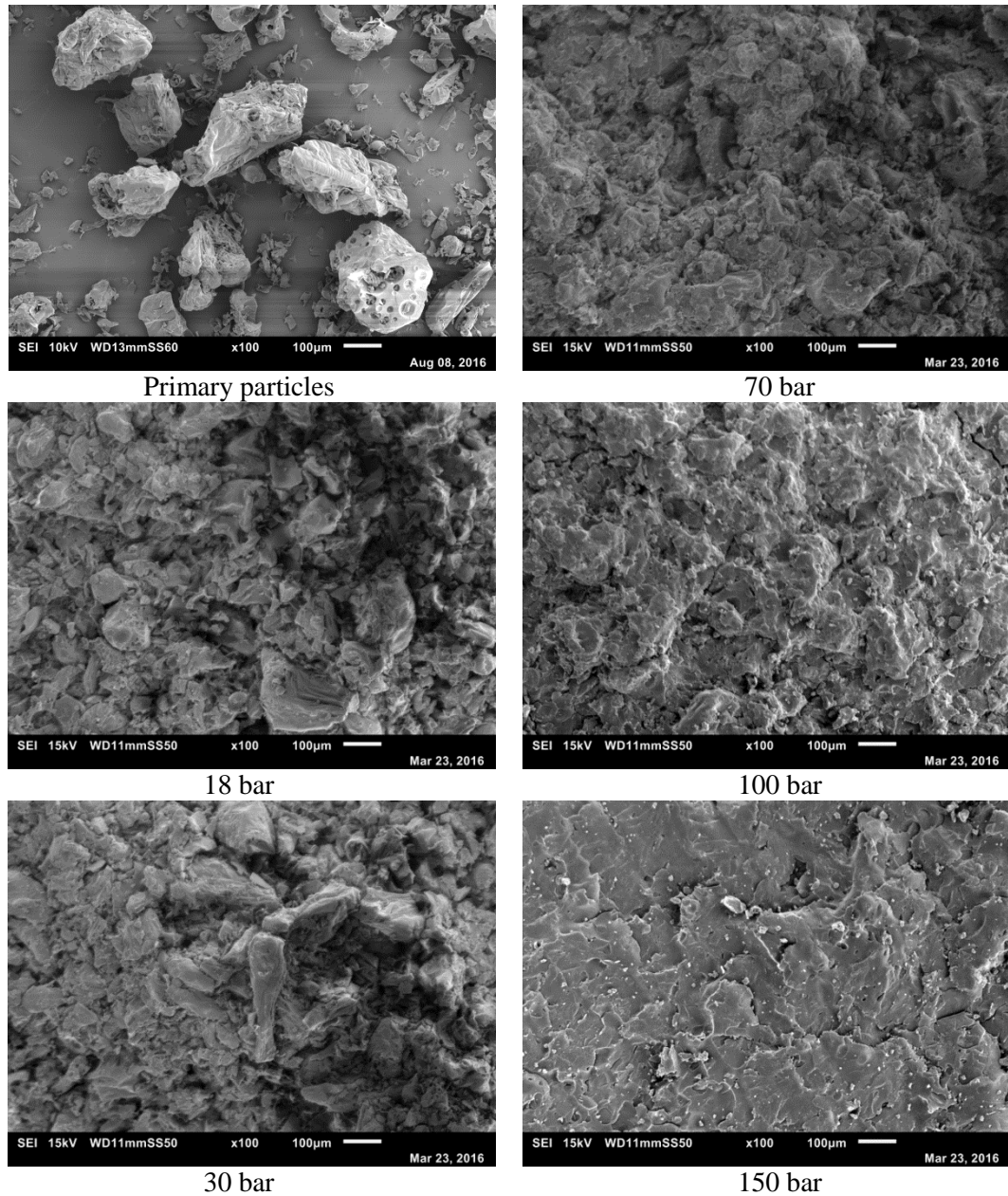


Figure 5-10: SEM images of primary particles and ribbon surface of Glucidex<sup>®</sup>6 produced at different hydraulic pressures

Figure 5-11 shows the SEM images of primary particles and ribbon surface of Tylpor 604 produced at different hydraulic pressures. It can be seen from the figure that at low pressures of 18 and 30 bar, it is easy to distinguish the individual primary particles and there is no sign of fracture. This indicates plastically deformable material. At higher pressures of 70 and 100 bar, it is not easy to identify individual primary particles on the ribbon surface. As the pressure increased further, the ribbon surface became smoother with flatten particles. This is supported by Figure A- 4 which is an image of 230 bar ribbon surface with higher magnification. It can be seen from the image that the projected area of the particles on the ribbon surface is bigger than the area of the original primary particles before compaction.

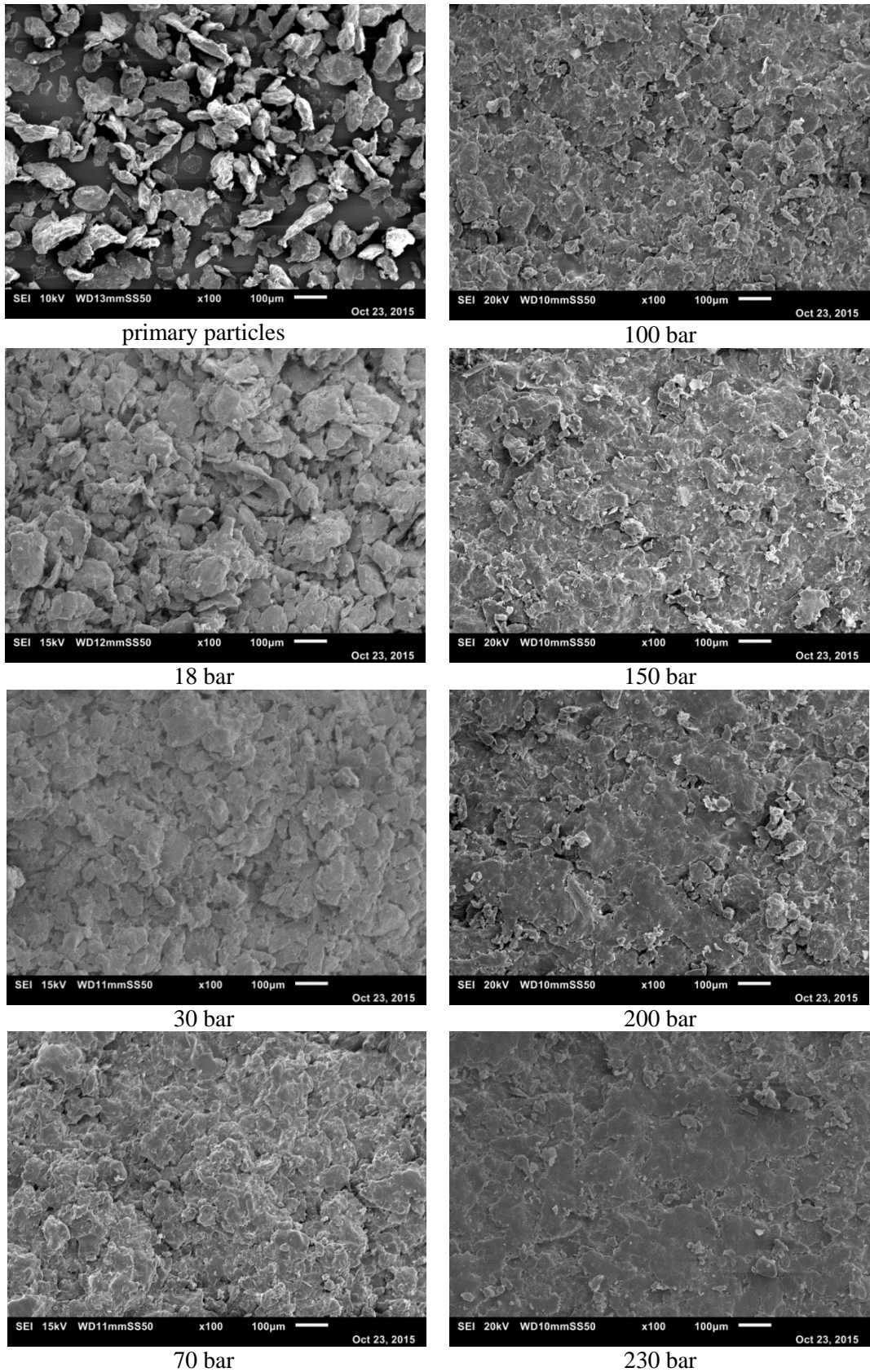


Figure 5-11: SEM images of primary particles and ribbon surfaces of Tylpor 604 at different hydraulic pressures

Figure 5-12 shows SEM images captured for primary particles and ribbon surface of Pharmatose 200M at different hydraulic pressures. It can be seen from the figure that at low pressure of 18 bar, it is difficult to see individual particles. This could be a sign of fracture. It is not the case with the plastically deformable materials where the single particles deformed but still can be identified specially at low pressures at 18 and 30 bar except the mentioned special case of Glucidex<sup>®</sup>6. At higher pressure of 100 bar, the ribbon surface still have some particles with a size smaller than the original size of the primary particles which could be another indication of fracture. The fracture and insignificant plastic deformation explain why Pharmatose 200M did not produce strong ribbon compared to the material that exhibit significant plastic deformation. Figure A- 5 (Appendix A) shows clearly small particles on the ribbon surface compared to the size of primary particles.

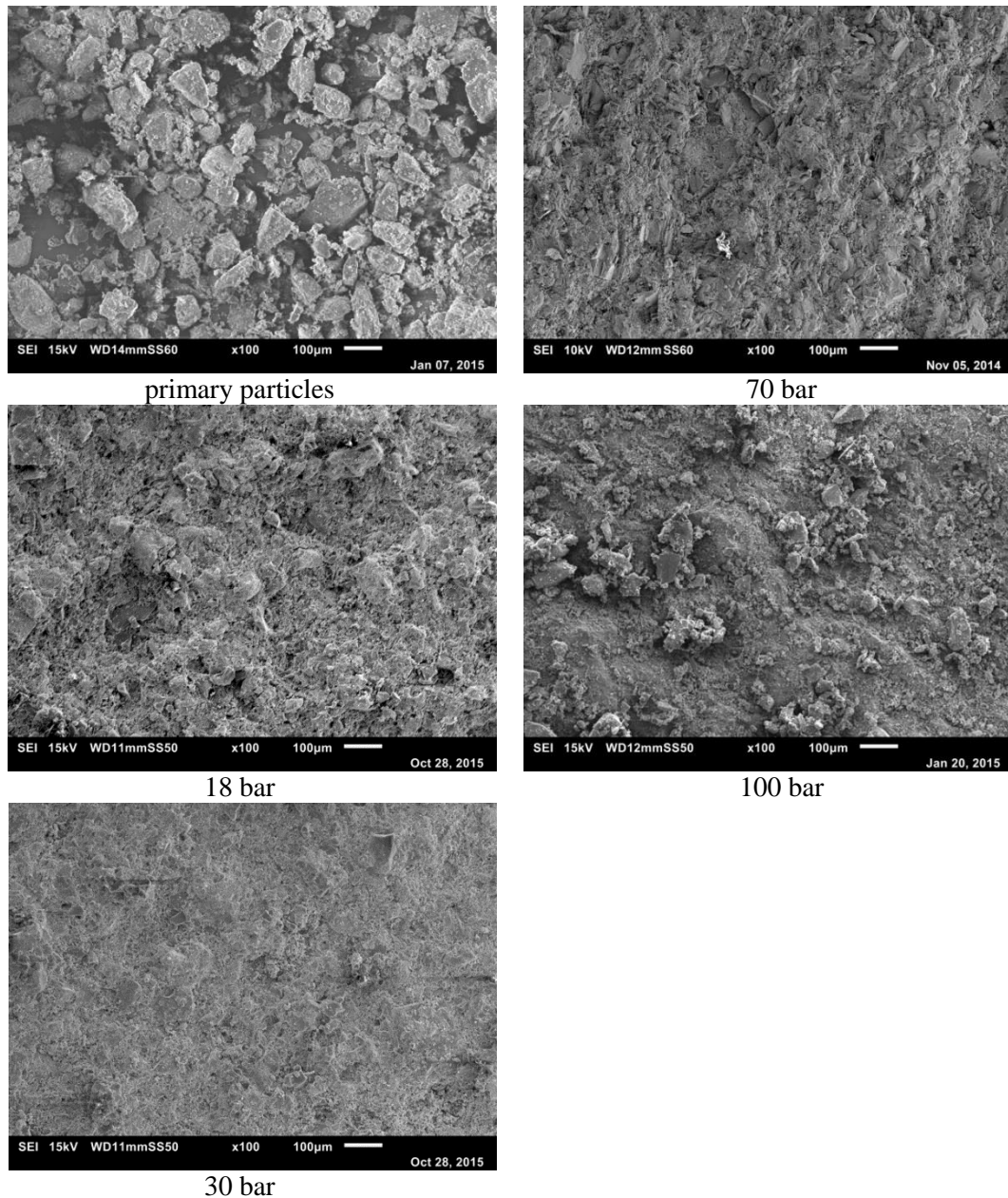


Figure 5-12: SEM images of primary particles and ribbon surfaces of Pharmatose 200M at different hydraulic pressures

Figure 5-13 shows SEM images produced from sodium carbonate at different hydraulic pressures. It can be seen from the figure that even at lowest pressure of 70 bar, it is not possible to identify any individual primary particle and this is due to the high brittleness of sodium carbonate. All the particles exhibited extensive fracture even at low pressures which lead to producing flat ribbon surface. Previous investigation of the fracture behavior of sodium carbonate in Section 4.1.3 showed that the particles of this material are very fragile and they are fractured by applying low force. Although the particles are fractured it did not produced strong ribbon and as shown in Figure 5-3. Figure A- 6 in Appendix A confirms the fracture of the primary particles where particles with small size can be seen on the 230 bar ribbon surface.

Figure 5-14 shows SEM images of primary particles and ribbon surfaces of calcium carbonate at different hydraulic pressures. It is not easy to see the individual particles clearly on the ribbon surfaces of different hydraulic pressures due to the small size of the particles. But the rough surface of the ribbon at different hydraulic pressures suggested that neither plastic deformation nor fracture happened at low pressures. At high pressures of 200 and 230 bar, there are some flat areas on the ribbon surfaces with small particles. The same could be seen in Figure A- 7 in Appendix A.

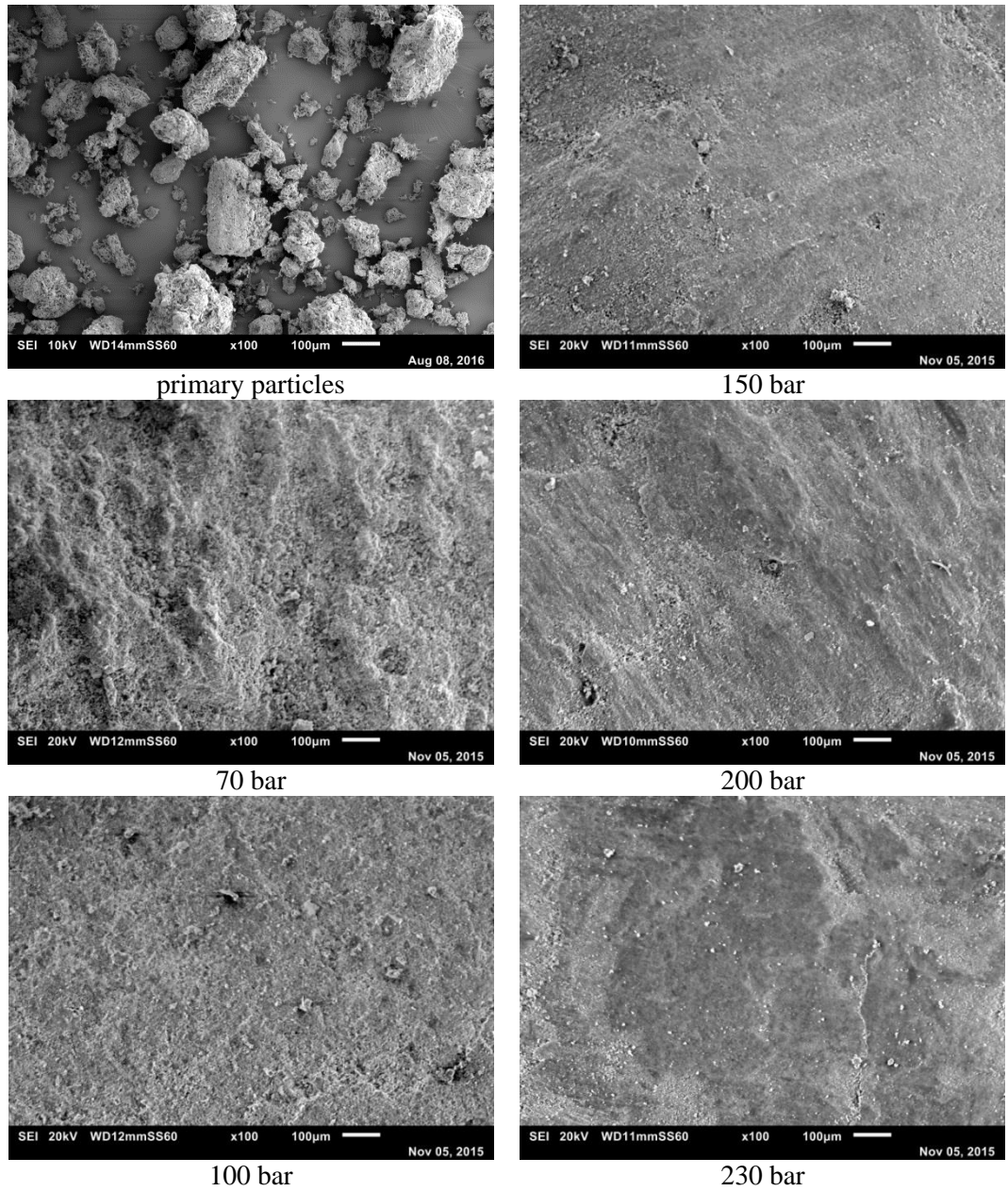


Figure 5-13: SEM images of ribbon surface of sodium carbonate produced at different hydraulic pressures

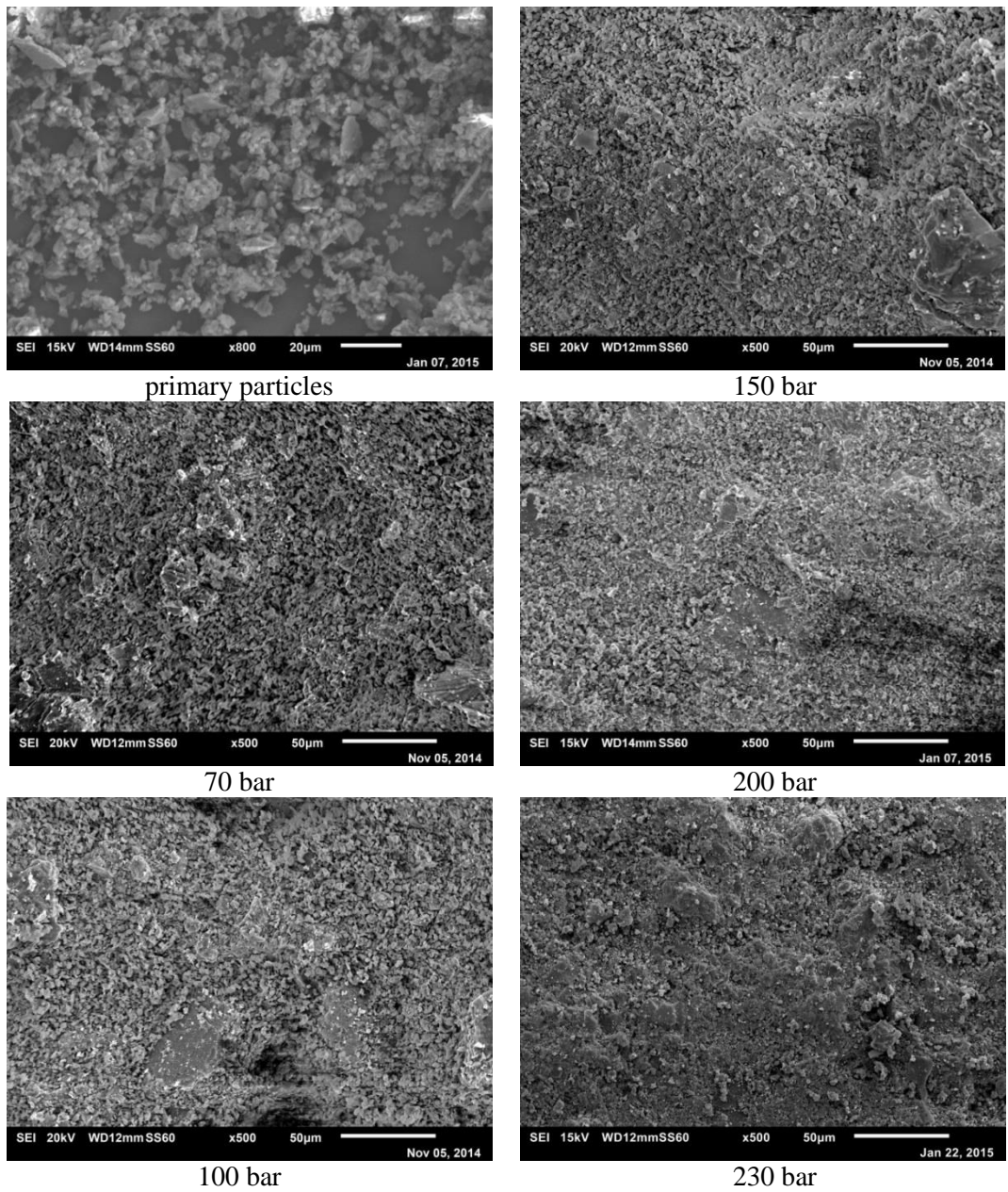


Figure 5-14: SEM images of calcium carbonate primary particles and ribbons surface produced at different hydraulic pressures



### 5.3.2 Single particle hardness and ribbon width

Although the width of the roller used in this study is 40 mm, as shown in Figure 5-15, the ribbon produced using different materials had different width.



Figure 5-15: Image of the roller showing its width

Figure 5-16 shows image of ribbons produced using different materials at hydraulic pressure of 70 bar. The image clearly shows the difference in the width of the ribbons produced by different materials.

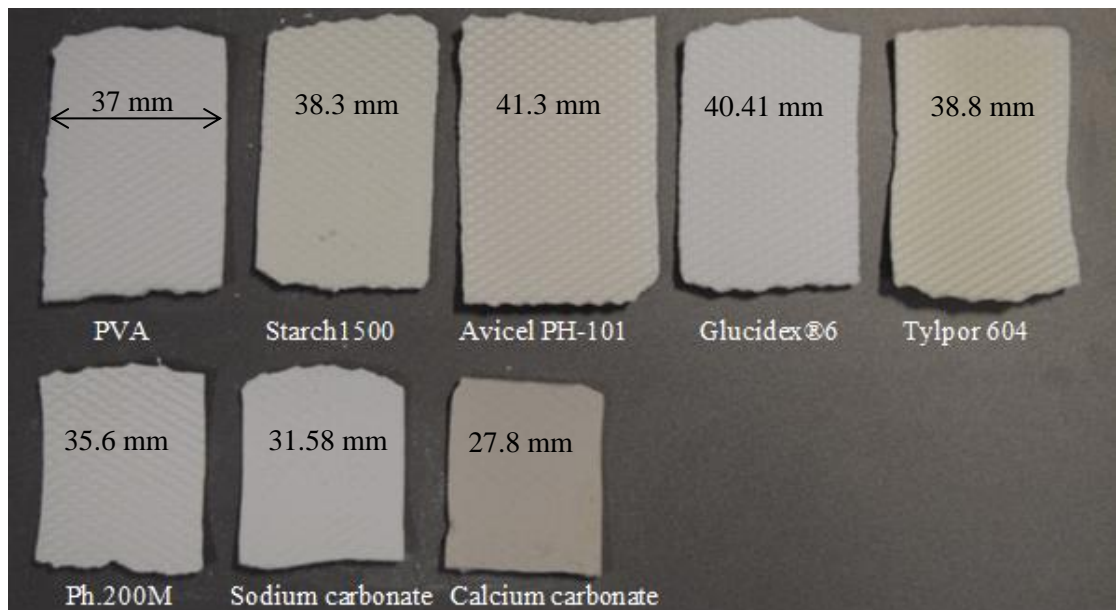


Figure 5-16: Ribbons produced by different materials at hydraulic pressure of 70 bar

The ribbon edges of some material were irregular. For this reason the width of the ribbon was determined by averaging the width of 10 ribbons. This was done using a slide digital caliper of 0.01mm resolution. Figure 5-17 shows the ribbon width of different materials represented by their nano-indentation hardness. The x-axis is the nano-indentation hardness and the y-axis is the ribbon width. It can be seen from Figure 5-17 that at lowest hydraulic pressure of 18 bar, the plastically deformable materials with medium hardness range of 0.44 to 0.7 GPa produced wider ribbons compared to other materials with width range between 36.7 to 38 mm. Materials of low hardness, PVA and starch, produced ribbon with the width of 36.7 and 36.1

mm respectively. The ribbon of partially plastic/brittle Pharmatose 200M was narrow compared to other plastically deformable material with a width of 35 mm. The case was almost the same with the ribbons of different materials produced at 30 bar and the difference between the width of plastically deformable material and brittle material, Pharmatose 200M, increased. At hydraulic pressure of 70 bar and above, all plastically deformable material with medium hardness range produced full ribbon width equal to the width of the roller i.e 40 mm or even more. At high pressure the particles of the deformable materials deformed and push the side cheek plates and that is the reason why the ribbon width is higher than 40 mm. Materials with low hardness produced less ribbon width. There was still a difference between the ribbon widths of deformable material in general and brittle/ hard material. It can be seen that the maximum width of sodium carbonate and calcium carbonate ribbon produced at maximum pressure of 230 bar were equal to 33 and 29.9 mm respectively which are narrower than other materials.

In summary, plastically deformable material with medium hardness range produced same width or wider ribbon compared to the plastically deformable materials with low hardness and that depends on the applied pressure. Both plastically deformable materials produced wider ribbon compared to the brittle material such as Pharmatose 200M and sodium carbonate. Calcium carbonate which is hard material produced narrowest ribbon compared to other materials at all hydraulic pressures.

The stress applied on the material between the rollers is not uniform as it is higher in the centre of the roller than the edges by approximately factor of three (Michel, 1994, Kleinebudde, 2004, Guigon et al., 2007, Cunningham et al., 2010, Miguélez-Morán et al., 2009, Yu, 2012). If the material is plastically deformable, the pressures experienced on the roller sides are sufficient to bond the particles together. Other reason of increasing the width is that the particles may squash and flatten which caused increase in the ribbon width. This is not the case with the brittle powders which produced significantly narrower ribbon compared to the plastically deformable materials. This is because either the applied pressure on the sides was not enough to bond the particles together or the particles did not exhibit significant plastic deformation so it did not squashed to increase the ribbon width.

Figure 5-18 shows how the ribbon width increased with increasing of hydraulic pressure. It can be seen from the figure that for all materials, increasing the hydraulic pressure caused an increase in the ribbon width. However the rate and the limit of the increase were different for different materials. Plastically deformable materials showed higher rate of width increase compared to the brittle hard materials for which even the maximum pressure was not enough to produce ribbon with full width of the roller. This can be seen clearly in Figure 5-19 where the ribbon widths of all materials were presented in one figure.

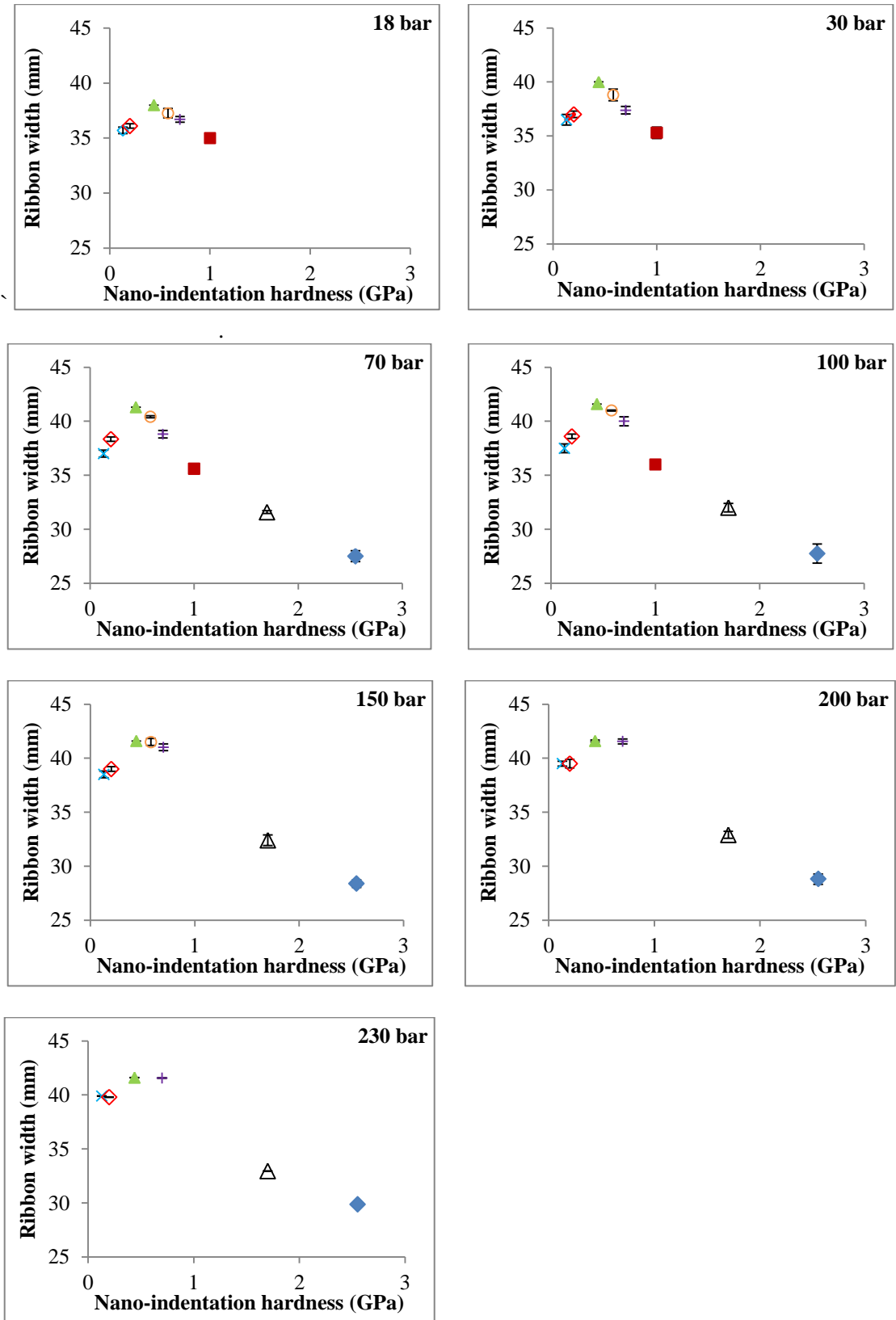


Figure 5-17: Ribbon width versus nano-indentation hardness of different materials at different applied hydraulic pressures

× PVA, ◇ Starch 1500, ▲ Avicel PH-101, ○ Glucidex®6, + Tylpor 604, ■ Pharmatose 200M, △ sodium carbonate, ◆ calcium carbonate

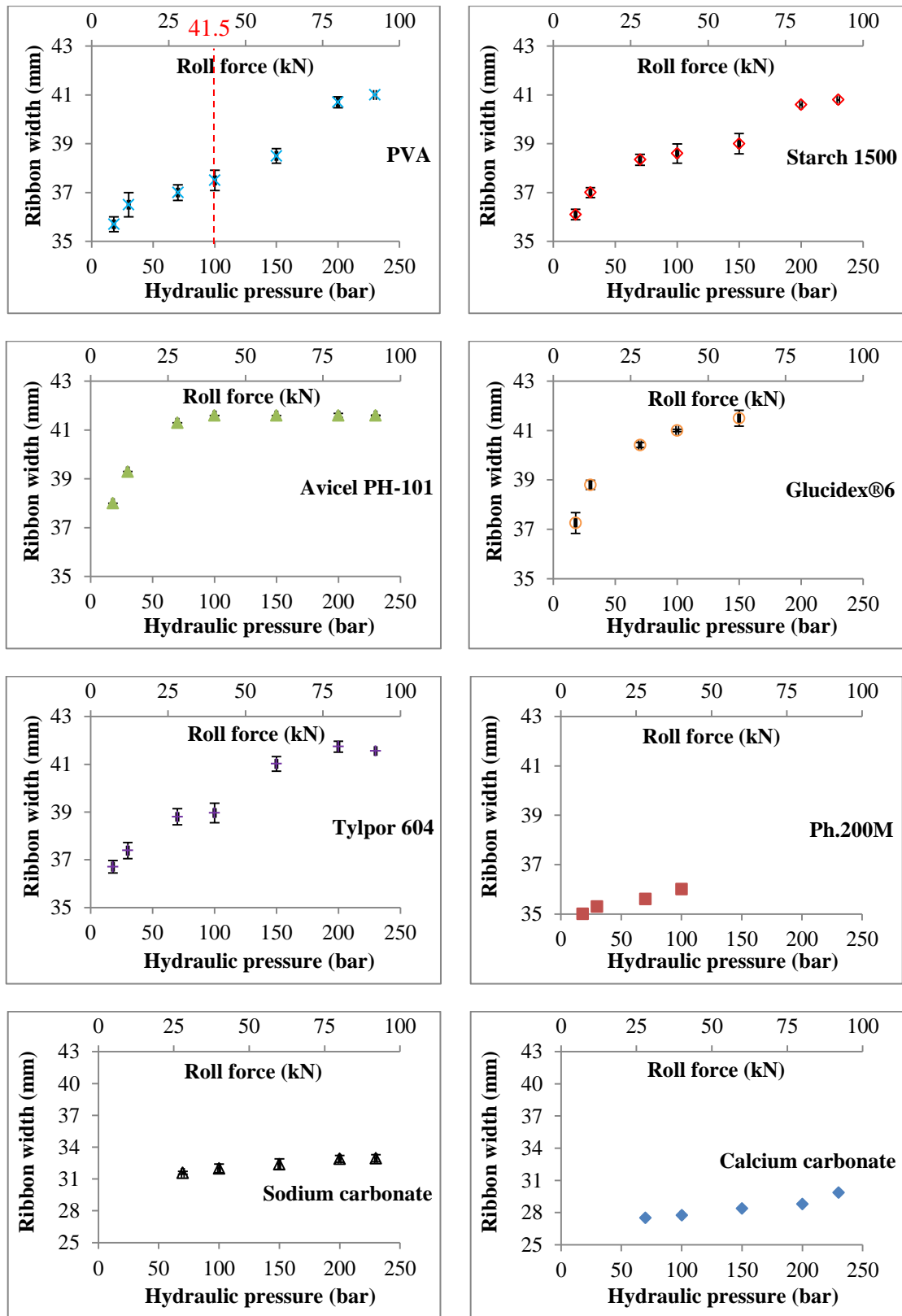


Figure 5-18: Ribbon width as a function of hydraulic pressure for different materials

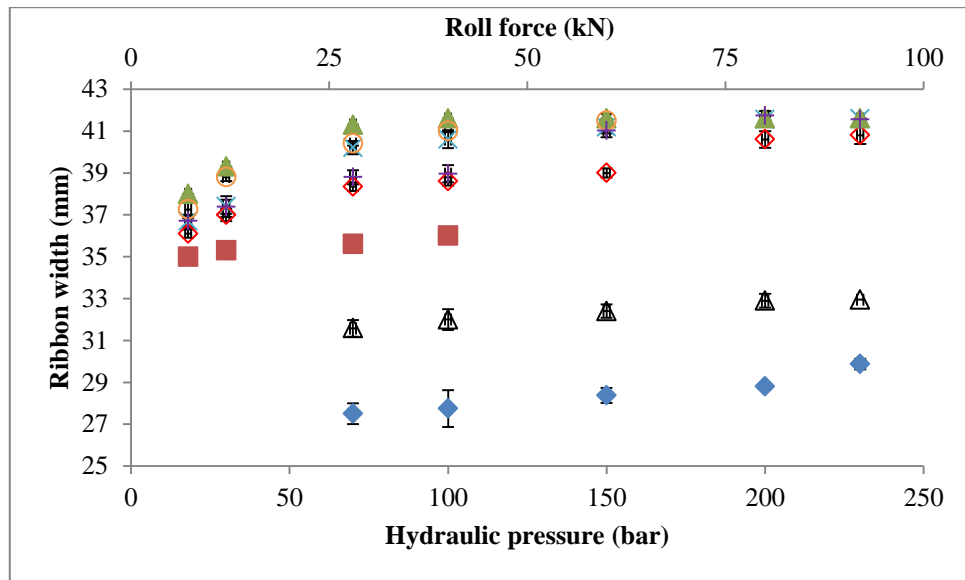


Figure 5-19: Comparison of ribbon width increase rate as a function of hydraulic pressure for different materials

× PVA, ◇ Starch 1500, ▲ Avicel PH-101, ○ Glucidex<sup>®</sup>6, + Tylpor 604, ■ Pharmatose 200M, △ sodium carbonate, ◆ calcium carbonate

### 5.3.3 Amount of fines produced during roller compaction

One of the disadvantages of roller compactor is producing big amount of fines (Inghelbrecht and Remon, 1998a). In industry, the fines is recycled to the feeding hopper but this causes limited problem if there is only one material in the process or if the composition of the fines is the same as the composition of the feed. For the case in which the feed is a mixture of materials and the fines composition is different than the composition of the feed, the recycling could result in inhomogeneity of the product (Kleinebudde, 2004). For this reason, it is important to determine and investigate the amount of fines produced from roller compaction of different materials.

The fines in this study is defined as the weight of the un-compacted powder with particle size equal or less than the maximum size of the primary powder of the material. This had been determined by sieving the entire product of roller compaction process which consists of ribbons, flakes and fines. This had been collected for 1 minute after achieving the steady state conditions of hydraulic pressure and roller gap. Figure 5-20 shows the percentage of fines determined for different materials at different hydraulic pressures. It can be seen from the figure that at low hydraulic pressures of 18 and 30 bar, the softest materials, PVA and starch, and the hardest materials, sodium carbonate and calcium carbonate, produced biggest amount of fines compared to the plastically deformable materials with medium hardness range. At hydraulic pressure of 70 bar, the fines produced from the softest materials decreased dramatically. Although the fines percentage produced from the hard materials decreased, it was still the highest among other materials. At higher hydraulic pressures, plastically deformable materials with low and medium hardness produced small percentage of fines followed by partially deformable Pharmatose 200M. For hard materials, i.e. sodium carbonate and calcium carbonate, the percentage of fines still high compared to other materials.

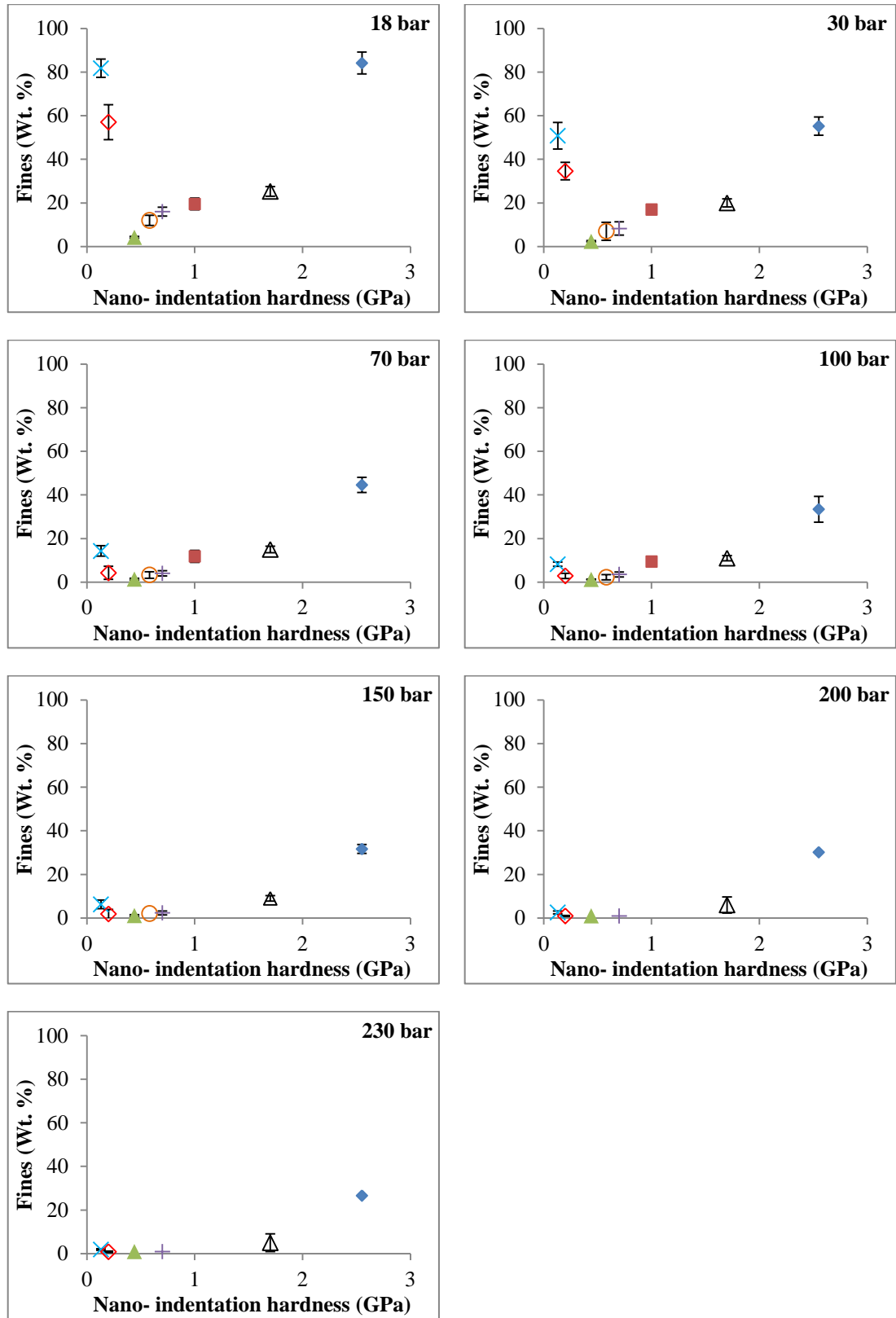


Figure 5-20: Fines wt. % as a function of applied hydraulic pressure for different materials  
 × PVA, ◇ Starch 1500, ▲ Avicel PH-101, ○ Glucidex<sup>®</sup>6, + Tylpor 604, ■ Pharmatose 200M, Δ sodium carbonate, ◆ calcium carbonate

The reasons for the powder that passed through the rollers but not getting agglomerated and staying as primary particles can be; the poor bonding between the particles and this is related to the mechanical properties of the material. This especially happened at the edges of the roller as the stress applied there is less than the stress applied at the centre (Miguélez-Morán et al., 2008, Miguélez-Morán et al., 2009, Lim et al., 2011, Muliadi et al., 2013).

The flowability of the powder could affect the amount of fines in two different ways that contradict each other; if the powder is poorly flowing, it may not spread uniformly across the roller width and this will cause more fines due to the inconsistency of the applied stress. The other source of the fines is the leakage of the powder through the space between the rollers and the cheek plates (Parrott, 1981, Kleinebudde, 2004). This fines will increase if the material is flowable.

Two methods were used in this study to indicate the flowability of the powder; flow function coefficient and angle of repose. The flow function coefficient (*ffc*) was determined by a ring shear cell tester RST-XS.s (Dr. Dietmar Schulze, Germany) and as described in Section 3.2.3.1. The repose angle of the powders was determined using angle of repose tester (Mark 4, powder research limited). Table 5-2 shows the flow function coefficient (*ffc*) measured by a ring shear cell tester for different materials.

Table 5-2: Flow function coefficient (*ffc*) of different materials

Material	Flow function coefficient ( <i>ffc</i> )
calcium carbonate	2.6 ± 0
Pharmatose 200M	3.55 ± 0.07
Avicel PH-101	4.35 ± 0.07
Tylpor 604	5.15 ± 0.07
sodium carbonate	5.3 ± 0
Glucidex <sup>®</sup> 6	9.1 ± 0.85
Starch 1500	12 ± 2
PVA	14.7 ± 1.5

According to Jenike (1964), the powders flow behaviour is classified as follows:

- $ffc < 1$  not flowing (Extremely poor flowability)
- $1 < ffc < 2$  very cohesive (very poor flowability)
- $2 < ffc < 4$  cohesive (poor flowability)
- $4 < ffc < 10$  easy-flowing (fair flowability)
- $ffc > 10$  free flowing (good flowability)

It can be seen from the table that PVA and starch are freely flowing powders as *ffc* for both materials is higher than 10. Avicel PH-101, Glucidex<sup>®</sup>6, Tylpor 604, and sodium carbonate

are easy flowing powders. Pharmatose 200M and calcium carbonate are cohesive poorly flowing materials.

Table 5-3 shows the determined angle of repose for different materials. The values confirmed the previous results of the ring shear cell tester. It can be seen from the table that PVA and starch have less angle of repose which means they have better flowability compared to other materials. Pharmatose 200M and calcium carbonate have the highest angles which is an indication of cohesive and poorly flowing powder.

Table 5-3: Angle of repose for the powders

<b>Material</b>	<b>Angle of Repose (°)</b>
Poly vinyl alcohol (PVA)	30.1 ± 3.9
Starch 1500	32.8 ± 0.9
Glucidex®6	35.68 ± 0.2
Sodium carbonate	38.28 ± 1.2
Tylpor 604	38.6 ± 3.1
Avicel PH-101	40.8 ± 0.4
Pharmatose 200M	43.88 ± 3.2
calcium carbonate	46.05 ± 2.4

According to the results in Tables 5-2 and 5-3, PVA and starch are both free flowing and can distribute uniformly across the roller but may leak more from the sides. Pharmatose 200M and calcium carbonate may not distribute uniformly across the roller but would leak less. During the experiments, the powder that leaked from the sides of the roller was collected and weighed. Then the percentages of the leaked powder were determined by dividing the amount of fines leaked from the sides of the roller by the total amount of fines. It was found that the percentage of the leaked powder in the total amount of fines is relatively small. It is the highest for PVA powder with a value of 5 % whereas the smallest percentage was for Tylpor 604 and sodium carbonate with a value of 1%. The small percentage of the leaked powder from the roller sides indicates that the main reason of the fines was the weak bonding between the particles during the compaction.

Despite the good flowability of PVA and starch powder, their percentage of fines was high at hydraulic pressures of 18 and 30 bar. It can be seen from Figure 5-4 and Figure 5-5 that the ribbon strength is very low for these two materials. This suggests that the mechanical properties are responsible for the weak bonding and consequently the big amount of fines.

Calcium carbonate is poorly flowing powder compared to other materials and the nano-indentation hardness is the highest. The ribbon strength of calcium carbonate is the weakest compared to other materials for all hydraulic pressures and as shown in Figure 5-4 and



Figure 5-5. For this reason, the mechanical properties and may be the flowability of the powder are together responsible for the big amount of the fines. However, the ribbon strength of calcium carbonate was weak across the whole width of the ribbon including the centre and the sides. In the centre, there should be enough amount of powder which consequently received the highest stress but despite of this the ribbon is weak. This might indicate that the weak bonding, more fines, is mainly caused by the mechanical properties of the primary powders rather than the poor flowability of the material.

It can be concluded from the above discussion that the mechanical properties of the powder is the main reason of the fines.

Figure 5-21 shows the relation between the amount of fines and the ribbon strength for different materials. It can be seen from the figure that for all materials; as the ribbon strength increased, the amount of fines decreased. This is because the ribbon strength is an indication of the bonding between the particles. Higher ribbon strength means a good bonding so there will be a small amount of un-granulated primary particles left. For PVA and starch, there is a big margin of change in the amount of fines and this is believed due to the big change in the ribbon strength from very weak ribbon at low pressure to the ribbon with good strength at high pressure. For Avicel PH-101, Glucidex<sup>®</sup> 6 and Tylpor 604, although the difference in the ribbon strength produced at low and high pressure is big, the ribbon strength at low pressure was relatively high compared to the ribbon strength of PVA and starch. The amount of fines is low even at low pressure due to the good bonding. For this reason, the reduction in the amount of fines for these three materials with increasing the pressure is not as big as that for PVA and starch. For Pharmatose 200M, medium change in the amount of fines was accompanied by medium change in the ribbon strength. For the hard materials, sodium carbonate and calcium carbonate, there was no big increase in the ribbon strength as well as no big decrease in the amount of fines upon increasing the pressure. This relation between the amount of fines and the ribbon strength confirms that the fines is mainly resulted from the poor bonding of the particles rather than the poor flowability.

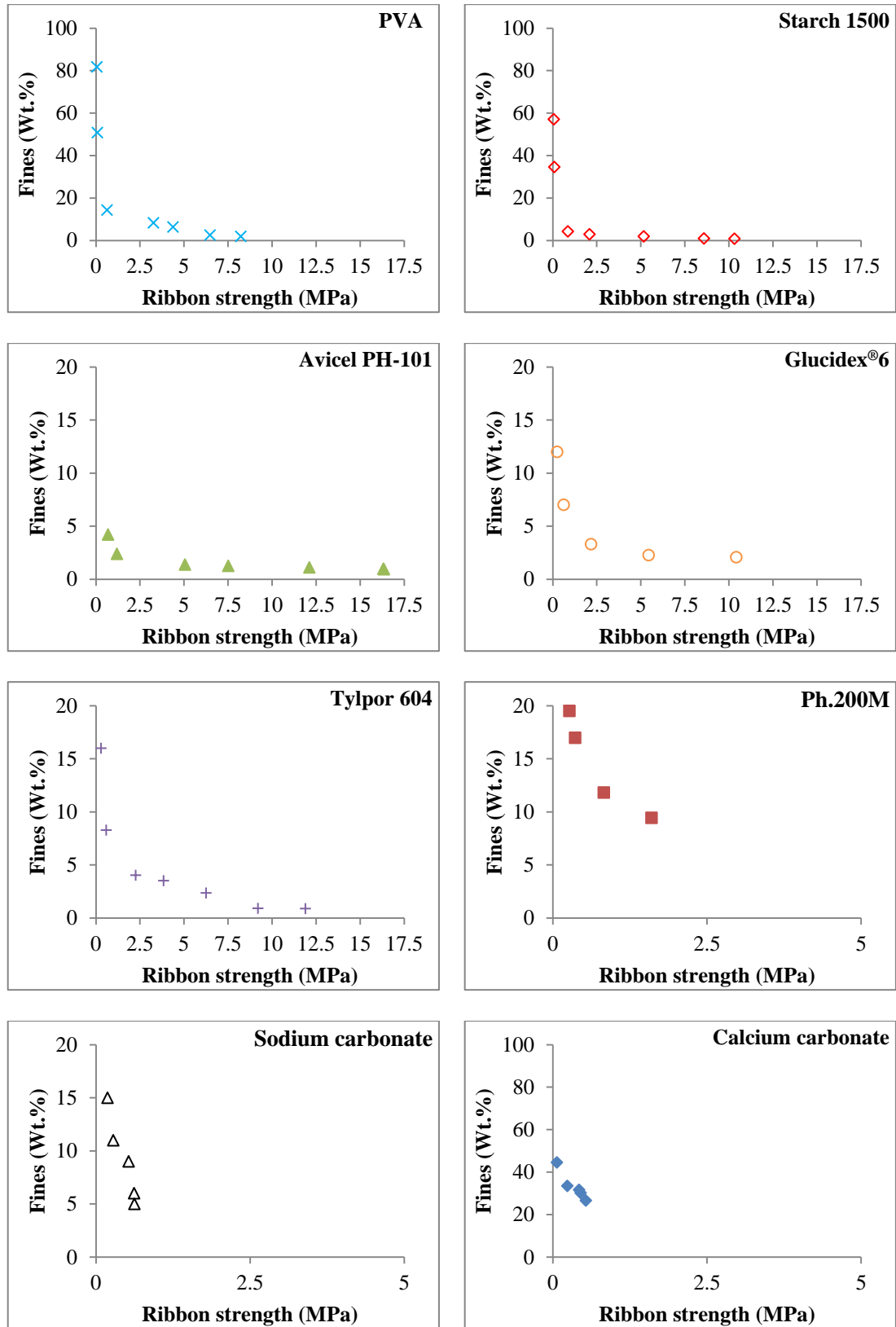


Figure 5-21: The amount of fines as a function of ribbon strength for different materials

Figure 5-22 shows how the applied hydraulic pressure affects the amount of fines. It can be seen from the figure that for all eight materials, increasing the hydraulic pressure caused a decrease in the amount of fines. This is because higher hydraulic pressure means higher stress applied on the materials which resulted in a better bonding between the particles. These results are in agreement with the literatures. Heiman et al. (2015) reported that increasing the pressure of the roller compactor caused a decrease in the amount of fines produced by hydroxypropyl methylcellulose. Dumarey et al. (2011) concluded that increasing the hydraulic pressure of roller compactor decreased the amount of fines produced by different grades of microcrystalline cellulose. The same observations were reported by Bacher et al. (2007) upon compaction of different powder types of calcium carbonate.

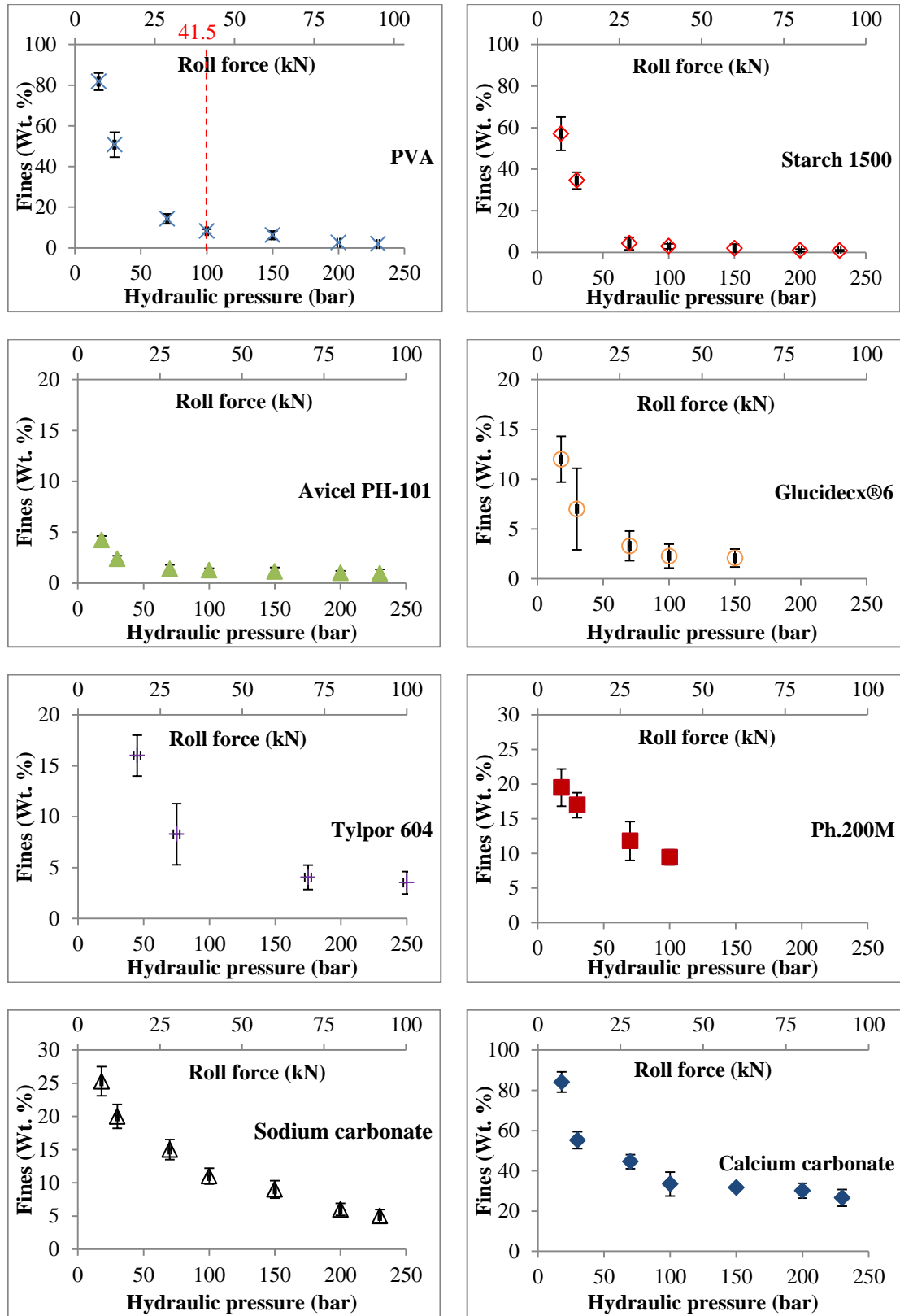


Figure 5-22: Fines % as a function of applied hydraulic pressure for different materials

### 5.3.4 Ribbon surface temperature and temperature profile

The aim of the study in this section is to measure the increase in the temperature during roller compaction process for range of materials and investigate if there is any link between the mechanical properties of the single primary powder and the increase in the temperature and the temperature profile across the ribbon width. Infrared thermal camera was used to measure the temperature of the ribbon online during the production.

#### 5.3.4.1 Measuring the thermal emissivity

The emissivity is one of the most important factors to be considered while measuring the temperature by thermal camera (Flir, 2011). The emissivity of the material is a measure of how much radiation is emitted from an object compared to a perfect black body. The emissivity of all ribbons under investigation was measured using the methods explained in Section 3.4.2.1. Table 5-4 shows measured emissivity values for different materials.

Table 5-4: Measured emissivity for different materials

Material	Emissivity
PVA	0.99
Starch 1500	0.99
Avicel PH-101	0.88
Glucidex®6	0.99
Tylpor 604	0.95
Pharmatose 200M	0.98
Sodium carbonate	0.98
calcium carbonate	0.95

#### 5.3.4.2 Ribbon temperature

The temperature of the ribbon produced by different materials using different hydraulic pressures were measured online using a FLIR SC655 thermal image camera with a frame rate of 50 frame/s. The online thermal imaging setup is shown in Figure 3-14. The camera was facing the two rotating rollers. The recording of one minute video was started after achieving the steady state of required hydraulic pressure and roller gap. FLIR R&D software used to analyse the images and to determine the average temperature at different times in the video for each experiment.

Figure 5-23 shows thermal images of the ribbon of different materials, produced at 100 bar, along with the colour scale as an indication of temperature; the lighter the colour the higher the temperature. These images were taken during the production just after the ribbons exit from the area between the two rotating rollers. It can be seen from the images that although the ribbons produced using the same hydraulic pressure; the temperature is different for different materials.

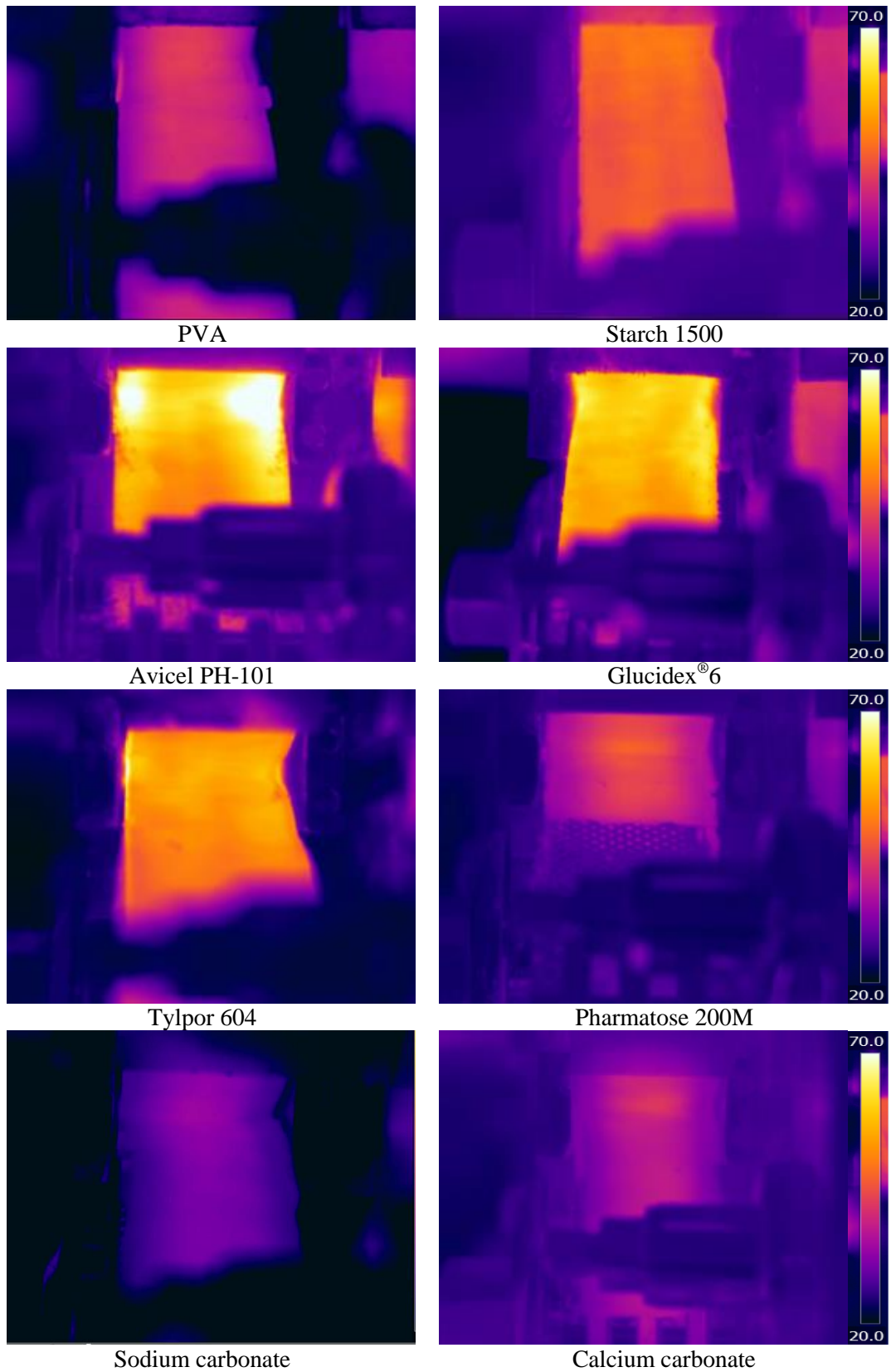


Figure 5-23: Thermal images for ribbon of different materials produced at 100 bar hydraulic pressure

Figure 5-24 shows how the maximum ribbon temperature of different materials changes with increasing the hydraulic pressures. The x-axis is the hydraulic pressure and the y-axis is the maximum ribbon surface temperature. It can be seen from the figure that increasing the hydraulic pressure caused an increase in the temperature of the ribbon for all materials. Increasing the temperature during the compaction of the powder is caused by different exothermic processes. At early stage of the compaction and during the rearrangement step, a collision and sliding of the particles with each other may contribute to the increase in the temperature. Then upon increasing the pressure, plastic deformation in addition to the fracture could happen and cause an increase in the temperature. The friction between the particle-particle and particle-surface of the equipment could be another important reason for increasing the temperature during the compaction process as shown for the uniaxial powder compaction process (Hanus and King, 1968, Ketolainen et al., 1993). The plastic deformation, fracture and the friction increase as the hydraulic pressure increase and this is the reason for increasing the temperature. Such increase in the temperature of ribbon has been seen by Osborne et al. (2013) upon roller compaction of dextrose syrup, microcrystalline cellulose and sodium chloride. Their results pointed out that the hydraulic pressure applied during the roller compaction is the most significant parameter that caused the increase in the temperature and there is a clear relation between the hydraulic pressure and the ribbon temperature. It can be seen from Figure 5-24 that the ribbon temperature and the increase of the temperature with increasing the hydraulic pressure are both material dependent.

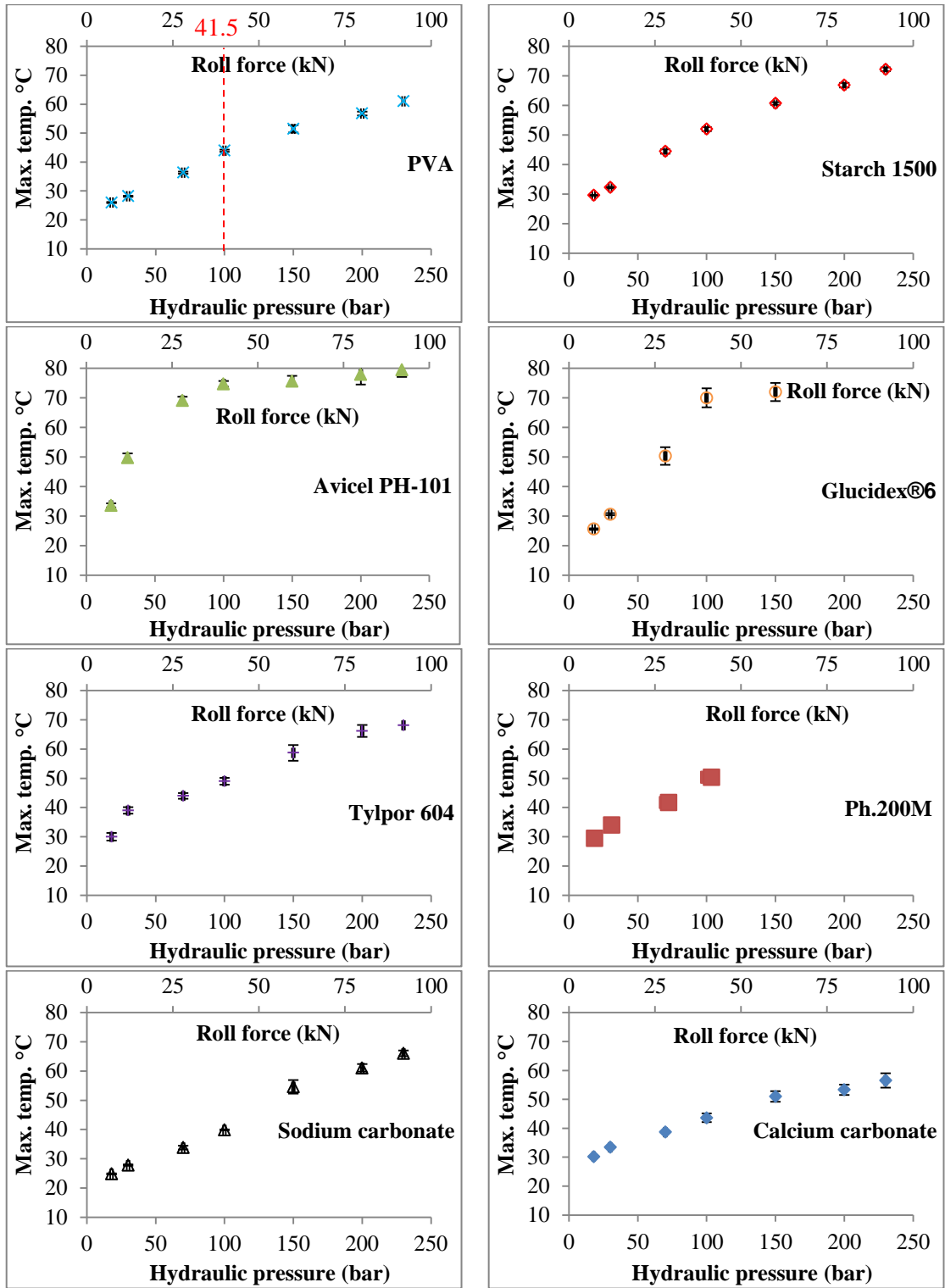


Figure 5-24: Maximum ribbon surface temperature for different materials at different hydraulic pressures



Figure 5-25 shows a comparison of maximum ribbon temperature increasing rate with hydraulic pressure for different materials. The figure shows clearly that some materials generate more heat than others. It can be seen that for the most hydraulic pressures, Avicel PH-101, Glucidex®6 and Tylpor 604 produced ribbon with higher temperature than other materials.

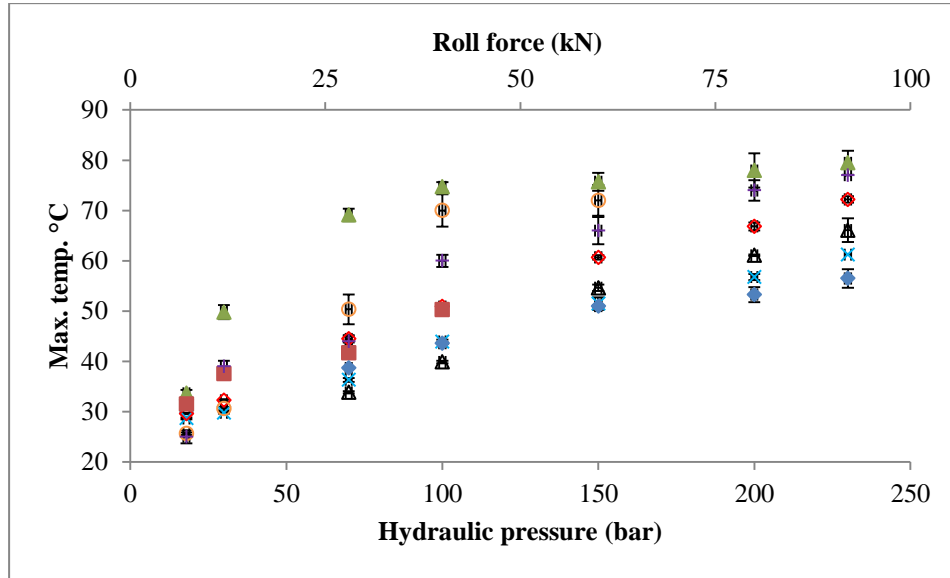


Figure 5-25: Comparison of ribbon maximum temperature for different materials at different hydraulic pressures

× PVA, ◇ Starch 1500, ▲ Avicel PH-101, ○ Glucidex®6, + Tylpor 604, ■ Pharmatose 200M, Δ Sodium carbonate, ◆ Calcium carbonate

Figures 5-26 and 5-27 show the temperature profile across ribbon width of different materials. The y-axis is the temperature of the ribbon surface and the x-axis is the distance across ribbon width in mm. The profiles have been determined using Flir R&D software by plotting a line across the ribbon width then exporting the temperature profile data every 6 seconds of the 1 minute movie. It can be seen from the figures that the temperature profile is different for different materials. Almost two profiles can be seen, the first one is higher temperature in the centre of the ribbon compared to the temperature at the sides. This is the case for all profiles of PVA, starch, Pharmatose 200M, sodium carbonate and calcium carbonate in addition to some profiles of other materials at low pressures. The second profile is lower temperature in the centre of the ribbon compared to the temperature at the sides. This can be seen with some profiles of Avicel PH-101, Glucidex®6 and Tylpor 604 at some hydraulic pressures.

According to the previous conclusion from Figure 5-24, for all materials, increasing the hydraulic pressure caused an increase in the ribbon surface temperature. Based on this, the first temperature profile, with higher temperature at the centre, could be explained as the stress applied at the centre of the ribbon is higher than the stress applied at the sides which caused the temperature to be higher at the centre compared to the sides. The pressure profile, ribbon density and porosity distribution across roller width had been investigated previously in different studies (Schönert and Sander, 2002, Miguélez-Morán et al., 2008, Miguélez-Morán et al., 2009, Cunningham et al., 2010, Lim et al., 2011, Michrafy et al., 2011, Muliadi et al., 2013). The general conclusion of these studies is the stress applied on the centre of the ribbon

is higher than the stress applied on the sides. For this reason the temperature profile for some material at some hydraulic pressure in Figs 5-26 and 5-27 followed this pressure distribution.

For the second temperature profile which is opposite to the previous one, higher temperature at the ribbon sides compared to the centre. This profile can be seen with the materials of medium hardness range (0.44- 0.7 GPa) at some hydraulic pressures.

For Avicel PH-101, the temperature profile of 18 bar is showing higher temperature at the centre than the sides. Then at 30 bar and above, the profiles are opposite and showing higher temperatures at the sides compared to the centre. This behavior believed to be due to the high friction between the ribbon and the side cheek plates. As Avicel PH-101 is plastically deformable powder, the particles deformed and produced wide ribbon of 40 mm width (see Figure 5-18) which is equal to the width of the roller. The powder or the ribbon pushed the side cheek plates and that caused high friction with the wall. The internal area of the cheek plate that contacts the powder or the ribbon was scratched or engraved due to the high friction with the ribbon side and as shown in Figure 5-28. The friction between the ribbon sides and the cheek plate generates heat and consequently increased the temperature at the ribbon sides to become higher than the temperature at the centre. This is the reason that caused heat generation at the sides. The ribbon width of Avicel PH-101 at hydraulic pressures 30 bar is 40 mm and it is even more than 40 mm at higher hydraulic pressures. This explains the high friction between ribbon and the side cheek plates.

For Glucidex<sup>®</sup>6, the temperature profiles at 18 and 30 bar are showing higher temperature at the centre than the sides. The ribbon width at these two hydraulic pressures, as it can be seen from Figure 5-18 are 37.3 and 38.8 mm respectively. At these two pressures, the stresses were not enough to produce full width ribbon so there was no friction between the ribbon and the side cheek plates and this is the reason for having normal temperature profile. At hydraulic pressures of 70 bar and above, the ribbons are wide with full width of the roller or more. This caused high friction with the cheek plates and consequently generates heat at the sides.

For Tylpor 604, at 18, 30 and 70 bar, the temperature profiles showing higher temperature at the centre than the sides. At hydraulic pressure of 100 bar and above, the temperature profiles are showing higher temperature at the sides compared to the centre. It can be noticed that the ribbons produced at 100 bar and above having the full width of 40 mm or more.

It can be concluded that under high pressure, the particles of plastically deformable material with medium hardness range between 0.44-0.7 GPa produce wide ribbon and that caused friction with the side cheek plates which consequently increased the temperature. That means the plastic deformation is indirect reason to increase the temperature during roller compaction process.

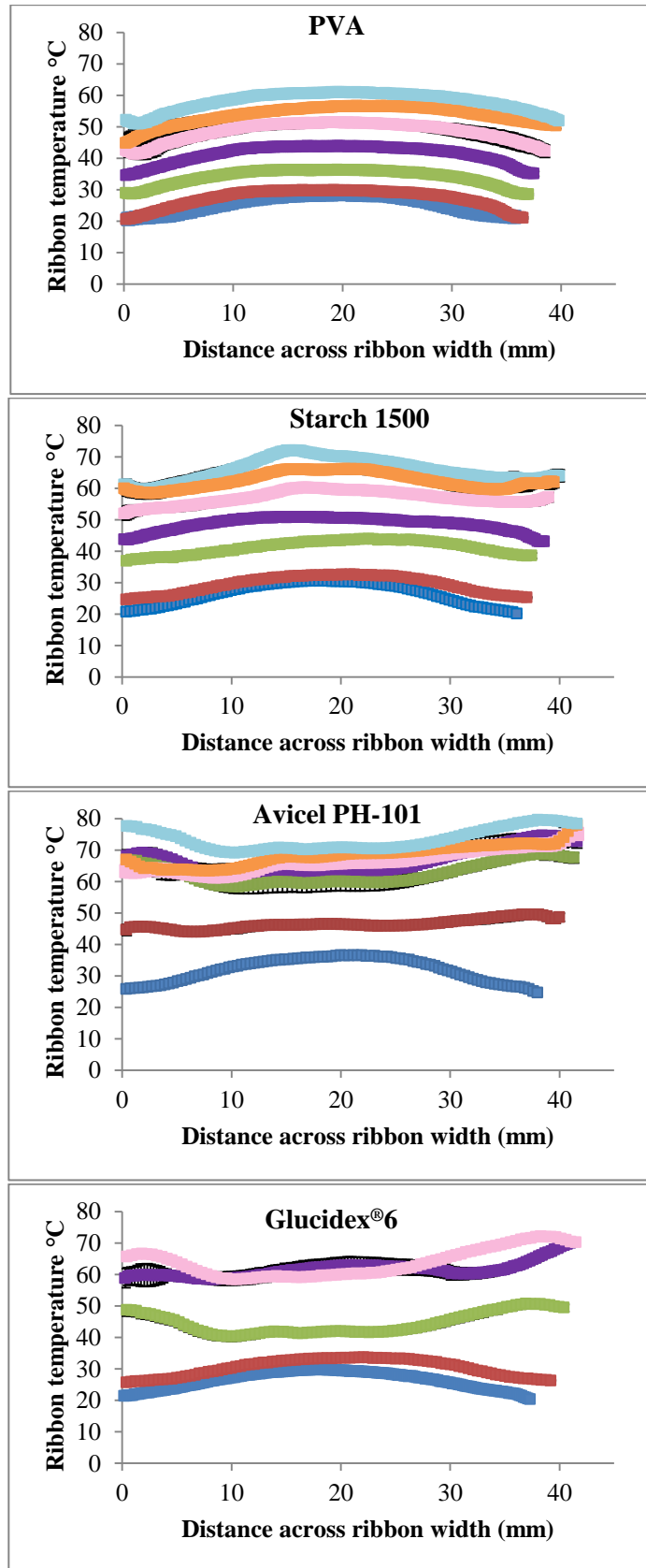


Figure 5-26: Temperature profile of different materials at different hydraulic pressures

■ 18 bar, ■ 30 bar, ■ 70 bar, ■ 100 bar, ■ 150 bar, ■ 200 bar, ■ 230 bar

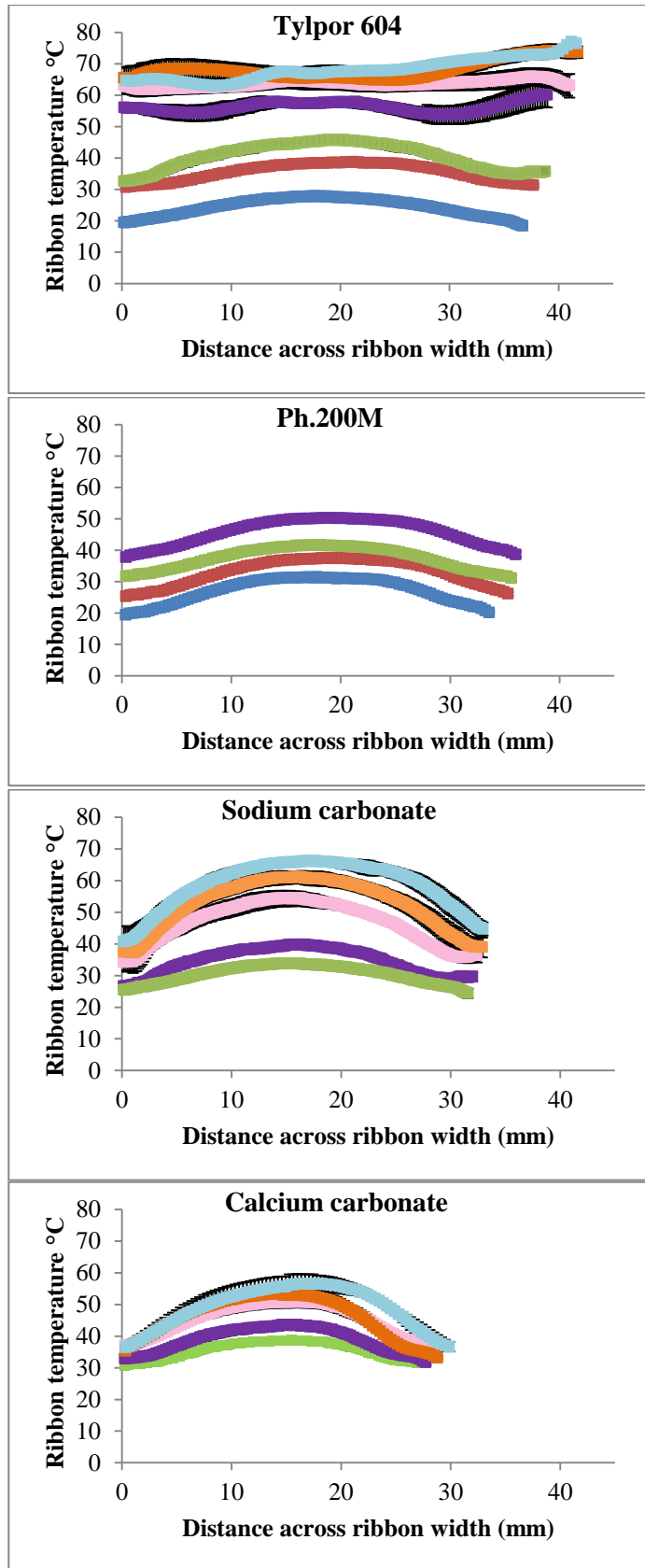


Figure 5-27: Temperature profile of different materials at different hydraulic pressures

■ 18 bar, ■ 30 bar, ■ 70 bar, ■ 100 bar, ■ 150 bar, ■ 200 bar, ■ 230 bar

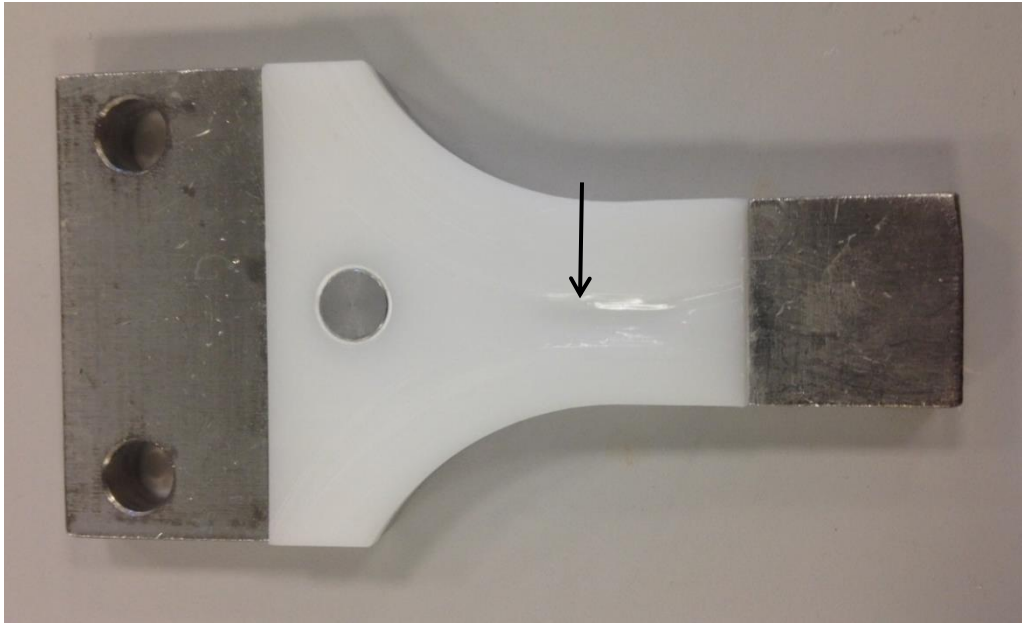


Figure 5-28: Scratched cheek plate due to the friction with the ribbon during roller compaction process

Based on previous discussion of different temperature profiles across the ribbon width, it is obvious that for some materials at some hydraulic pressures, the maximum temperature is caused by the friction with the cheek plates. In order to investigate the relation between the plastic deformation and the increase in the temperature during the roller compaction process it is more relevant to consider the temperature at the centre of the ribbon rather than the maximum temperature which could be at the sides.

Figure 5-29 shows the surface temperature at the centre of the ribbon for different materials, represented by their nano-indentation hardness, produced at different hydraulic pressures. It can be seen from the figure that the ribbon of Avicel PH-101 has the highest temperature among other materials for almost all hydraulic pressures. This could be due to the good deformability of this material even at low hydraulic pressure. At low pressure of 18 bar, the ribbon temperature of different materials are close to each other. At low pressure, the plastic deformation of the material is not significant. As it can be seen that even the partially deformable Pharmatose 200M produced ribbon with relatively high temperature. At 30 bar, temperature of PVA and starch are less than other materials. At this pressure, these two materials produced very weak ribbon with big amount of fines as it can be seen from Figure 5-3 and Figure 5-20 respectively. This is an indication of low plastic deformability of these two materials at low pressure and this is believed to be the reason behind the difference between the temperatures of these two materials with the temperature of other materials. At pressure more than 100 bar, the temperature of the ribbon produced by plastically deformable material with medium hardness range, 0.44-0.7 GPa, are almost the highest among other materials. It can be seen also that the temperature of the starch ribbon increased with increasing the hydraulic pressure more than the temperature of PVA and this is could be due to the plastic deformation of starch at high pressure. Figure 5-29 shows that the temperature of PVA and the hard materials, sodium carbonate and calcium carbonate are the lowest among other materials for all hydraulic pressures. PVA exhibited low plastic deformation due to the significant viscoelasticity as discussed in the next section. Sodium carbonate and calcium carbonate are hard materials so the plastic deformation is not significant.

The relation between the plastic deformation of the material and the rise in temperature has been investigated in different field, neither for compaction process nor for powder. Kapoor and Nemat-Nasser (1998) and Hodowany et al. (1999) confirmed this relation between the high strain plastic deformation of different metal alloys and the increase in the temperature. Rittel (1999) confirmed the same relation but for glassy polymer. These studies showed that part of the mechanical energy of plastic deformation is converted to a heat.

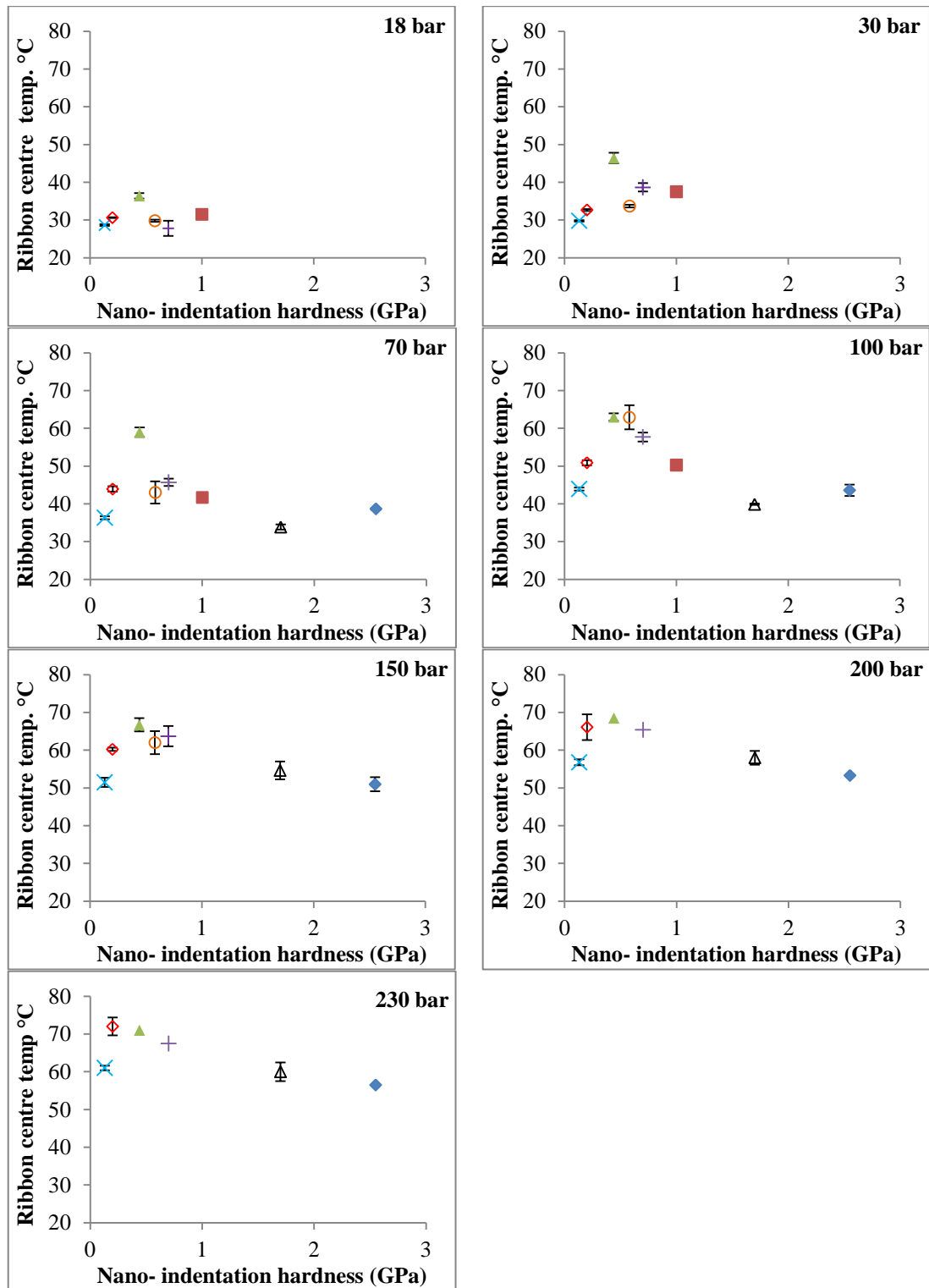


Figure 5-29: Temperature of the ribbon centre for different materials at different hydraulic pressures

× PVA, ◇ Starch 1500, ▲ Avicel PH-101, ○ Glucidex®6, + Tylpor 604, ■ Pharmatose 200M, △ Sodium carbonate, ◆ Calcium carbonate

### 5.3.5 Investigating the behaviour of the low hardness material (PVA and starch)

The SEM images of PVA and starch in Figures 5-6 and 5-8 respectively suggest that the particles of these two materials did not experience significant plastic deformation especially at low hydraulic pressures despite the low nano-indentation hardness. This unexpected behaviour resulted in producing narrow and weak ribbons with relatively big amount of fines.

PVA and starch are both polymers. Polyvinyl alcohol is synthetic polymer whereas the starch is natural. It has been reported by Rees and Rue (1978) that the plastic deformation of starch is time dependant. This means holding the load for longer time will cause more plastic deformation of the powder. Palzer (2011) stated that starch is one of the materials that behave viscoelastically under low speed of compression and one of the important factors to cause plastic deformation is the dwell time. Chang et al. (2008) investigated the roller compaction of the pregelatinized starch. They showed that starch produced weak ribbon at low pressure but the strength improved too much upon increasing the pressure. They attributed this to the viscoelasticity of this material. At low pressure it exhibit elastic deformation rather than plastic deformation.

Different forms of PVA, such as sponge, showed different mechanical properties upon compressing using different strain rates (Karimi et al., 2014, Wang et al., 2001). This is an indication of viscoelastic behaviour.

Heiman et al. (2015) stated that using high roller speed in roller compaction process led to produce weak ribbon. This is especially pronounced with plastically deformable materials (Wu et al., 2010). This may indicates that the plastically deformable materials are viscoelastic as well.

In order to investigate the viscoelasticity of the powder, several methods have been used in the literatures (Malamataris et al., 1992). One of the methods is applying a load on a powder bed and holding the punch at constant position and measure the decrease in the force with time (David and Augsburger, 1977). Another method is using different loading rates and measure the difference in the height and the strength of the compact (Malamataris et al., 1992). The creeping behaviour of the powder was also used to indicate the viscoelasticity of the powder which includes holding a constant stress on the powder bed over a period of time and measure the difference in the height of the compact (Staniforth and Patel, 1989).

The main experiments of the roller compactor in this study were carried out at roller speed of 3 rpm. Consequently, the tip speed of the roller of 120 mm diameter is 1130 mm/min. This could be considered as a compaction speed by assuming that the powder is moving at the same speed as the roller.

On the other hand, the nano-indentation test was carried out using loading time of 5 seconds. The penetration rate of the tip could be determined by dividing the maximum displacement before starting holding the load (see Figure 4-9) by loading time. For PVA, the displacement is around 150 nm so the loading rate is 0.0018 mm/min. The displacement of the starch is 140 nm so the loading rate is 0.00168 mm/min.



This big difference between the compaction rate in the roller compactor and the penetration rate in the nano-indenter may cause a difference in the mechanical behaviour of the material if it is showing significant viscoelasticity.

The viscoelasticity of all materials used in this study was investigated. The lower roller speed of the roller compactor used in this study is limited to 3 rpm. This speed is already been used in the experiments. On the other hand, the nano-indenter works with limited loading rate. For these two reasons, uniaxial compression of a powder bed was used instead to investigate the viscoelasticity of the materials. The test has been carried out using material testing machine, Instron 3367, with a wide range of loading rate.

### **5.3.5.1 Viscoelasticity experiment**

To investigate the viscoelasticity of the materials, the creeping behaviour of the powder under constant stress for a specific time was considered. The creep is the displacement of the powder bed during applying a constant load for period of time (constant stress over time). The creep was investigated using two loading rates; 0.01 mm/min. and 100 mm/min. The test involved compressing 0.2 gram of powder in a die of 10 mm diameter and 10 mm height. For the two loading rates; the punch moved down until the force arrived to 3000 N. Then the load kept constant at 3000 N for 2 hours. Figure 5-30 shows the force displacement curves resulted from the test. The y-axis is the applied force and the x-axis is the powder bed displacement. The figure compared the compaction of the powder bed using two loading rates. In addition, the creep (extension) of the powder bed while holding the maximum load for two hours is also shown in the figure.

It can be seen from the figure that for all materials and for the most force values, the displacement of the powder bed at low loading rate is high compared to the displacement using high loading rate. Table 5-5 shows the difference in the in-die powder bed height of different loading rates at maximum load for all materials. It can be seen from the table that PVA and starch showed the largest difference. Upon applying the load at low rate, more time was available for the particles to rearrange their positions in the bed. In addition, more time may cause more elastic and plastic deformation in addition to the fracture. For these reasons, the difference in the height of the bed could not be considered due to the plastic deformation only.

The second observation that could be seen from the figure is that the creep of PVA and starch are large compared to other materials. This is the case for both used loading rates. Table 5-6 shows the creep values for all powders at two different loading rates. It can be seen from the table that the material of low nano-indentation hardness showed more creep and the opposite for hard materials. According to the results, PVA and starch showed the largest creep (viscoelasticity) among other materials. It can be noticed from the table that the creep value is low with using low loading rate and it is high with using high loading rate. Upon using low loading rate, the material have more time to deform plastically during the loading time so it will deform less during holding time. This is not the case with using higher loading rate where the material experienced less plastic deformation and showed more plastic deformation during load holding time.

The above results may explain why the PVA and starch did not produce strong ribbon especially at low hydraulic pressures. Due to the viscoelasticity of these two materials, the

loading rate during roller compaction process was too high to cause enough permanent plastic deformation to produce strong ribbon.

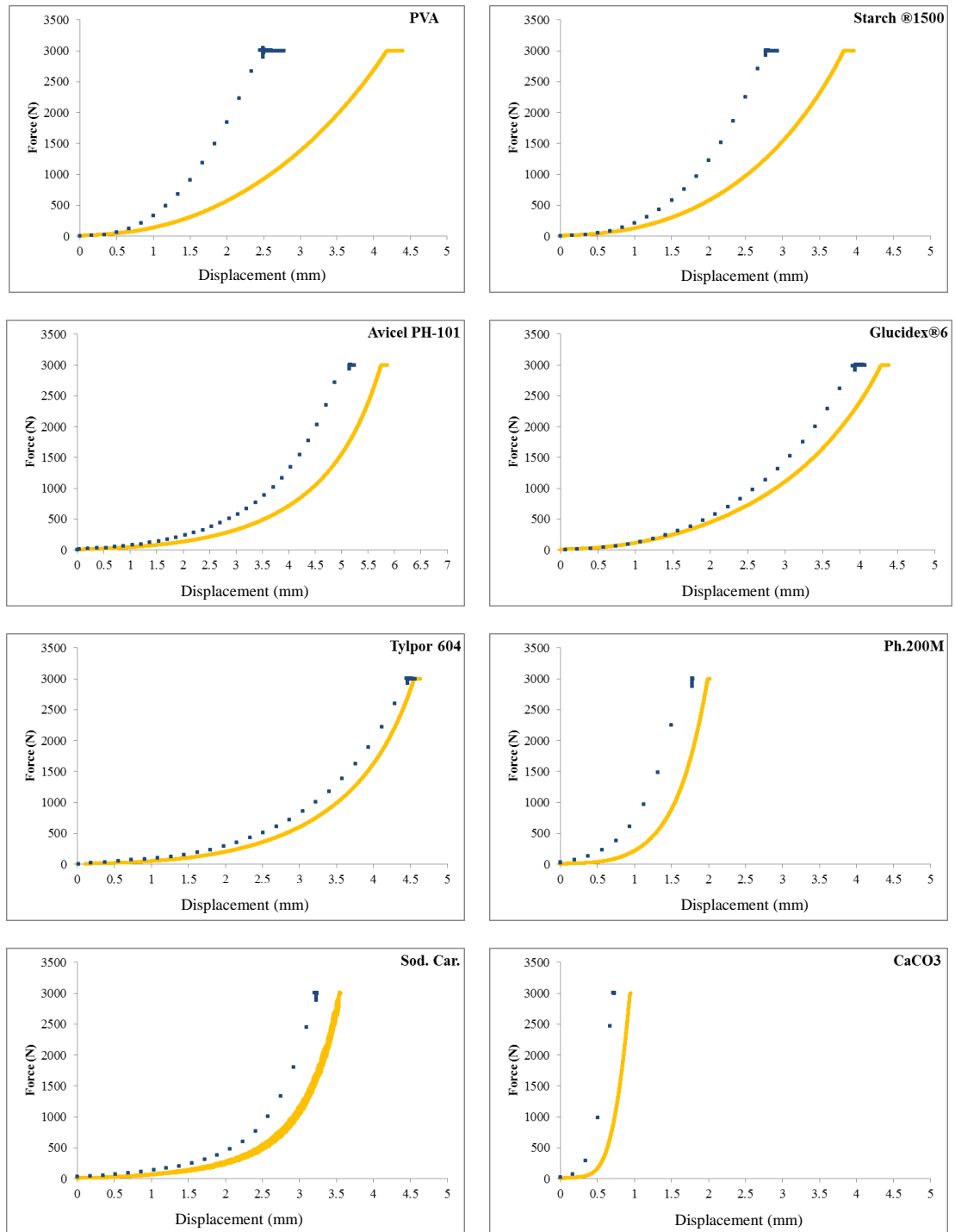


Figure 5-30: Compression of different powders at different strain rates with holding maximum load for 2 hours (■ 100 mm/min. ■ 0.01 mm/min.)

Table 5-5: The difference between the displacements at maximum load for the two different loading rates

<b>Material</b>	<b>Difference in the displacement (mm) at maximum load (3000N) (displacement at 0.01 mm/min - displacement at 100 mm/min)</b>
PVA	1.677
Starch 1500	1.057
Avicel PH-101	0.594
Glucidex®6	0.346
Tylpor 604	0.077
Pharmatose 200M	0.209
Sodium carbonate	0.308
Calcium carbonate	0.231

Table 5-6: Creep of different powders at different loading rates

<b>Material</b>	<b>Nano indentation hardness (GPa)</b>	<b>Creep at 100 mm/min (mm)</b>	<b>Creep at 0.01 mm/min in (mm)</b>
PVA	0.13	0.268	0.219
Starch1500	0.24	0.156	0.135
Avicel PH-101	0.44	0.132	0.118
Glucidex®6	0.58	0.122	0.100
Tylpor 604	0.7	0.094	0.082
Pharmatose 200M	1	0.025	0.004
Sodium carbonate	1.7	0.02	0.001
Calcium carbonate	2.55	0.015	0.001

The creep of different materials at 0.01 mm/min that listed in Table 5-6 are permanent as investigated by measuring the out-die height of the bed before and after holding the maximum load for two hours. The creep at 100 mm/min is not permanent because the bed height before holding the load was recovered but after holding the load, the height did not change. With using a high loading rate of 100 mm/min, the viscoelastic materials deformed less and according to the available time limit of holding the load.

In order to investigate whether the difference in the bed height in Figure 5-30 is reversible or permanent, there is a need to compare the out die compact heights, after removing the load,

produced by two different loading rates. Table 5-7 shows the difference in the height and the strength of the compacts produced by different loading rates. The difference in the height is determined by subtracting the out die height of the compact produced at 0.01 mm/min from the height of the compact produced at 100 mm/min. The strength of the compact was determined according to the following equation;

$$\text{compact strength} = \frac{2F_{\text{comp.}}}{\pi D_{\text{comp.}} H_{\text{comp.}}} \quad \text{Eq. 5-1}$$

Where

compact strength in MPa

$F_{\text{comp.}}$  The force required to break the compact in Newton

$D_{\text{comp.}}$  Diameter of the compact in mm

$H_{\text{comp.}}$  Height of the compact in mm

It can be seen from the table that PVA and starch showed big difference in both the height and the strength of the tablets which is suggesting that compaction behaviour of these two materials are significantly affected by the loading rates. Some materials showed a difference in the tablet height but insignificant change in the tensile strength such as Avicel PH-101, Glucidex<sup>®</sup>6, Tylpor 604 and Pharmatose 200M. Some materials did not show neither change in the height nor in the tablet strength such as sodium carbonate and calcium carbonate.

Table 5-7: The difference in the height and strength of the compacts produced by different loading rates

Material	Difference in height of the compacts produced by 0.01 mm/min. and 100 mm/min. (mm)	Difference in the strength of the compacts produced by 0.01 mm/min. and 100 mm/min. (%)
PVA	0.8	566
Starch 1500	0.7	309
Avicel PH-101	0.3	4
Glucidex <sup>®</sup> 6	0.2	4
Tylpor 604	0.23	2
Pharmatose 200M	0.12	0
Sodium carbonate	0	0
Calcium carbonate	0	0

## **5.4 Measuring the nano indentation hardness of the ribbon**

Reducing the tableability is one of the reported problems of the granules produced by roller compactor (Herting and Kleinebudde, 2008, Sun and Kleinebudde, 2016). Different studies investigated the reason behind this behaviour. One of the main reported possible reasons is the work of hardening that happening during the roller compaction which reduces the plastic deformation of the granules compared to raw primary powder. Herting and Kleinebudde (2008) measured the yield strength of the granules resulted from crushing the ribbons that produced at different compaction pressures. They showed that the yield strength of the granules increased as the roller compaction pressure increased. They explained this as a work of hardening effect. The yield strength was determined by uniaxial die compression using Heckel's approach. The granules are usually larger than the primary powder with less surface area. This makes the comparison of the yield strength for both primary powder and granules difficult as there might be an effect of particle size in addition to the effect of the plastic deformation (Sonnergaard, 1999). Both could be responsible for changing the yield strength. There is a need to use a relevant method to trace the change in the plastic deformation only of the powder after being roller compacted.

The main aim of the study in this section is to measure the nano-indentation hardness of the ribbons produced at different hydraulic pressures of 30, 70, 100, 150, 200 and 230 bar. Three materials were investigated; Avicel PH-101, Pharmatose 200M and calcium carbonate. These materials were chose to represent plastically deformable, partially plastic/brittle and hard/brittle material respectively. The ribbons of three materials were produced using the same experiment that was described in Section 5.2.

### **5.4.1 Preparing the ribbon to nano indentation test**

To keep the ribbon stable and flat during the nano-indentation test, the ribbons were mounted in a resin and hardener. Two volumes of resin mixed with one volume of hardener. Both materials are KEP Epoxy type supplied by Kemet, UK. These two materials were chose as both of them are used for cold mounting so they are suitable for materials that are sensitive to the heat. Both materials were mixed until getting a homogeneous mixture. Then the mixture poured in a plastic die where the ribbon placed at the bottom. This process is carried out in specially designed evacuated system to remove undesirable air bubble that generat during pouring the mixture. The air bubble might disturb the structure of the mold and consequently affect the nano indentation test. The hardening time for the mixture is 10 hours at 25 °C (Kemet, 2016). Figure 5-31 shows mounted ribbons.

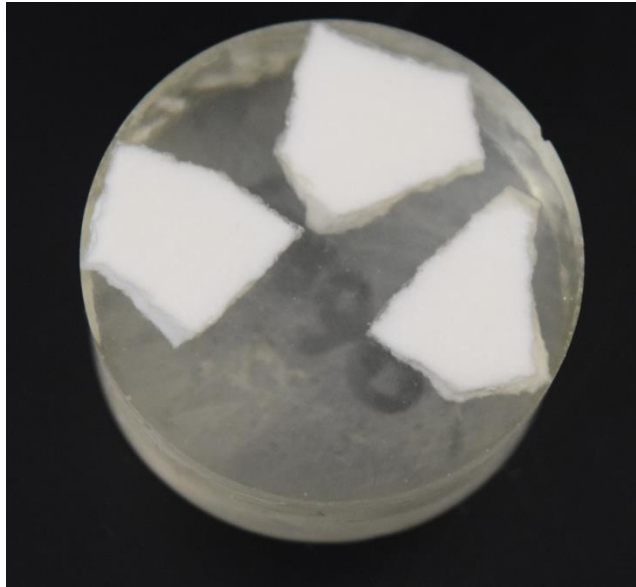


Figure 5-31: Ribbon mounted and prepared for nano indentation test

#### 5.4.2 Measuring the nano indentation hardness

The same Berkovich tip and the same load of 200  $\mu\text{N}$  were used to indent the ribbon surface to determine the nano-indentation hardness. The only difference between the ribbon and the single particle is that the ribbon surface may have bridges that bond the particles to each other and it is not clear whether these bridges have the same hardness of the particle or not. For this reason and to cover big area, the ribbon was divided into five areas of 20  $\mu\text{m}^2$  each. The distance between each area and another is at least 1 cm. During the test, each area had 9 indents so the total number of indents was 40 for each material. This was done by creating an automatic script using the software of the nano-indenter. The determined hardness was averaged for these 40 tests.

#### 5.4.3 Results and discussion

Figure 5-32 shows the measured hardness of the ribbon produced by different materials at different hydraulic pressures. It can be seen from the figure that for Avicel PH-101, the hardness of the ribbon produced at 30, 70 and 100 bar is 0.44 GPa which is equal to the hardness of the single primary particles that listed in Table 4-2. Further increase in the pressure caused an increase in the hardness of the material. The hardness of the ribbon produced at 230 bar is 0.55 GPa so the total change in the ribbon hardness compared to the primary powder is 25 %.

For Pharmatose 200M, There was no change in the hardness of the ribbon at 30, 70 and 100 bar. The ribbon produced at higher pressure was not suitable for analysis due to the presence of crack on the surface.

For calcium carbonate, it can be seen that there is a small change in the hardness of the ribbon at 200 and 230 bar. The maximum change in the ribbon hardness compared to the primary powder is 7 % but if the error bar taken into consideration it can be seen that there is almost no change in the hardness.

It can be concluded that the ribbon hardness of plastically deformable materials increased at certain compaction pressure compared to the hardness of the primary particle. The hardness of the hard material is almost the same even after compacted at high pressure.

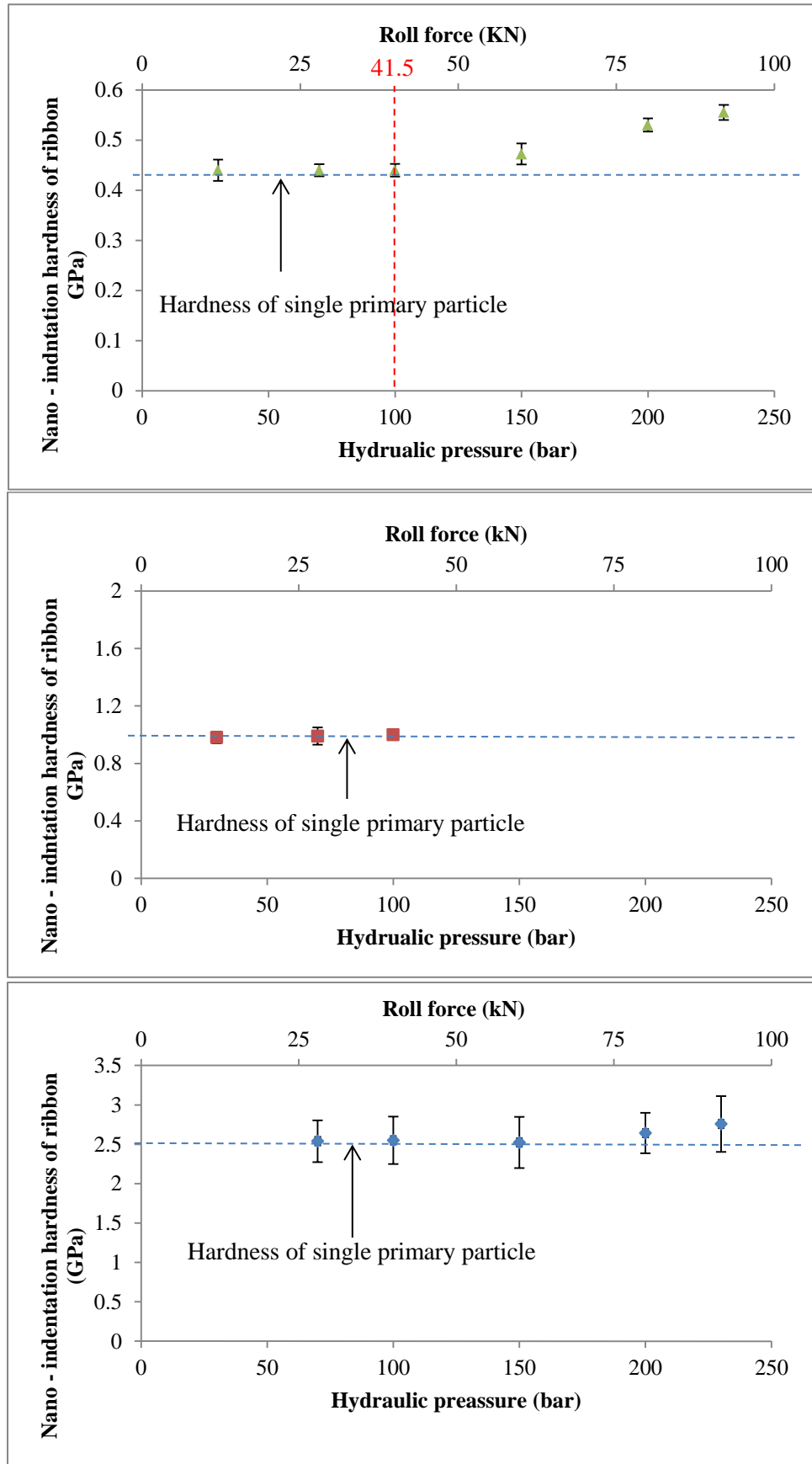


Figure 5-32: Nano- indentation hardness of ribbon produced by different materials at different hydraulic pressures



The results in Figure 5-32 can be more useful and used universally regardless of the used roller compactor if only the hydraulic pressure is converted to stress that applied at the material. For this reason, Johanson’s theory was used to determine the maximum stress at each hydraulic pressure. The accuracy of Johanson’s theory to determine the maximum stress applied to the material was validated by Bindhumadhavan et al. (2005). It was shown that the theory is quite accurate in determining the maximum stress applied on the materials. The details of the calculation are explained in Section 2.5.1.1. The first step is determining the nip angle for the three materials. The determined nip angle for Avicel PH-101 is equal to 21° whereas it is equal to 10 and 8° for Pharmatose 200M and calcium carbonate respectively. Then, the maximum stress applied at the material was determined using Eq. 2-21. Table 5-8 summarizes the results.

Table 5-8: Maximum normal stress applied to the material at different hydraulic pressure

Hydraulic pressure (bar)	Roll force (kN)	Maximum normal stress applied on the materials by the rollers (GPa)		
		Avicel PH-101	Ph.200M	Calcium carbonate
20	8.29	0.021	0.05	0.052
30	12.44	0.0315	0.075	0.078
40	16.59	0.042	0.1	0.104
60	24.88	0.063	0.150	0.155
70	29.03	0.073	0.176	0.181
80	33.17	0.084	0.201	0.207
100	41.47	0.105	0.251	0.259
120	49.76	0.126	0.301	0.311
140	58.05	0.147	0.351	0.362
150	62.2	0.157	0.376	0.388
160	66.35	0.168	0.401	0.414
180	74.64	0.189	0.451	0.466
200	82.94	0.210	0.501	0.518
215	89.16	0.226	0.539	0.557
230	95.38	0.241	0.577	0.595

### 5.5 Comparing the maximum stress with the yield stress

The two accepted mechanisms of powder compaction are plastic deformation and/or fracture. For these two processes to happen, the particles of the powder need to exceed the yield point.

By comparing the values of the yield stress of the material listed in Table 4-4 with the maximum applied stress during roller compaction process that listed in Table 5-8. It can be seen that the applied stress on Avicel PH-101 during the roller compaction is higher than the yield stress of the material at hydraulic pressure of 20 bar and above. The yield stress of

Avicel PH-101 particles is 0.007 GPa. By comparing this number to the applied stress listed in Table 5-8, it can be seen that even at 20 bar, the applied stress is higher than the yield stress by 3 times and this increase with increasing the applied stress. This may explain why the ribbons of Avicel PH-101 are strong at almost all the applied pressure. For Pharmatose 200M, the particles start to yield around 60 bar. The yield stress of Pharmatose 200M is 0.168 GPa. It can be seen that at pressure of 140 bar, the applied stress is only double the value of yield stress which might explain why the strength of the Pharmatose 200M ribbon is weaker than the MCC.

For calcium carbonate, the maximum stress applied for all hydraulic pressures are less than the yield stress of the material except at 230 bar where the stress is close to the yield. This also might explain why the ribbon of calcium carbonate is too weak compared to other materials.

## 5.6 Conclusion

This study showed that the plastic deformation of the powder undergoing roller compaction is important and plays an important role in controlling the strength of the compact. In addition, the results showed that the nano-indentation hardness and viscoelastic behaviour are both important to indicate the plastic deformation of the powder.

It was found that the powder with very low or high nano-indentation hardness produce weak ribbons especially at low pressures. The best ribbons were produced by plastically deformable materials with medium range of nano-indentation hardness.

Materials with very low hardness showed significant viscoelastic behaviour. The particles of these materials did not exhibit significant plastic deformation under high compaction rate, which used in the roller compactor, compared to the low penetration rate used in the nano-indentation test. For these materials, caution needs to be taken when using nano-indentation hardness as an indication of plastic deformation for the roller compaction process.

On the other hand, brittle materials produced weak ribbon compared to plastically deformable materials and this suggests that the plastic deformation of the particle is more important than the fracture in controlling the product quality.

The study showed that the increase in the temperature during roller compaction process is affected by hydraulic pressure. For this reason, for some materials, the temperature can be used instead of pressure as an online indication of the stress that applied on the powder. It is also shown that the nano-indentation hardness of the single primary particle is related to the temperature profile across the ribbon width. Using high hydraulic pressure to process plastically deformable materials could cause a significant increase in the temperature.

Based on the results of this chapter, the nano-indentation hardness and the viscoelastic behaviour of the powder could be used as a good tool to predict the behaviour of the powder undergoing roller compaction and consequently predicting the ribbon properties.

The results of this study suggest using the creep values to relatively characterise the mechanical properties of the powders since it is related to the nano-indentation hardness of the material.

This chapter investigated the effect of the mechanical properties of the primary particles on the different ribbon properties. This is the first step that helps choosing the right formula for

the roller compaction process. The next chapter will investigate the behaviour of the primary powder in the slip and nip zones using Avicel PH-101 as a feed.

# Chapter 6 Determining the nip angle and powder compaction progress

## 6.1 Introduction

Understanding the behaviour of the powder undergoing roller compaction is important for the industry as it will improve the design and the scaling up of the equipment to achieve required product quality. The maximum stress acting on the powder in addition to the nip angle and stress distribution between the rollers are important parameters in the compaction process (Guigon et al., 2007). It has been shown that the average ribbon density depends on the maximum applied stress and the nip angle (Miguélez-Morán et al., 2008). Knowing these two values and keep it constant is essential for the scale up of the roller compactor to get the same product quality (Allesø et al., 2016).

Many approaches were proposed to determine the stress distribution acting on the materials between the rollers and to determine the nip angle as described in Section 2.5.1. However, Johanson's theory is the first and the most commonly used method as it needs measuring some powder flow properties and compressibility to determine the nip angle and then the maximum stress. On the other hand and in order to determine the stress distribution acting on the powder between the rollers, there is a need to measure the stress at the nip angle which is difficult (Bindhumadhavan et al., 2005).

Despite the valuable and pioneering contributions in the literatures, there is still a need to study the compaction process in more details due to the discrepancies and challenges in previous works. For instance, the mechanical properties of the powder and the friction between the particle- particle and the particle- roller surface are suggested to play an important role in the compaction process. However, measuring the friction properties of the powder by the shear cell does not simulate the actual powder situation in the roller compactor and the geometry/material of the roller surface (Bindhumadhavan et al., 2005). In addition, Johanson's theory for example does not take in consideration the effect of roller speed on the nip angle and on the maximum stress applied on the powders.

Hence, in this study an alternative new method has been suggested to determine the nip angle, by measuring the mechanical properties of the real pre-compacted body of Avicel PH-101 (Al-Asady et al., 2016). The results were used to explain how the process parameters affect different properties of the ribbon such as width, strength and temperature in addition to the amount of un-granulated powder, fines, during the roller compaction process.

## 6.2 Material properties of Avicel PH-101

Microcrystalline cellulose, Avicel PH-101, was used as a primary powder in the roller compaction experiments. The particle size distribution of the powder is shown in Figure 6-1. The y- axis of the curve is the cumulative undersize distribution based on volume and the x- axis is the particle size in micrometre. The  $D_{10}$ ,  $D_{50}$  and  $D_{90}$  are 21, 62 and 122  $\mu\text{m}$  respectively. The mean value for the sphericity is 0.749. The SEM image of the particles is the same that shown in Figure 3-3 in Section 3.1.3.

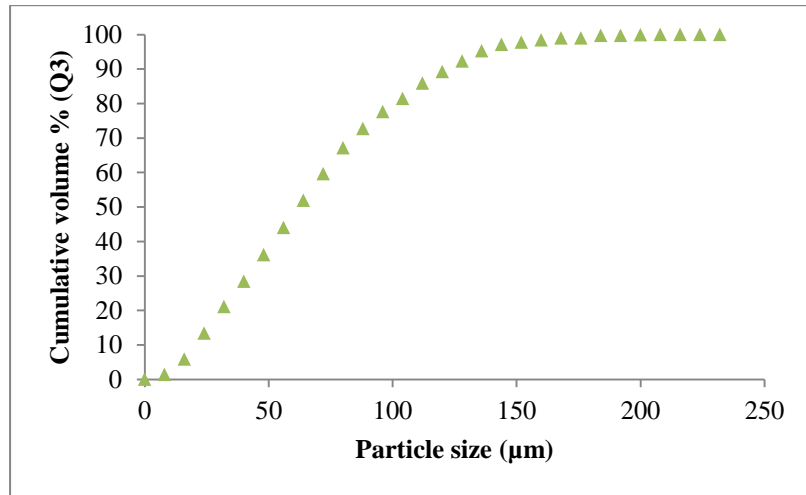


Figure 6-1: Particle size distribution of the Avicel PH-101

As mentioned previously in Section 2.5.1, Johanson’s theory can be used to determine the nip angle and the maximum stress applied on the powder. To apply this theory, powder flow properties and compressibility factor should be determined.

A ring shear cell tester (Schulze RST-XS, Germany) was used to measure the flow properties (effective angle of internal friction,  $\delta_E$ , and angle of wall friction,  $\phi_w$ ) of the Avicel PH-101 powder and as described in more details in Section 3.2.3.1.

The compressibility factor (K) was determined by the method that described in Section 3.2.3.3 using the logarithmic plot of the pressure versus bulk density (Figure 6-2) and according to Eq. 2-19.

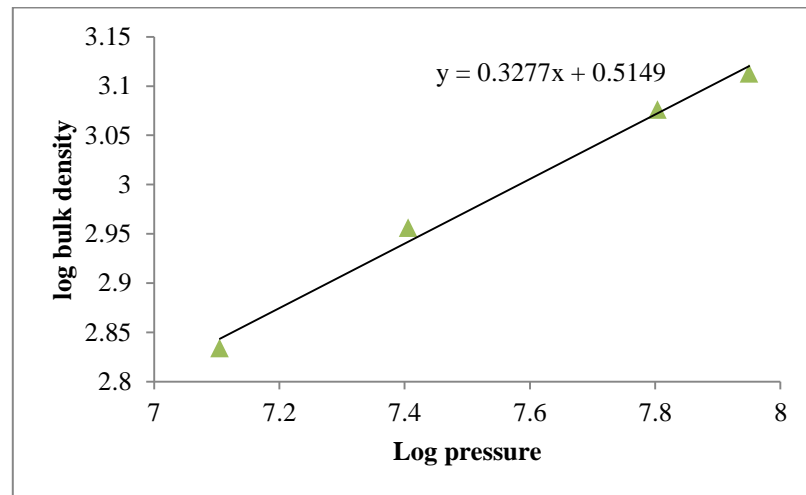


Figure 6-2: Pressure density relationship

Table 6-1 shows the compressibility factor and the determined flow properties of the Avicel PH-101 in addition to the true density of the powder as supplied by the manufacturer.

Table 6-1: Flow properties and compressibility factor of the Avicel PH-101 primary powder

Effective angle of internal friction ( $\delta_E$ )°	Angle of wall friction ( $\phi_w$ )°	Compressibility factor (K)	True density (Kg/m <sup>3</sup> )
36.4	27.2	3	1561

### 6.3 Calculation the nip angle by Johanson's theory

The material properties that listed in Table 6-1 were used along with Johanson's theory to determine the nip angle for different process conditions.

Johanson (1965) suggests that the pressure gradients in the slip and nip regions are equal at the nip angle so the nip angle can be found by solving the following equation:

$$\left(\frac{d\sigma}{dx}\right)_{Slip} = \left(\frac{d\sigma}{dx}\right)_{Nip} \quad \text{Eq. 2-20}$$

Using Eq. 2-15 and Eq. 2-18, the above equation can be written as follows:

$$\frac{4\sigma_\theta \left(\frac{\pi}{2} - \theta - \nu\right) \tan\delta_E}{\frac{D}{2} \left(1 + \frac{G}{D} - \cos\theta\right) \cot(A - \mu) - \cot(A + \mu)} = \frac{K\sigma_\theta \left(2\cos\theta - 1 - \frac{G}{D}\right) \tan\theta}{\frac{D}{2} \left[\frac{d}{D} + \left(1 + \frac{G}{D} - \cos\theta\right)\cos\theta\right]}$$

Where  $\theta$  is the angular position at the roller surface,  $G$  is the roller gap,  $D$  is the roller diameter,  $d$  is the depth of roller indentation and the parameter  $A$  is defined by following equation:

$$A = \frac{\theta + \nu + \frac{\pi}{2}}{2} \quad \text{Eq. 2-16}$$

Where  $\nu$  is an acute angle between the tangent to the roll surface and the direction of the major principal stress ( $\sigma_1$ ) (Figure 2-4) and it is given by

$$\nu = \frac{1}{2} \left( \pi - \sin^{-1} \frac{\sin\phi_w}{\sin\delta_E} - \phi_w \right) \quad \text{Eq. 2-17}$$

And  $\mu$  can be calculated by the following equation:

$$\mu = \frac{\pi}{4} - \frac{\delta_E}{2}$$

The values for the parameters mentioned in the previous equations are listed in Table 6-2.

Table 6-2: The values of the parameters used to calculate the nip angle

Effective angle of internal friction, $\delta_E$ (radians)	0.64
Angle of wall friction, $\phi_w$ (radians)	0.47
acute angle between the tangent to the roll surface and the direction of the major principal stress, $\nu$ (radians)	0.89
Roller gap, $G$ (m)	0.003
Roller diameter, $D$ (m)	0.12
$\mu$ (radians)	0.48
Compressibility factor, $K$	3
Roller indentation depth, $d$ (m)	0.002
Roller width, $W$ (m)	0.04

Figure 6-3 shows the pressure gradient at the slip zone (The left side of Eq. 2-20) and the nip zone (The right side of Eq. 2-20) as a function of angular roll position. The pressure gradients are equal only at the nip angle (Johanson, 1965) so the angular position at which the two curves intersect is the nip angle. The determined nip angle from this figure is 21°. According to Johanson’s theory, this angle is the same for different hydraulic pressures and different roller gaps as the effect of changing the gap is too small and it does not change the term  $G/D$  in Eq. 2-20 significantly.

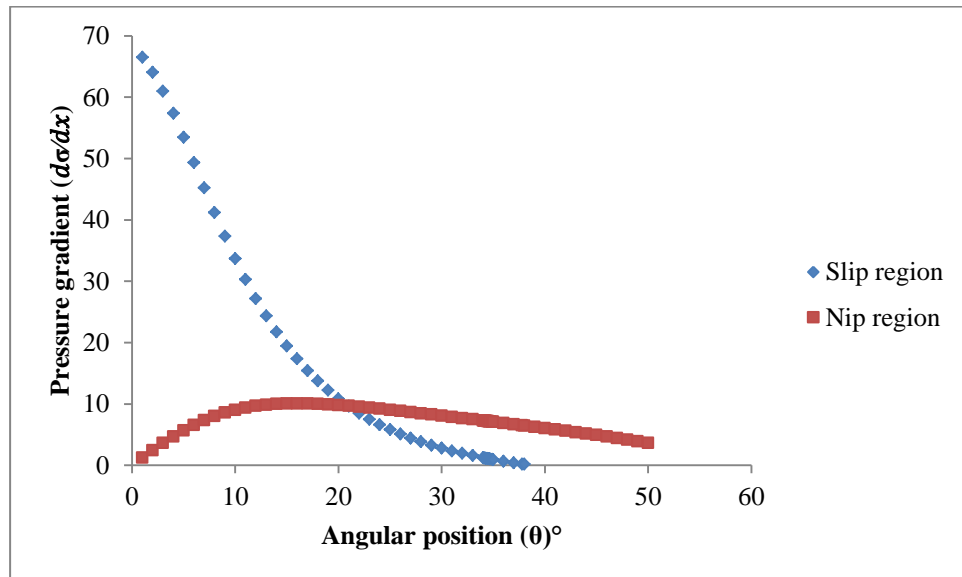


Figure 6-3: The pressure gradients at slip and nip zones as a function of angular roll position

## 6.4 Production of the pre-compacted body

The pre-compacted body, as shown in Figure 6-4, is defined as the powder or the compact in the space between the rollers, which starts at the beginning of the contact between the powder and the roller and ends at the minimum gap/separation between the two rollers as shown in Figure 6-5.



Figure 6-4: Pre-compacted body of Avicel PH-101 and the ribbon

Figure 6-5 shows also different angular roll positions at which the indentation by Shore A hardness tester has been carried out. Angle zero, which corresponds to a minimum gap between the two rollers, was determined using Bosch PCL-10 cross line laser level which produces cross laser line. The vertical line aligned with the roller centres and as shown in Figure 6-6. This will ensure precise determination of all other angular roll positions. The other angles were then determined using tangent inverse function.

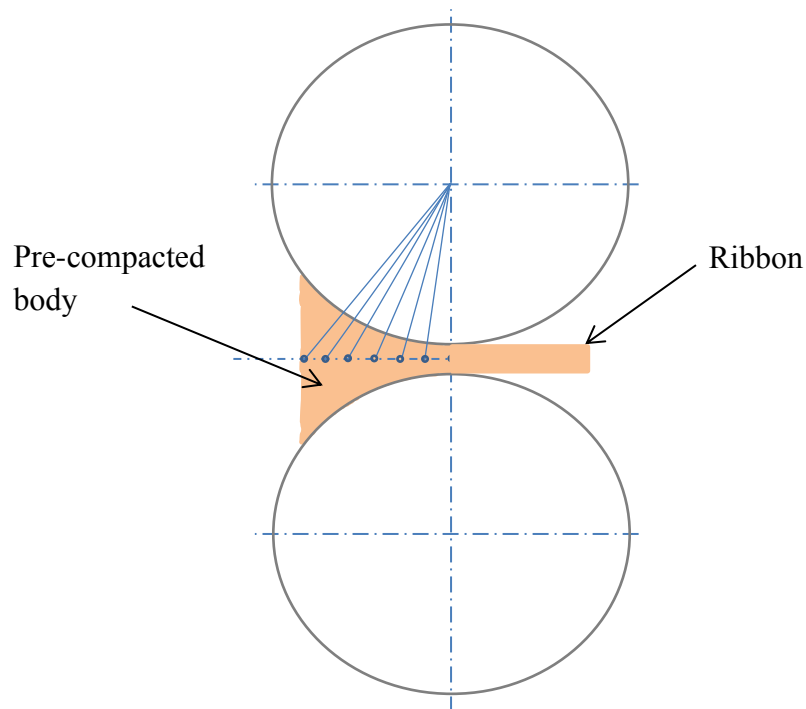


Figure 6-5: Indentation of the pre-compacted body at different angular roll positions



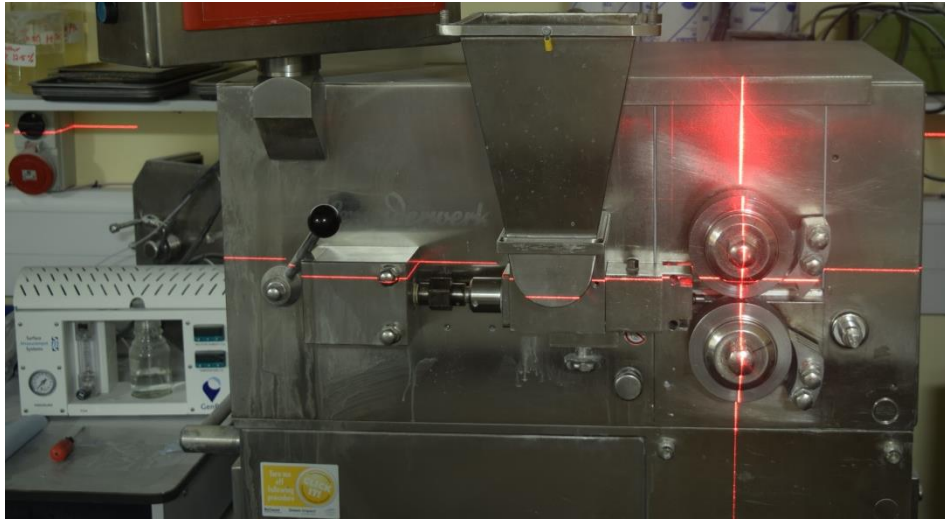


Figure 6-6: Cross line laser level

Prior to ribbon production, the powders were conditioned in humidity chamber at 40% RH and 20 °C as explained in Section 3.1.9. This is to remove the effect of different relative humidity in the store or in the laboratory which might affect the compaction behaviour and the flowability of some powders and as shown by different studies (Wu et al., 2010, Osborne et al., 2013, Omar et al., 2016). The powder conditioned to 40 % RH because it is close to the humidity of the laboratory so it is easy to maintain the humidity during the experiment.

Humidity generator was used to maintain the humidity during roller compaction experiment as explain in Section 3.3. In this study, the effect of three parameters: roller speed, hydraulic pressure and roller gap were investigated. Table 6-3 shows the experimental design for three different sets. It is worth to mention that the automatic feedback system that keeps the roller gap constant was switched on for all the experiments in this study.

Table 6-3: Experimental design of roller compactor experiments

Set title	Hydraulic pressure (bar)	Roll speed (rpm)	Roll gap (mm)
Effect of roll speed	Constant at 70	3,4,5,6 and 7	Constant at 1.5
Effect of hydraulic pressure	18, 30, 70, 100, 150, 200 and 230	Constant at 3	Constant at 1.5
Effect of roll gap	Constant at 70	Constant at 3	1, 1.5, 2 and 2.5

## 6.5 Characterisation of the pre-compacted body and ribbon

### 6.5.1 Mechanical properties (Hardness)

The mechanical properties of the pre-compacted body were measured using Shore A digital hardness tester supplied by Omnitron, UK. The tester is manufactured to meet the DIN, ISO and ASTM standards. Shore A tester produces hardness value between 0 and 100 with resolution of 0.1.

The Shore hardness is an indication of the resistance of the material to indentation. The indentation is carried out by pushing protruding tip, connected to a spring, of 0.79 mm diameter against the body under test until a firm non-destructive contact between the interface panel of the tester and the body is achieved. Figure 6-7 (a) shows the tip shape and the dimension of the Shore A hardness tester and Figure 6-7 (b) shows the tip when pushed against the body.

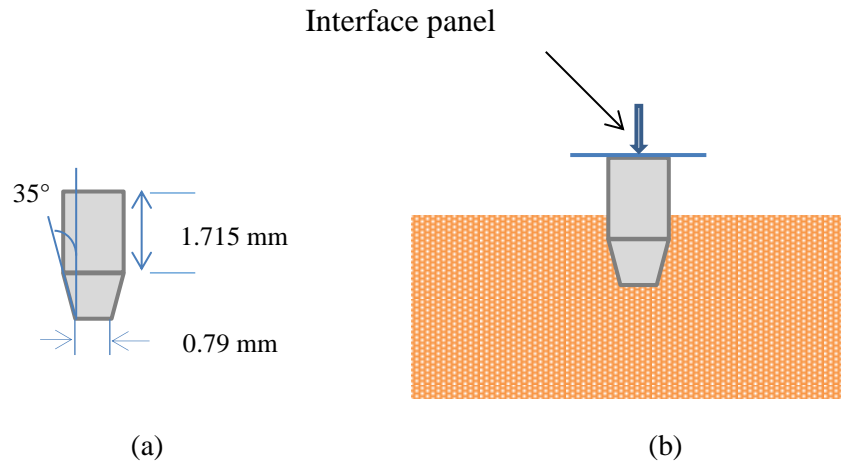


Figure 6-7: Dimension and shape of Shore A hardness tester tip

### 6.5.2 Porosity of pre-compacted body and ribbon

To measure the porosity of the pre-compacted body at different angular roll positions, a non-destructive X-ray tomography, MicroCT 35 (Scanco medical AG, Switzerland), was used. All of the X-ray experiments were carried out using a voltage of 45 kV and consequently current of 177  $\mu$ A and power of 8 Watt. It was found that the 45 kV is the most appropriate voltage for the density of the material being studied which produce images with clear details for analysis. The voxel size used was 3.5  $\mu$ m. Figure 6-8 shows an X-ray image for a slice of ribbon. The X-ray images were analysed using ImageJ software to determine the porosity by considering the black colour in the sample as an air and the white as solid material. The range of 16-bit grey scale level is between 0 and 65,535; zero is complete black whereas 65,535 is complete white. As the number increased, the colour becomes whiter. Prior to determining the porosity of any sample, there was a calibration step to define the black area which represents the air in the sample. This is done by determining the grey scale of the black area that surrounds the sample. Each sample was sliced to 240 pieces then the porosity of the sample was determined by averaging the porosity for these slices. The porosity is determined by dividing the number of black pixel (which represents the air in the sample) by the total number of the pixel which represents air and solid. More details description of the technique could be found elsewhere (Maire et al., 2001, Falcone et al., 2004, Dadkhah et al., 2012).

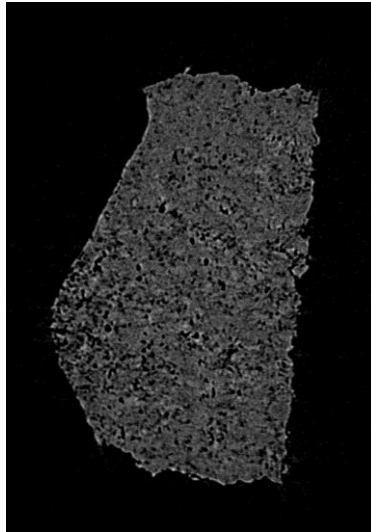


Figure 6-8: X-ray image of one slice of ribbon

Other ribbon properties such as ribbon strength and temperature were measured using the same procedures described in Chapter 3.

## **6.6 Results and discussion**

In this section, the effect of roller speed, hydraulic pressure and roller gap on the hardness and porosity of the pre-compacted body, nip angle, ribbon width and strength, amount of fines and the temperature of the ribbon surface were investigated and discussed.

### **6.6.1 Effect of roll speed**

With reference to Table 6-3, the roller speed was changed from 3 to 7 rpm with a step of 1 rpm. All other parameters were kept constant; hydraulic pressure at 70 bar and roll gap at 1.5 mm. Figure 6-9 shows the hardness of the pre-compacted body at different angular roll positions and at different roller speeds. The y-axis is the Shore A hardness and the x-axis is the angular roll position.

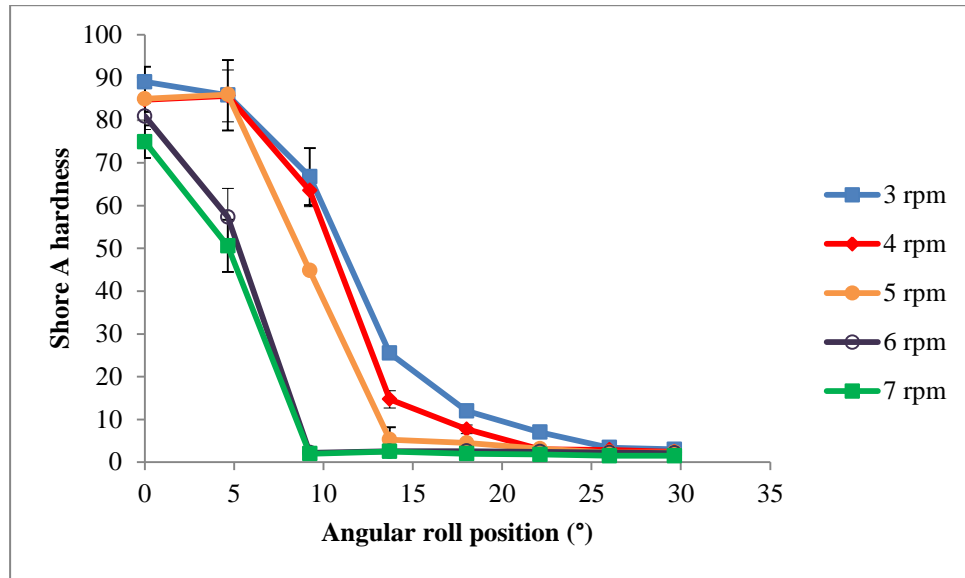


Figure 6-9: Hardness of the pre-compacted body of Avicel PH-101 at different angular roll positions and at different roller speeds

Figure 6-9 shows that the powder compaction zone starts at higher angular positions when the rollers rotate at lower speeds. This means the powder subjected to a high pressure for longer time compared to the powder that compacted at higher roller speeds. The biggest difference in the hardness of the pre-compacted body can be seen between 3 rpm and 7 rpm roll speed. Also the smallest difference can be noticed between roll speed of 6 and 7 rpm. The figure shows early gradual increase in the hardness of the pre-compacted body at 3 rpm compared to the rapid but late increase of the hardness for the roll speed of 6 and 7 rpm.

For all the curves in Figure 6-9, the area under the curve for each speed is representative of two things; first, the progress of the compaction process as it indicates the rate at which the hardness increases as approaching the minimum gap at angle zero. Second the size of the compaction zone. Figure 6-10 shows the area under the curve of hardness versus angular roll position for different roller speeds. All the areas under the curves were determined using the trapezium rule.

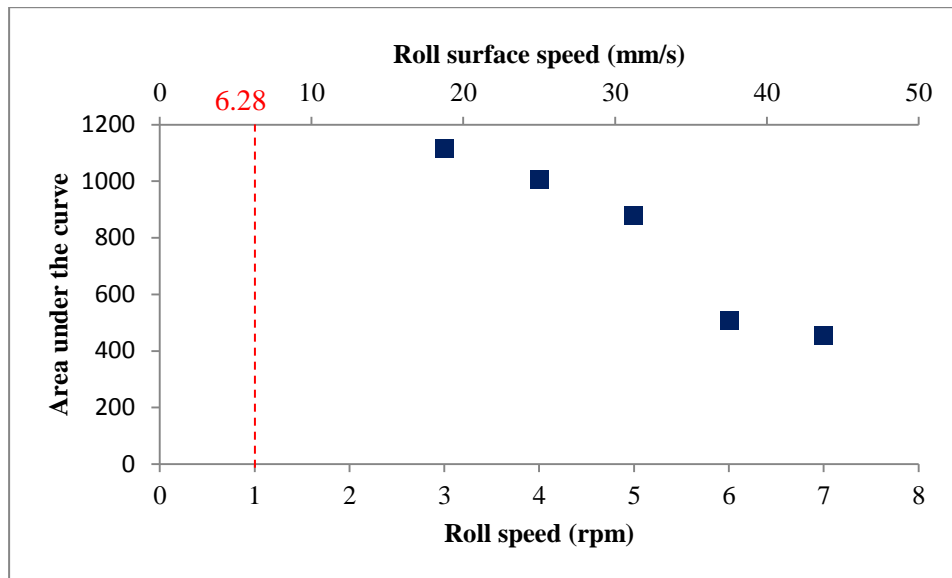


Figure 6-10: Area under the curve (hardness versus angular roll position) for different roll speed

The nip zone is defined by two criteria; particles move at the same speed as the roller and the pressure starts to increase significantly (Johanson, 1965, Bindhumadhavan et al., 2005, Yu et al., 2012). An increase in the pressure should be accompanied by an increase in the hardness of the pre-compacted body especially if the powder is deformable such as Avicel PH-101. This is the idea upon which this research is based. In this study, the nip angle is considered as the angle at which the hardness of the pre-compacted body starts to increase significantly. Figure 6-11 shows the determined nip angle for each roller speed. The error bars in this figure and in all figures in this study represent the standard deviation. Five hardness values were averaged for each angular roll position. It can be seen from the figure that an increase in roller speed from 3 to 7 rpm caused a decrease in the nip angle from 26 to 9° respectively.

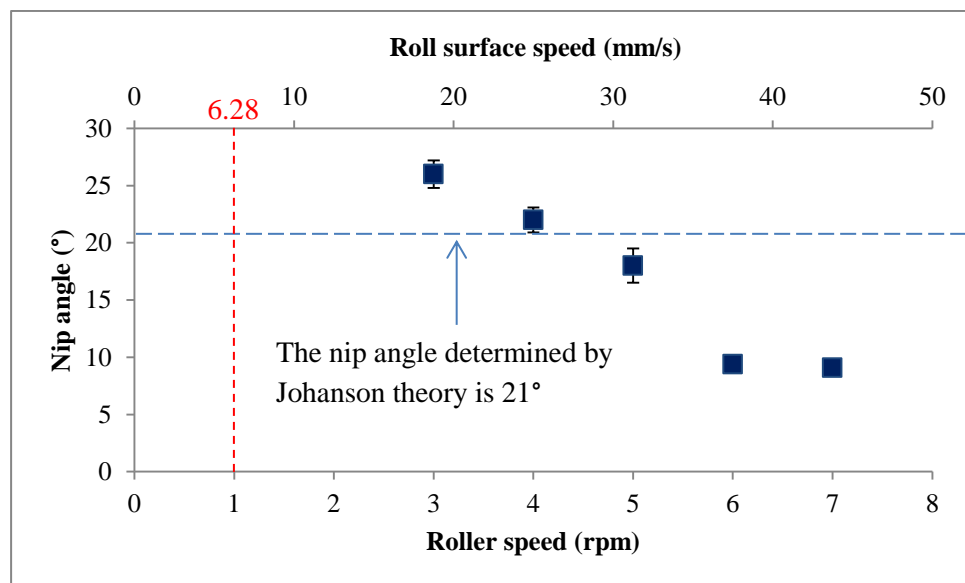


Figure 6-11: Determined nip angle as a function of roller speed

The calculated nip angle by Johanson's theory is 21°. By comparing the range of the nip angles determined by the new method with the nip angle calculated by Johanson's theory, it

can be seen that the Johanson's nip angle is approximately the same as the nip angle at roller speed of 4 rpm, However at 3 and 5 rpm the nip angle deviates from the 21°, at higher roller speeds of 6 and 7 rpm the deviation is even greater. As previously explained, the nip angle is an indication of the size of the compaction zone. Based on this, big nip angle means gradual powder compaction and big compaction zone which are better for two reasons; first, more air will be removed from the powder which helps the compaction process. The effect of the air on the compaction of metal powder was investigated by Spinov et al. (1967). It was shown that the air has negative effect on the ribbon quality. Trapped air in the powder bed will cause voids in the ribbon and reduce its width (Kleinebudde, 2004, Bindhumadhavan et al., 2005). Second, some powder exhibit viscoelasticity which means to cause plastic deformation, the applied load should be hold for specific time.

Decreasing the nip angle with increasing the roller speed could be due to the slipping of the particles on the roller surface. As the rollers rotate faster, the particles were not able to move at the same speed as the roller. So it will not be grabbed by the roller and that reduced the amount of the stress applied to the particles.

Figure 6-12 shows how the feeder screw speed changes with changing roller speed. It can be seen from the figure that as the roller speed increase, the screw speed increase too. The feedback system of the roller compactor maintains a constant gap by varying the speed of the screw feeder to supply enough material to the compaction zone. According to this, the screw speed increased to supply more powder to the compaction zone in order to maintain the gap and pressure to the set values.

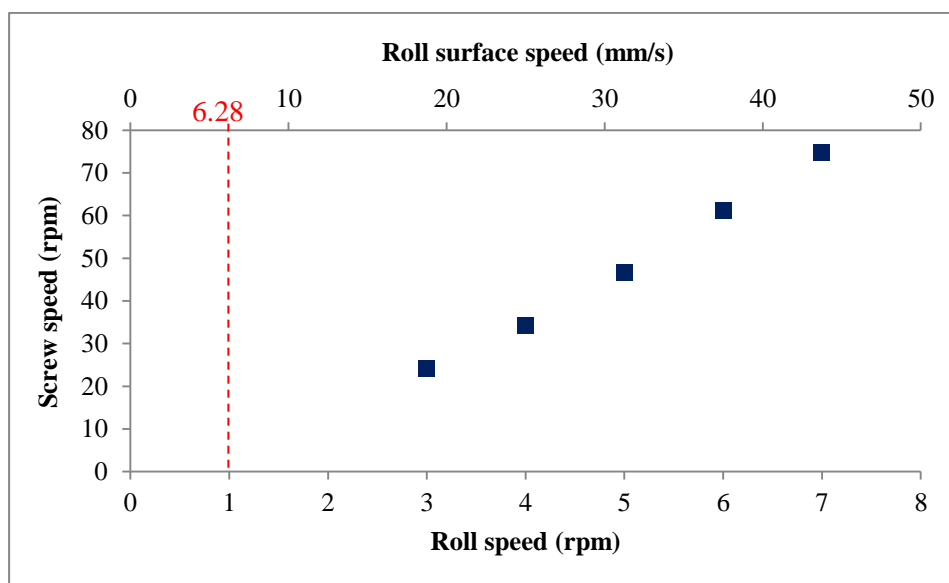
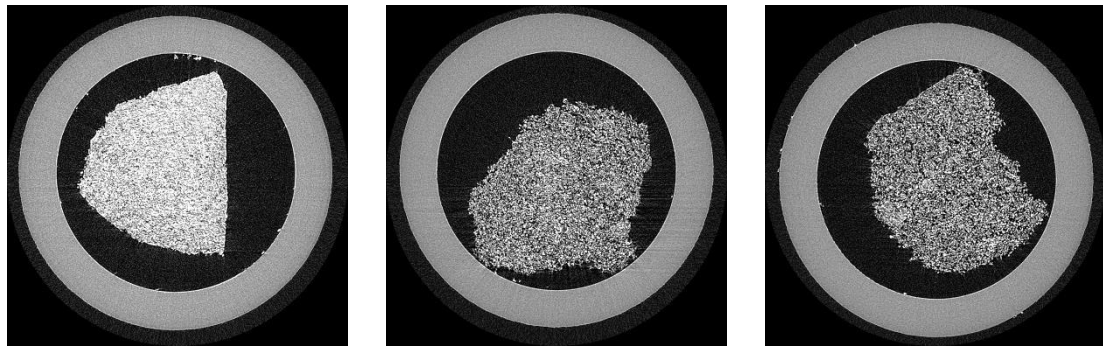


Figure 6-12: Screw speed as a function of roller speed for Avicel PH-101

The porosity of the pre-compacted body at different angular roll positions at roller speed of 3 rpm was determined using a non-destructive X-ray tomography technique. Figure 6-13 shows three slices of pre-compacted body at different angular roll positions. It can be seen that as the angular roll position decreases the structure of the pre-compacted body becomes less porous.



At 5°

At 18°

At 30°

Figure 6-13: Three X-ray slices of the pre-compacted body at different angular roll position

Figure 6-14 shows how the porosity of the pre-compacted body changes with changing the angular roll position. It is worth to mention that all the pieces used to measure the porosity were taken from the side of the pre-compacted body. It is expected that the effect of changing the porosity is opposite to the effect of changing the hardness as there is a pressure density relation. It can be seen from the figure that as the angular roll position decreased the porosity decreased too and this is because of increasing the stress as the powder moves towards the minimum gap.

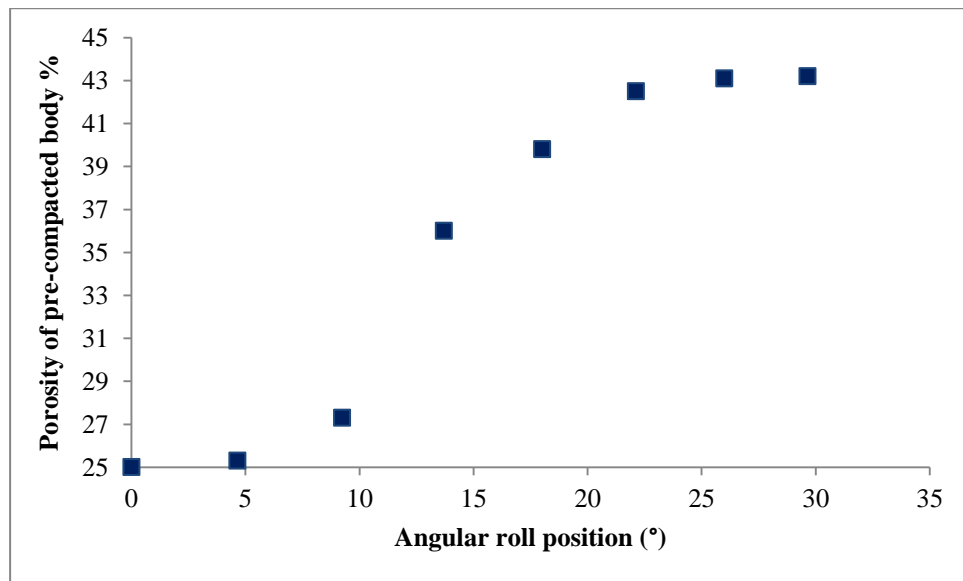


Figure 6-14: Porosity of the pre-compacted body at different angular roll positions and roll speed of 3 rpm

Figure 6-15 shows how the ribbon width changes with roller speed. The whole width of the roller used is equal to 40 mm. It can be seen from Figure 6-15 that the width of the ribbon produced at roller speed of 3 rpm is 40 mm, which is equal to the width of the roller. As the roller speed increased further the ribbon width decreased by about 1 mm at 6 and 7 rpm. This may be attributed to the late but rapid increase in the hardness of the pre-compacted body at roll speed of 6 and 7 rpm which make it difficult for the air to escape during the compaction process. This has undesired effect on the process. Increasing roller speed caused a decrease in the size of the compaction zone and as shown by Figure 6-9 which resulted in a decrease of the powder compaction time.

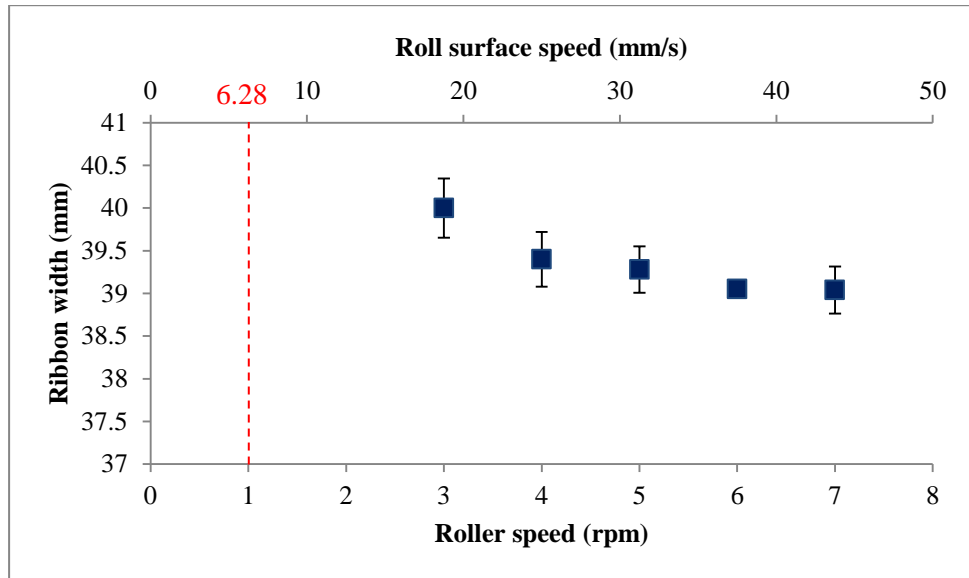


Figure 6-15: Ribbon width versus roller speed

Figure 6-16 shows the ribbon strength as a function of the roller speed. It can be seen that there is a limited effect of roller speed on the ribbon strength except at the highest speed of 7 rpm, at which the ribbon strength dropped significantly. Previous study by Bindhumadhavan et al. (2005) showed that the peak stress applied to the powder decreased as the roller speed increased which consequently caused a decreased in the ribbon strength. This is clear in Figure 6-9 where the hardness at zero angular roll position is the lowest at roll speed of 7 rpm. The case is the same for the area under the curve at speed of 7 rpm and as shown in Figure 6-10 which indicates late and rapid compaction which has negative effect on the process as discussed earlier.

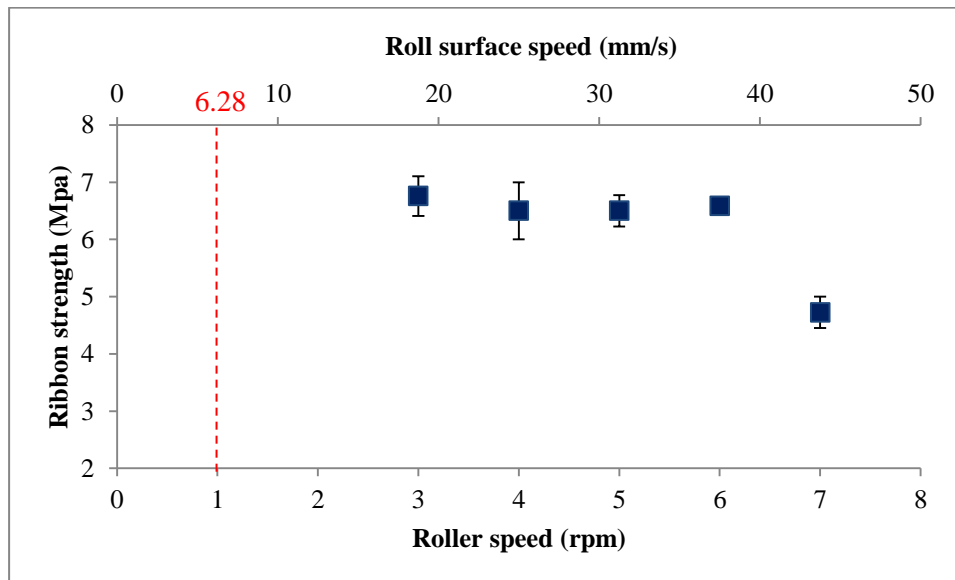


Figure 6-16 : Ribbon strength versus roller speed

Figure 6-17 shows the measured porosity for the ribbon centre at different roller speeds. It can be seen from the figure that increasing the roller speed from 3 to 7 rpm caused an increase in ribbon porosity from 22 to 24 respectively. As the roller speed increase, the nip angle



decreased and as shown in Figure 6-11. In addition, the maximum stress applied to the powder may also decrease upon increasing the speed due to more air in the bed. These two reasons might cause increase in the porosity. It can be noticed that the porosity of the centre of the ribbon produced at roller speed of 3 rpm is lower than the porosity of the pre-compacted body at angular roll position of zero in Figure 6-14. This is because the centre of ribbon exhibit more stress during the compaction process than the edges (Guigon et al., 2007) from which the sample of pre-compacted body has been taken.

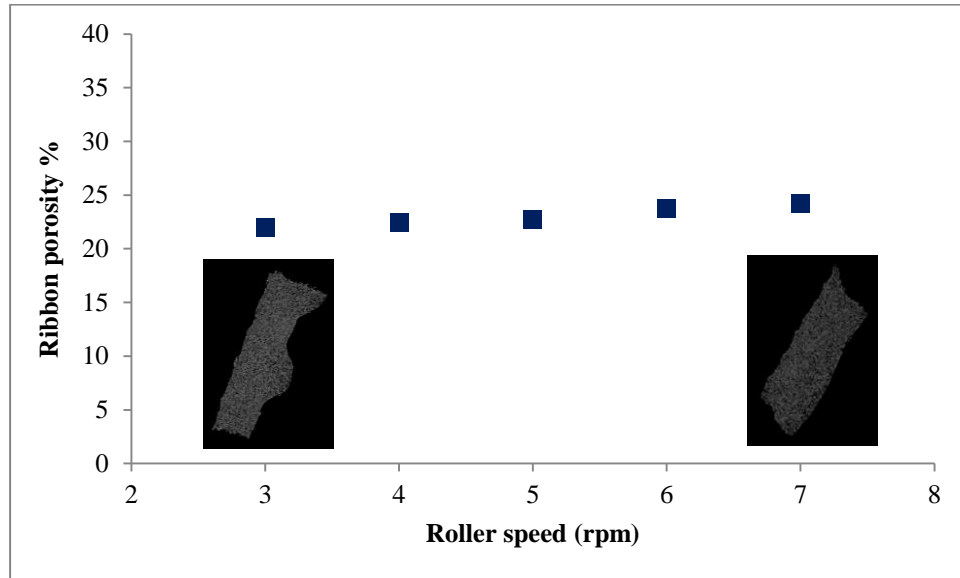


Figure 6-17: Ribbon porosity versus roller speed

Figure 6-18 shows how the percentage of fines changes with the changing of the roller speed. The percentage of fines in this study is defined as the weight of un-granulated powder recuperated after compaction, of size equal or below 150  $\mu\text{m}$ , divided by the total weight of the product. This is determined by separating the fines from the ribbon by sieving. It can be seen from Figure 6-18 that increasing the roller speed caused a small increase in the percentage of fines when taking the error bar into consideration. This could be because of decreasing the nip angle with increasing the roller speed. Consequently, more air trapped in the system in addition to shorter compaction time.

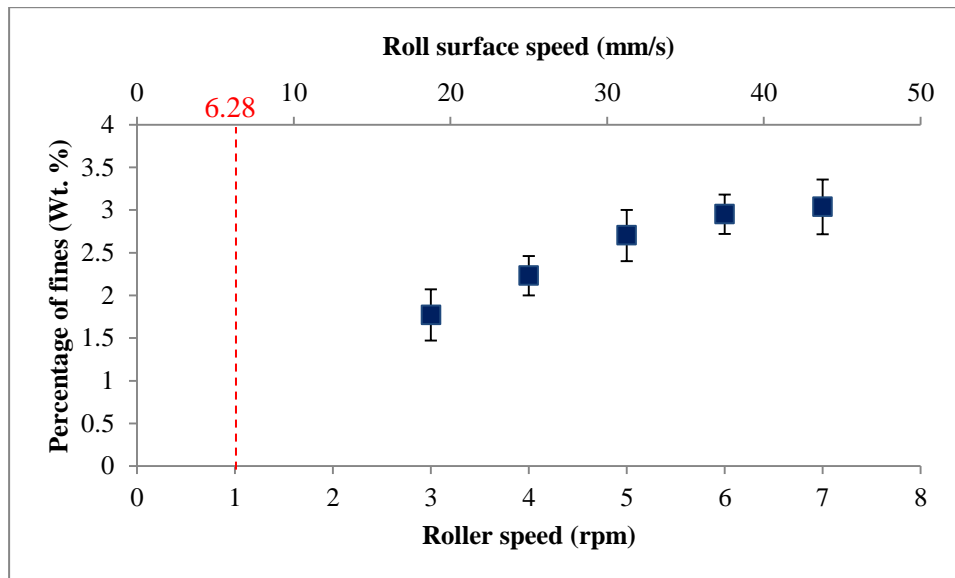


Figure 6-18: Percentage of fines versus roller speed

Figure 6-19 shows the maximum temperature of the ribbon as a function of roller speed. It is clear that as the roller speed increased the temperature increased too. It can be seen from Figure 6-9 that the increase in the hardness of the pre-compacted body is late but with faster rate at high roller speed compared to the gradual increase in the hardness at the lower roller speed. This fast increase in the hardness may have been caused by rapid increase in the applied stress, which could be a reason for the increase in the temperature at high roller speed compared to the low speed. Increasing the screw speed with increasing the roller speed, as shown in Figure 6-12, might cause an increase in the powder internal friction which could participate in generating more heat and raising the temperature. Another reason for recording high temperature at high roller speed could be the less available time for the heat to dissipate from the ribbon that moves faster. Such an increase in the temperature with increasing roller speed was seen by Osborne (2013) during the roller compaction of sodium chloride powder. It was attributed to the increase in the powder friction.

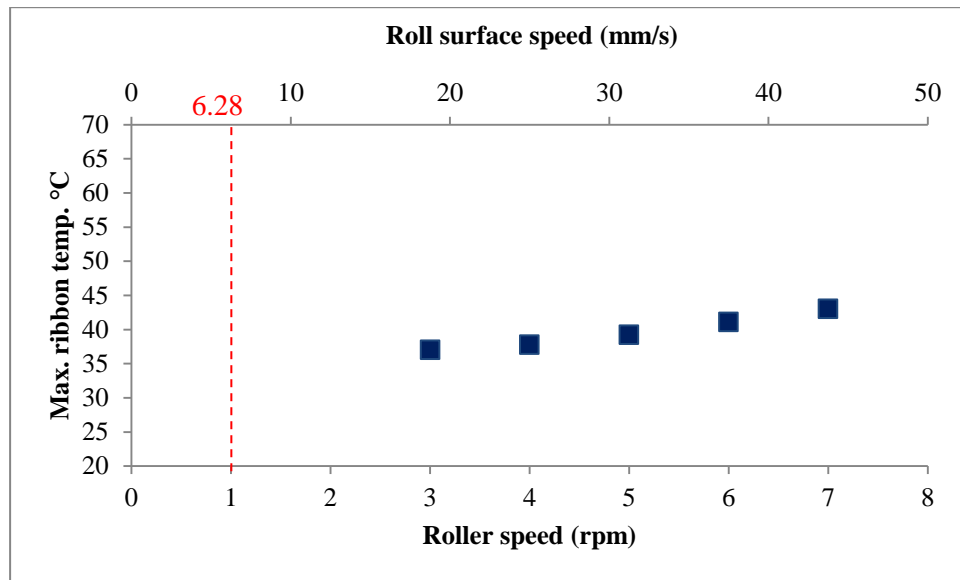


Figure 6-19: Maximum ribbon temperature for different roller speeds

### 6.6.2 Effect of hydraulic pressure

The applied pressure by the rollers is the most important process parameter that affects the ribbon properties and compaction process. As shown in Table 6-3, the experiments of this set were carried out at different hydraulic pressures of 18, 30, 70, 100, 150, 200 and 230 bar and at constant roller speed of 3 rpm and constant roller gap of 1.5 mm.

Figure 6-20 shows how the Shore A hardness of the pre-compacted body at different angular roll positions is affected by changing the hydraulic pressure. It can be seen from the figure that the hardness starts to increase at higher angular roll position as the applied hydraulic pressure becomes higher compared to lower hydraulic pressure at which the hardness starts to increase at lower angular roll position but the increase is rapid as it can be seen for pressures of 18 and 30 bar. There are no hardness values for the pre-compacted body produced at 18 and 30 bar at angles greater than  $14^\circ$  as the structures of the pre-compacted bodies were too weak, and as a result the Shore A hardness tester when immersed in the powder bed did not yield a meaningful result. Also it can be noticed from Figure 6-20 that there is a large discrepancy between the hardness at different angular roll position of 18 and 30 bar compared to the hardness of the pre-compacted body produced at higher pressures. As the hydraulic pressure increased, the stress applied to the powder was more which caused the powder to pre-compact. In addition, more pressure caused more friction between the particles and the rollers which might help the particles to be grabbed by the rollers at earlier stage of compaction.

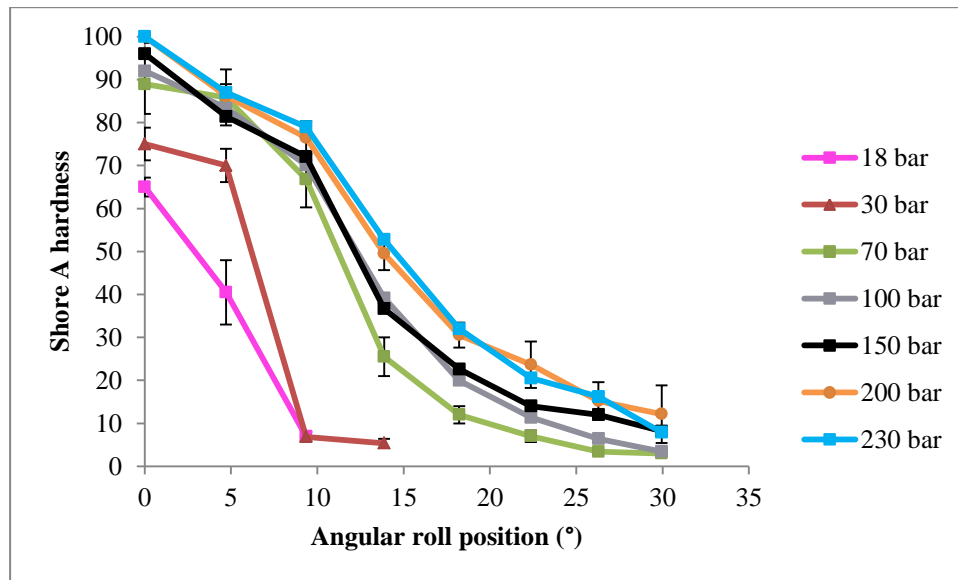


Figure 6-20: Shore A hardness for different angular roll position at different hydraulic pressures

Figure 6-21 shows the area under the curves of Figure 6-20. It can be observed that in general, the area under the curve increases as the hydraulic pressure increases but there is a small difference of 10 and 1 arbitrary unit of the area under the curve upon increasing the pressure from 100 to 150 bar and from 200 to 230 bar respectively. As mentioned earlier, the area under the curve represents the size of the compaction zone and the rate at which Shore A hardness increase. That explains why the difference is small between the areas under the curves of these hydraulic pressures because the sizes of the compaction zone and the rates of increasing the hardness are close as it can be seen in Figure 6-20.

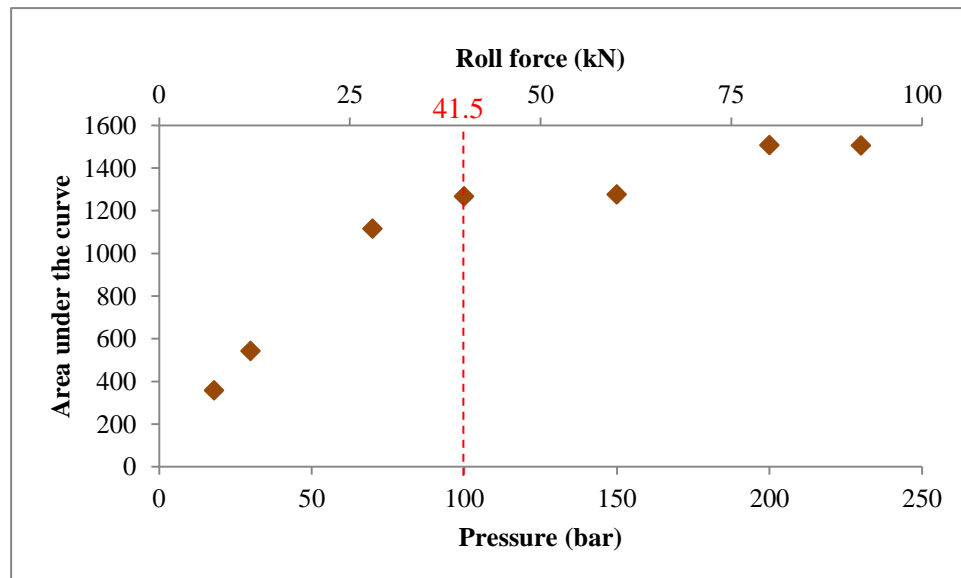


Figure 6-21: Area under the curve (hardness versus angular roll position) for different hydraulic pressures

The nip angle, defined in this study as the angle at which the hardness starts to increase significantly, is plotted against the hydraulic pressure in Figure 6-22. There is no significant

difference between the nip angle at pressure of 18 and 30 bar. Also there is no large difference in the nip angle at pressure of 100, 150, 200 and 230 bar. Almost three values of the nip angle can be distinguished in Figure 6-22; 7° at 18 and 30 bar, 26° at hydraulic pressure of 70 bar and 30° at all other higher pressures.

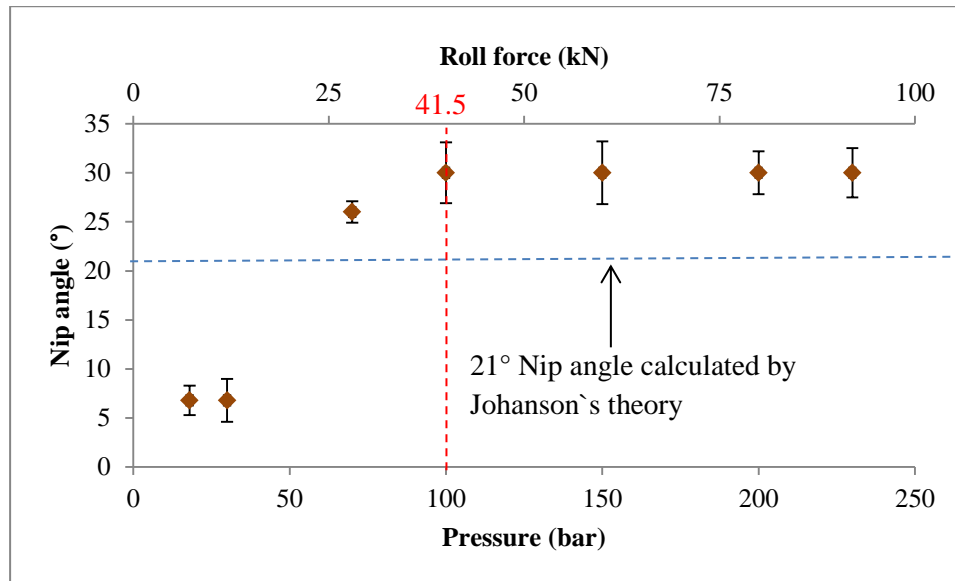


Figure 6-22: Determined nip angle for different hydraulic pressure

Figure 6-23 shows how the screw speed of the feeder change upon changing the hydraulic pressure due to feedback gap control system turned on. It can be seen from the figure that in general, increasing the hydraulic pressure caused an increase in the screw speed. However the change is less compared to that happened due to the change of roller speed. There is no difference between the screw speed of 18 and 30 bar. Also the difference is very small within the range of hydraulic pressure between 70 and 150 bar. The case is the same for the difference between 200 and 230 bar.

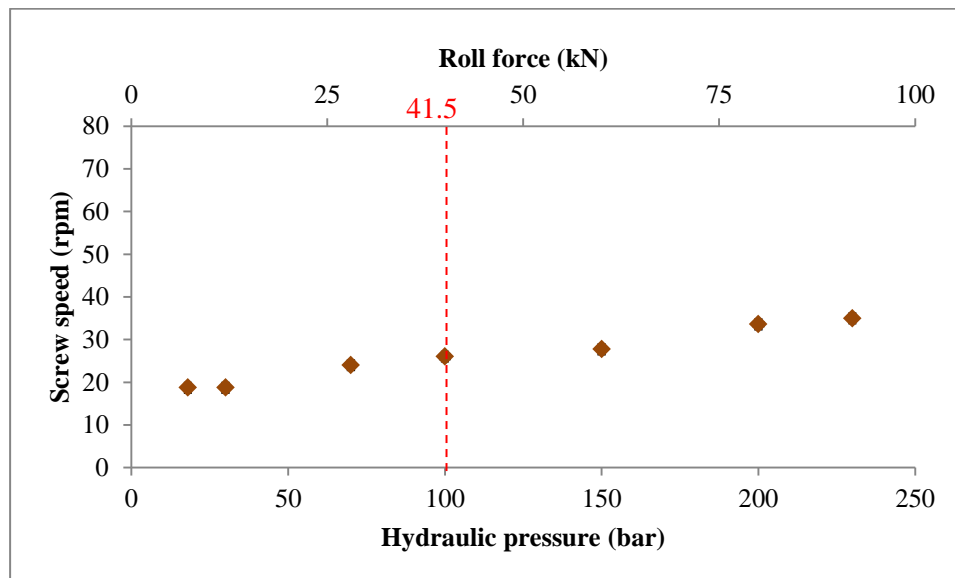


Figure 6-23: Screw feeder speed as a function of hydraulic pressure for Avicel PH-101

Figure 6-24 shows the porosity of the pre-compacted body produced at hydraulic pressure of 100 bar and at different angular roll positions. It can be seen that as the angular roll position decrease, the porosity decrease too which indicate more densification of the powder.

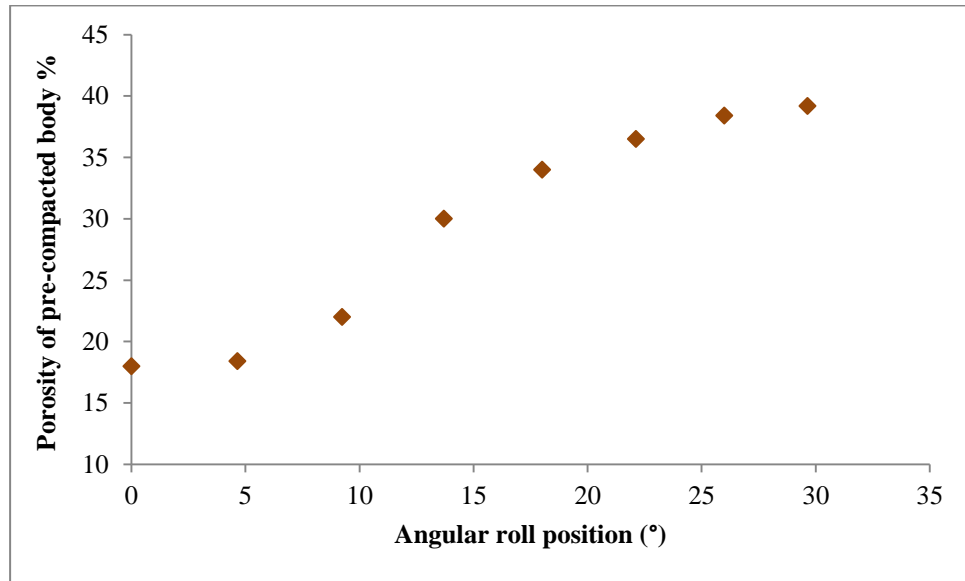


Figure 6-24: Porosity of pre-compacted body at different angular roll positions produced at 100 bar hydraulic pressure

Ribbon width is a function of the applied pressure and deformability of the powder (Al-Asady et al., 2015). Figure 6-25 shows how the ribbon width changes with changing the applied hydraulic pressure. Increasing the hydraulic pressure caused an increase in the ribbon width and it reached the full roller width of 40 mm at 70 bar. Then shows further increase at 100 and 150 bar. Above 150 bar, there is no more change in ribbon width. This may be due to the fact that there is no more space as the roller full width is 40 mm and the space between the roller and the cheek plate is also limited.

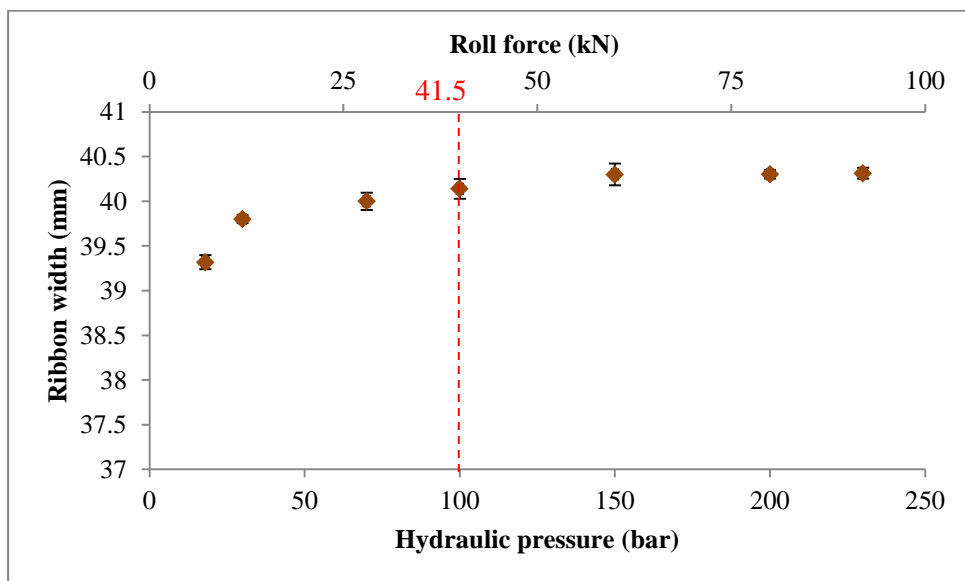


Figure 6-25: Ribbon width as a function of hydraulic pressure

The strength of the ribbon is greatly affected by changing the hydraulic pressure; the higher the hydraulic pressure, the higher is the ribbon strength. This relationship is shown in Figure 6-26. There was no ribbon long enough to test the ribbon strength at pressure of 200 and 230 bar, as the ribbon broke into two pieces from the middle at those pressures. Although the ribbon breaks into two pieces, the pieces are very strong. This is a common problem in the roller compaction process (Kleinebudde, 2004, Guigon et al., 2007) and it is explained as a capping phenomenon (Hakanen and Laine, 1993). Ritter and Sucker (1980) showed that the capping increase as the compression pressure that used to make tablet increase.

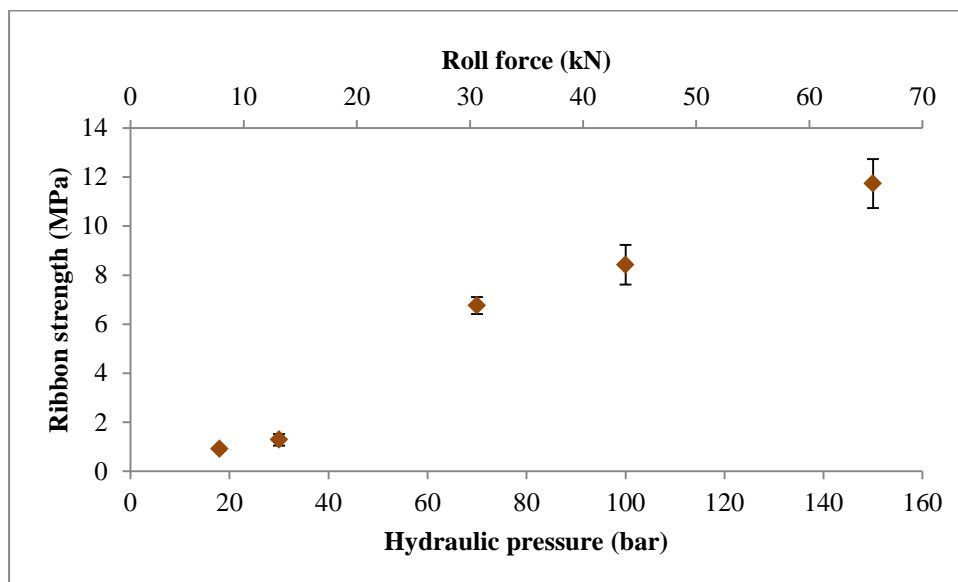


Figure 6-26: Ribbon strength as a function of hydraulic pressure

Figure 6-27 shows how the porosity of the centre area of the ribbon is changing with increasing the hydraulic pressure. As the hydraulic pressure increase the ribbon porosity decreased. This is because the maximum applied stress and the nip angle increased. Also as mentioned previously, the hardness of the pre-compacted body increased gradually for the pressure of 70 bar and above compared to the sudden increase at lower pressure of 18 and 30 bar. This could be the reason for the big decrease in porosity as the pressure increased from 30 and 70 bar.

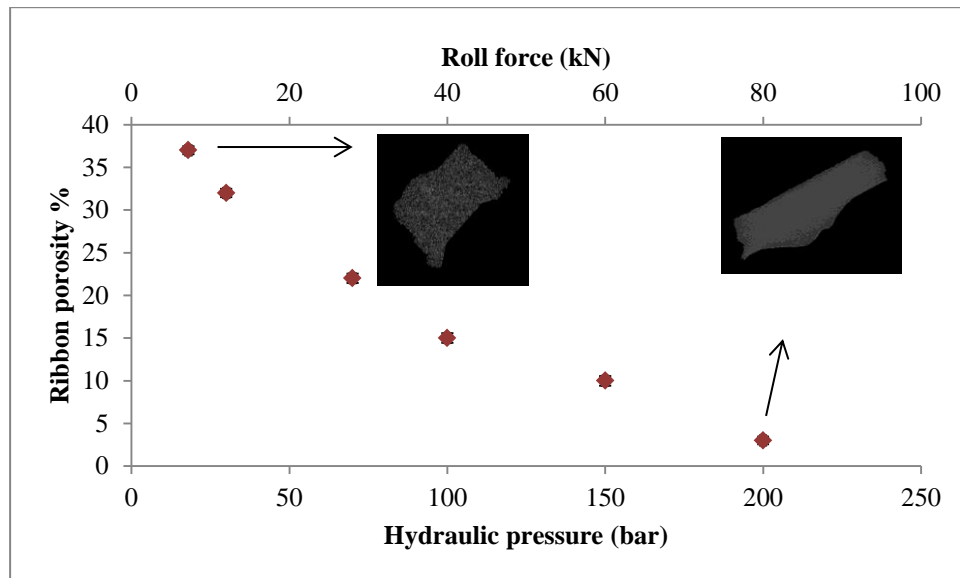


Figure 6-27: Porosity of the ribbon centre as a function of hydraulic pressure

As the hydraulic pressure increased there may be a greater chance for the particles to be granulated and bonded to each other. This caused a decrease in the weight percentage of fines as shown in Figure 6-28. There is no significant decrease in the percentage of fines as the pressure increase from 70 bar to 200 bar. This is likely because the applied stress on the powder at 70 bar was enough to granulate most of the powder and the extra pressure above 70 bar did not cause further reduction in the percentage of fines.

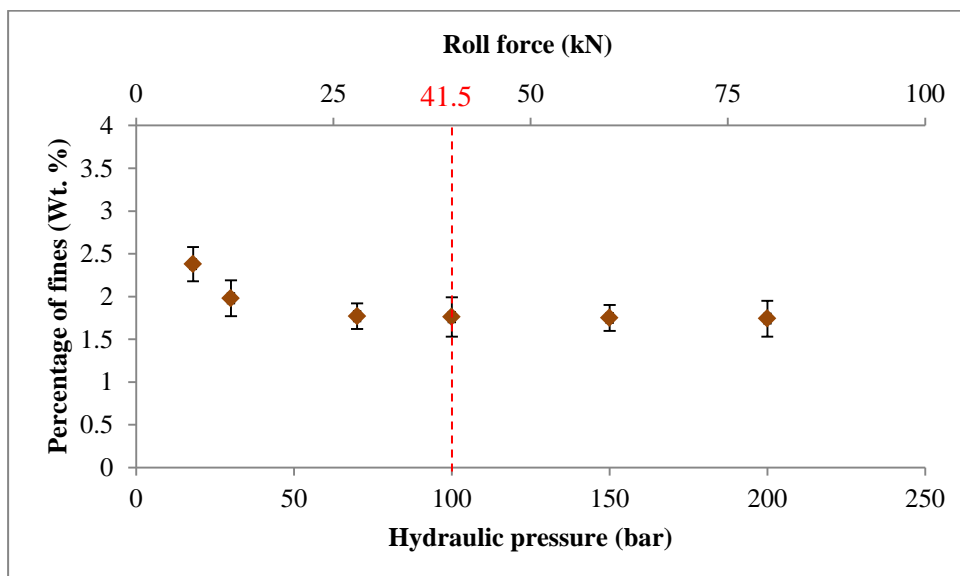


Figure 6-28: Percentage of fines versus hydraulic pressure

Figure 6-29 shows how the maximum ribbon temperature increased with increasing the hydraulic pressure. The main two reasons for the temperature to increase are the deformation of the particle and friction of particle-particle and particle-surface. It is known that an increase in the hydraulic pressure caused deformation of the particles (Al-Asady et al., 2015) and as shown previously in Figure 5-9. It can be seen from Figure 6-20 that the Shore A hardness of the pre-compacted body produced at 18 bar suddenly increased from 7 at angular roll position of around 9.3° to 40.5 at angular position of 5°. For the pre-compacted body produced at 30 bar, the hardness increased from 7 to 70 upon decrease in the angular roll position from 9.3°



to 5° respectively. A sudden increase in the hardness of the pre-compacted body was seen before with pre-compacted body produced at high roller speed of 6 and 7 rpm. At these roller speeds the temperature of the ribbon was also higher. This is likely due to the higher friction at higher speed compared to the lower speeds. Figure 6-20 and Figure 6-29 suggests that the deformation is may be more important factor to raise the temperature than the friction. Increasing the screw speed with increasing hydraulic pressure (see Figure 6-23) might contribute in generating some heat due to the internal powder friction in the compaction area.

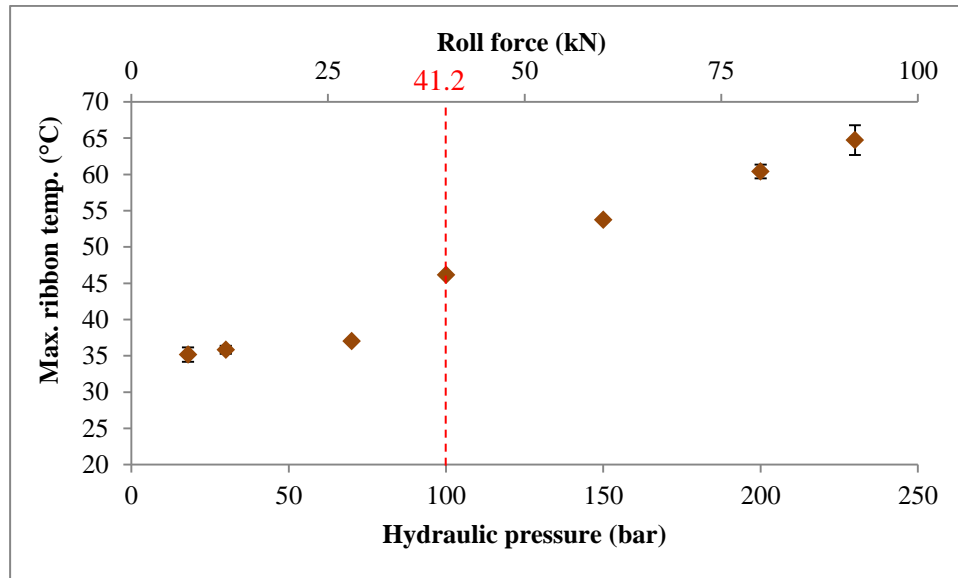


Figure 6-29: Ribbon temperature as a function of hydraulic pressure

### 6.6.3 Effect of roller gap

Figure 6-30 shows the measured Shore A hardness at different angular roll positions of the pre-compacted body produced at different roller gaps of 1, 1.5, 2 and 2.5 mm. It can be seen that the Shore A hardness of the pre-compacted body at 2.5 mm gap starts to increase at earlier stage of compaction at higher angular roll position compared to that produced at narrower gap. This trend is almost applicable for all other curves of hardness at different roller gaps.

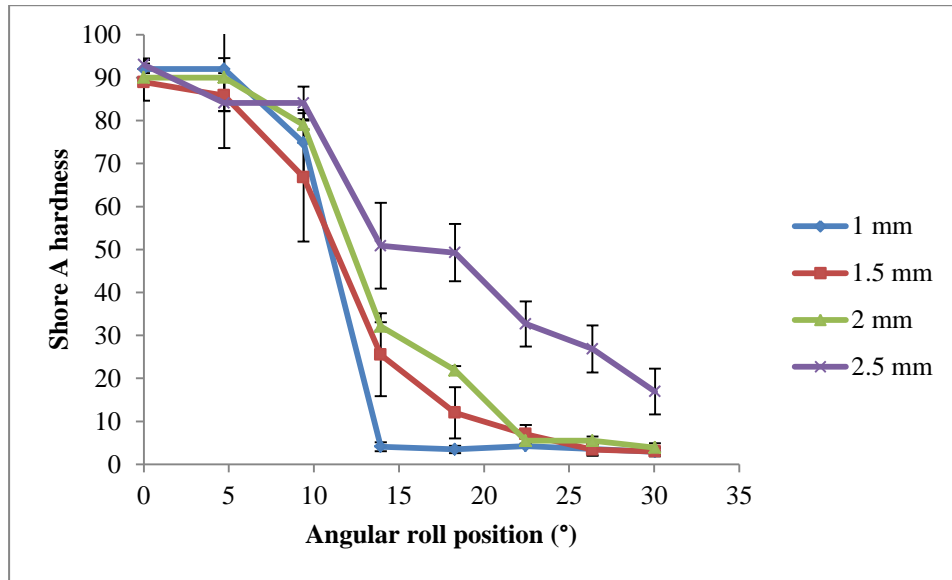


Figure 6-30: Shore A hardness at different angular roll position at different roll gap

Figure 6-31 shows the determined area under each curve in Figure 6-30. The figure suggests that the area under the curve is a function of roller gap. The higher the roller gap, the higher the area under the curve. As explained earlier, the area under the curve is an indication of the size of the compaction zone and the rate at which the hardness increase. For the largest value of the roller gap of 2.5 mm, the area under the curve is big because the size of the compaction zone is big. This means a gradual compaction of the powder.

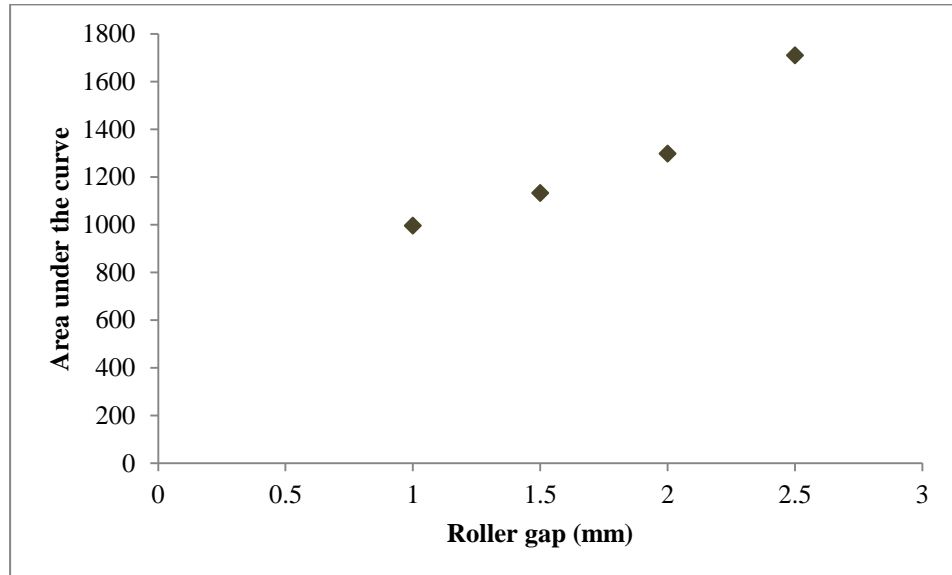


Figure 6-31: Area under the curve of the hardness-Angular roll position curves at different gaps

As indicated in Figure 6-30, the hardness of the pre-compacted body increased at different rates with angular roll position at different roller gaps. For this reason the nip angle is different for each roller gap. Figure 6-32 shows how the nip angle is changing with changing

of the roller gap. As the roller gap increases the nip angle increase too. The nip angle changes from 14° to 30° upon increasing the roller gap from 1 to 2.5 mm respectively.

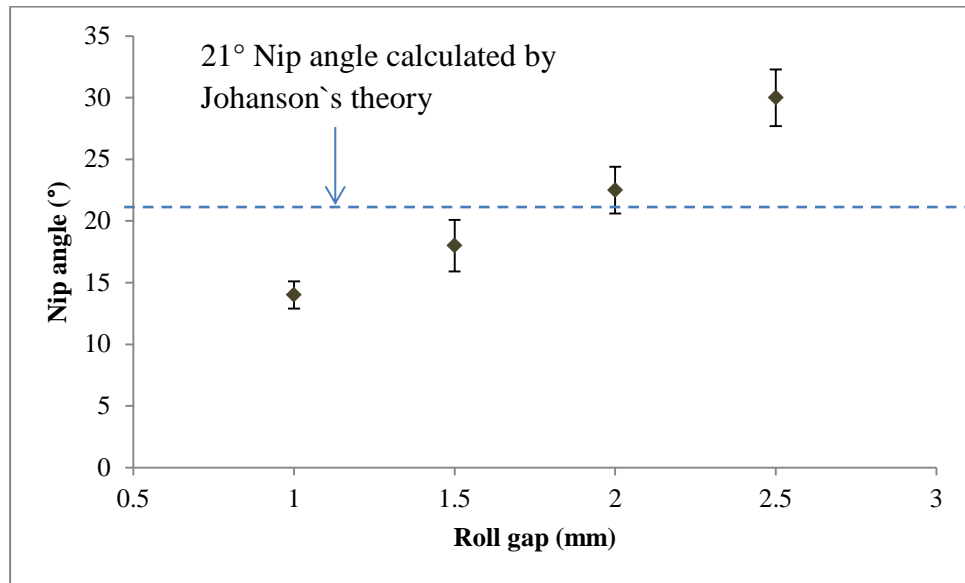


Figure 6-32: Determined nip angle for different roll gaps

The increase of the nip angle with increasing the gap was observed by Bindhumadhavan et al. (2005) and Yu et al. (2012) as the determined nip angle increased with increasing the roll gap for specific limit. Johanson (1965) stated that the nip angle does not change with changing the roller gap because changing the gap will not change the term  $G/D$  significantly in Eq. 2-20.

Figure 6-33 shows the effect of changing the roller gap on the speed of the feeding screw. The figure shows significant increase in the screw speed from 15 to 57 rpm upon increasing the roller gap from 1 to 2.5 mm respectively. Large gap needs more materials to maintain the pressure value. This increase in the amount of material may affect the hardness of the pre-compacted body. Feeding more material to the pre-compaction area may cause more densification/compaction which may lead to increase the hardness of the pre-compacted body which consequently affected the nip angle at different roller gaps.

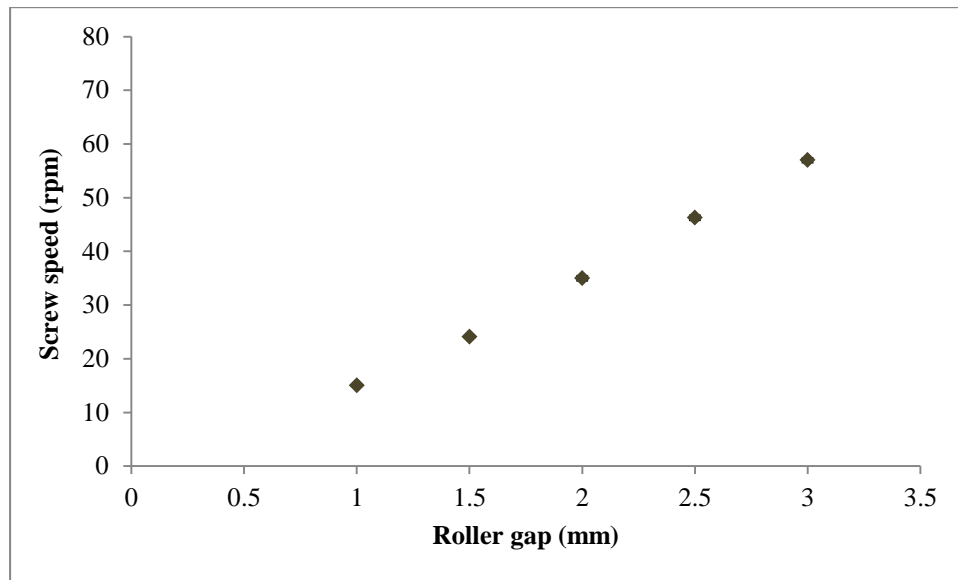


Figure 6-33: Screw speed as a function of roller gap for Avicel PH-101

Figure 6-34 shows how the porosity of the pre-compacted body produced at 2.5 mm gap changes with changing the angular roll position. It can be seen that as the angular roll position decreased, the porosity decreased too. The porosity changed from 36.7 % to 23 % upon changing the angular roll position from 30° to 0° respectively. This is due to the fact that the pressure applied to the powder increase as the powder approaching the minimum gap between the two rollers (Johanson, 1965, Bindhumadhavan et al., 2005).

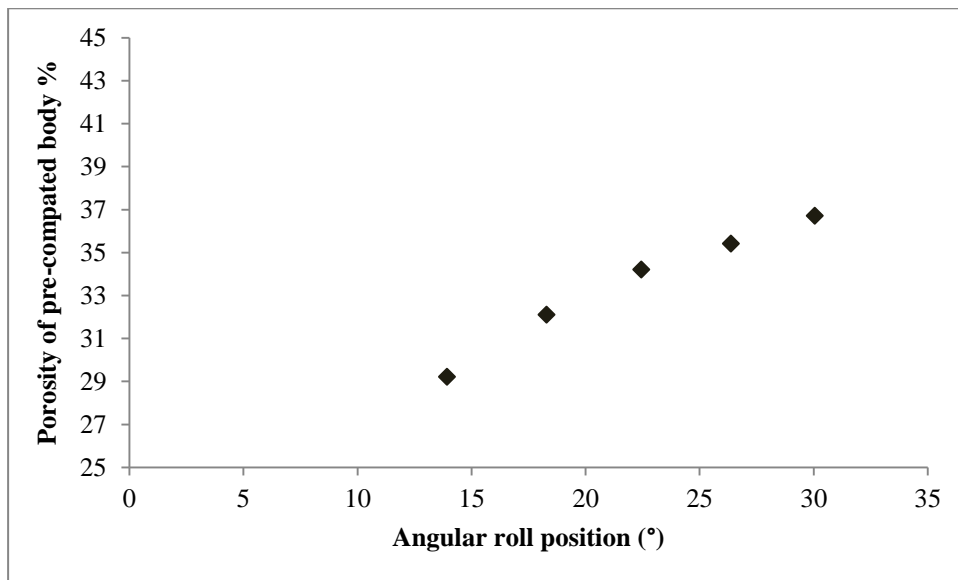


Figure 6-34: Porosity of pre-compacted body at different angular roll position produced using 2.5 mm roll gap

Figure 6-35 shows the width of the ribbon as a function of the roller gap. There is a slight increase in ribbon width of about 0.5 mm or less upon increasing the roller gap from 1 to 2.5 mm. It can be seen from Figure 6-32 that the nip angle is high at large roller gap which means more compaction time. Figure 6-30 shows that the increase of the Shore A hardness is gradual which let more air to be removed from the process and there is more time for the particles to

rearrange and deform which led to more efficient compaction process. The effect of the trapped air in the bed on the ribbon width has been investigated by Spinov et al. (1967) which supports the argument.

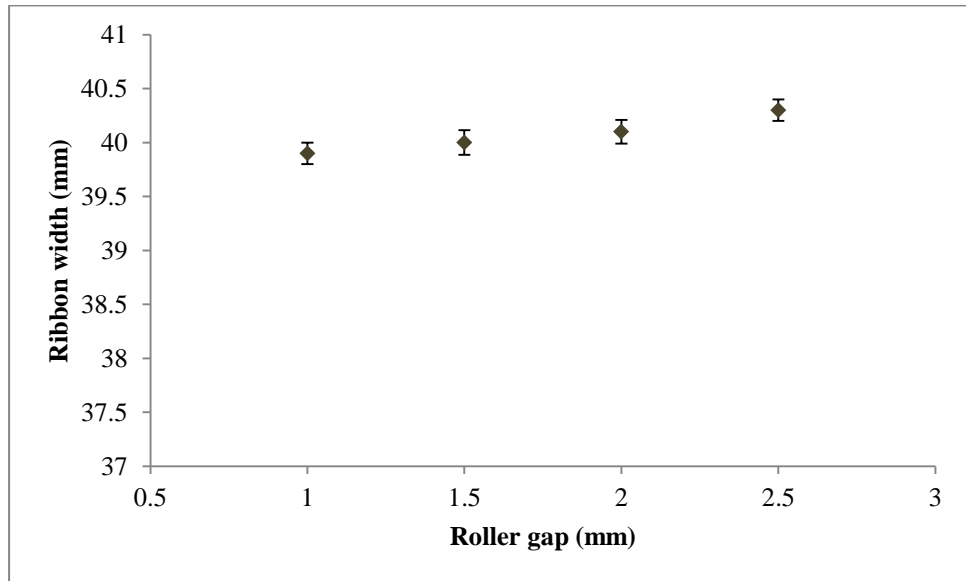


Figure 6-35: Width of the ribbon as a function of roller gap

Figure 6-36 shows that the ribbon strength is almost not changing upon increasing the roller gap from 1 to 2.5 mm. The figure suggests that there is no big change in the stress applied to the material at different roller gaps.

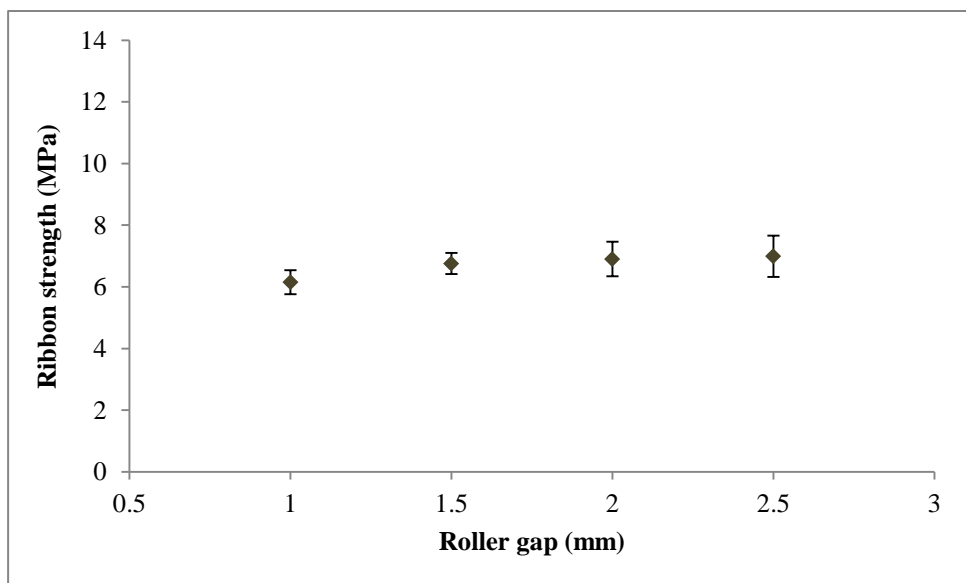


Figure 6-36: Ribbon strength versus roller gap

Figure 6-37 shows how the porosity of the centre of ribbon changes with changing the roller gap. There is an increase in the porosity around 1.5 % upon increasing the gap from 1 to 2.5 mm. Increasing the roller gap caused an increase in the height of the powder bed between the

two rollers at the minimum gap. This increase in the height caused the particles to receive less stress by the rollers compared to the particles in a bed with less height.

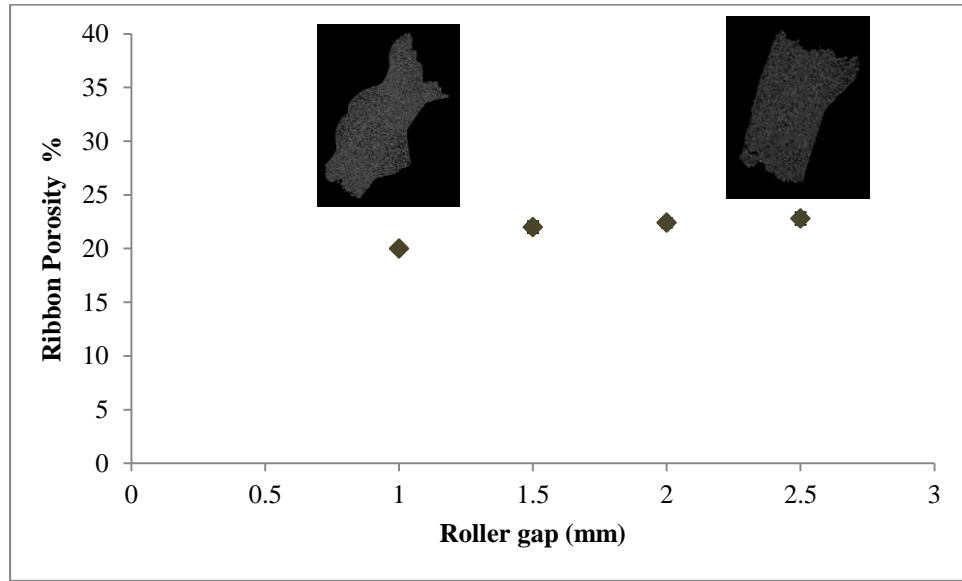


Figure 6-37: Ribbon porosity at different roll gap

As shown in Figure 6-38, there is almost no change in the percentage of fines at different roll gaps. This is may be because the range of the applied stresses on the material under different roller gaps was sufficient to granulate most of the Avicel PH-101 powder.

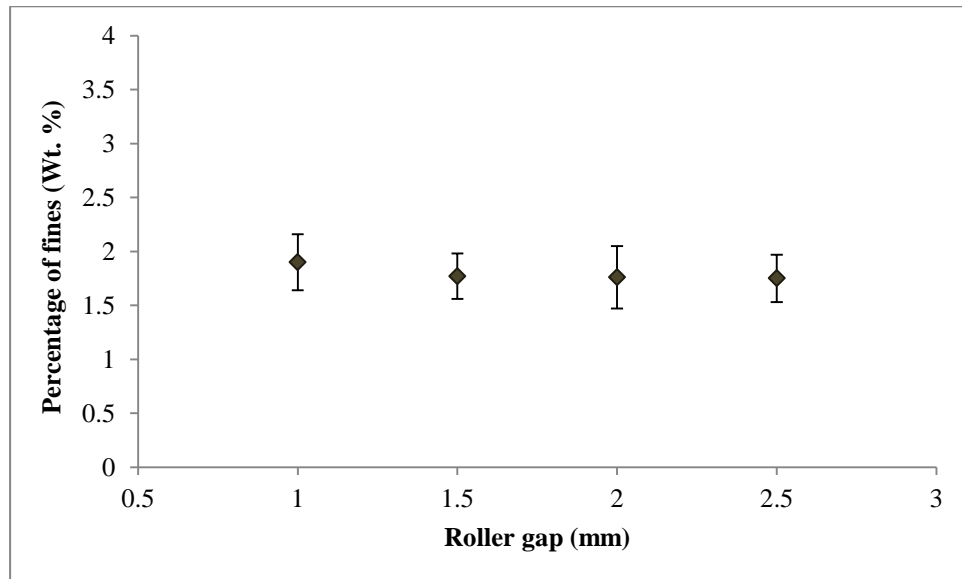


Figure 6-38: Percentage of fines for different roll gap

Figure 6-39 shows the change in maximum ribbon temperature upon a change in the roller gap. An increase in the roller gap caused increase in the maximum ribbon temperature. This could be again due to the increase of the area under the curve of the Shore A hardness which means more compaction time, better rearrangement and more deformation of particles. Increasing the screw speed with increasing the roller gap (See Figure 6-33) might cause

increase in the internal friction of the powder in the compaction area which consequently generate heat and caused an increase in the temperature.

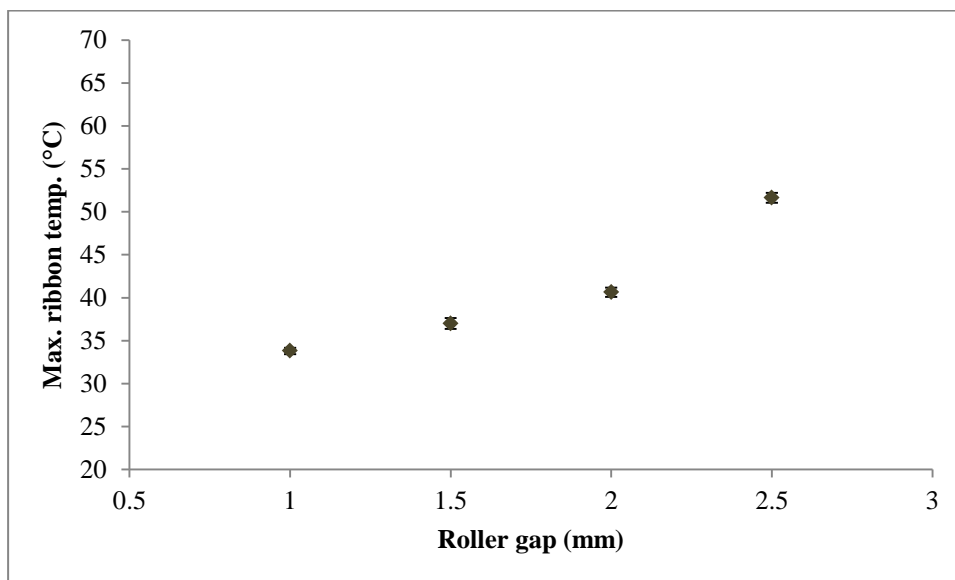


Figure 6-39: Maximum ribbon temperature as a function of roller gap

#### 6.6.4 Other materials

More experiments were carried out to measure the shore A hardness of the pre-compacted body produced from Pharmatose 200M and calcium carbonate. The aim is to investigate whether the new technique of measuring the hardness of the pre-compacted body can be used with different type of materials. Figure A- 8 (Appendix A) shows the shore A hardness of the pre-compacted body at different angular roll positions. The pre-compacted body of both materials was produced using a hydraulic pressure of 70 bar, roller speed of 3 rpm and roller gap of 1.5 mm. It can be seen from the figure that in general, the hardness of the pre-compacted body of calcium carbonate is less than the hardness of the Pharmatose 200M at different angular roll position. The hardness of the Pharmatose 200M is also less than that of the Avicel PH-101 (Figure 6-20). The nip angle that determined from Figure A- 8 is equal to  $5^{\circ}$  and  $9^{\circ}$  for calcium carbonate and Pharmatose 200M respectively. These values are close to the values of the nip angle that determined by Johanson's theory for these two materials (Section 5.4.3). This may confirms that the new technique could be also used for different materials with different mechanical properties.

#### 6.7 Conclusion

In this study a new method was presented to determine the nip angle of the Avicel PH-101 powder undergoing roller compaction. The method consists of using the Shore A hardness of the pre-compacted body at different angular roll positions. The proposed method successfully detects the change in the nip angle as a function of different process parameters, such as roll speed, hydraulic pressure and roller gap. The results showed that the roll speed has a large effect on the nip angle; an increase in the roller speed significantly decreases the nip angle.

The method proposed in this study was also able to track the progress of the compaction process as the powder moves towards the minimum gap. The results showed an early gradual increase of the hardness of the pre-compacted body at low roll speed compared to late but

rapid compaction at higher speed. Early gradual increase in the hardness is good for the compaction process as it gives more time for the powder to be under stress and more time for the air to escape from the process. This study suggests using the area under the curve of the Shore A hardness as an indication for the progress of compaction process as the powder moves towards the minimum gap. Big area means early gradual increase of the pre-compacted body hardness.

Investigating the effect of hydraulic pressure on the nip angle showed three regions of nip angle; at 18 and 30 bar the nip angle is around 7°. At 70 bar the nip angle around 26° and at hydraulic pressure of 100, 150, 200 and 230 bar the nip angle is around 30°. Increasing the hydraulic pressure also caused an increase in the area under the curve of the hardness which is good for the compaction process.

Increasing the roller gap caused an increase in the nip angle but did not show a big change in the ribbon properties of Avicel PH-101. Increasing the area under the curve with increasing the gap may compensate the decreasing of the stress.

The temperature, especially in the centre, of the outlet ribbon is reflecting the three process parameters together; hydraulic pressure, roller speed and roller gap so it is an indication of what happened to the powder during the compaction process. For this reason, it can be related to the ribbon properties.

The new method of determining the nip angle can be used to scale up the roller compaction process as there is no any assumption made to measure it and all the real affecting process and formulation parameters were taken into consideration.



# Chapter 7 Stress distribution across roller width

## 7.1 Introduction

More understanding of the roller compaction process is necessary to optimize the efficiency and to improve the quality of the product. It is clear from the literatures in Chapter 2 that one of the reported problems associated with roller compaction process is the inhomogeneity of the ribbon quality across the width. Consequently, the granules resulted from crushing of the ribbon centre may have different properties than the granules of the side. In addition, large amount of fines is produced at the side of the roller compared to the centre. Producing homogeneous ribbon is considered of great importance to the industry (Muliadi et al., 2013) however it is a challenge (Miguélez-Morán et al., 2008).

Another problem of the roller compactor is producing big amount of fines (Un-granulated powder). For hard materials such as calcium carbonate, the amount of fines is considerably high and difficult to reduce for a given system as shown in Section 5.3.3.

Funakoshi et al. (1977) used a rim roller instead of cheek side plates system with inclined wall of the rim at different angles. They found that using a rim roller with angle of 65° produced less amounts of fines. The same findings is confirmed by Parrott (1981) who used rim roller with concave-convex design. This improvement however is limited to a specific type of rollers (rim roller) and not tested on the roller with the side cheek plate. In addition, the inclination was only on the wall of the rim roller and not along the whole roller width. This might limit the pressure uniformity across the roller width.

In this chapter, the stress distribution across the ribbon width was investigated in different ways including a new technique involving online measurement of the temperature profile across the ribbon width. Based on the results, a new roller with a novel design was built and tested (Salman et al., 2016). Ribbon width, fines, local porosity across ribbon width, pressure and temperature profiles across the ribbon for both the flat standard and the new curved roller were measured and compared.

## 7.2 Materials and methods

Three materials (As received from the suppliers) were used in this study; microcrystalline cellulose (Avicel PH-101),  $\alpha$ -lactose monohydrate (Pharmatose 200M) and calcium carbonate. These materials were chose due to different mechanical attributes.

### 7.2.1 Ribbon production

Ribbons were produced using the same method that described in Section 3.3 with three different hydraulic pressures of 30, 70 and 100 bar at fixed roller gap and speed of 1.5 mm and 3 rpm respectively. There were no ribbons produced from calcium carbonate at hydraulic pressure of 30 bar. The ribbons were produced using two types of rollers; standard flat roller and the new curved built roller which explained in Section 7.3.2.

## 7.2.2 Determining the pressure profile shape across roller width

To determine the shape of the pressure profile across the roller width; a pre-scale film (Fujifilm, UK) was used (Osborne, 2013). The film changes its colour according to the applied pressure. It consists of two layers; micro-encapsulated colour-forming layer and colour developing layer as shown in Figure 7-1. When the stress is applied to the film, the microcapsules break and the colour forming materials react with the colour developing material to cause red patches appear on the film.

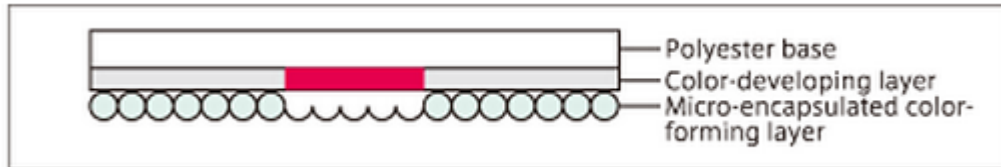


Figure 7-1: Pressure film (Fuji film)

Then the stress applied to the film can be determined from the relation between the color density and the stress according to the chart supplied by Fuji film and as shown in Figure 7-2.

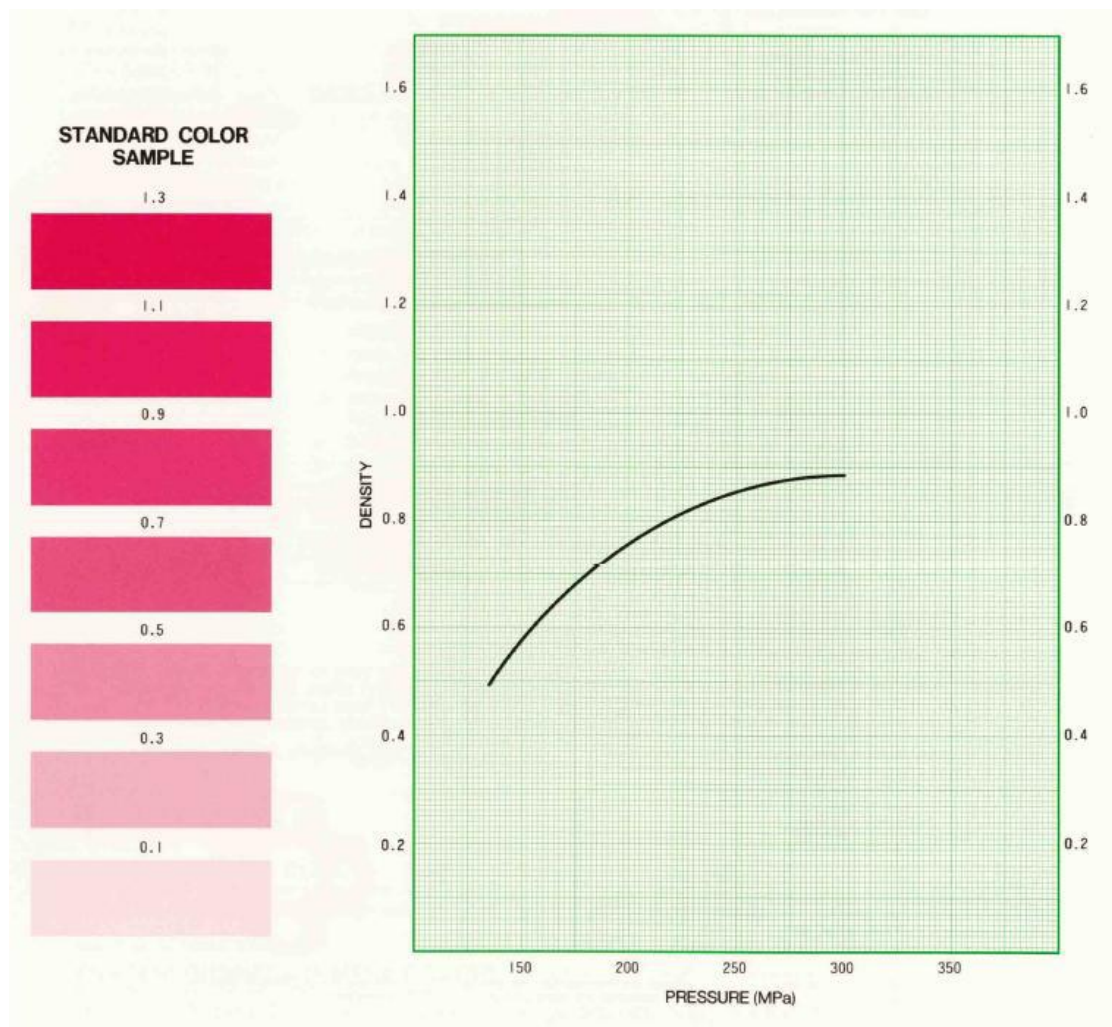


Figure 7-2: Pressure density chart supplied by Fujifilm (Fujifilm, 2012)

### 7.2.3 Measuring the porosity of the ribbon centre and side

The porosity of the ribbon centre and sides were determined by X-ray tomography and as described in Section 6.5.2.

### 7.2.4 Measuring the temperature profile across ribbon width

The temperature of the exiting ribbon from the rollers was recorded online using thermal imaging camera (FLIR SC655). The camera was positioned facing the point between the rollers where the ribbon was produced. The setup of thermal camera is shown in Figure 3-14. The videos of 1 min duration were analysed and the temperature profile along the width of the ribbon was measured. The temperature profile presented in this study is an average of 10 profiles determined at different time of the experiments.

## 7.3 Results and discussion

### 7.3.1 Flat standard rollers setup

The results in Sections 7.3.1.1- 3 are for experiments that were carried out using the two standard rollers of flat knurled surfaces. Figure 7-3 shows the setup used.

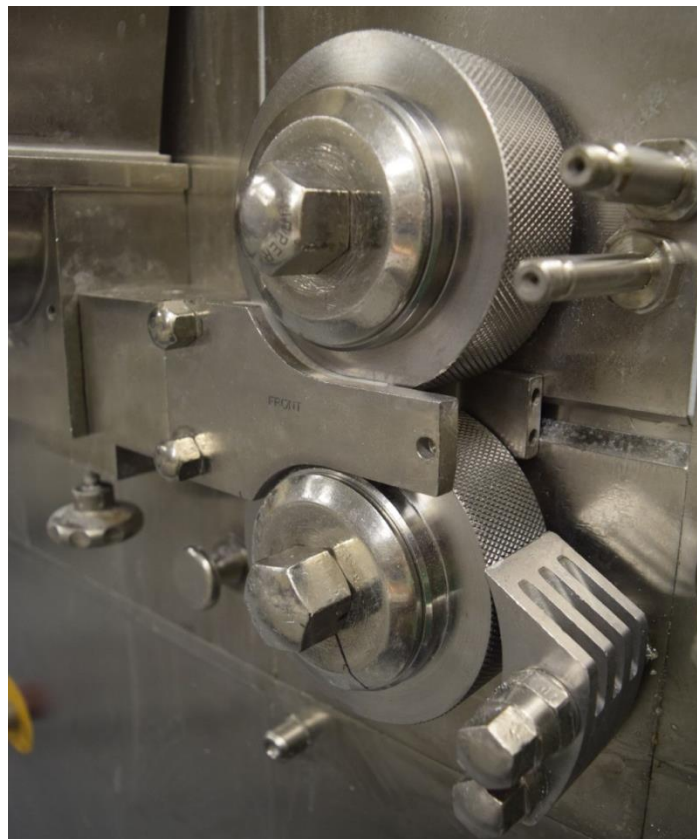


Figure 7-3: Two flat knurled rollers

#### 7.3.1.1 Pressure profile across ribbon width

The pressure profiles were determined using the pressure film (See Section 7.2.2). A piece of the film was inserted between the rollers during the production. Figure 7-4 shows a pressure film used with different materials at hydraulic pressure of 100 bar. It can be seen from the all used pressure films that the colour intensity in the centre is more than that at the sides of the

ribbon. This indicates that more stress acted on the materials at the centre than the sides. Previous study conducted by Miguélez-Morán et al. (2009) showed that the density at the centre of the MCC ribbon is higher than that at the sides. Another study by Muliadi et al. (2013) showed that the ribbon density is higher at the centre than the sides. They also compared the experimentally determined density distribution with the one predicted by the finite element method (FEM) and both methods agreed that the centre of the ribbon is denser than the sides.

It can be seen from Figure 7-4 that the colour of the pressure film used with calcium carbonate is darker compared to that of Pharmatose 200M which is also darker than the pressure film of Avicel PH-101. This is because harder material resulted in more stress applied to the film. These results confirm the results in Table 5-8 where the stress applied on different powder was calculated by Johanson's theory.

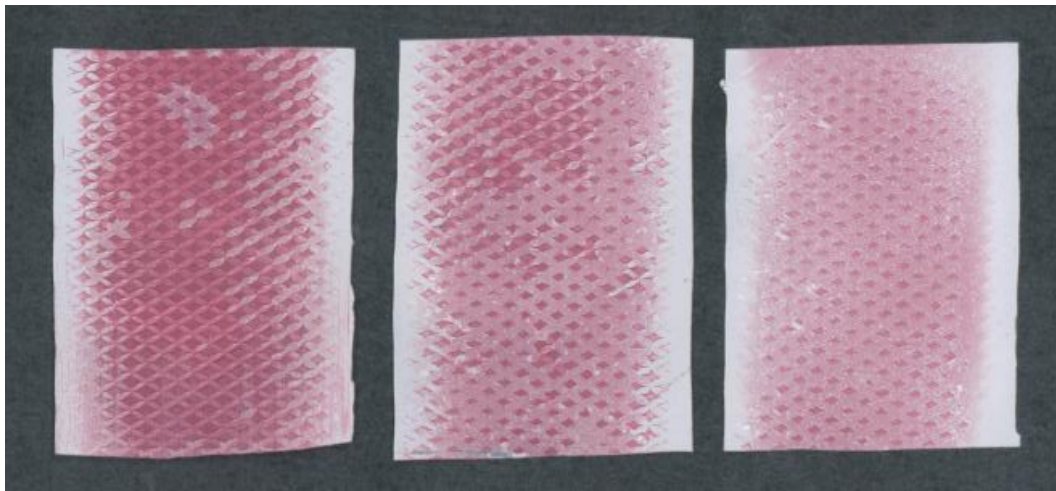


Figure 7-4: Pressure films after passed through the rollers (Left: Calcium carbonate, middle: Pharmatose 200M and right: Avicel PH-101)

Figure 7-5 shows an image of calcium carbonate ribbon taken during the production process. The image clearly shows that the ribbon sides are not well compacted compared to the centre.



Figure 7-5: Image of calcium carbonate ribbon during compaction showing un-compacted ribbon sides compared to the centre

### 7.3.1.2 Temperature profile across ribbon width

It has been shown in Section 5.3.4 that increasing the hydraulic pressure caused an increase in the ribbon surface temperature. This proved to be true for all materials.

Figure 7-6 shows the temperature profile across ribbon width for three materials; calcium carbonate, Pharmatose 200M and Avicel PH-101 using different hydraulic pressures. It can be seen from the figure that the temperature profile of calcium carbonate and Pharmatose 200M showing higher temperature at the centre than the sides. This is because the stress acting on the centre of the roller is higher than that at the sides. Higher stress caused an increase in the temperature of the ribbon centre as a result of more deformation and/or breakage in addition to the friction. It can be seen from the figure that the case is different for the temperature profile of the Avicel PH-101. At hydraulic pressure of 30 bar the temperature at the centre is higher than the temperature at the sides. However, increasing the hydraulic pressure to 70 and 100 bar caused the profiles to be the opposite with higher temperature at the sides than the centre. The whole width of the roller used to produce the ribbon is 40 mm. The width of the Avicel PH-101 ribbon produced at 30 bar is less than 40 mm and as shown in Figure 7-6 but for ribbon produced at 70 and 100 bar the width is 40 and 41 mm respectively. It is believed that during ribbon production, the ribbon with this width was in contact with the cheek plates and this caused increase in the temperature due to the high friction.

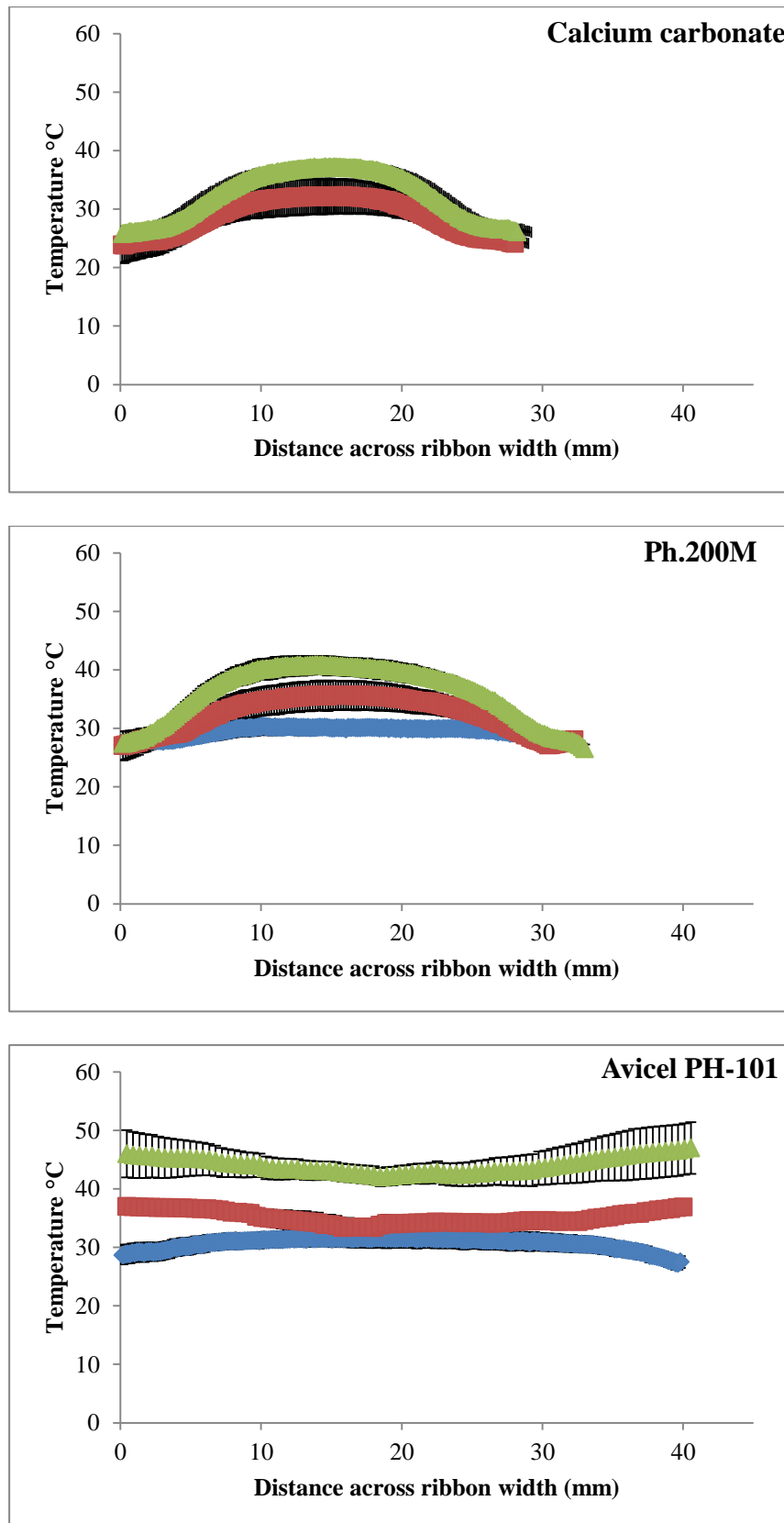


Figure 7-6: Temperature profile for different materials at different hydraulic pressures

◆ 30 bar, ■ 70 bar, ▲ 100 bar

### 7.3.1.3 Changing the colour of Avicel PH-101 powder after roller compaction

It has been noticed during the experiments of this study that there was a change in the colour of Avicel PH-101 after being compacted at hydraulic pressure of 150 bar and above. The ribbon centre was darker than the sides and as shown in Figure 7-7. Changing the colour of Avicel PH-101 powder after roller compaction were noticed by Wu et al. (2010). They also noticed that the colour mainly changed at the middle of the ribbon rather than the sides which is consistent with the results in this study. They explained the change of the colour to be caused by the hydrolysis and caramelisation process of glucose monomer which is resulted from processing at elevated pressure and temperature. Changing the colour of microcrystalline cellulose powder was investigated by Vanhatalo and Dahl (2014) while studying the effect of the acid hydrolysis on the MCC. They stated that changing the colour of MCC powder to brown with caramel smell is due to the caramelisation of the powder which consists mainly of dehydration and condensation reactions.

It is reasonable to expect that the temperature at the sides of Avicel PH-101 ribbon produced at 150 bar is higher than the centre because the ribbon width is also expected to be higher than 40 mm (The ribbon width at 100 bar is 41mm). In addition, it is also expected that the pressure profile at 150 bar has similar shape of that at 100 bar (see Figure 7-4) with higher colour intensity at the centre compared to the sides. This means the pressure and the colour profile have the same shape which is different than the temperature profile. From this comparison it can be concluded that changing the colour is mainly because of the applied pressure and not because of the temperature.



Figure 7-7 : Avicel PH-101 ribbon produced at 150 bar with dark colour at the centre part of the ribbon

### 7.3.2 Design of the new curved roller

From previous results and discussion, it is clear that the sides of the ribbon are less compacted and received less stress compared to the centre. This is true for the ribbons produced by different materials at different hydraulic pressures.

Based on these results, a novel design for a new roller has been suggested (Salman et al., 2016). The new design consists of a convex surface and as illustrated in Figure 7-8. The

curvature of the roller surface can be described as an arc of a circle with radius of 101 mm. The difference in the height between the centre and the side of the roller is 2 mm. The width and the diameter of the roller are 40 and 120 mm respectively. The roller was manufactured in-house at University of Sheffield by the technicians of the Chemical and Biological Engineering Department. The image of the roller is shown in Figure 7-9. The surface geometry was designed in a way to avoid the poor compaction at the roller edges by decreasing the available gap as moving from the roller centre along the rollers width towards the edges.

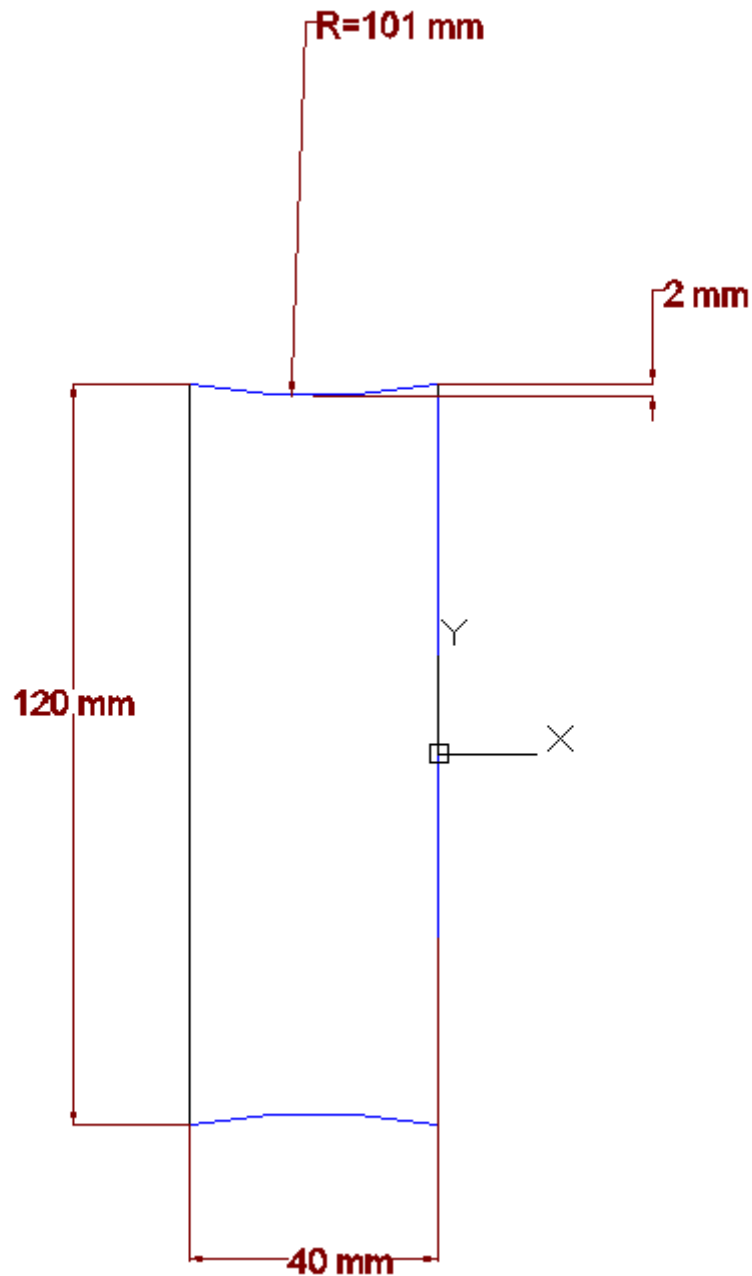


Figure 7-8: The design of the new roller



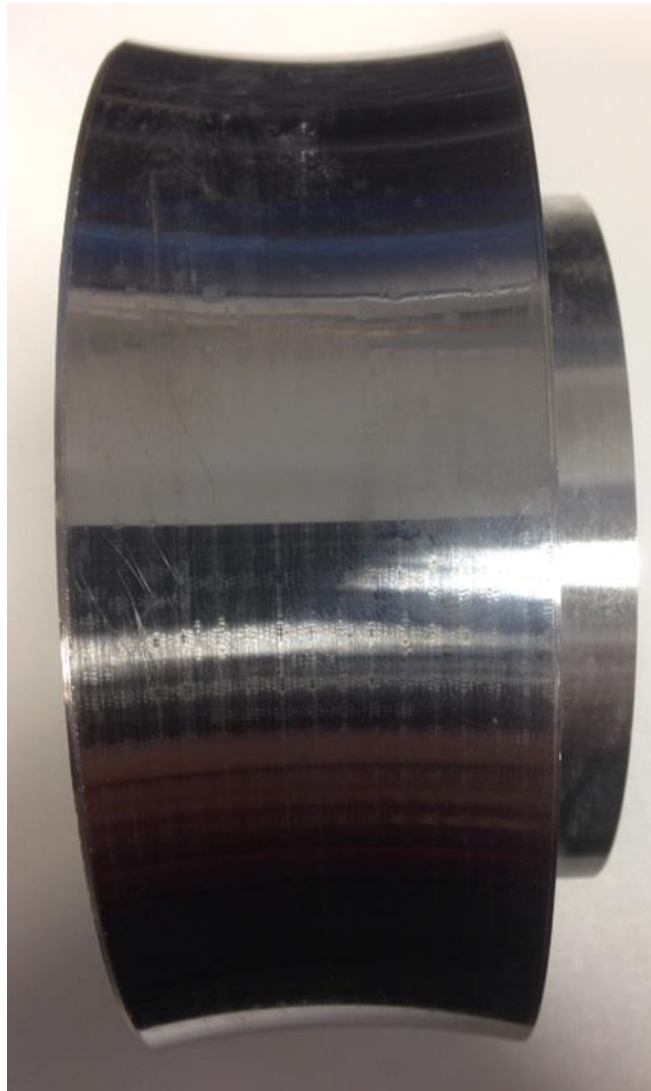


Figure 7-9: Image of the new roller built at the University of Sheffield

The same experimental design and ribbon characterisation methods that used previously with flat rollers were used with new curved roller setup. Figure 7-10 shows the setup used consisting of new curved roller at the top and flat standard roller at the bottom.

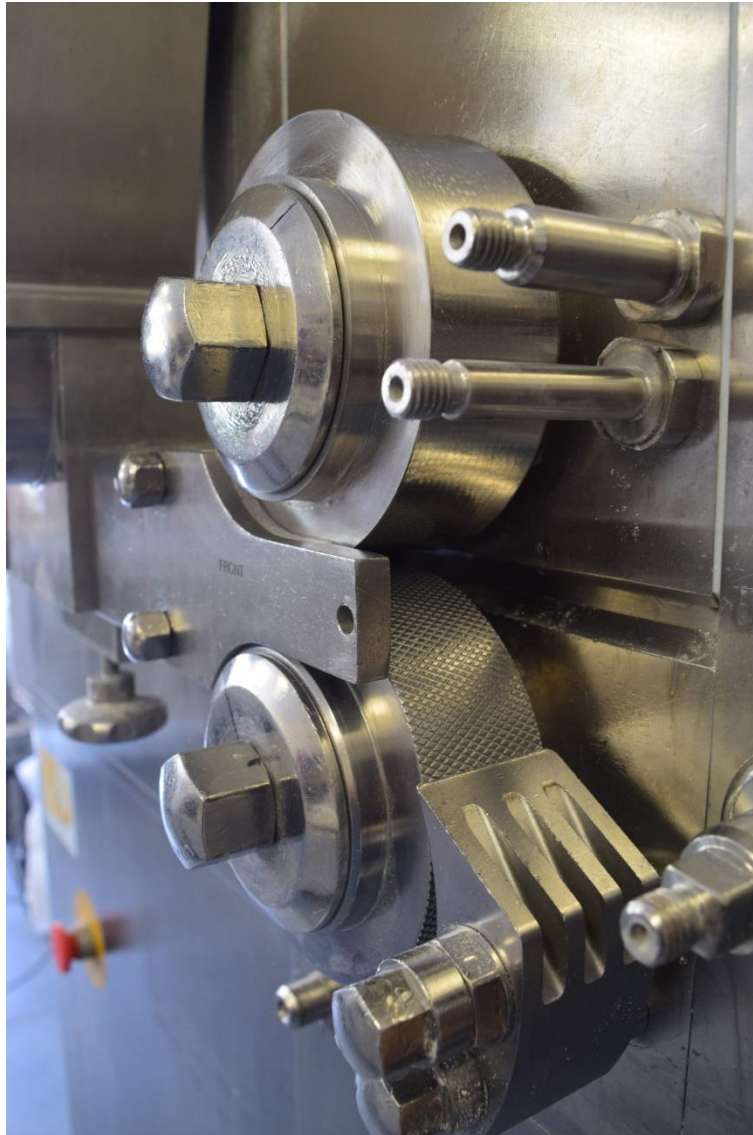


Figure 7-10: Experimental setup showing new curved roller and standard knurled flat roller

### 7.3.2.1 Pressure profile across the ribbon width

Figure 7-11 shows the pressure films used with three materials. It can be seen from the pressure films that the edges are darker than the centre which indicates more stress applied on the material at the edge of the roller compared to the stress applied at the centre. These pressure profiles are opposite to that using the standard rollers and as shown in Figure 7-4. Using new roller caused the pressure profile to be higher at the edges than the centre and that is because the gap at the edge is less which caused the powder to be compacted at higher pressure than the side.

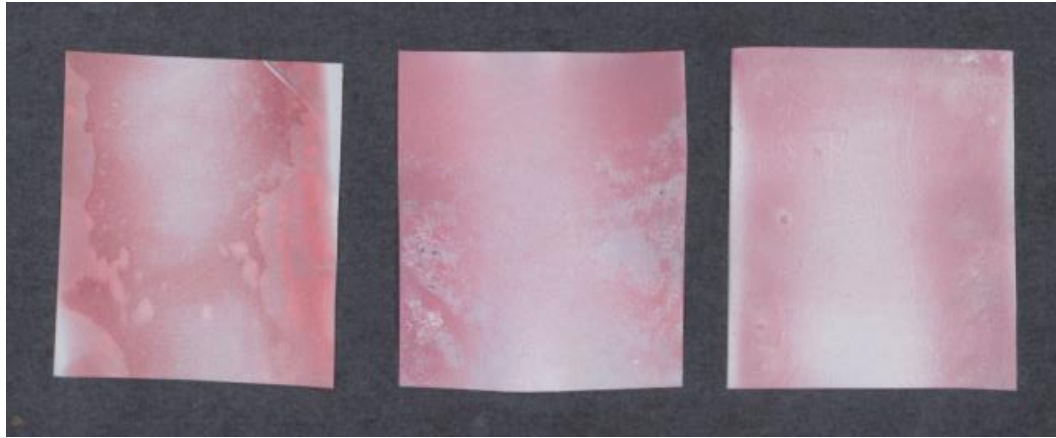


Figure 7-11: Pressure films after passing between the rollers at 100 bar

(Left: Calcium carbonate, Middle: Pharmatose 200M and right: Avicel PH-101)

### 7.3.2.2 Temperature profile across ribbon width

Temperature profiles across the ribbon width of three materials using the new roller are shown in Figure 7-12. It can be seen from the figure that for all materials, the temperature of the ribbon sides is higher than that at the centre. This is opposite to the temperature profiles of calcium carbonate and Pharmatose 200M at all pressures and of Avicel PH-101 at 30 bar in Figure 7-6. In addition, it can be noticed from Figure 7-12 that using the curved roller resulted in more uniform temperature distribution for calcium carbonate and Pharmatose 200M compared to the temperature profiles of these materials using the flat roller as shown in Figure 7-6. The surface geometry of the new roller caused a balance in the applied stress across the ribbon width. The small stress that supposed to be applied at the roller sides has been compensated by a decreasing gap across the roller width towards the roller sides. This decreased the difference in the stress applied at the centre and the sides of the roller and hence resulted in more uniform temperature profiles.

For Avicel PH-101, the temperature profiles at different hydraulic pressures show clear difference between the temperature at the sides and that at the centre. For hydraulic pressure of 30 bar, the width of the MCC ribbon is 39 mm which is less than the width of the roller. Despite of this, the temperature at the sides is higher than the centre. This suggests that the high temperature at the side is caused by a higher stress applied at the sides compared to the centre as there was no contact between the powder and the cheek plate. At higher pressure of 70 and 100 bar, the ribbon was produced with full width of 40 mm or higher so the heat generated at the sides was a contribution of the high stress applied to the sides and the friction with the cheek plate.

It can be seen from Figure 7-12 that for all materials, increasing the hydraulic pressure caused an increase in the temperature along the ribbon width. This confirms the previous conclusion that increasing the pressure caused an increase in the temperature regardless of the roller type. It can also be seen from Figure 7-12 that the temperature of Avicel PH-101 is higher than the temperature of other two materials.

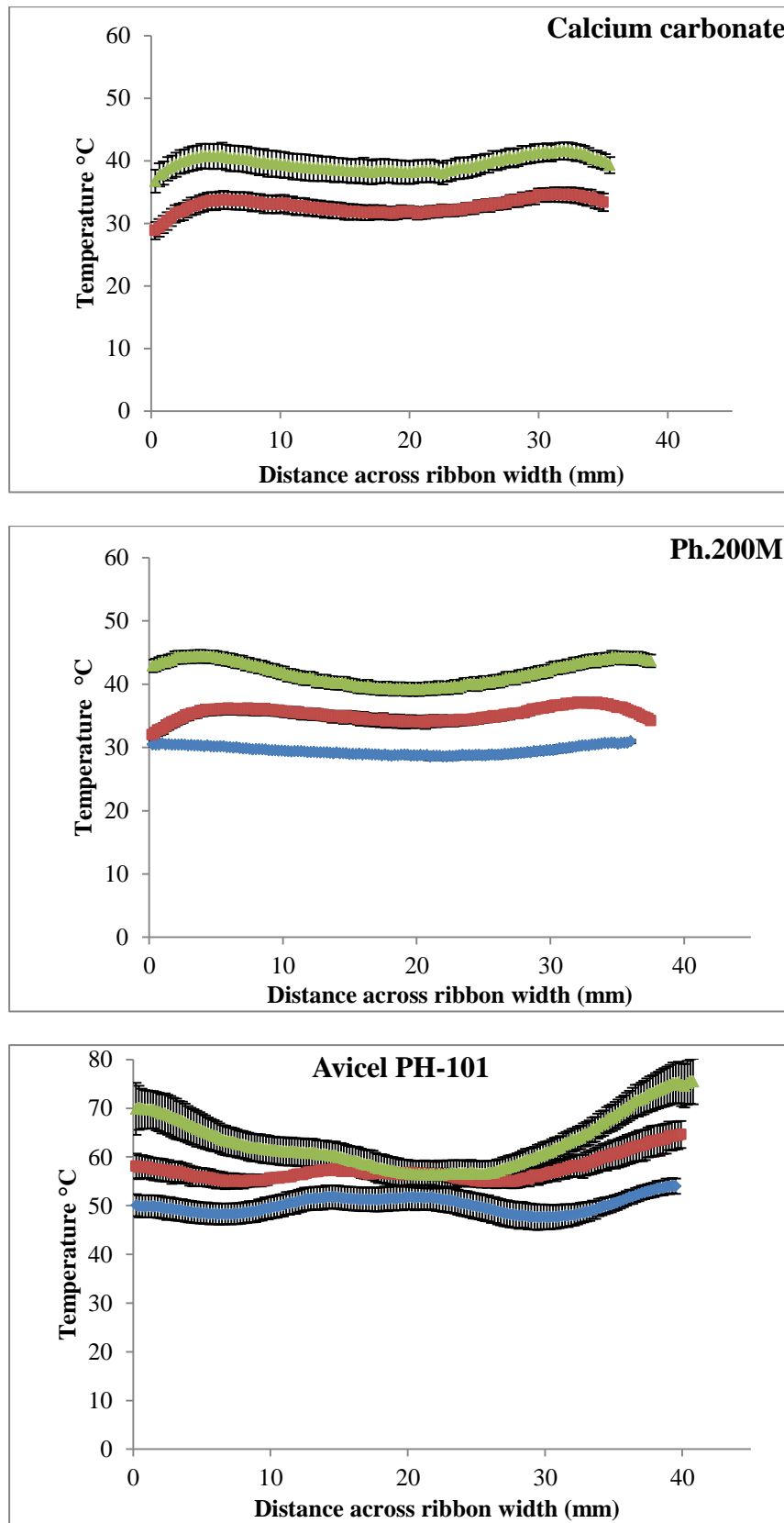


Figure 7-12: Temperature profile across the ribbon width of different materials at different hydraulic pressures produced using the new roller (◆ 30 bar, ■ 70 bar, ▲ 100 bar)

### 7.3.2.3 Changing the colour of Avicel PH-101 powder after roller compaction

Figure 7-13 shows an image of the Avicel PH-101 ribbon produced at 150 bar using the new roller. It can be seen from the image that the dark color is on the sides whereas the centre is almost white. This is opposite to the color profile of the ribbon produced using standard roller (See Figure 7-7). This is another indication that the stress applied on the sides of the roller is higher than the stress applied on the centre.

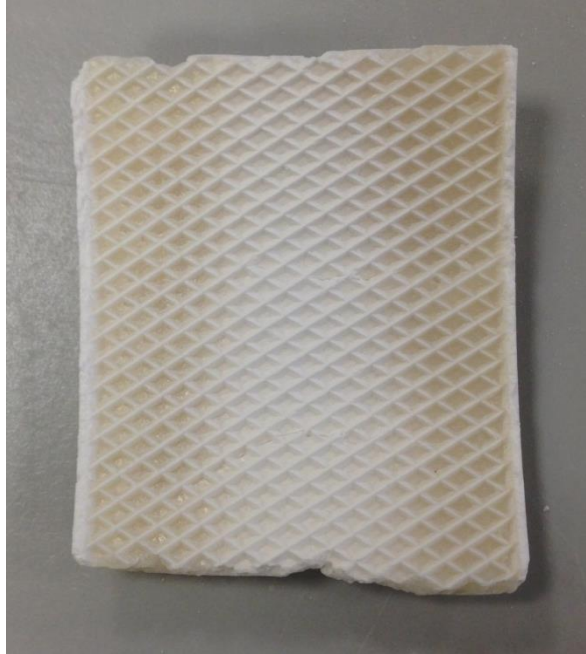


Figure 7-13: Avicel PH-101 ribbon produced at 150 bar using the new roller

## 7.3.3 Comparison of ribbon properties and percentage of fines produced by two types of roller

### 7.3.3.1 Ribbon width

The width of the ribbon produced by different materials was measured using digital caliper with a resolution of 0.01. Figure 7-14 shows a comparison between the width of the ribbons produced by the new curved roller and the standard flat roller in addition to the images of the ribbons produced by two roller types. The x-axis is the hydraulic pressure and the y-axis is the ribbon width in mm. It is clear from the figure that for calcium carbonate and Pharmatose 200M, the ribbon produced by the curved roller is wider compared to that produced by the standard flat roller. This is true for the three used hydraulic pressures. The ribbon of calcium carbonate showed significant increase in the width by around 7 mm followed by Pharmatose 200M with a difference of around 5 mm. There was almost no difference in the width of the Avicel PH-101 ribbons produced by the two different rollers. This is because even with using the flat roller, the ribbon width was almost equal to the full width of the roller. This is due to the good deformability of the Avicel PH-101 as shown in Chapter 5.

Calcium carbonate is hard material compared to other two materials and as determined in Section 4.1.2. For this reason, the ribbon produced by the standard flat roller was narrow as the pressure applied at the sides was not enough to bond the particles together. The surface geometry of the new curved roller helped the particles to bond to each other even at the sides of the roller as there was sufficient pressure applied on the materials due to the smaller gap

compared to the centre. The case is the same for Pharmatose 200M but with less sensitivity as the pressure applied at the side of the standard roller was relatively enough to bond the particles and creates relatively wide ribbon.

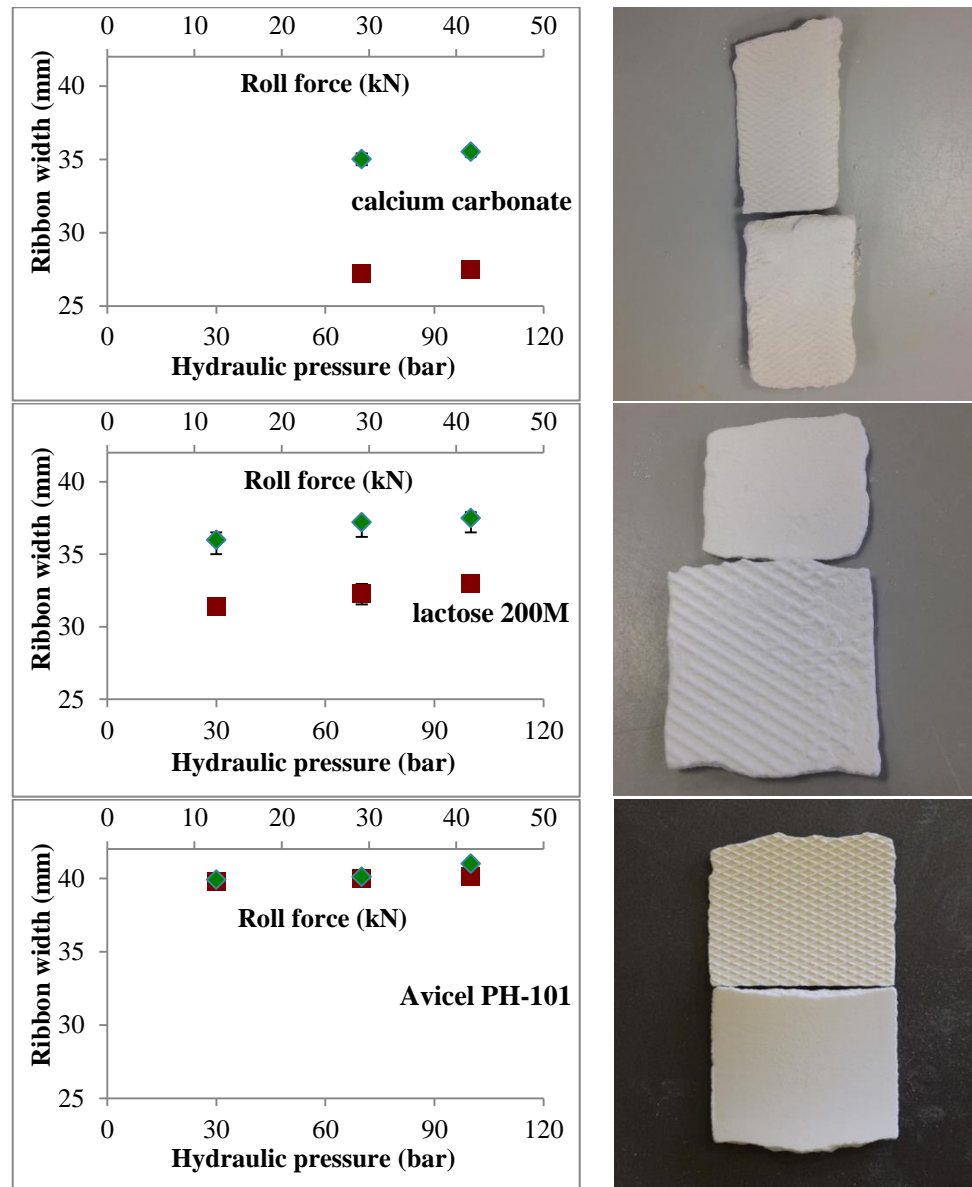


Figure 7-14: Comparison of ribbon width produced by the curved and the flat roller (■ flat roller, ◆ Curved new roller) – Ribbons in the images; Bottom: curved roller, top: flat roller

### 7.3.3.2 Amount of fines

Figure 7-15 shows a comparison of the weight percentage of fines produced by different materials at different hydraulic pressures using the flat and the curved new rollers. The x-axis is the hydraulic pressure and the y-axis is the weight percentage of the fines collected during roller compaction experiments. It can be seen from the figure that the percentage of fines of calcium carbonate and Pharmatose 200M produced with the curved new roller is less compared to that of flat roller. For Avicel PH-101, there is almost no difference in the percentage of fines. As seen in Section 7.3.3.1, the width of the ribbon increased by using the new curved roller which means more particles granulated and bonded to each other. It can be

seen from Figure 7-15 that the reduction in the amount of fines upon using the new curved roller is the highest for calcium carbonate followed by Pharmatose 200M. This trend is similar to the trend of increasing the ribbon width that discussed in Section 7.3.3.1 and it is related to the mechanical properties of the primary particles. The more the plastic deformation of the primary powder, the smaller the reduction in the amount of fines and the opposite for the hard material. This result is useful for industry because the hard material usually produces large amount of fines and it is important to reduce it. For plastically deformable materials such as Avicel PH-101, the amount of fines is already small so it is not a big issue.

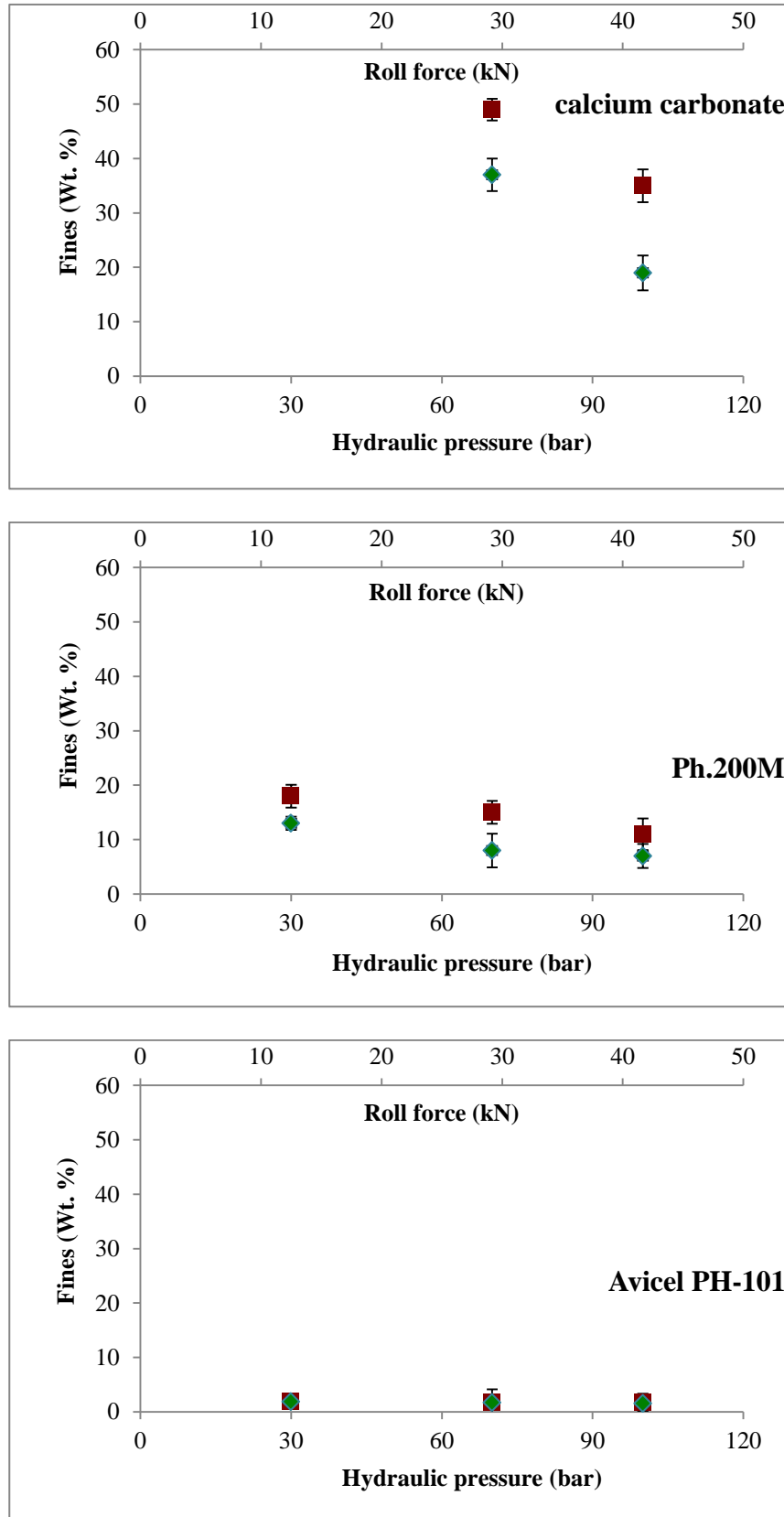


Figure 7-15: Comparison of the percentage of fines produced from different materials at different pressures using the flat and the curved rollers ( ■ flat roller, ◆ curved new roller)



### 7.3.3.3 Porosity of the side and centre of the ribbon

Table 7-1 shows the porosity of the side and the centre of the ribbon produced from different materials at different hydraulic pressure using the flat roller. The porosity has been determined using the X-ray tomography method that described in Section 6.5.2. It can be seen from the table that for all materials; the ribbon sides are more porous than the centre. This is because the stress applied on the centre of the ribbon is higher than that applied on the sides.

Table 7-1: Porosity of the side and the centre of the ribbon for different materials and hydraulic pressures using standard flat roller

Material	Porosity % - Flat roller					
	30 bar		70 bar		100 bar	
	Side	Centre	Side	Centre	Side	Centre
Calcium carbonate			14	5	11	2.5
Pharmatose 200M	28	17	23	8	20	4
Avicel PH-101	40	32	27	22	16	13

Table 7-2 shows the porosity of side and centre of the ribbon produced from different materials at different hydraulic pressure using the curved new roller. It can be seen from the table that the porosity of the centre and the sides are closer to each other in comparison to that in case of the flat roller. The more uniform stress applied by the curved new roller resulted in more uniform porosity across the ribbon width.

Table 7-2: Porosity of the side and the centre of the ribbon for different materials and hydraulic pressures using curved roller

Material	Porosity % - Curved roller					
	30 bar		70 bar		100 bar	
	Side	Centre	Side	Centre	Side	Centre
Calcium carbonate			11	8	6.2	4.7
Pharmatose 200M	24	26	18.5	19.03	11.25	12.5
Avicel PH-101	32	30	15.6	16.8	8.5	9.2

To quantify the difference between the porosity of the side and the centre of the ribbon, a new term ( $\Delta\phi$ ) was proposed. The term is defined as follows:

$\Delta\phi$ = Absolute value of the difference between the porosity of the side and the centre of the ribbon

Figure 7-16 shows the values of  $\Delta\phi$  for different materials and for different hydraulic pressures using the curved and flat roller setups. It can be seen from the figure that using the curved roller decreased the value of the  $\Delta\phi$  significantly. This means that the difference between the porosity of the centre and the side are minimised. This is due to the more uniform stress applied across the curved roller width and as previously explained.

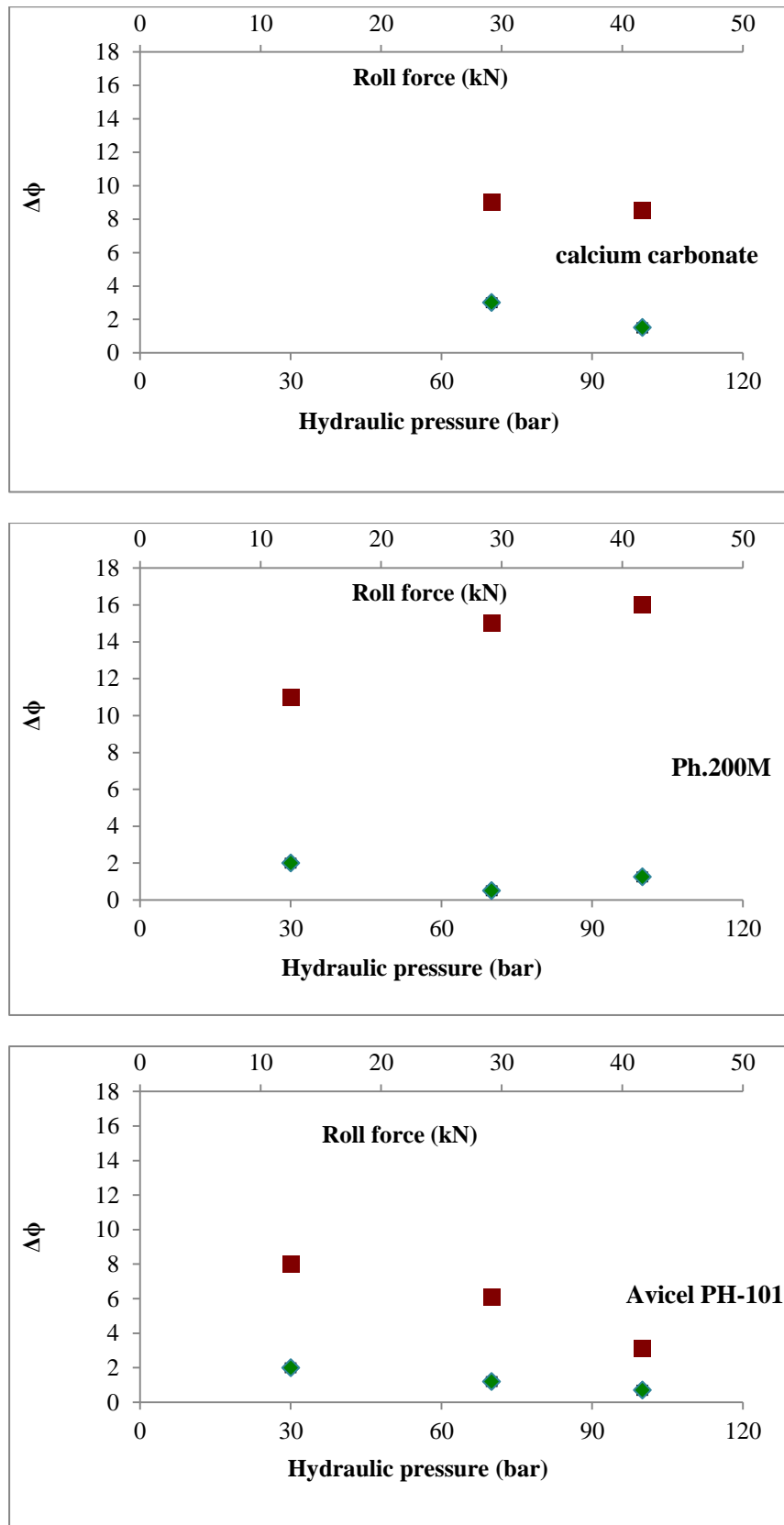


Figure 7-16: The value of  $\Delta\phi$  for different material using the flat roller (■) and the curved new roller (◆)

### **7.3.4 Comparison of ribbon quality of different materials produced by the curved and flat roller**

Ribbons from different materials such as polyvinyl alcohol, starch, maltodextrin and sodium carbonate were produced using the new curve roller and the flat roller setups. The ribbon width and the weight percentage of fines were determined and compared. Table A-1 in appendix A shows the results. It can be seen from the table that the curved roller reduced the amount of fines and increased the ribbon width for all materials. This confirms that the curved roller is useful to improve the quality of the ribbon produced from different materials.

## **7.4 Conclusion**

The pressure distribution across ribbon width was investigated using different methods. This was carried out by determining the pressure, temperature and colour profile across ribbon width in addition to determining the porosity at the side and the centre of the ribbon.

The results showed that the pressure distribution across the roller width significantly affects the width of the ribbon and the percentage of fines (un-granulated powder) in addition to the local porosity across the ribbon width. Based on these findings, a new roller with a novel design was built and tested (Salman et al., 2016). The new curved roller successfully produced significantly wider ribbon with fewer amounts of fines compared to the standard flat roller. In addition, the curved new roller reduced the heterogeneity of the porosity across the ribbon width.

As shown in this chapter and in Chapter 5, there is a clear relationship between the temperature of the ribbon of all materials and the applied pressure. Increasing the pressure caused an increase in the ribbon temperature. Based on this relation, this study suggests using the temperature distribution across the ribbon width as a new novel technique to determine the stress distribution applied on the powder during roller compaction process. Caution to be taken for plastically deformable material at high pressure, as these materials deforms during the compaction process and produce ribbon with full roller width which causes significant friction with the wall and that can generate heat which might mislead the results of the stress distribution. Using such an online technique during roller compaction process is especially useful for the industry.

# Chapter 8 Mechanical properties and granule size distribution

## 8.1 Introduction

In the industry, the roller compactor in most of the cases is used in combination with a crusher system to produce granules with better flowability and more bulk density compared to the primary powders. The size distribution is one of the most important granule properties (Perez-Gandarillas et al., 2016). The size dramatically affects the properties of the granules and the tablet made of it such as the friability (Ingelbrecht et al., 1997, Jeon et al., 2011).

Each industry targets a specific granule size depends on how the granules used downstream. In Pharmaceutical industry, the granules could be used to produce immediate release tablet, capsule, sachet, dry powder for suspension. Each of these products requires specific granule size.

Understanding the crushing process and the parameters that affect the granule size is important for the industry as it can be used to control and predict the granule size distribution for a given parameters and that will reduce the needs for the trial and error.

It was mentioned in the literatures that milling of strong compact produced larger granules compared to that produced from weak compact (Sheskey et al., 1994). The granule size distribution resulted from crushing the ribbon was previously used as an indication of ribbon strength (Osborne et al., 2013). However, the process is not well understood due to the complexity and strong dependence on the properties of the feed powders and on the crushing parameters such as rotor speed and mesh size.

In this chapter, the correlation between the mechanical properties of the ribbon and the granule size distribution resulted from crushing the ribbon was investigated. The study covers different materials with different mechanical properties. In addition, the effect of hydraulic pressure, crusher speed and crusher mesh size were investigated. Then the granule size distributions were fitted to Rosin- Rammler equation of two parameters. The parameters of the equation were correlated to the properties of the ribbon and single primary particle.

## 8.2 Materials and methods

Three materials were used in this study; MCC (Avicel PH-101),  $\alpha$ -lactose monohydrate (Pharmatose 200M) and calcium carbonate. These materials were chose to cover different mechanical properties; Avicel PH-101 is plastically deformable material, Pharmatose 200M is partially plastic/ brittle and calcium carbonate is hard/brittle material.

The particle size distributions of the primary powder are shown in Figure 8-1. The x-axis is the particle size and the y-axis is the undersize cumulative % based on volume.

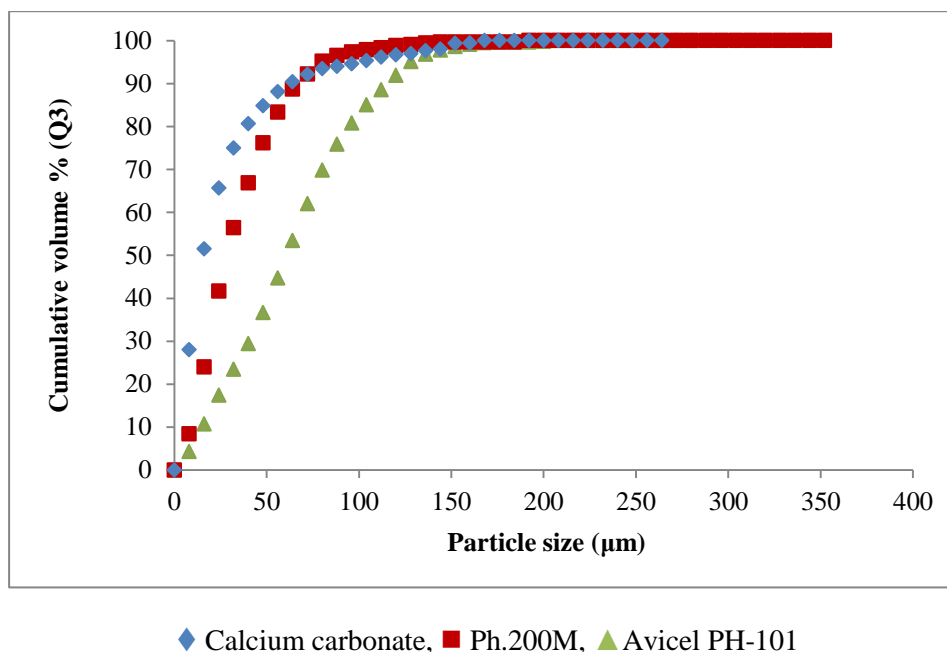


Figure 8-1: Particle size distribution of the three primary powders

### 8.2.1 Powder preparation

Prior to any experiment, all the powders were conditioned in the humidity chamber at relative humidity of 40% and temperature of 20 °C for three days.

### 8.2.2 Ribbon production

The same system that is described in Section 3.3 was used to produce ribbon of three different materials. Different hydraulic pressures of 30, 70 and 100 bar were used along with fixed roller gap and speed of 1.5 mm and 3 rpm respectively. To keep powder humidity constant during the experiments, the feed hopper was covered with a lid and continuously supplied with conditioned air of 40% RH supplied by humidity generator (Gen RH supplied by surface measurement system, UK).

The ribbon of calcium carbonate produced at hydraulic pressure of 30 bar was very weak and difficult to handle. For this reason, it was not considered in this study.

### 8.2.3 Ribbon characterization

#### 8.2.3.1 Ribbon hardness

The hardness of the ribbon, at the centre, of different materials produced at different hydraulic pressure was determined. The test comprised of applying load of 70 N by a sapphire ball indenter of 2 mm diameter. The indenter image is shown in Figure 8-2. The image captured using an optical microscope (VHX-5000, Keyence VHX digital microscope).



Figure 8-2: Sapphire ball that used as indenter to determine the hardness of the ribbon

The ball attached to the flat punch of the mechanical testing machine (Zwick Roell, Germany). The maximum load was held on the sample for 30 seconds then removed. The diameter of the resulted impression in two directions was measured using a microscope (VHX-5000, Keyence). Figure 8-3 shows an example of the impression left, after removing the load, on the surface of Pharmatose 200M ribbon. Then the cross sectional area was determined using the average of the two measured diameters. The hardness has been calculated by dividing the applied maximum load by the cross sectional area of the impression.

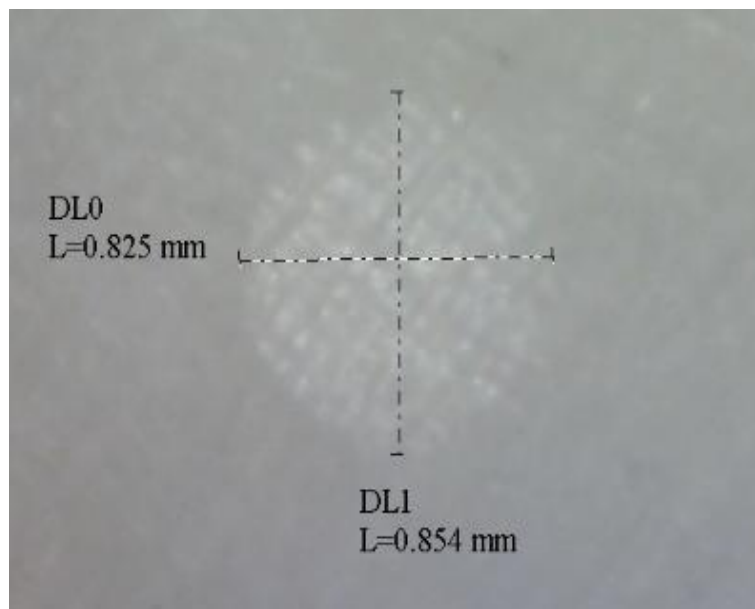


Figure 8-3: Typical impression resulted from the indentation of Pharmatose 200M ribbon surface

### 8.2.3.2 Ribbon strength

The strength of the ribbons produced by different materials for different hydraulic pressures were determined using three point bend test that described in Section 3.4.1. At least ten pieces of good non-broken ribbon were tested and averaged.

### 8.2.4 Crushing of the ribbon

The ribbons produced by different materials at different hydraulic pressures were separated from the fines and from the small broken pieces (flakes). About 100 gram of ribbons (approximately 3 cm long each) produced at a given condition was crushed for 1 minute using a rotary bar mill attached to the roller compactor. The crusher is shown in Figure 8-4. The crushing system consists of two rotors; Pre crusher and fines crusher. The granules passed through a U shaped screening mesh of different sizes at the top and the bottom. The granules passed through the mesh by rotors. The rotor speed range is between 30-100 rpm. The distance between the rotors and the mesh is kept constant for all experiments. This is achieved by using a collar ring that could be adjusted to control the space between the mesh and the blades of the rotors.

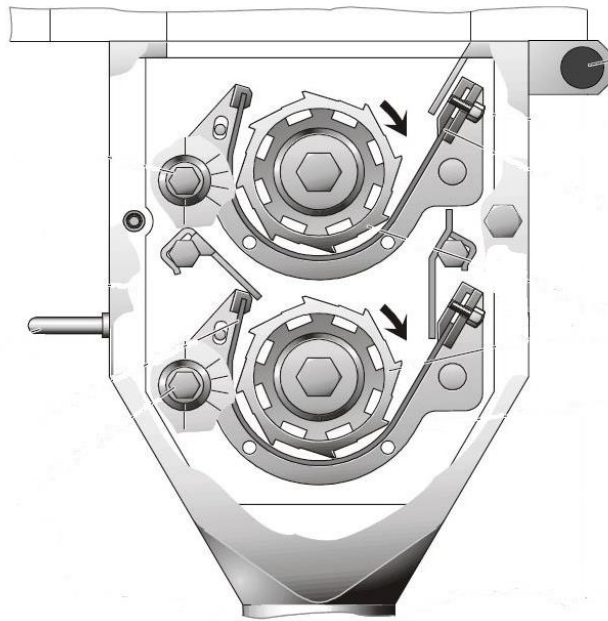


Figure 8-4: Crusher system used to crush the ribbons (Alexanderwerk)

### 8.2.5 Measuring the granule size distribution

The granule size distributions resulted from crushing the ribbons were determined using CAMSIZER<sup>®</sup>XT manufactured by Retsch Technology, Germany. The device is able to measure a particle size from 1  $\mu\text{m}$  to 3 mm. To ensure that the sample of the granules is representative for the bulk of the granules, a chute splitter sampler was used. It consists of a V-shaped trough. The granules are halved into two parts then one of these parts is halved again. This process is repeated many times until the desired quantity of the sample is obtained.

### 8.2.6 Crusher fines

In addition to the fines that is left after compaction, there is also fines coming from the crusher. The crusher fines is defined in this study as the volume % of the granules/powder with size under the size of the primary powder. This is determined by comparing the granule size distribution with the primary particle size distribution.

### 8.3 Design of the experiments

In this chapter, the granule size distribution resulted from crushing the ribbons of different materials were investigated as a function of different parameters. The study consists of three sets; effect of hydraulic pressure (Roll force), effect of crusher speed and the effect of the crusher mesh size. Table 8-1 shows the design of the experiments for the three sets.

Table 8-1: Experimental design of the three different sets

Set title	Roller compactor parameters			Crusher parameters	
	Hydraulic pressure (bar)	Roller speed (rpm)	Roller gap (mm)	Mesh size (mm)	Crusher speed (rpm)
Effect of hydraulic pressure (Roll force)	30, 70 and 100 (Roll force of 12.4, 29 and 41.5 kN)	3	1.5	1.6 & 2.15	40
Effect of crusher speed	100 (Roll force of 41.5 kN)	3	1.5	1.6 & 2.15	30, 70 and 100
Effect of mesh size	100 (Roll force of 41.5 kN)	3	1.5	0.63 & 1 1.6 & 2.15 2 & 3.15	40

## 8.4 Results and discussions

### 8.4.1 Ribbon hardness

The hardness of the ribbon centre produced using different materials at different hydraulic pressures is listed in Table 8-2. Each number is average of five measurements.

Table 8-2: Hardness of ribbon centre produced by different materials at different hydraulic pressure

Material	Hardness of the ribbon produced at 30 bar (GPa)	Hardness of the ribbon produced at 70 bar (GPa)	Hardness of the ribbon produced at 100 bar (GPa)
Avicel PH-101	0.04	0.20	0.24
Pharmatose 200M	0.0045	0.09	0.12
Calcium carbonate	-----	0.0012	0.0098



It can be seen from the table that the hardness of Avicel PH-101 ribbon is higher than the hardness of other materials and this is applied for all hydraulic pressures. The used indenter is a sphere of 2 mm diameter. Indenter with this size was landed on a ribbon area that consists of many primary particles as illustrated in Figure 8-5. Because of this big indenter size and relatively high applied force, the determined hardness value was influenced mainly by the strength of the bonding between the particles and not by the plastic deformation of these particles. This is confirmed by the results in Table 8-2. The ribbon hardness of Avicel PH-101 is the highest despite the lowest hardness of the single primary particle. High ribbon hardness could be explained by the strong bonding between the primary particles. The hardness of the Pharmatose 200M ribbon is medium whereas the lowest hardness was determined for the calcium carbonate ribbon. It is known from Chapter 4 that calcium carbonate is hard material and it is not producing a strong ribbon as the bonds between the particles are very weak.

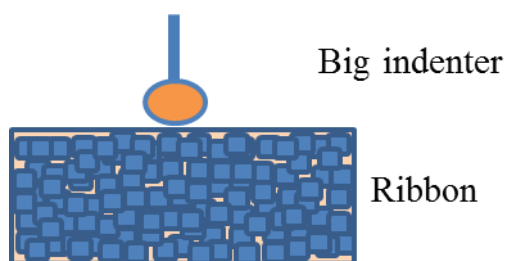


Figure 8-5: Illustration of ribbon hardness measurement concept

The case is different for measuring the nano-indentation hardness where a small indenter was used to apply low force on a single primary particle and as shown in Figure 8-6. The determined value of the hardness is affected by the plastic deformation of the material.

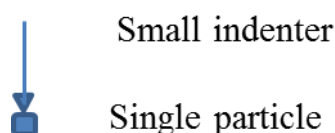


Figure 8-6: Illustration of the nano-indentation hardness measurement concept

It can be also noticed from Table 8-2 that for all materials, increasing the hydraulic pressure caused an increase in the hardness of the ribbon. This is because increasing the hydraulic pressure caused an increase in the strength of the bonding between the particles.

#### 8.4.1.1 Ribbon strength

The ribbon strength was measured using three points bent test described in Section 3.4.1. Table 8-3 shows the tensile strength of the ribbon produced by different materials at different hydraulic pressures. It can be seen from the table that the strength of the Avicel PH-101 ribbon is the highest among other materials and in general, increasing the hydraulic pressure caused an increase in the ribbon strength for all materials. These results are in agreement with the results of the ribbon hardness as both showing the same trend. This is another

confirmation that the hardness of the ribbon reflecting the ribbon strength and not the plastic deformation.

Table 8-3: Tensile strength of the ribbon of different materials produced at different hydraulic pressures

Material	Tensile strength of the ribbon produced at 30 bar (MPa)	Tensile strength of the ribbon produced at 70 bar (MPa)	Tensile strength of the ribbon produced at 100 bar (MPa)
Avicel PH-101	1.3	6.8	8.4
Pharmatose 200M	0.36	0.87	1.7
Calcium carbonate	-----	0.07	0.26

## 8.4.2 Granule size distribution

### 8.4.2.1 Effect of roller force

In order to investigate the effect of hydraulic pressure on the granule size distribution, ribbons produced from three materials at different hydraulic pressures were crushed using 40 rpm crusher speed and mesh size of 1.6 mm at the bottom and 2.15 mm at the top. Figure 8-7 shows a comparison of the granule size distributions. The y-axis is the cumulative % based on the volume and the x-axis is the granule size. The presented granule size is average of three repetitions for each condition. It can be seen from the figure that the granule size distribution of calcium carbonate is smaller than that of Pharmatose 200M and Avicel PH-101. The figure also shows that the granule size distribution of the Pharmatose 200M and Avicel PH-101 are almost the same for the same hydraulic pressure except a small difference at 70 and 100 bar where Pharmatose 200M produced smaller granules at small size classes.

The figure suggests that using the granule size as indication of the ribbon strength is not always applicable.

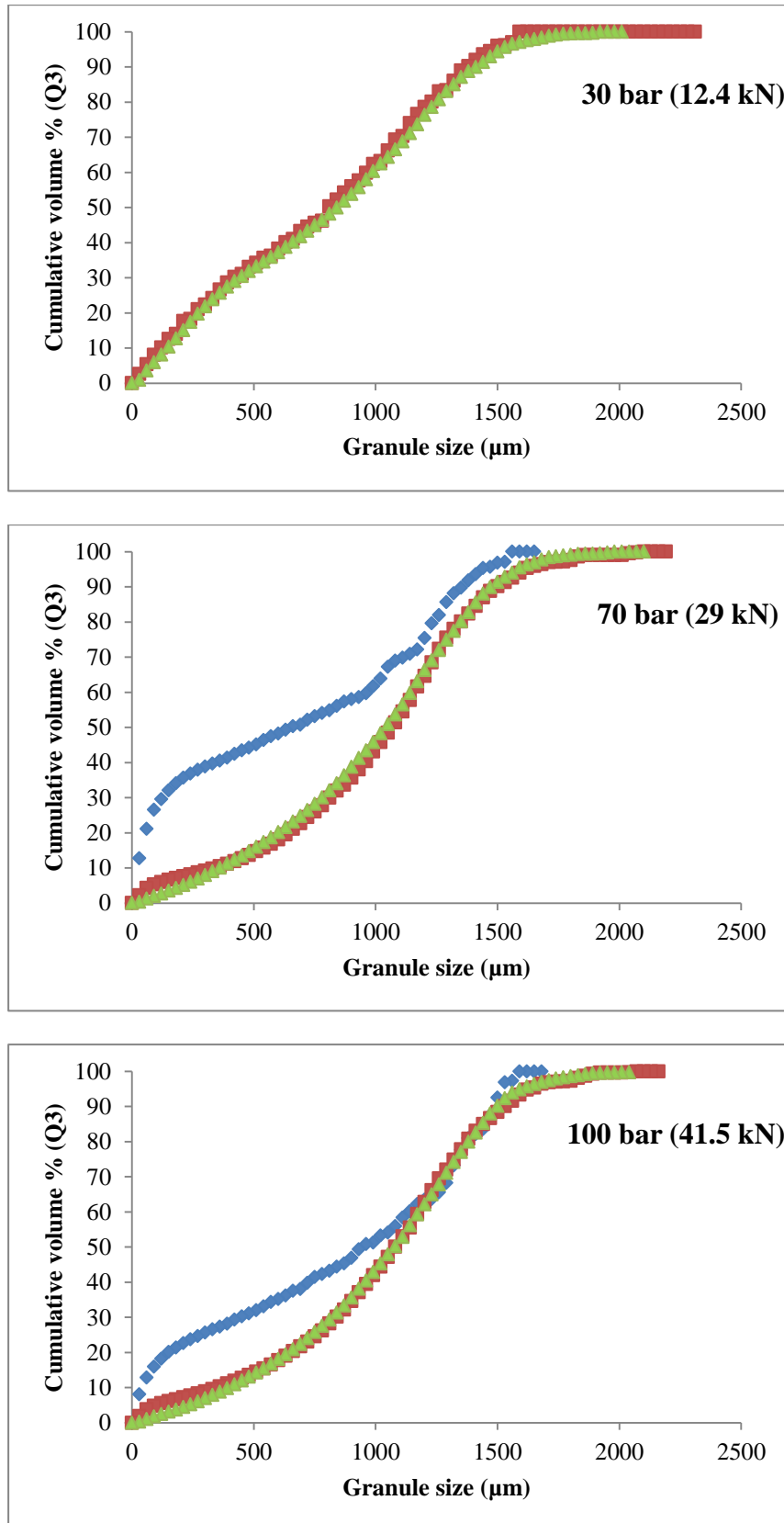


Figure 8-7: Granule size distribution of different materials produced at different hydraulic pressures (♦ Calcium carbonate, ■ Ph.200M, ▲ Avicel PH-101)

Calcium carbonate ribbon is weak as it can be seen from Tables 8-2 and 8-3. Upon crushing, the ribbon broke into small granules and may even turned back to primary particle as there is no strong bond to hold the particles to each other.

Large fragments of Pharmatose 200M and Avicel PH-101 in the sample indicate a resistance to breakage compared to weak ribbon of calcium carbonate. This was supported by the ribbon hardness and strength data that listed in Tables 8-2 and 8-3.

Although the ribbon strength of Avicel PH-101 is higher than that of Pharmatose 200M, the granules size distributions are almost the same for different hydraulic pressures. The crushing force applied to the ribbons during the crushing process is governed mainly by the size of the mesh that the granules need to pass through (Sakwanichol et al., 2012). This is because the ribbon pieces are continuously sheared by the rotating blades until they become small enough to pass through the mesh. The used mesh size of 1.6 and 2.15 mm are relatively big and it was relatively easy for the granules to pass through it without being hit many times by the rotating blades. For this reason, there was no difference in the granule size distribution of these two materials.

Figure 8-8 shows the crusher fines of different materials as a function of hydraulic pressure. It can be seen from the figure that the fines produced by calcium carbonate is the highest among other materials followed by Pharmatose 200M and the less fines produced by crushing of Avicel PH-101. It can be seen from the figure that as the hydraulic pressure increased, the crusher fines decreased and this is because increasing the pressure created a strong bond between the particles and it was not easy to break it compared to the ones produced by lower pressure. Freitag et al. (2005) investigated the amount of crusher fines for four different magnesium carbonate powder. They reported that all materials showed a decrease in the amount of fines upon increasing the pressure of roller compactor which is in agreement with the results of this study. Figure 8-8 shows that the decreasing rate of the fines of calcium carbonate is high and this is believed to be due to a high increasing rate of ribbon strength and hardness with increasing the pressure. This is especially affects the percentage of fines when the ribbon is very weak such as the ribbon of calcium carbonate at 70 bar. For Pharmatose 200M and Avicel PH-101, the ribbon are strong, even at low pressure, compared to the calcium carbonate ribbon so the percentage of fines are less sensitive to the increase in the ribbon strength.

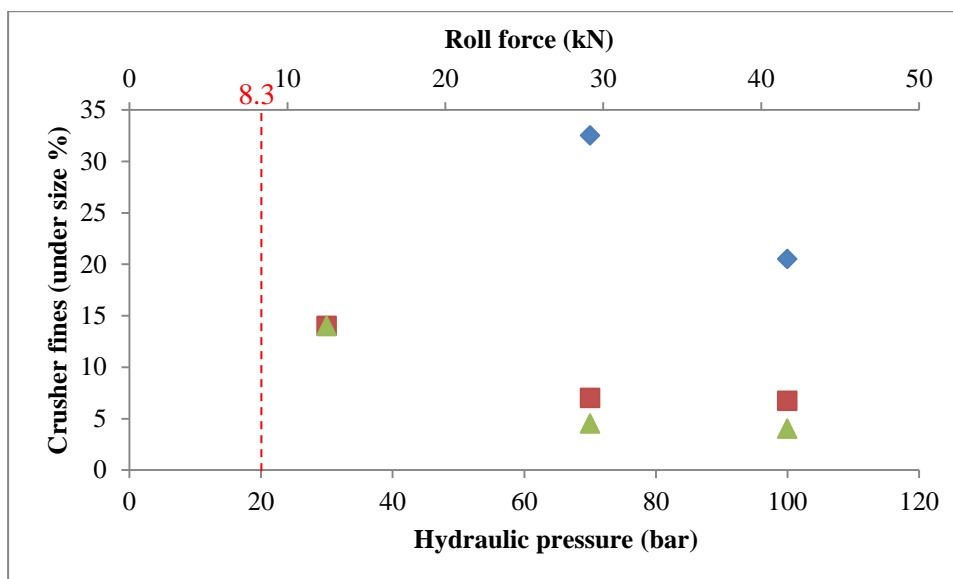


Figure 8-8: Crusher fines produced by different materials using different hydraulic pressures

(♦ Calcium carbonate, ■ Ph.200M, ▲ Avicel PH-101)

The data of Figure 8-7 will be presented in a different way to compare the granule size for the ribbon produced at different hydraulic pressures for each material. Figure 8-9 shows a comparison of granule size distributions resulted from crushing ribbons of each materials produced at different hydraulic pressures. For Avicel PH-101, there is almost no difference between the granules of 70 and 100 bar but it can be noticed that the granules of 30 bar is smaller than the granules of other two pressures. It can be seen from Tables 8-2 and 8-3 that there is no big difference between ribbon hardness and strength of 70 and 100 bar whereas the hardness and the strength of the ribbon produced at 30 bar are much less. Weaker ribbons mean less resistance to the breakage so the applied crusher force was enough to break the 30 bar ribbon into small pieces.

The case is almost the same for the ribbon of Pharmatose 200M at different hydraulic pressures. There is significant difference between the granule size distributions resulted from crushing of 30 bar ribbon compared to the granule size distribution of the 70 and 100 bar. It can be seen also that there is no difference between the granules size of 70 and 100 bar.

By comparing the granule size distribution of the calcium carbonate at 70 and 100 bar, it can be seen that increasing the hydraulic pressure of the roller compactor caused an increase in the granule size. This is because of the same reason that caused a big decrease in the percentage of fines in Figure 8-8.

Freitag et al. (2005) reported that the mean diameter of magnesium carbonate granules increased upon increasing the roll force of the roller compactor. Another study conducted by Sakwanichol et al. (2012) also showed an increase in the granule size of a powder mixture upon increasing the force of the roller compactor. Osborne et al. (2013) investigated the effect of the roller compactor pressure on the granule size of maltodextrin powder. They showed an increase of the granule size upon increasing the pressure.

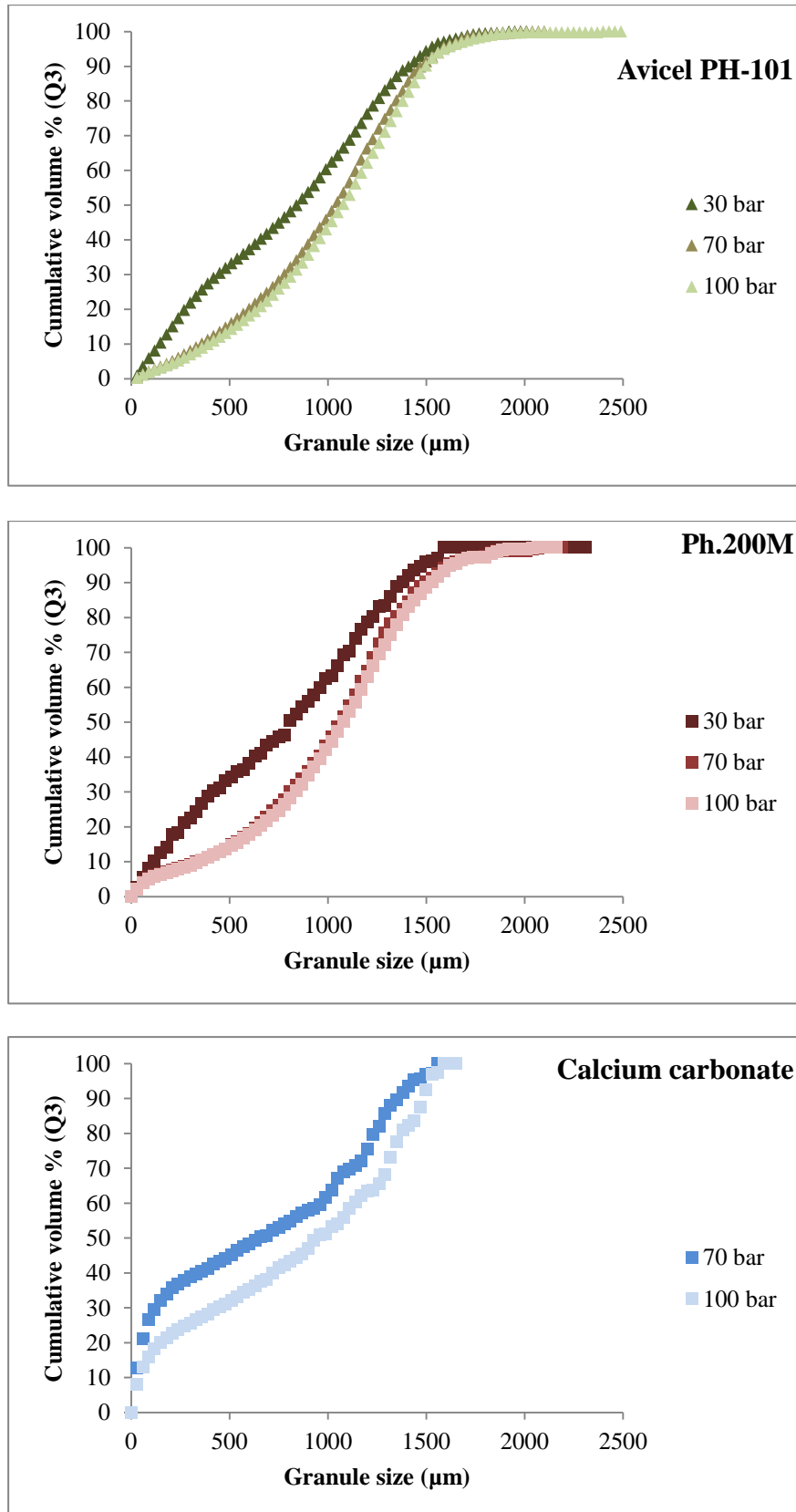


Figure 8-9: Comparing the granule size distribution of each material at different hydraulic pressures

### 8.4.3 Effect of crusher speed

Different crusher rotor speeds of 30, 70 and 100 rpm were used as input parameter to crush the ribbons. The granule size distribution and the amount fines were measured as output parameters. All other parameters were kept constant during the experiments and as illustrated in Table 8-1. Figure 8-10 shows a comparison of the granule size distribution resulted from crushing the ribbons of different materials produced at different rotor speeds. It can be seen from the figure that for different crusher speeds, the granules of calcium carbonate within approximately the first half of the size class (x-axis) is smaller than the granules of the other two materials; Pharmatose 200M and Avicel PH-101. At higher size classes, calcium carbonate has almost the same size compared to other materials. This means that calcium carbonate produced a lot of small and big granules in the same time. Calcium carbonate produced smaller granules than other two materials because the ribbon is weaker compared to other materials and as shown in Tables 8-2 and 8-3. On the other hand and although Avicel PH-101 produced larger granule size compared to Pharmatose 200M, the difference was small. The reason for this was relatively big mesh size of 1.6 mm at the bottom and 2.15 mm at the top of the crusher. Using a mesh of a big size means that the ribbon does not need to break to very small pieces in order to pass through the mesh and this removes the effect of different ribbon strength.

Figure 8-10 confirms the conclusion from Figure 8-7 that the granule size could not be always used as indication of the ribbon strength. The granule size affected by the roller compactor and crusher process parameters.

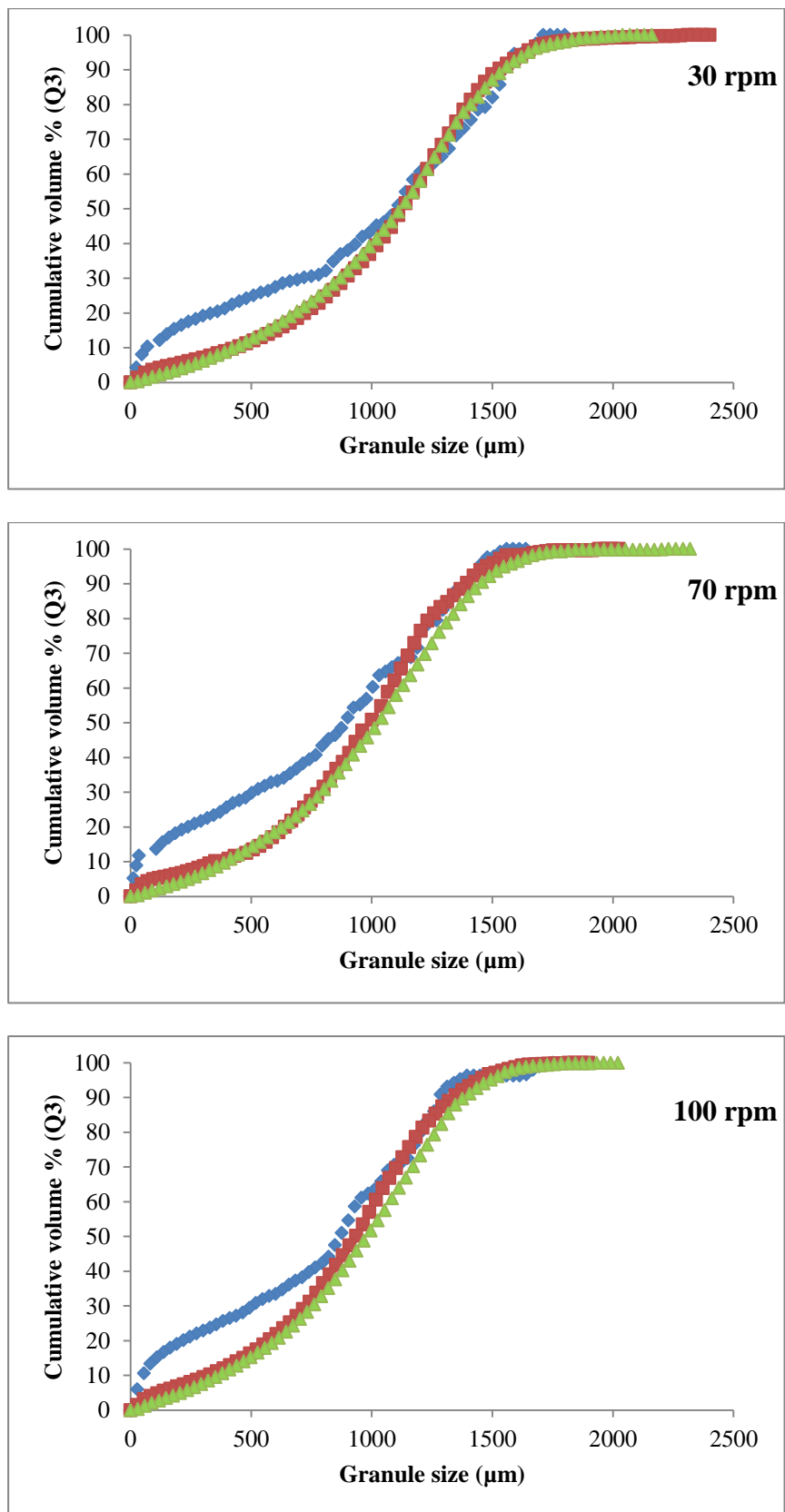


Figure 8-10: Granule size distribution of different materials produced at different rotor speeds

(♦ Calcium carbonate, ■ Ph.200M, ▲ Avicel PH-101)



The granules size distribution resulted from crushing the ribbons of each material at different crusher speeds are shown in Figure 8-11. These are the same data of Figure 8-10 but presented in a different way. It can be seen from the figure that for the three investigated materials, increasing the crusher speed caused a decrease in the granule size distribution. As the crusher rotor speed increase, there will be more chance for the ribbon to be scratched by the blades and the mesh wires which caused a decrease in the granule size. The effect of the crusher rotor speeds on the granule size has been investigated previously. Sakwanichol et al. (2012) showed that the granule size resulted from crushing of MCC ribbon decreased with increasing rotor speed. They also showed an increase in the amount of fines with increasing rotor speed. Their results are consistent with a study conducted by Lee and Evertsson (2011) using cone mill. They showed that increasing the rotation speed cause an increase in the amount of fines and decrease in the size of the product. This was attributed to the bigger crushing zone and the applied stress on the feed materials. Meghwal and Goswami (2014) stated that the speed of the rotor is highly affected the force applied on the material during the crushing process.

Figure 8-12 shows the amount of fines produced by crushing of different materials as a function of crusher rotor speed. It can be seen from the figure that as the speed increase, the fines increase too and this is due to the same reason of decreasing the granule size distribution that discussed in the previous paragraph.

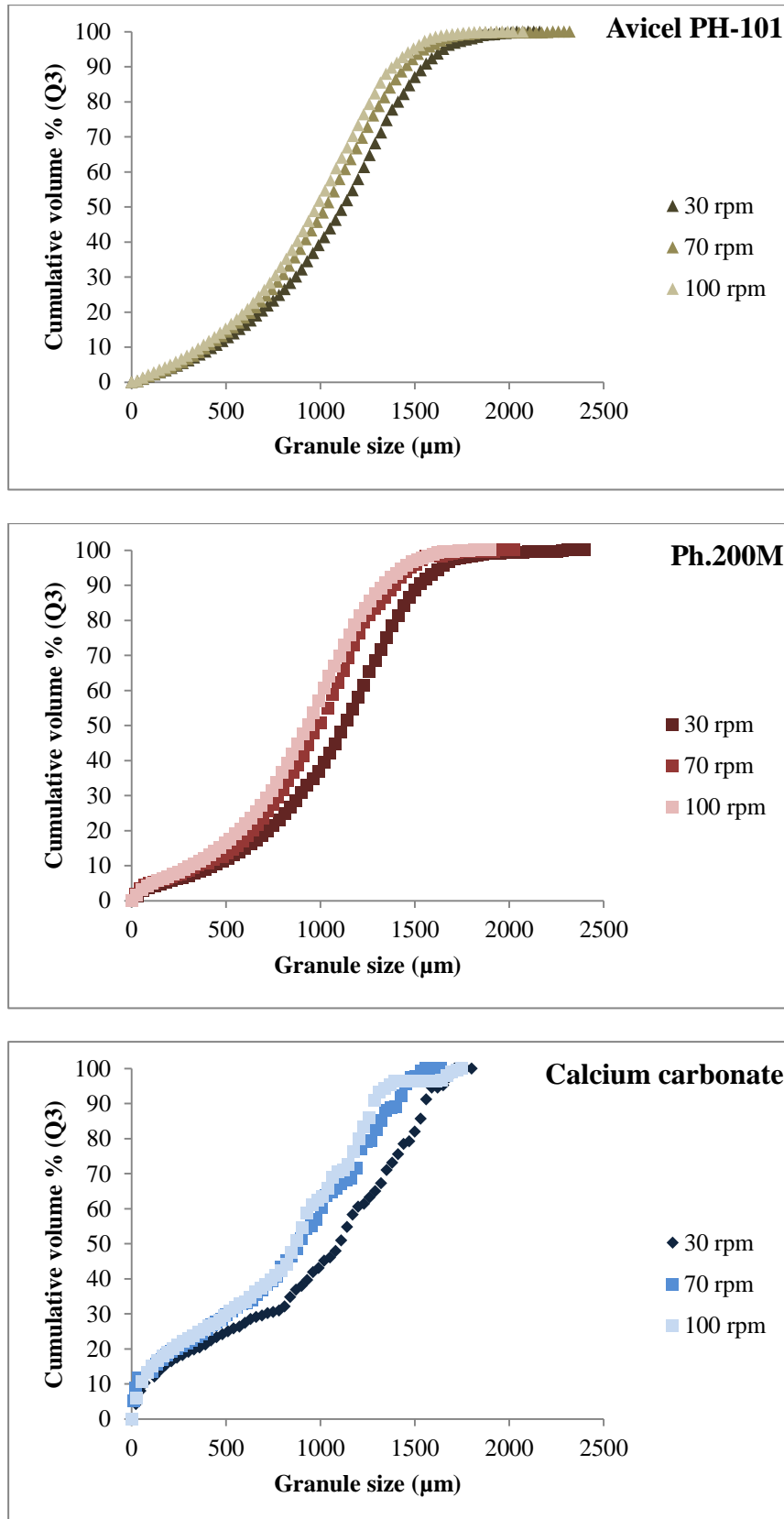


Figure 8-11: Comparing the granule size distribution of each material at different rotor speeds

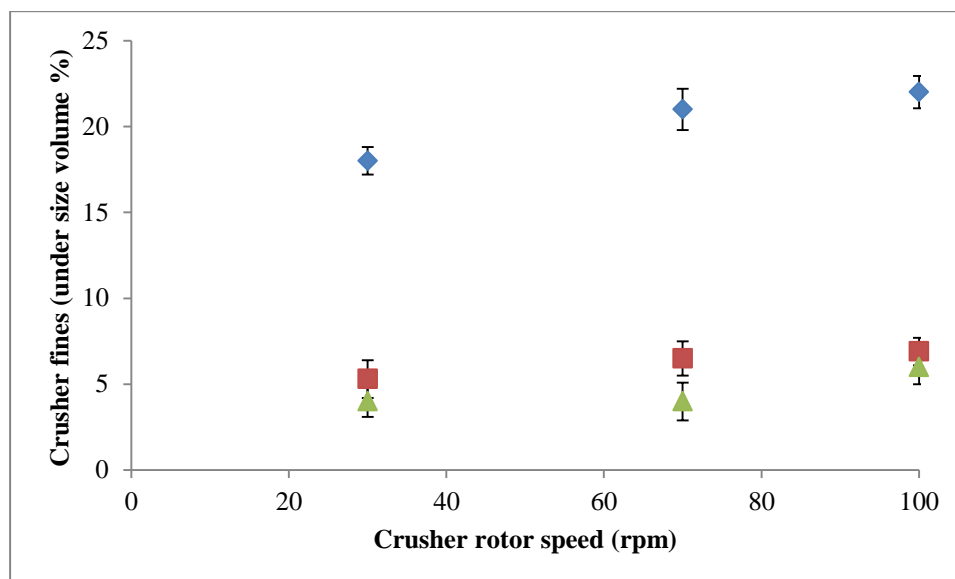


Figure 8-12: Crusher fines produced by different materials using different rotor speeds

(♦ Calcium carbonate, ■ Ph.200M, ▲ Avicel PH-101)

#### 8.4.4 Effect of crusher mesh size

To investigate the effect of the mesh size on the granule size distribution, experiments were carried out to crush the ribbons produced from different materials at hydraulic pressure of 100 bar using three mesh sizes; 0.63- 1 mm, 1.6- 2.15 mm and 2- 3.15 mm. Figure 8-13 shows a comparison of the granules size of the three materials resulted from crushing the ribbon of 100 bar using different mesh sizes. It can be seen from the figure that using the smallest mesh size of 0.63 and 1 mm caused a difference in the granule size distribution of different materials. Avicel PH-101 produced large granules compared to the granules of the Pharmatose 200M which is also larger than the granules of the calcium carbonate. This is the only set of parameters that resulted in a clear difference in the granule size of all three materials and for all size classes. Strong ribbon produced large granules and the opposite for the weak ribbon. For this set of parameters, the granule size can be used as an indication of the ribbon strength.

Using bigger mesh sizes of 1.63- 2.5 mm and 2- 3.15 mm almost removed the difference between the granules size of Avicel PH-101 and Pharmatose 200M but still produced small size of calcium carbonate granules compared to the granule size of other materials.

Using a small mesh size caused more contact between the ribbon and the mesh as the material needs to be smaller to pass through the mesh. The ribbon was rubbed more by the mesh which caused a decrease in the granule size. Strong ribbon such as ribbon of Avicel PH-101 survived more on the mesh and resisted the breakage as it has the highest strength. For this reason it produced larger granules compared to other materials. The same things happened to the Pharmatose 200M ribbon which produced larger granules than calcium carbonate.

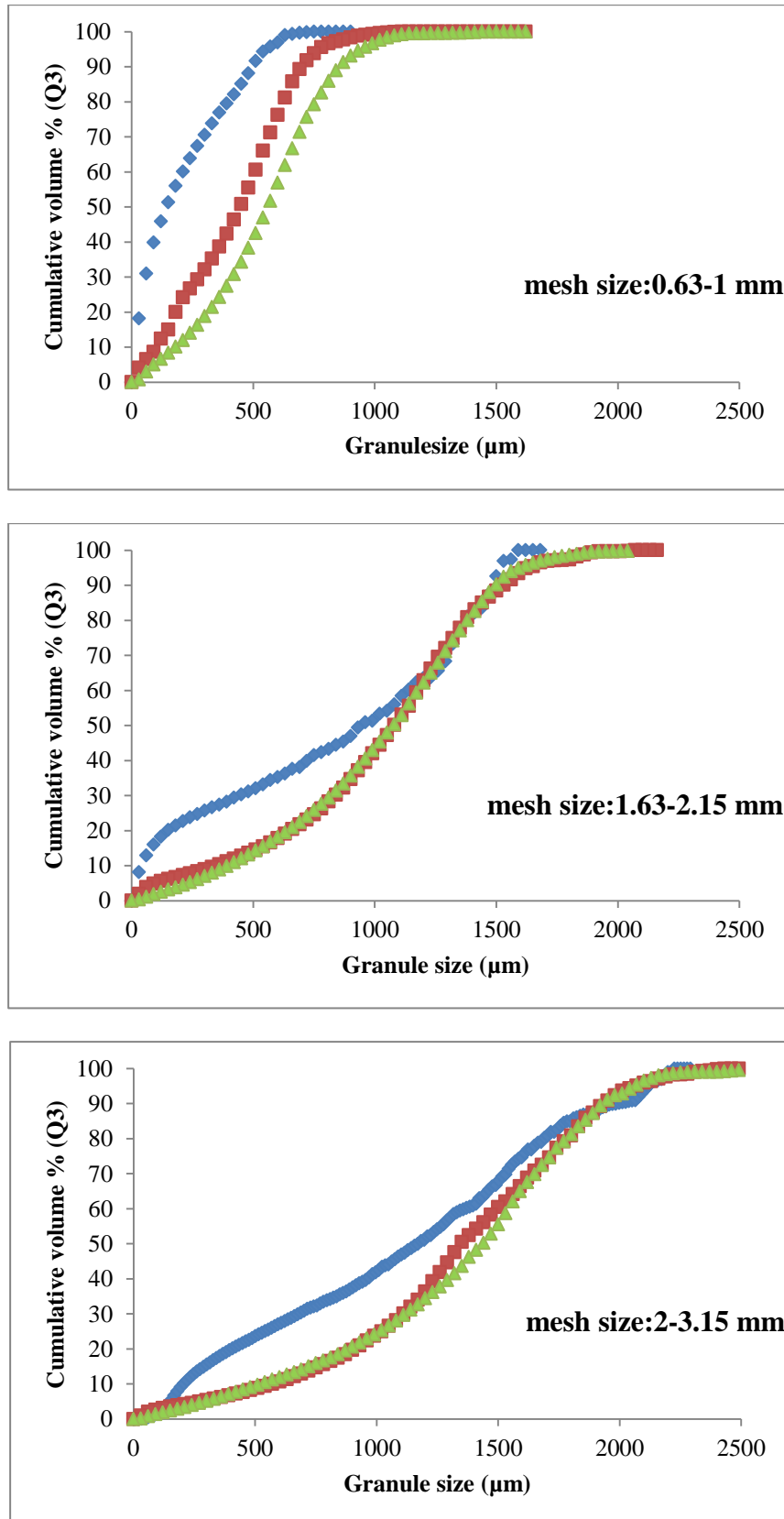


Figure 8-13: Granule size distribution of different materials produced at different mesh sizes

(♦ Calcium carbonate, ■ Ph.200M, ▲ Avicel PH-101)

Figure 8-14 shows a comparison of the crusher fines produced by different materials using different mesh sizes. It can be seen from the figure that for all mesh sizes, calcium carbonate produced the largest amount of fines compared to other materials followed by Pharmatose 200M and the smallest amount of fines was for Avicel PH-101. The figure shows a clear difference in the amount of fines produced by different materials with using the smallest mesh size of 0.63- 1 mm. As the mesh size increased, the difference in the fines produced by different materials decreased.

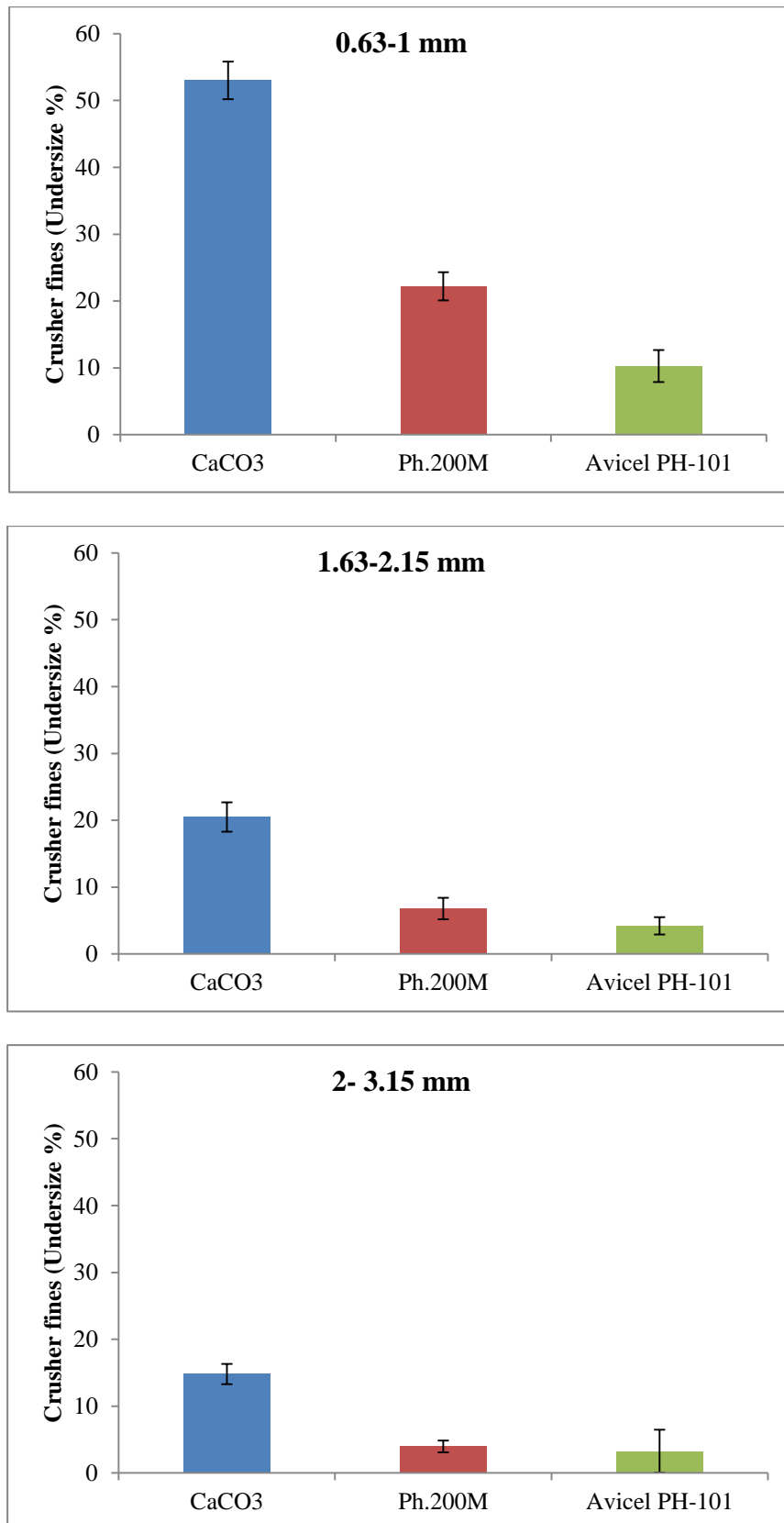


Figure 8-14: Crusher fines produced by different materials using different mesh sizes

### 8.4.5 Fitting the granule size distribution to Rosin-Rammler equation

The previous results of the granule size distributions for different materials showed that the granule size can be used as indication of the ribbon strength upon using a small mesh size of 0.63- 1 mm. Using larger mesh size resulted in an insignificant difference in the granule size between the Pharmatose 200M and Avicel PH-101. The difference stills insignificant for different hydraulic pressures of roller compactor and for different rotor speeds of the crusher.

The particle size distribution can be presented in different ways. It can be presented as a table or commonly presented as a curve which is showing the percentage of each class versus the particle size. The other way to represent the particle size distribution is by mathematical formula. This is considered to be the best among other methods mainly for two reasons; first it is easy to extrapolate and interpolate. Second the constants in the mathematical formula could be correlated with the process parameters or even with the material properties that of interest to the process. That helps in prediction of the particle size.

Many mathematical formulas have been developed to represent the particle size distribution including the 3 and 4 parameters formula. Although they provide high accuracy, their application is limited due to the complexity (Djamarani and Clark, 1997).

In this study, the granule size distributions resulted from crushing the ribbons of three materials using the smallest mesh size of 0.63- 1 mm were fitted to Rosin- Rammler equation. Using of a small mesh size resulted in a correlation between ribbon mechanical properties and the granule size. In this case, the constants of Rosin- Rammler equation can be correlated to the strength and the hardness of the ribbon.

Rosin-Rammler equation is suitable to describe the skewed particle size distribution of the powder in which significant amounts of powder are either large or small (Allen, 1997). The equation could be written as mentioned in Section 2.7.3 (Eq.2-30):

$$Y = 1 - \exp\left(\frac{-x}{x_0}\right)^n \tag{Eq.2-30}$$

Where

Y Cumulative % undersize of size x

n Uniformity constant which is an indication of spreading of particles

$x_0$  Size parameter at which 63 % of the particles pass through

The linear form of the equation can be derived to be:

$$\log \ln \left[ \frac{1}{1-Y} \right] = n \log x - n \log x_0 \tag{Eq. 2-31}$$

This is an equation of a line.  $x_0$  is defined as the size at which  $\ln \left[ \frac{1}{1-Y} \right] = 1$

Where n is the slope of the line

The fittings were carried out by nonlinear model fit regression using Mathematica 9 software code (Appendix A).

Figure 8-15 shows the results of the fitting. For all materials, dark color is the experimental data whereas the continuous light color line is the data predicted by Rosin-Rammler equation. It can be seen from the figure that for all materials, the predicted granule size is quite close to the experimental one.  $x_0$  is the size at which 63% of the particles will pass through. An increase in the  $x_0$  means larger granules whereas  $n$  is the uniformity constant. Small  $n$  value indicates less difference between the particle volume percentages (density size distribution) of different size classes.



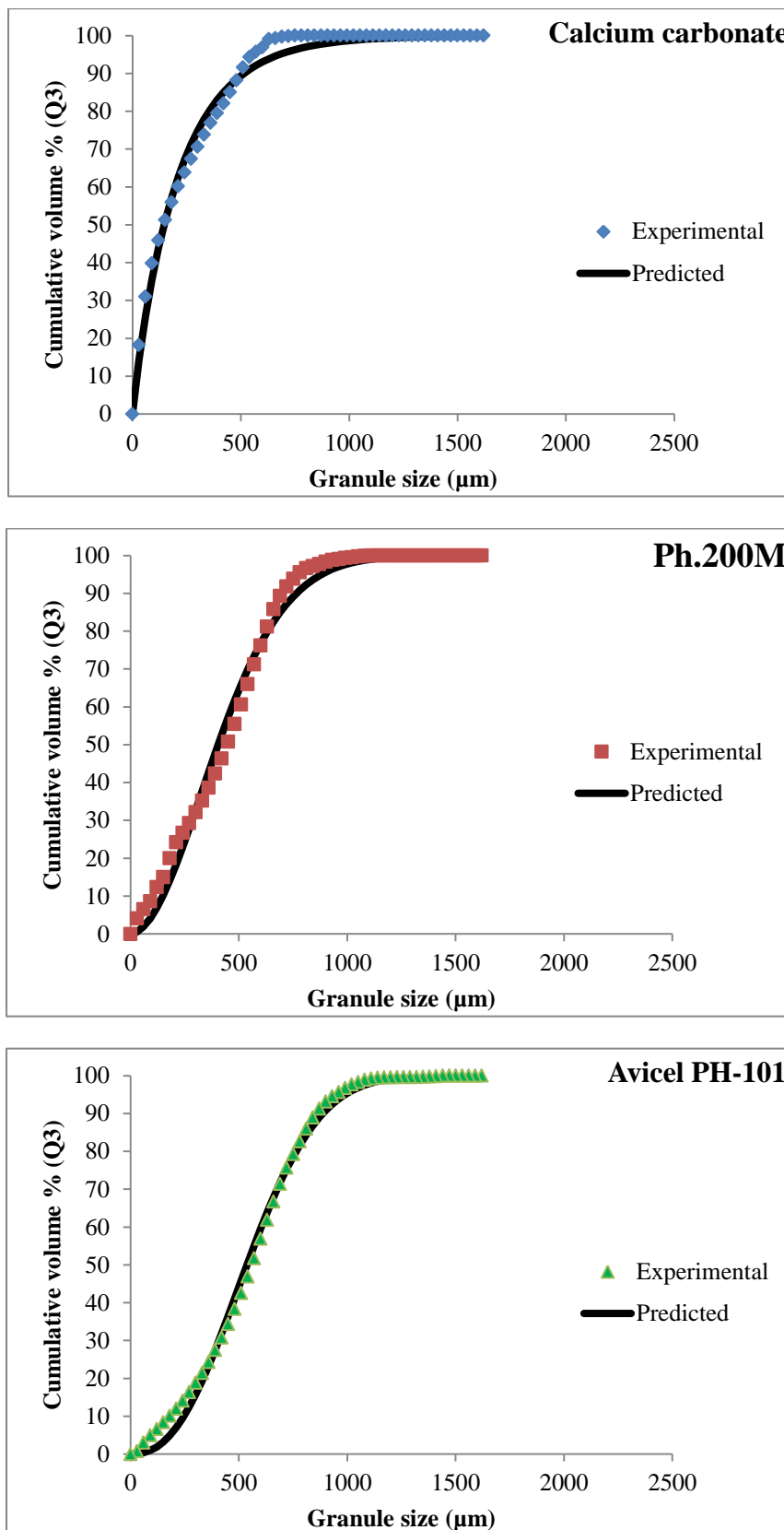


Figure 8-15: Experimental and predicted granule size distribution of different materials produced from crushing ribbons of 100 bar using mesh size of 0.63-1 mm

Figure 8-16 shows the relationship between the two constants of Rosin- Rammler equation and the strength of the ribbon produced at 100 bar. It can be seen from the figure that the values of both constants increased upon increasing the strength of the ribbon.

Figure 8-17 shows similar relationship but with the nano- indentation hardness of the single primary particle. It can be seen that as the hardness increase, the value of the two constants decreased. This is because powder with high nano-indentation hardness produced weak ribbon and consequently small granules.

The relationships between the two Rosin-Rammler constants and ribbon strength or nano-indentation hardness of the primary single particle can be used to predict the whole granule size distribution for a given system by measuring the strength of the ribbon or the nano-indentation hardness of the single primary particle.

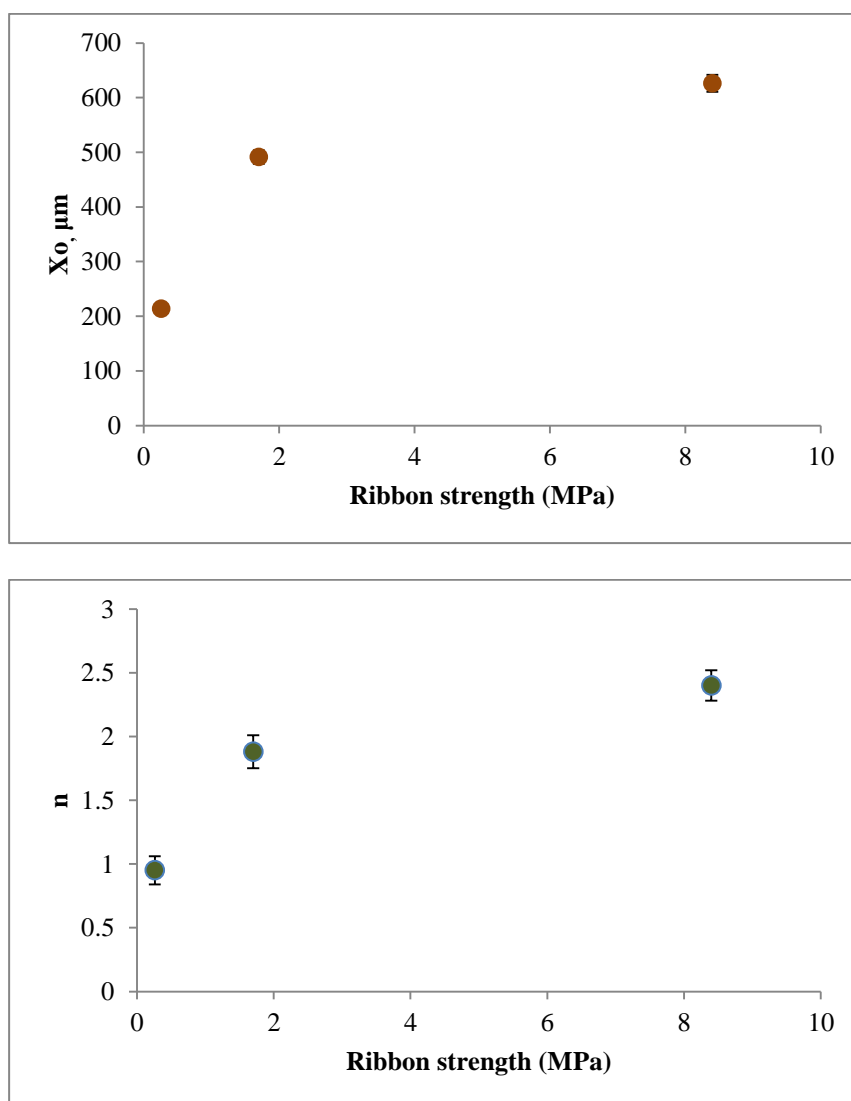


Figure 8-16: Relation between the ribbon strength of different materials produced at 100 bar and the two constants of Rosin- Rammler equation

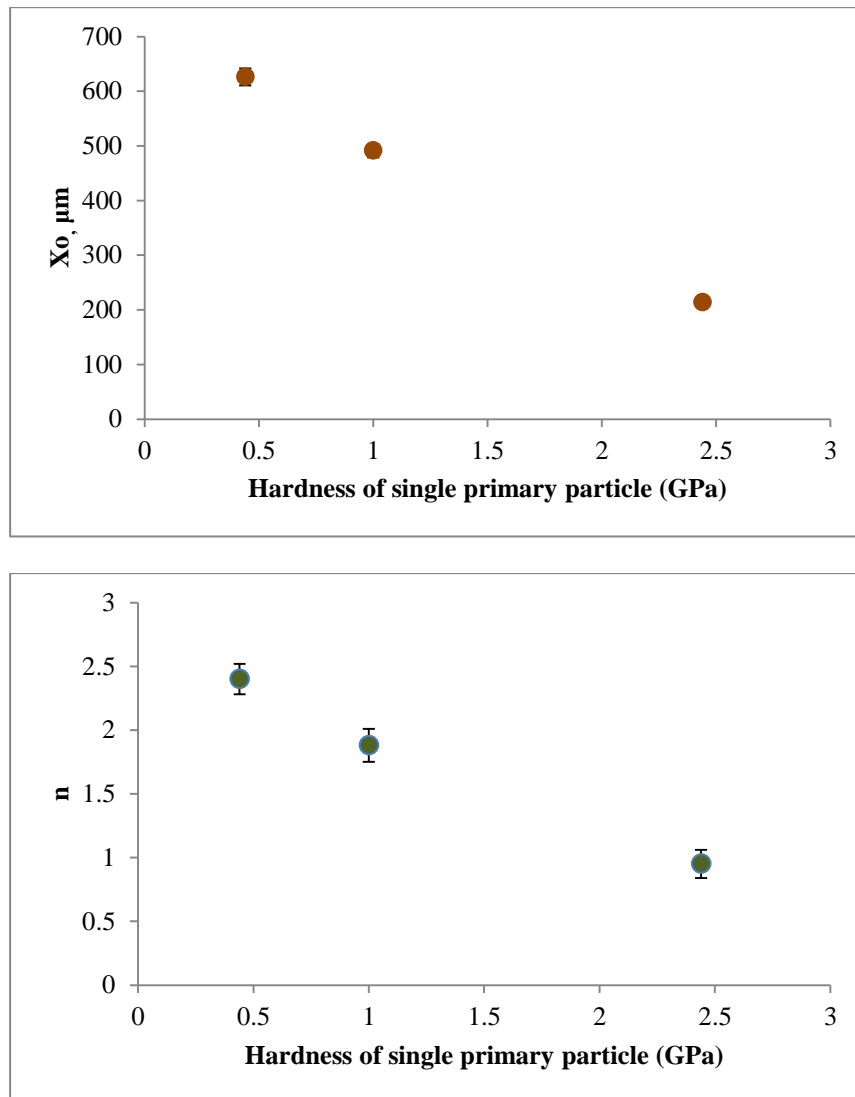


Figure 8-17: Relation between nano- indentation hardness of the single primary particle of different materials and the two constants of Rosin- Rammler equation

## 8.5 Conclusion

The aim of the study in this chapter is to investigate the relationship between the mechanical properties of the ribbon or primary powder with the granule size distribution resulted from crushing the ribbon. This relationship was investigated with a ribbon produced from different materials using different hydraulic pressures. The crusher speed and the mesh size are the two crusher parameters that have been considered in the study. It was found that the mechanical properties of the ribbon are not always control the granule size. The study showed that the ribbon with higher strength and high hardness produced larger granule size compared to the weak ribbon. This is always true only upon using small mesh size. Fitting the granule size distribution to Rosin– Rammler equation of two parameters was successful and therefore it can be used in industry to predict the granule size distribution by measuring the mechanical properties of the ribbon or measuring the nano-indentation hardness of the single primary particle.

## Chapter 9 Conclusion and future work

### 9.1 Conclusion

This study showed that the mechanical properties of the primary powder, pre-compacted body and the ribbon play an important role in the compaction process and control the product quality.

The main aim of this thesis is to suggest a tool to predict the product quality of the roller compaction process by using the hardness of single primary particle. If this is successful, it can be used by different industries. The aim was achieved successfully and the optimum hardness range of a single primary particle that produces good compact was suggested and therefore the important ribbon properties such as ribbon strength, ribbon width, amount of fines and ribbon temperature could be predicted. It was concluded that both the hardness and the viscoelasticity of the material are necessary to indicate the plastic deformation of the powder. The study also concluded that the plastically deformable material such as microcrystalline cellulose loses the ability to plastically deform upon compaction. This loss is only happened within a specific range of applied stress which should be avoided especially where the roller compaction process is followed by tableting.

This work has suggested a novel method to measure the nip angle and to track the progress of the compaction process using the mechanical properties of the pre-compacted body. The method takes into consideration the real data of the powder properties and the parameters of the compaction process. Hence, the effect of roller speed and the shear stress applied to the powder during roller compaction process and other parameters are included. The method concluded that the roller speed has a big effect on the nip angle and hence the time at which the powder will be under significant stress during the compaction process. It was experimentally proven that the nip angle predicted by Johanson's theory is applied for the medium roller speed while the theory failed at high and low roller speed.

This study suggested a new method to improve the stress distribution across the roller width by using a new specially designed curved roller (Salman et al., 2016). The study showed that using the new roller significantly increased the ribbon width, decreased the amount of fines and reduced the heterogeneity across the ribbon width. In addition, the new roller helped to efficiently granulate the difficult/ hard material such as calcium carbonate. This is especially useful for some industries where there is no option other than using specific type of material.

The study concluded that the granule size distribution resulted from crushing the ribbon of different materials can be used as an indication of the mechanical properties of the ribbon only when small mesh size is used in the crusher. Upon using a small mesh size, strong ribbon produces larger granules compared to the granules of the weak ribbon.

## **9.2 Future work**

### **9.2.1 Measuring the fracture toughness of single primary particle**

This study measured the plastic deformation by the nano-indentation test whereas the fracture behavior was determined qualitatively by a compression of a single particle. Measuring the fracture toughness of the single primary particle is possible using a nano-indenter that can apply high load to cause a fracture of the particle. If this is carried out successfully, it can be used to find a link between fracture toughness and the product quality of roller compaction process in addition to the size of the granules resulted from crushing of the ribbon.

### **9.2.2 Online measuring of the nip angle**

This study showed a clear relationship between increasing the temperature during roller compaction process and the stress applied on the material. The nip angle is defined as the angle at which the stress applied on the powder starts to increase significantly. An increase in the stress will consequently cause an increase in the temperature. Then the nip angle could be defined as the angle at which the temperature starts to increase significantly. The temperature at different angular roll positions could be measured using a thermal camera window fitted to the cheek plate. Measuring the temperature using a thermal camera is online during the compaction process which means the nip angle can be also determined online.

### **9.2.3 Trying different geometry of the curved roller**

The work in this study has shown that using the curved roller improved the quality of the ribbon produced by roller compaction process. More changes to the surface geometry may further improve the product quality. It would be interesting to optimize the geometry of the roller curvature such as using different curvatures with different radius to find the geometry that produces the best product quality.

### **9.2.4 Monitoring the compaction process by measuring the temperature**

This study showed that the temperature is reflecting the process parameters; hydraulic pressure, roller gap and speed together and it is a response of what happening to the powder during the compaction process. For this reason, it can be used in an online automatic feedback system to control the quality of the ribbon.

### **9.2.5 Plastic deformation at different temperature and humidity**

This work has shown that the plastic deformation that the material exhibits during the roller compaction process play a vital role in bonding the particles to each other to form strong compact. For some materials, the plastic deformation could change with changing the temperature and the moisture content. If this is proven to be true by measuring the nano-indentation hardness under different temperature and relative humidity then it can be used to improve the quality of the product.

## References

- ABDEL-GHANI, M., PETRIE, J. G., SEVILLE, J. P. K., CLIFT, R. & ADAMS, M. J. 1991. Mechanical properties of cohesive particulate solids. *Powder Technology*, 65, 113-123.
- ABURUB, A., MISHRA, D. & BUCKNER, I. 2007. Use of Compaction Energetics for Understanding Particle Deformation Mechanism. *Pharmaceutical Development & Technology*, 12, 405-414.
- ADAMS, M. J. & MCKEOWN, R. 1996. Micromechanical analyses of the pressure-volume relationship for powders under confined uniaxial compression. *Powder Technology*, 88, 155-163.
- AL-ASADY, R. B., DHENGE, R. M., HOUNSLOW, M. J. & SALMAN, A. D. 2016. Roller compactor: Determining the nip angle and powder compaction progress by indentation of the pre-compacted body. *Powder Technology*.
- AL-ASADY, R. B., OSBORNE, J. D., HOUNSLOW, M. J. & SALMAN, A. D. 2015. Roller compactor: The effect of mechanical properties of primary particles. *International Journal of Pharmaceutics*, 496, 124-136.
- ALLEN, T. 1997. *Particle size measurement*, London, Chapman and Hall.
- ALLESØ, M., HOLM, R. & HOLM, P. 2016. Roller compaction scale-up using roll width as scale factor and laser-based determined ribbon porosity as critical material attribute. *European Journal of Pharmaceutical Sciences*, 87, 69-78.
- AM ENDE, M. T., MOSES, S. K., CARELLA, A. J., GADKARI, R. A., GRAUL, T. W., OTANO, A. L. & TIMPANO, R. J. 2007. Improving the Content Uniformity of a Low-Dose Tablet Formulation Through Roller Compaction Optimization. *Pharmaceutical Development & Technology*, 12, 391-404.
- AMEYE, D., KELEB, E., VERVAET, C., REMON, J. P., ADAMS, E. & MASSART, D. L. 2002. Scaling-up of a lactose wet granulation process in Mi-Pro high shear mixers. *European Journal of Pharmaceutical Sciences*, 17, 247-251.
- ANTIKAINEN, O. & YLIRUUSI, J. 2003. Determining the compression behaviour of pharmaceutical powders from the force–distance compression profile. *International Journal of Pharmaceutics*, 252, 253-261.
- ARMSTRONG, N. A. 1989. Time-dependent factors involved in powder compression and tablet manufacture. *International Journal of Pharmaceutics*, 49, 1-13.
- ASKELAND, D. R. 1998. *The Science and Engineering of Materials*, Cheltenham, UK, Stanley Thomas Ltd.
- ATKINS, A. G. & MAI, Y.-W. 1986. Deformation transitions. *Journal of Materials Science*, 21, 1093-1110.
- BACHER, C., OLSEN, P. M., BERTELSEN, P., KRISTENSEN, J. & SONNERGAARD, J. M. 2007. Improving the compaction properties of roller compacted calcium carbonate. *International Journal of Pharmaceutics*, 342, 115-123.

- BALAKRISHNAN, A., PIZETTE, P., MARTIN, C. L., JOSHI, S. V. & SAHA, B. P. 2010. Effect of particle size in aggregated and agglomerated ceramic powders. *Acta Materialia*, 58, 802-812.
- BARSOUM, M. W. & RADOVIC, M. 2011. Elastic and Mechanical Properties of the MAX Phases. *Annual Review of Materials Research*, 41, 195-227.
- BI, M., ALVAREZ-NUNEZ, F. & ALVAREZ, F. 2014. Evaluating and Modifying Johanson's Rolling Model to Improve its Predictability. *Journal of Pharmaceutical Sciences*, 103, 2062-2071.
- BINDHUMADHAVAN, G., SEVILLE, J. P. K., ADAMS, M. J., GREENWOOD, R. W. & FITZPATRICK, S. 2005. Roll compaction of a pharmaceutical excipient: Experimental validation of rolling theory for granular solids. *Chemical Engineering Science*, 60, 3891-3897.
- BOLHUIS, G. K. & CHOWHAN, Z. T. 1996. Materials for direct compaction. *Pharmaceutical powder compaction technology*, 71, 419-500.
- BOZIC, D. Z., DREU, R. & VRECER, F. 2008. Influence of dry granulation on compactibility and capping tendency of macrolide antibiotic formulation. *International Journal of Pharmaceutics*, 357, 44-54.
- BROZ, M. E., COOK, R. F. & WHITNEY, D. L. 2006. Microhardness, toughness, and modulus of Mohs scale minerals. *American Mineralogist*, 91, 135-142.
- BUCKNER, I. S., FRIEDMAN, R. A. & WURSTER, D. E. 2010. Using compression calorimetry to characterize powder compaction behavior of pharmaceutical materials. *Journal of Pharmaceutical Sciences*, 99, 861-870.
- BUCKTON, G. 2012. Intermolecular bonding forces. *Pharmaceutical Powder Compaction Technology, Second Edition*. New Jersey: CRC Press.
- BULTMANN, J. M. 2002. Multiple compaction of microcrystalline cellulose in a roller compactor. *European Journal of Pharmaceutics and Biopharmaceutics*, 54, 59-64.
- CELIK, M. 2011. *Pharmaceutical powder compaction technology*, London, Informa Healthcare, 2011.
- CHANG, C., ALVAREZ-NUNEZ, F., RINELLA JR, J., MAGNUSSON, L.-E. & SUEDA, K. 2008. Roller Compaction, Granulation and Capsule Product Dissolution of Drug Formulations Containing a Lactose or Mannitol Filler, Starch, and Talc. *AAPS PharmSciTech*, 9, 597-604.
- CHEN, W., LI, M., ZHANG, T., CHENG, Y.-T. & CHENG, C.-M. 2007. Influence of indenter tip roundness on hardness behavior in nanoindentation. *Materials Science and Engineering: A*, 445-446, 323-327.
- CHEONG, Y. S., REYNOLDS, G. K., SALMAN, A. D. & HOUNSLOW, M. J. 2004. Modelling fragment size distribution using two-parameter Weibull equation. *International Journal of Mineral Processing*, 74, Supplement, S227-S237.
- COHN, R., HEILIG, H. & DELORIMIER, A. 1966. Critical evaluation of the compactor. *Journal of Pharmaceutical Sciences*, 55, 328-331.

- CUNNINGHAM, J. C., WINSTEAD, D. & ZAVALIANGOS, A. 2010. Understanding variation in roller compaction through finite element-based process modeling. *Computers & Chemical Engineering*, 34, 1058-1071.
- DADKHAH, M., PEGLOW, M. & TSOTSAS, E. 2012. Characterization of the internal morphology of agglomerates produced in a spray fluidized bed by X-ray tomography. *Powder Technology*, 228, 349-358.
- DAVID, S. T. & AUGSBURGER, L. L. 1977. Plastic flow during compression of directly compressible fillers and its effect on tablet strength. *Journal of Pharmaceutical Sciences*, 66, 155-159.
- DEC, R. T., ZAVALIANGOS, A. & CUNNINGHAM, J. C. 2003. Comparison of various modeling methods for analysis of powder compaction in roller press. *Powder Technology*, 130, 265-271.
- DJAMARANI, K. M. & CLARK, I. M. 1997. Characterization of particle size based on fine and coarse fractions. *Powder Technology*, 93, 101-108.
- DUMAREY, M., WIKSTRÖM, H., FRANSSON, M., SPARÉN, A., TAJARABI, P., JOSEFSON, M. & TRYGG, J. 2011. Combining experimental design and orthogonal projections to latent structures to study the influence of microcrystalline cellulose properties on roll compaction. *International Journal of Pharmaceutics*, 416, 110-119.
- FALCONE, P. M., BAIANO, A., ZANINI, F., MANCINI, L., TROMBA, G., MONTANARI, F. & DEL NOBILE, M. A. 2004. A Novel Approach to the Study of Bread Porous Structure: Phase-contrast X-Ray Microtomography. *Journal of Food Science*, 69, FEP38-FEP43.
- FARBER, L., HAPGOOD, K. P., MICHAELS, J. N., FU, X.-Y., MEYER, R., JOHNSON, M.-A. & LI, F. 2008. Unified compaction curve model for tensile strength of tablets made by roller compaction and direct compression. *International Journal of Pharmaceutics*, 346, 17-24.
- FIELD, J. E., FARHAT, M. & WALLEY, S. M. 2014. Comminution limit (CL) of particles and possible implications for pumped storage reservoirs. *Journal of Materials Science*, 49, 3780-3784.
- FISCHER-CRIPPS, A. C. 2011. *Nanoindentation: Mechanical Engineering Series 1*, New York, Springer Verlag.
- FLIR. 2011. *Thermal imaging guidebook for building and renewable energy applications* [Online]. Available: [http://www.flirmedia.com/MMC/THG/Brochures/T820325/T820325\\_EN.pdf](http://www.flirmedia.com/MMC/THG/Brochures/T820325/T820325_EN.pdf).
- FRANKS, G. V. & LANGE, F. F. 1999. Mechanical behavior of saturated, consolidated, alumina powder compacts: effect of particle size and morphology on the plastic-to-brittle transition. *Colloids and Surfaces A: Physicochemical and Engineering Aspects*, 146, 5-17.
- FREEMAN, T., VOM BEY, H., HANISH, M., BROCKBANK, K. & ARMSTRONG, B. 2016. The influence of roller compaction processing variables on the rheological properties of granules. *Asian Journal of Pharmaceutical Sciences*, 11, 516-527.



- FREITAG, F. & KLEINEBUDDE, P. 2003. How do roll compaction/dry granulation affect the tableting behaviour of inorganic materials? Comparison of four magnesium carbonates. *European Journal of Pharmaceutical Sciences*, 19, 281-289.
- FREITAG, F., RUNGE, J. & KLEINEBUDDE, P. 2005. Coprocessing of Powdered Cellulose and Magnesium Carbonate: Direct Tableting Versus Tableting After Roll Compaction/Dry Granulation. *Pharmaceutical Development & Technology*, 10, 353-362.
- FUJIFILM. 2012. *Prescale pressure measurement film* [Online]. Available: <http://www.fujifilm.com/products/prescale/>.
- FUNAKOSHI, Y., ASOGAWA, T. & E., S. 1977. Use of a novel roller compactor with a concavo-convex roller pair to obtain uniform compacting pressure. *Drug. Dev. Ind. Pharm.*, 6, 555-573.
- GELDART, D., ABDULLAH, E. C., HASSANPOUR, A., NWOKE, L. C. & WOUTERS, I. 2006. Characterization of powder flowability using measurement of angle of repose. *China particuology*, 04, 104-107.
- GOVEDARICA, B., ILIĆ, I., ŠIBANC, R., DREU, R. & SRČIČ, S. 2012. The use of single particle mechanical properties for predicting the compressibility of pharmaceutical materials. *Powder Technology*, 225, 43-51.
- GROUP, P. M. R. 1999. Comparison of computer models representing powder compaction process. *Powder Metallurgy*, 42, 301-311.
- GUIGON, P. & SIMON, O. 2003. Roll press design—influence of force feed systems on compaction. *Powder Technology*, 130, 41-48.
- GUIGON, P., SIMON, O., SALEH, K., BINDHUMADHAVAN, G., ADAMS, M. J. & SEVILLE, J. P. K. 2007. Roll Pressing. *Handbook of Powder Technology*. Amsterdam, Netherlands: Elsevier.
- GUPTA, A., PECK, G. E., MILLER, R. W. & MORRIS, K. R. 2005. Influence of ambient moisture on the compaction behavior of microcrystalline cellulose powder undergoing uni-axial compression and roller-compaction: A comparative study using near-infrared spectroscopy. *Journal of Pharmaceutical Sciences*, 94, 2301-2313.
- GUPTA, A. & YAN, D. S. 2006. Chapter 2 - Particle Size Estimation and Distributions. In: GUPTA, A. & YAN, D. S. (eds.) *Mineral Processing Design and Operation*. Amsterdam: Elsevier Science.
- HAKANEN, A. & LAINE, E. 1993. Acoustic emission during powder compaction and its frequency spectral analysis. *Drug Dev. Ind. Pharm.*, 19, 2539-2560.
- HANUS, E. J. & KING, L. D. 1968. Thermodynamic effects in the compression of solids. *Journal of Pharmaceutical Sciences*, 57, 677-684.
- HARIRTIAN, I. & MICHAEL, J. 2000. Determination of mechanical strength same material double-layer rectangular tablets. *DARU Journal of Pharmaceutical Sciences*, 8, 22-27.
- HE, X., SECREAST, P. J. & AMIDON, G. E. 2007. Mechanistic study of the effect of roller compaction and lubricant on tablet mechanical strength. *Journal of Pharmaceutical Sciences*, 96, 1342-1355.

- HECKEL, R. W. 1961. Density-Pressure relationships in powder compaction. *Trans. Metall. Soc. AIME*, 221, 671-675.
- HEIMAN, J., TAJAROBI, F., GURURAJAN, B., JUPPO, A. & ABRAHMSÉN-ALAMI, S. 2015. Roller compaction of hydrophilic extended release tablets—Combined effects of processing variables and drug/matrix former particle size. *AAPS PharmSciTech*, 16, 267-277.
- HERTING, M. G. & KLEINEBUDDE, P. 2007. Roll compaction/dry granulation: Effect of raw material particle size on granule and tablet properties. *International Journal of Pharmaceutics*, 338, 110-118.
- HERTING, M. G. & KLEINEBUDDE, P. 2008. Studies on the reduction of tensile strength of tablets after roll compaction/dry granulation. *European Journal of Pharmaceutics and Biopharmaceutics*, 70, 372-379.
- HIESTAND, H. E. N. & SMITH, D. P. 1984. Indices of tableting performance. *Powder Technology*, 38, 145-159.
- HODOWANY, J., RAVICHANDRAN, G., ROSAKIS, A. J. & ROSAKIS, P. 1999. Partition of plastic work into heat and stored energy in metals. *Experimental Mechanics*, 40, 113-123.
- HOLMAN, L. E. 1991. The compaction behaviour of particulate materials. An elucidation based on percolation theory. *Powder Technology*, 66, 265-280.
- HSU, S.-H., REKLAITIS, G. V. & VENKATASUBRAMANIAN, V. 2010. Modeling and Control of Roller Compaction for Pharmaceutical Manufacturing. Part I: Process Dynamics and Control Framework. *Journal of Pharmaceutical Innovation*, 5, 14-23.
- HYSITRON 2006. Triboscope For dimension Series SPM software Version 8.0 User Manual. In: HYSITRON (ed.). Minneapolis, USA.
- HYSITRON. 2013. *TS 70 TriboScope®* [Online]. USA. Available: <http://phi-gmbh.eu/wp-content/uploads/2013/10/TS-70-TriboScope.pdf> [2013].
- HYSITRON. 2016. *Hysitron Nanoindenter* [Online]. USA. Available: <http://bm3.unl.edu/hysitron-nanoindenter#details>.
- INGHELBRECHT, S. & PAUL REMON, J. 1998. The roller compaction of different types of lactose. *International Journal of Pharmaceutics*, 166, 135-144.
- INGHELBRECHT, S., REMON, J.-P., DE AGUIAR, P. F., WALCZAK, B., MASSART, D., VAN DE VELDE, F., DE BAETS, P., VERMEERSCH, H. & DE BACKER, P. 1997. Instrumentation of a roll compactor and the evaluation of the parameter settings by neural networks. *International Journal of Pharmaceutics*, 148, 103-115.
- INGHELBRECHT, S. & REMON, J. P. 1998a. Reducing dust and improving granule and tablet quality in the roller compaction process. *International Journal of Pharmaceutics*, 171, 195-206.
- INGHELBRECHT, S. & REMON, J. P. 1998b. Roller compaction and tableting of microcrystalline cellulose/drug mixtures. *International Journal of Pharmaceutics*, 161, 215-224.

- IVESON, S. M. & PAGE, N. W. 2004. Brittle to Plastic Transition in the Dynamic Mechanical Behavior of Partially Saturated Granular Materials. *ASME. J. Appl. Mech.*, 71, 470-475.
- JENIKE, A. 1964. Storage and flow of solids. *Buletin of the University of Utah*.
- JEON, I., GILLI, T. & BETZ, G. 2011. Evaluation of roll compaction as a preparation method for hydroxypropyl cellulose-based matrix tablets. *Journal of Pharmacy and Bioallied Sciences*, 3, 213-220.
- JOHANSON, J. R. 1965. A Rolling Theory for Granular Solids. *Journal of Applied Mechanics*, 32, 842-848.
- JOHNSON, K. L. 1985. *Contact Mechanics*, Cambridge, UK, Cambridge University Press.
- KAFUI, K. D. & THORNTON, C. 2000. Numerical simulations of impact breakage of a spherical crystalline agglomerate. *Powder Technology*, 109, 113-132.
- KAPOOR, R. & NEMAT-NASSER, S. 1998. Determination of temperature rise during high strain rate deformation. *Mechanics of Materials*, 27, 1-12.
- KARIMI, A., NAVIDBAKHSI, M. & HAGHI, A. M. 2014. An Experimental Study on the Structural and Mechanical Properties of Polyvinyl Alcohol Sponge Using Different Stress–Strain Definitions. *Advances in Polymer Technology*, 33.
- KATASHINSKII, V. P. 1966. Analytical determination of specific pressure during the rolling of metal powders. *Soviet Powder Metallurgy and Metal Ceramics*, 5, 765-772.
- KATASHINSKII, V. P. & SHTERN, M. B. 1983a. Stress-strain state of powder being rolled in the densification zone. *Soviet Powder Metallurgy and Metal Ceramics*, 22, 972-976.
- KATASHINSKII, V. P. & SHTERN, M. B. 1983b. Stressed-strained state of powder being rolled in the densification zone. I. Mathematical model of rolling in the densification zone. *Soviet Powder Metallurgy and Metal Ceramics*, 22, 882-885.
- KATASHINSKII, V. P. & VINOGRADOV, G. A. 1965. Investigation into the compactability of metal powders during rolling. *Soviet Powder Metallurgy and Metal Ceramics*, 4, 356-361.
- KATASHINSKII, V. P., VINOGRADOV, G. A. & KALUTSKII, G. Y. 1975. Nonuniformity of strain and stress distribution over the width of rolled powder strip. *Soviet Powder Metallurgy and Metal Ceramics*, 14, 976-979.
- KAWAKITA, K. & LÜDDE, K.-H. 1971. Some considerations on powder compression equations. *Powder Technology*, 4, 61-68.
- KEMET. 2016. *Cold Mounting Resins and Acrylics* [Online]. Available: <http://www.kemet.co.uk/products/metallography/cold-mounting-resin-systems> 2016].
- KENDALL, K. 1978. The impossibility of comminuting small particles by compression. *Nature*, 272.
- KETOLAINEN, J., ILKKA, J. & PARONEN, P. 1993. Temperature changes during tableting measured using infrared thermoviewer. *International Journal of Pharmaceutics*, 92, 157-166.

- KHOMANE, K. S. & BANSAL, A. K. 2013. Yield strength of microcrystalline cellulose: Experimental evidence by dielectric spectroscopy. *International Journal of Pharmaceutics*, 455, 1-4.
- KHOSSRAVI, D. & MOREHEAD, W. 1997. Consolidation Mechanisms of Pharmaceutical Solids: A Multi-Compression Cycle Approach. *Pharmaceutical Research*, 14, 1039-1045.
- KLEINEBUDDE, P. 2004. Roll compaction/dry granulation: pharmaceutical applications. *European Journal of Pharmaceutics and Biopharmaceutics*, 58, 317-326.
- KUHN, H. A. & DOWNEY, C. L. 1971. Deformation characteristics and plasticity theory of sintered powder materials. *International Journal of Powder Metallurgy*, 7, 15-25.
- LARSSON, I. & KRISTENSEN, H. G. 2000. Comminution of a brittle/ductile material in a Micros Ring Mill. *Powder Technology*, 107, 175-178.
- LEE, E. & EVERTSSON, C. M. 2011. A comparative study between cone crushers and theoretically optimal crushing sequences. *Minerals Engineering*, 24, 188-194.
- LEE, J., KIM, C. Y., JOO, M. & PARK, K. 2013. Uncertainty compensation methods for quantitative hardness measurement of materials using atomic force microscope nanoindentation technique. *Thin Solid Films*, 546, 448-452.
- LEE, K. M., YEO, C.-D. & POLYCARPOU, A. A. 2008. Relationship between scratch hardness and yield strength of elastic perfectly plastic materials using finite element analysis. *Journal of Materials Research*, 23, 2229-2237.
- LEUENBERGER, H. 1982. The compressibility and compactibility of powder systems. *International Journal of Pharmaceutics*, 12, 41-55.
- LEUENBERGER, H. 2001. New trends in the production of pharmaceutical granules: batch versus continuous processing. *European Journal of Pharmaceutics and Biopharmaceutics*, 52, 289-296.
- LIM, H., DAVE, V. S., KIDDER, L., NEIL LEWIS, E., FAHMY, R. & HOAG, S. W. 2011. Assessment of the critical factors affecting the porosity of roller compacted ribbons and the feasibility of using NIR chemical imaging to evaluate the porosity distribution. *International Journal of Pharmaceutics*, 410, 1-8.
- LIU, Y. & WASSGREN, C. 2016. Modifications to Johanson's roll compaction model for improved relative density predictions. *Powder Technology*, 297, 294-302.
- MAIRE, E., BUFFIÈRE, J. Y., SALVO, L., BLANDIN, J. J., LUDWIG, W. & LÉTANG, J. M. 2001. On the Application of X-ray Microtomography in the Field of Materials Science. *Advanced Engineering Materials*, 3, 539-546.
- MAL'TSEV, M. V. 1971. Investigation of metal powder rolling. *Soviet Powder Metallurgy and Metal Ceramics*, 10, 445-448.
- MALAMATARIS, S., REES, J. E. & HART, J. P. 1992. Influence of loading rate and packing fraction on visco-elastic behaviour of powder compacts. *Powder Technology*, 69, 231-238.

- MANGWANDI, C., CHEONG, Y. S., ADAMS, M. J., HOUNSLOW, M. J. & SALMAN, A. D. 2007. The coefficient of restitution of different representative types of granules. *Chemical Engineering Science*, 62, 437-450.
- MANGWANDI, C., JIANGTAO, L., ALBADARIN, A. B., DHENGE, R. M. & WALKER, G. M. 2015. High shear granulation of binary mixtures: Effect of powder composition on granule properties. *Powder Technology*, 270, Part B, 424-434.
- MANSA, R. F., BRIDSON, R. H., GREENWOOD, R. W., BARKER, H. & SEVILLE, J. P. K. 2008. Using intelligent software to predict the effects of formulation and processing parameters on roller compaction. *Powder Technology*, 181, 217-225.
- MEGHWAL, M. & GOSWAMI, T. K. 2014. Comparative study on ambient and cryogenic grinding of fenugreek and black pepper seeds using rotor, ball, hammer and Pin mill. *Powder Technology*, 267, 245-255.
- MEIER, M., JOHN, E., WIECKHUSEN, D., WIRTH, W. & PEUKERT, W. 2009. Influence of mechanical properties on impact fracture: Prediction of the milling behaviour of pharmaceutical powders by nanoindentation. *Powder Technology*, 188, 301-313.
- MICHEL, B. 1994. *Compactage en presse a rouleaux de poudres minerales*. PhD, Universite de Compiègne.
- MICHRAFY, A., DIARRA, H., DODDS, J. A. & MICHRAFY, M. 2011. Experimental and numerical analyses of homogeneity over strip width in roll compaction. *Powder Technology*, 206, 154-160.
- MIGUÉLEZ-MORÁN, A. M., WU, C.-Y., DONG, H. & SEVILLE, J. P. K. 2009. Characterisation of density distributions in roller-compacted ribbons using micro-indentation and X-ray micro-computed tomography. *European Journal of Pharmaceutics and Biopharmaceutics*, 72, 173-182.
- MIGUÉLEZ-MORÁN, A. M., WU, C. Y. & SEVILLE, J. P. K. 2008. The effect of lubrication on density distributions of roller compacted ribbons. *International Journal of Pharmaceutics*, 362, 52-59.
- MOHSIN, M., HOSSIN, A. & HAIK, Y. 2011. Thermal and mechanical properties of poly (vinyl alcohol) plasticized with glycerol. *Journal of Applied Polymer Science*, 122, 3102-3109.
- MOLLAN JR, M. J. & ÇELIK, M. 1996. The effects of lubrication on the compaction and post-compaction properties of directly compressible maltodextrins. *International Journal of Pharmaceutics*, 144, 1-9.
- MOODY, N. R., ADAMS, D. P., MEDLIN, D., HEADLEY, T., YANG, N. & VOLINSKY, A. 2003. Effects of diffusion on interfacial fracture of gold-chromium hybrid microcircuit films. *International Journal of Fracture*, 120, 407-419.
- MULIADI, A. R., LITSTER, J. D. & WASSGREN, C. R. 2012. Modeling the powder roll compaction process: Comparison of 2-D finite element method and the rolling theory for granular solids (Johanson's model). *Powder Technology*, 221, 90-100.
- MULIADI, A. R., LITSTER, J. D. & WASSGREN, C. R. 2013. Validation of 3-D finite element analysis for predicting the density distribution of roll compacted pharmaceutical powder. *Powder Technology*, 237, 386-399.

- NARAYAN, P. & HANCOCK, B. C. 2003. The relationship between the particle properties, mechanical behavior, and surface roughness of some pharmaceutical excipient compacts. *Materials Science and Engineering: A*, 355, 24-36.
- NESARIKAR, V. V., PATEL, C., EARLY, W., VATSARAJ, N., SPROCKEL, O. & JERZWESKI, R. 2012a. Roller compaction process development and scale up using Johanson model calibrated with instrumented roll data. *International Journal of Pharmaceutics*, 436, 486-507.
- NESARIKAR, V. V., VATSARAJ, N., PATEL, C., EARLY, W., PANDEY, P., SPROCKEL, O., GAO, Z., JERZEWSKI, R., MILLER, R. & LEVIN, M. 2012b. Instrumented roll technology for the design space development of roller compaction process. *International Journal of Pharmaceutics*, 426, 116-131.
- O'NEILL 1967. *Hardness Measurement of Metals and Alloys*, London, UK, Chapman and Hall Ltd.
- OLIVER, W. C. & PHARR, G. M. 1992. An improved technique for determining hardness and elastic modulus using load and displacement sensing indentation experiments. *Journal of Materials Research*, 7, 1564-1583.
- OLIVER, W. C. & PHARR, G. M. 2004. Measurement of hardness and elastic modulus by instrumented indentation: Advances in understanding and refinements to methodology. *Journal of Materials Research*, 19, 3-20.
- OMAR, C. S., DHENGE, R. M., OSBORNE, J. D., ALTHAUS, T. O., PALZER, S., HOUNSLOW, M. J. & SALMAN, A. D. 2015. Roller compaction: Effect of morphology and amorphous content of lactose powder on product quality. *International Journal of Pharmaceutics*, 496, 63-74.
- OMAR, C. S., DHENGE, R. M., PALZER, S., HOUNSLOW, M. J. & SALMAN, A. D. 2016. Roller compaction: Effect of relative humidity of lactose powder. *European Journal of Pharmaceutics and Biopharmaceutics*.
- OSBORNE, J. 2013. *Bonding Mechanisms Involved in the Roller Compaction of an Amorphous Food Material*. PhD, The University of Sheffield.
- OSBORNE, J. D., ALTHAUS, T., FORNY, L., NIEDERREITER, G., PALZER, S., HOUNSLOW, M. J. & SALMAN, A. D. 2013. Investigating the influence of moisture content and pressure on the bonding mechanisms during roller compaction of an amorphous material. *Chemical Engineering Science*, 86, 61-69.
- PALZER, S. 2009. Influence of material properties on the agglomeration of water-soluble amorphous particles. *Powder Technology*, 189, 318-326.
- PALZER, S. 2010. The relation between material properties and supra-molecular structure of water-soluble food solids. *Trends in Food Science & Technology*, 21, 12-25.
- PALZER, S. 2011. Agglomeration of pharmaceutical, detergent, chemical and food powders — Similarities and differences of materials and processes. *Powder Technology*, 206, 2-17.
- PARROTT, E. L. 1981. Densification of powders by concavo-convex roller compactor. *J Pharm Sci*, 70, 288-91.

- PATEL, B. A., ADAMS, M. J., TURNBULL, N., BENTHAM, A. C. & WU, C. Y. 2010. Predicting the pressure distribution during roll compaction from uniaxial compaction measurements. *Chemical Engineering Journal*, 164, 410-417.
- PATEL, J. K., KAPADIA, C. H. & OWEN, D. B. 1976. *Handbook of statistital distributions*, New York, Marcel Dekker.
- PATEL, S., KAUSHAL, A. M. & BANSAL, A. K. 2008. Compaction behavior of roller compacted ibuprofen. *European Journal of Pharmaceutics and Biopharmaceutics*, 69, 743-749.
- PELEG, M. 1996. Determination of the parameters of the Rosin-Rammler and beta distributions from their mode and variance using equation-solving software. *Powder Technology*, 87, 181-184.
- PEREZ-GANDARILLAS, L., PEREZ-GAGO, A., MAZOR, A., KLEINEBUDDE, P., LECOQ, O. & MICHRAFY, A. 2016. Effect of roll-compaction and milling conditions on granules and tablet properties. *European Journal of Pharmaceutics and Biopharmaceutics*.
- PERKINS, M., EBBENS, S. J., HAYES, S., ROBERTS, C. J., MADDEN, C. E., LUK, S. Y. & PATEL, N. 2007. Elastic modulus measurements from individual lactose particles using atomic force microscopy. *International Journal of Pharmaceutics*, 332, 168-175.
- PETER, S., LAMMENS, R. F. & STEFFENS, K.-J. 2010. Roller compaction/Dry granulation: Use of the thin layer model for predicting densities and forces during roller compaction. *Powder Technology*, 199, 165-175.
- PHARR, G. & OLIVER, W. 1992. Measurement of thin film mechanical properties using nanoindentation. *Mrs Bulletin*, 17, 28-33.
- PIETSCH, W. 1976. *Roll pressing*, London (etc.), London etc. : Heyden, 1976.
- PIETSCH, W. B. 2002. *Agglomeration processes: Phenomena, Technologies, Equipments*, weinheim, Wiley-VCH.
- PRIGGE, J. D. & SOMMER, K. 2011. Numerical Investigation of Stress Distribution during Die Compaction of Food Powders. *Particulate Science and Technology*, 29, 40-52.
- RAMBALI, B., BAERT, L., JANS, E. & MASSART, D. 2001. Influence of the roll compactor parameter settings and the compression pressure on the buccal bio-adhesive tablet properties. *International Journal of Pharmaceutics*, 220, 129-140.
- REES, J. E. & RUE, P. 1978. Time-dependent deformation of some direct compression excipients. *J. Pharm. Pharmacol*, 30, 601-607.
- REYNOLDS, G., INGALE, R., ROBERTS, R., KOTHARI, S. & GURURAJAN, B. 2010. Practical application of roller compaction process modeling. *Computers & Chemical Engineering*, 34, 1049-1057.
- RITTEL, D. 1999. On the conversion of plastic work to heat during high strain rate deformation of glassy polymers. *Mechanics of Materials*, 31, 131-139.
- RITTER, A. & SUCKER, H. 1980. Studies of variables that affect tablet capping. *Pharm. Tech.*, 3, 56-65.

- ROBERTS, R. J. & ROWE, R. C. 1987. Brittle/ductile behaviour in pharmaceutical materials used in tableting. *International Journal of Pharmaceutics*, 36, 205-209.
- ROBERTS, R. J., ROWE, R. C. & KENDALL, K. 1989. Brittle—ductile transitions in die compaction of sodium chloride. *Chemical Engineering Science*, 44, 1647-1651.
- ROMEIS, S., PAUL, J., HERRE, P., HANISCH, M., TAYLOR, R. N. K., SCHMIDT, J. & PEUKERT, W. 2015. In Situ Deformation and Breakage of Silica Particles Inside a SEM. *Procedia Engineering*, 102, 201-210.
- RUBINSTEIN, M. H. 1988. Tablets. In: AULTON, M. E. (ed.) *Pharmaceutics: The Science of Dosage Form Design*. Edinburgh: Churchill Livingstone.
- RUE, P. J. & REES, J. E. 1978. Limitations of Heckel relation for predicting powder compaction mechanisms. *J. Pharm. Pharmacol*, 30, 642-643.
- RUMPF, H. 1958. Basic principles and method of granulation *Che. Eng. Tech.*, 30, 144.
- SAKWANICHOL, J., PUTTIPIPATKHACHORN, S., INGENERF, G. & KLEINEBUDDE, P. 2012. Roll compaction/dry granulation: Comparison between roll mill and oscillating granulator in dry granulation. *Pharmaceutical Development and Technology*, 17, 30-39.
- SALMAN, A. D., OMAR, C. S. & AL-ASADY, R. B. 2016. Roller compactor: Improving the roller stress distribution along the roller width.
- SCHÖNERT, K. & SANDER, U. 2002. Shear stresses and material slip in high pressure roller mills. *Powder Technology*, 122, 136-144.
- SCHULZE, D. 2008. Discussion of testers and test procedures. *Powders and Bulk Solids: Behavior, Characterization, Storage and Flow*, 163-198.
- SCHULZE, D. 2010. *Powders and bulk solids : behavior, characterization, storage and flow*, Berlin New York, Springer.
- SHESKEY, P. J., CABELKA, T. D., ROBB, R. T. & BOYCE, B. M. 1994. Use of roller compaction in the preparation of controlled release hydrophilic matrix tablets containing methylcellulose and hydroxypropylmethylcellulose polymers. *Pharm. Tech.*, 18, 132–150.
- SIMON, O. & GUIGON, P. 2003. Correlation between powder-packing properties and roll press compact heterogeneity. *Powder Technology*, 130, 257-264.
- SKINNER, G., HARCUM, W., BARNUM, P. & GUO, J.-H. 1999. The Evaluation of Fine-Particle Hydroxypropylcellulose as a Roller Compaction Binder in Pharmaceutical Applications. *Drug Development & Industrial Pharmacy*, 25, 1121.
- SOH, J. L. P., FENG, W., BOERSEN, N., PINAL, R., PECK, G. E., CARVAJAL, M. T., CHENEY, J., VALTHORSSON, H. & PAZDAN, J. 2008. Utility of Multivariate Analysis in Modeling the Effects of Raw Material Properties and Operating Parameters on Granule and Ribbon Properties Prepared in Roller Compaction. *Drug Development & Industrial Pharmacy*, 34, 1022-1035.
- SONNERGAARD, J. M. 1999. A critical evaluation of the Heckel equation. *International Journal of Pharmaceutics*, 193, 63-71.



- SONNERGAARD, J. M. 2006. Quantification of the compactibility of pharmaceutical powders. *European Journal of Pharmaceutics and Biopharmaceutics*, 63, 270-277.
- SOUIHI, N., REYNOLDS, G., TAJAROBI, P., WIKSTRÖM, H., HAEFFLER, G., JOSEFSON, M. & TRYGG, J. 2015. Roll compaction process modeling: Transfer between equipment and impact of process parameters. *International Journal of Pharmaceutics*, 484, 192-206.
- SPINOV, V. A., VINOGRADOV, G. A. & KALUTSKII, G. Y. 1967. Influence of air on the rolling of powders. *Soviet Powder Metallurgy and Metal Ceramics*, 6, 673-675.
- SRIKANT, P., AKASH, J., MAHESH, D. & ASTIK, S. 2014. Roller Compaction Design and Critical Parameters in Drug Formulation and Development: Review. *International Journal of PharmTech Research*, 7, 90-98.
- STANIFORTH, J. N. & PATEL, C. I. 1989. Creep compliance behaviour of direct compression excipients. *Powder Technology*, 57, 83-88.
- SUN, C. C. & KLEINEBUDDE, P. 2016. Mini review: Mechanisms to the loss of tableability by dry granulation. *European Journal of Pharmaceutics and Biopharmaceutics*, 106, 9-14.
- SUNDAR, S., SAIN, M. & OKSMAN, K. 2011. Thermal characterization and electrical properties of Fe-modified cellulose long fibers and micro crystalline cellulose. *An International Forum for Thermal Studies*, 104, 841-847.
- TABOR, D. 1951. *The hardness of metals*, Oxford, UK, Oxford University Press.
- TAYLOR, L. J., PAPADOPOULOS, D. G., DUNN, P. J., BENTHAM, A. C., MITCHELL, J. C. & SNOWDEN, M. J. 2004. Mechanical characterisation of powders using nanoindentation. *Powder Technology*, 143-144, 179-185.
- THOORENS, G., KRIER, F., LECLERCQ, B., CARLIN, B. & EVRARD, B. 2014. Microcrystalline cellulose, a direct compression binder in a quality by design environment—A review. *International Journal of Pharmaceutics*, 473, 64-72.
- VANHATALO, K. & DAHL, O. 2014. Effect of Mild Acid Hydrolysis Parameters on Properties of Microcrystalline Cellulose. *BioResources*, 9, 4729-4740.
- VESILIND, P. A. 1980. The Rosin-Rammler particle size distribution. *Resource Recovery and Conservation*, 5, 275-277.
- VON EGGELKRAUT-GOTTANKA, S. G., ABED, S. A., MÜLLER, W. & SCHMIDT, P. C. 2002. Roller compaction and tableting of St. John's wort plant dry extract using a gap width and force controlled roller compactor. II. Study of roller compaction variables on granule and tablet properties by a 33 factorial design. *Pharmaceutical development and technology*, 7, 447-455.
- WALKER, E. E. 1923. The properties of powders. Part VI. The compressibility of powders. *Transactions of the Faraday Society*, 19, 73-82.
- WANG, Y., XIA, Y. & JIANG, Y. 2001. Tensile Behaviour and Strength Distribution of Polyvinyl-Alcohol Fibre at High Strain Rates. *An International Journal for the Science and Application of Composite Materials*, 8, 297-306.

- WEYENBERG, W., VERMEIRE, A., VANDERVOORT, J., REMON, J. P. & LUDWIG, A. 2005. Effects of roller compaction settings on the preparation of bioadhesive granules and ocular minitablets. *European Journal of Pharmaceutics and Biopharmaceutics*, 59, 527-536.
- WU, C. Y., HUNG, W. L., MIGUÉLEZ-MORÁN, A. M., GURURAJAN, B. & SEVILLE, J. P. K. 2010. Roller compaction of moist pharmaceutical powders. *International Journal of Pharmaceutics*, 391, 90-97.
- YU, S. 2012. *Roll compaction of pharmaceutical excipients* PhD, The University of Birmingham.
- YU, S., ADAMS, M., GURURAJAN, B., REYNOLDS, G., ROBERTS, R. & WU, C.-Y. 2013. The effects of lubrication on roll compaction, ribbon milling and tableting. *Chemical Engineering Science*, 86, 9-18.
- YU, S., GURURAJAN, B., REYNOLDS, G., ROBERTS, R., ADAMS, M. J. & WU, C.-Y. 2012. A comparative study of roll compaction of free-flowing and cohesive pharmaceutical powders. *International Journal of Pharmaceutics*, 428, 39-47.
- ZHANG, J., PEI, C., SCHIANO, S., HEAPS, D. & WU, C.-Y. 2016. The application of terahertz pulsed imaging in characterising density distribution of roll-compacted ribbons. *European Journal of Pharmaceutics and Biopharmaceutics*.

# Appendix

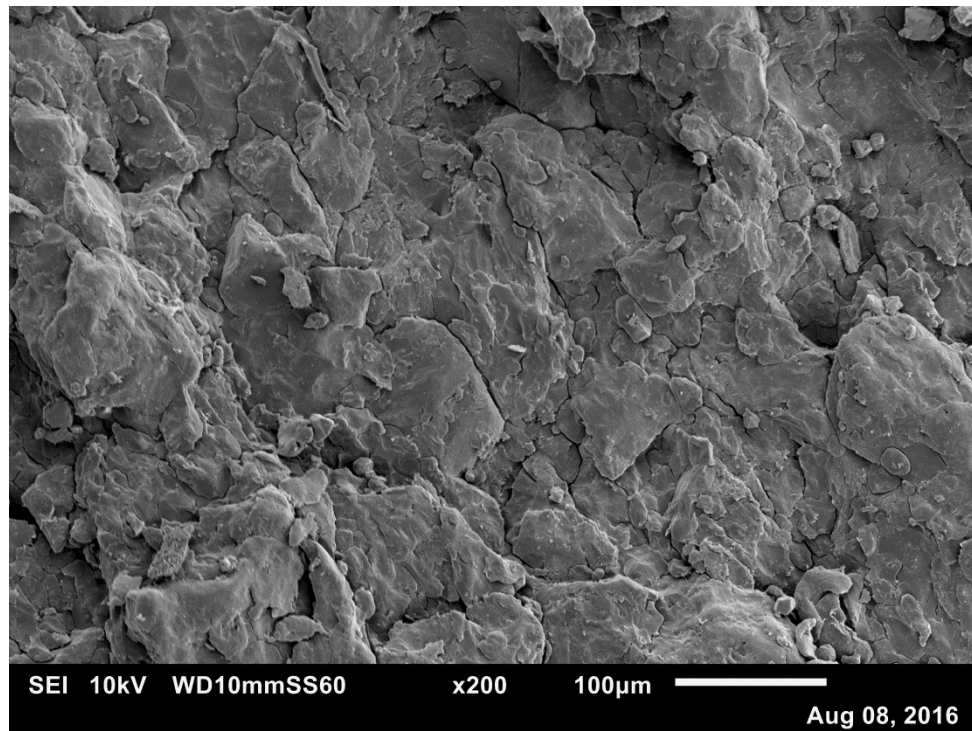


Figure A- 1: Image of Starch 1500 ribbon surface produced at 230 bar

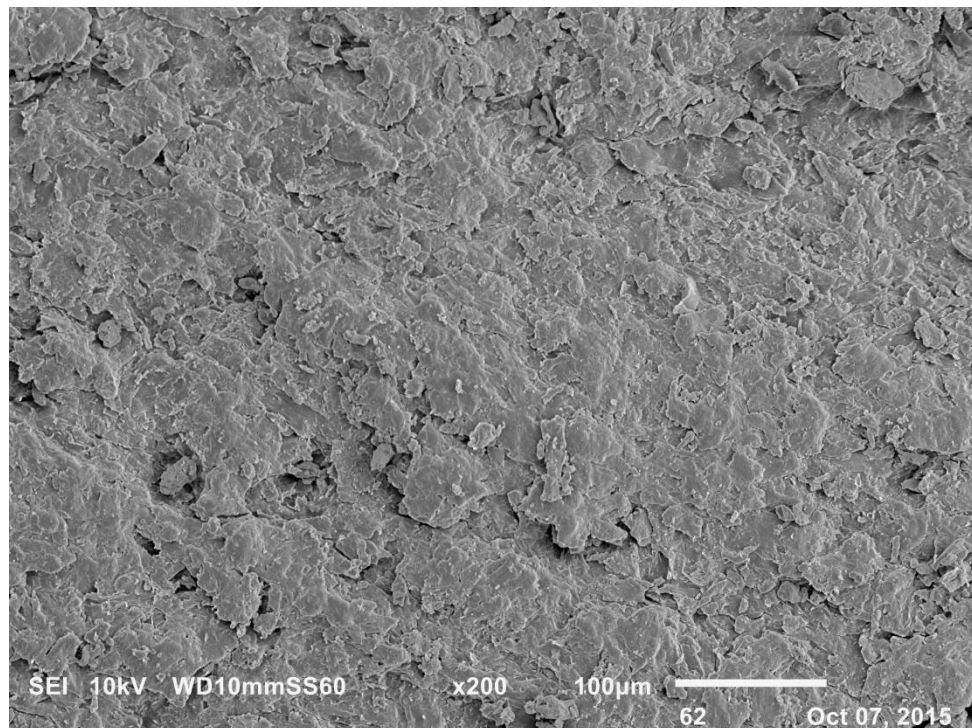


Figure A- 2: Image of Avicel PH-101 ribbon surface produced at 230 bar

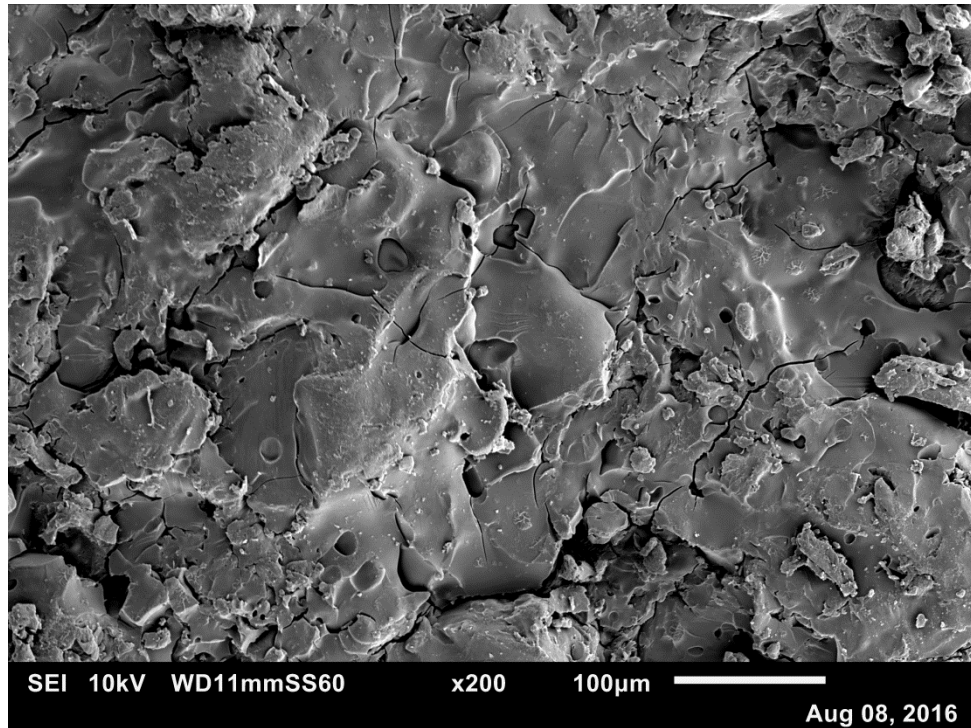


Figure A- 3: Image of Glucidex®6 produced at 150 bar

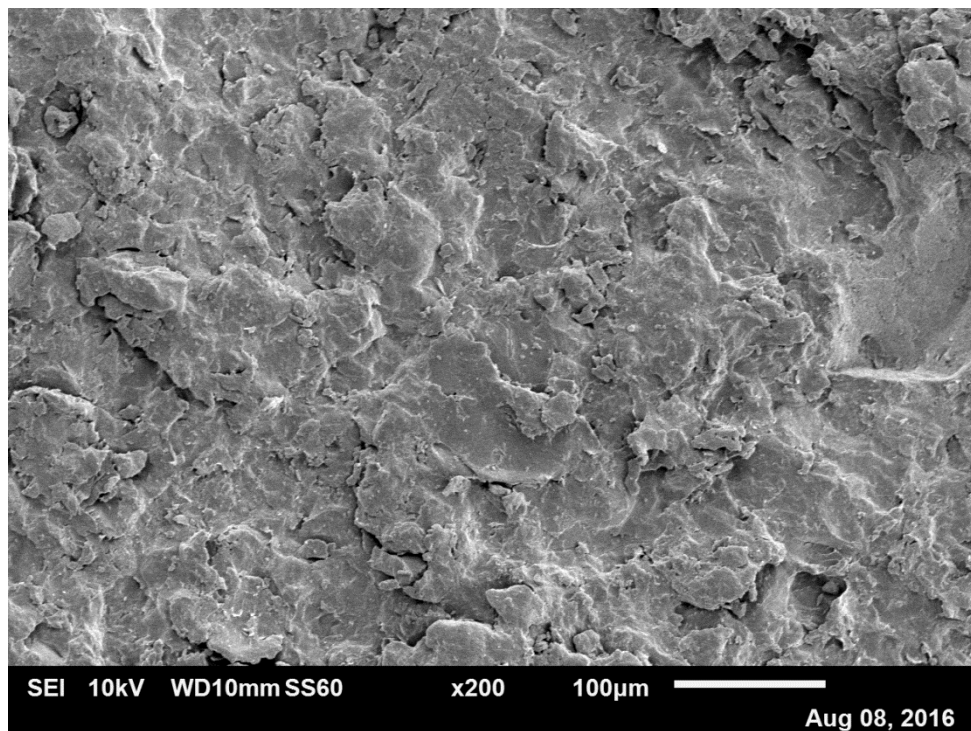


Figure A- 4: Image of Tylpor 604 ribbon surface produced at 230 bar

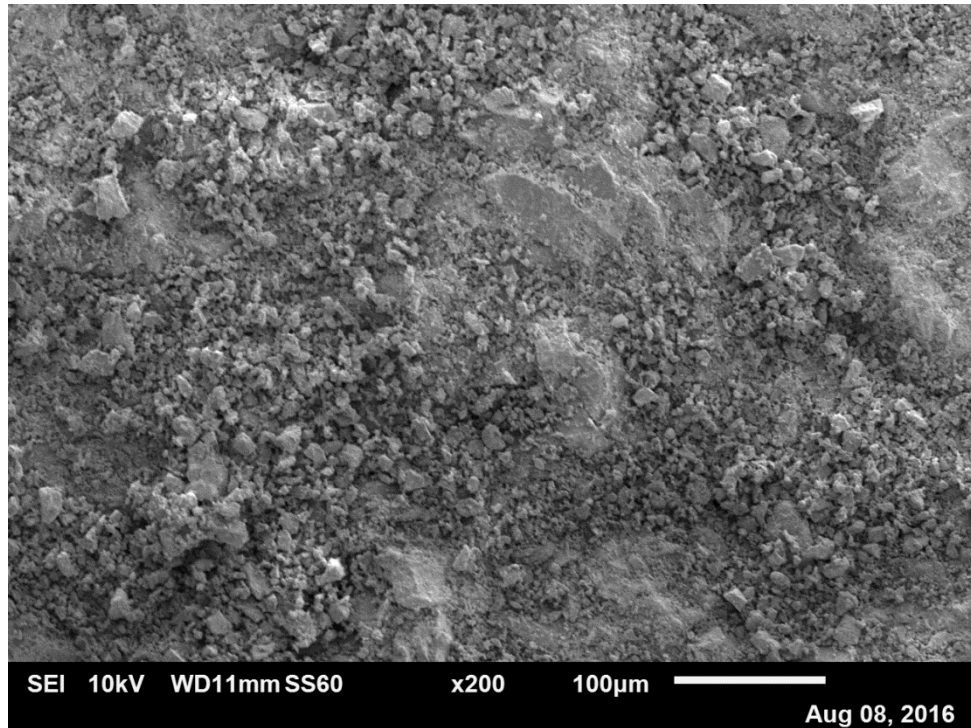


Figure A- 5: Image of Pharmatose 200M ribbon surface produced at 100 bar

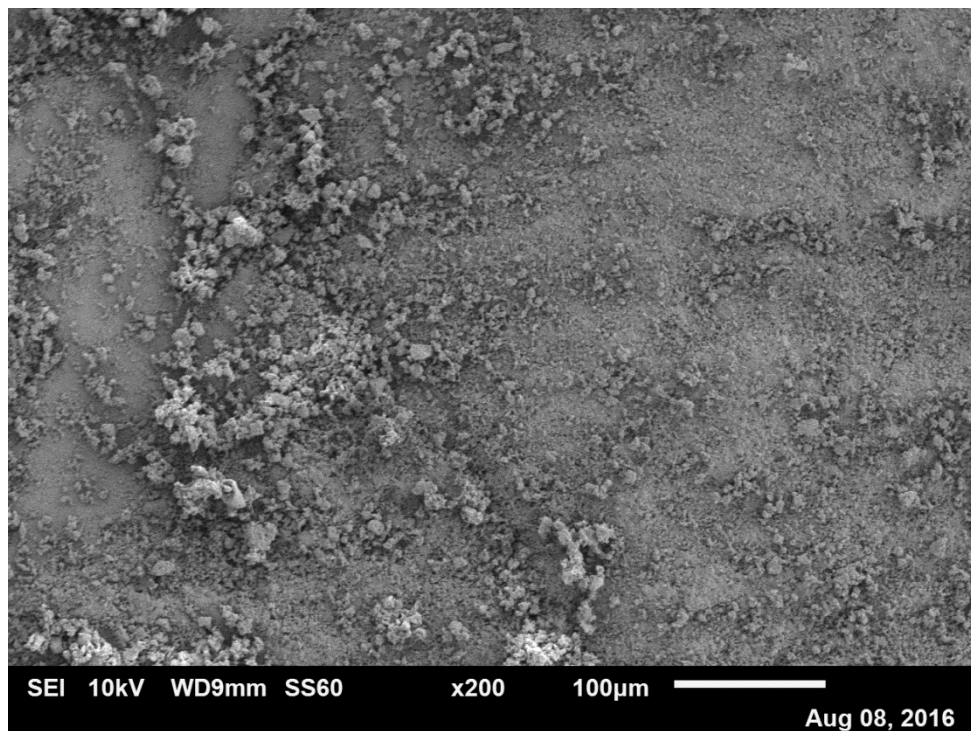


Figure A- 6: Image of sodium carbonate ribbon surface produced at 230 bar

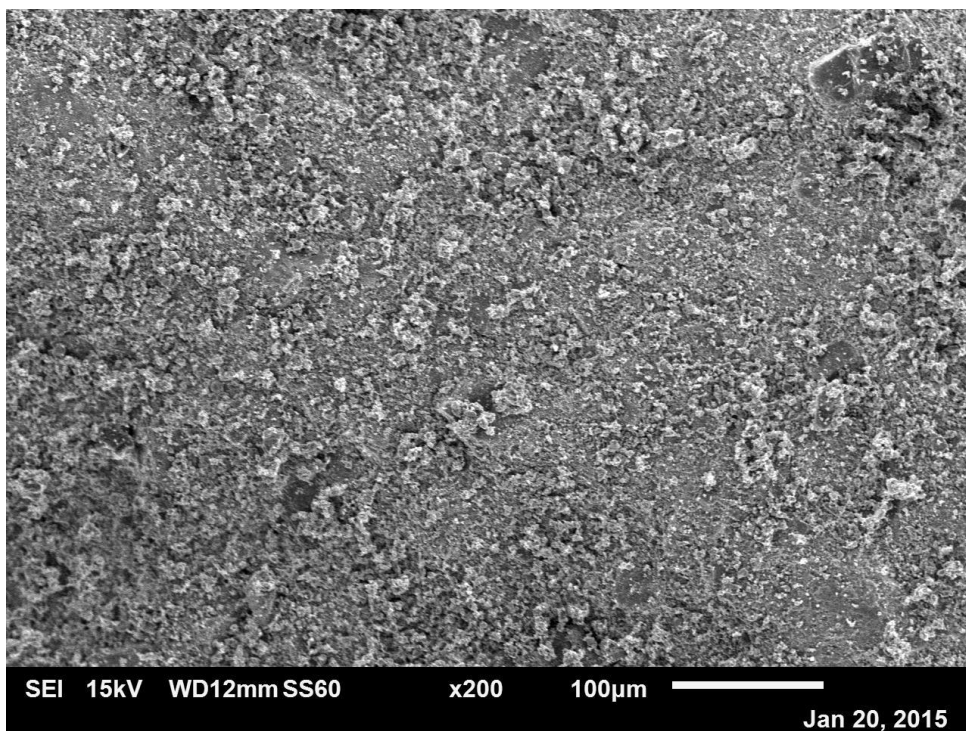


Figure A- 7: Image of calcium carbonate ribbon surface produced at 230 bar

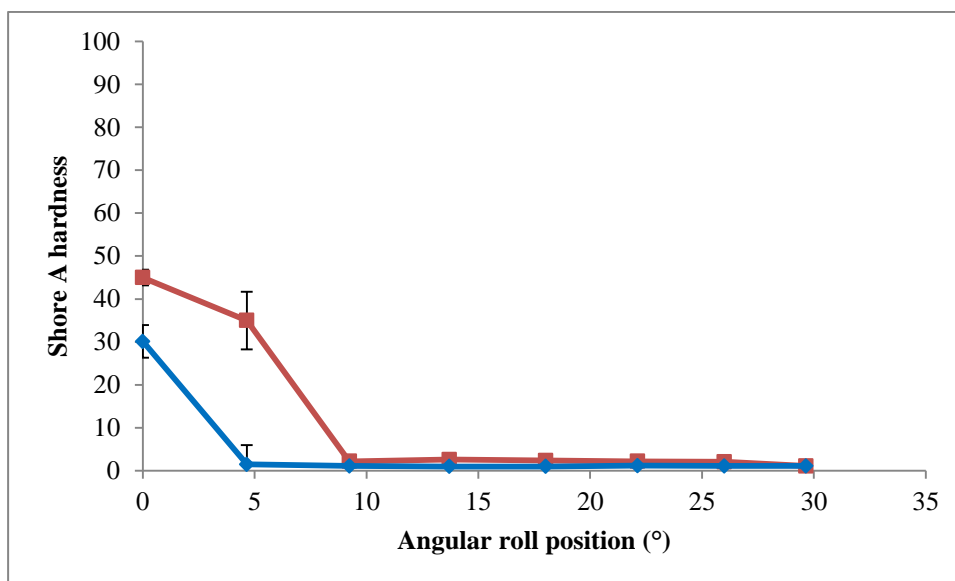


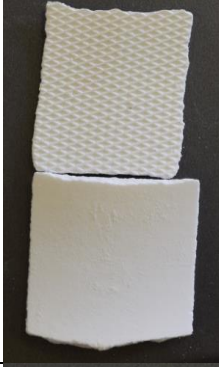
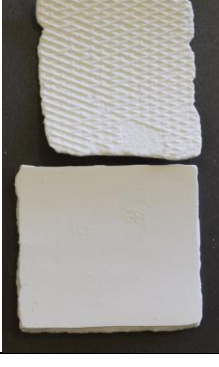


Figure A- 8: Shore A hardness of the pre-compacted body produced at 70 bar versus angular roll positions for Pharmatose 200M (■) and calcium carbonate (◆)

Table A-1: Comparison of the ribbon width and amount of fines for different materials using the flat and the curved roller

Material	Width (mm)		Fines Wt. %		Ribbon of standard roller (top) and curved roller (Bottom)
	Flat roller	Curved roller	Flat roller	Curved roller	
PVA	36.6	40	14	3.5	
Starch 1500	38	39.5	4.5	3.6	
Glucidex®6	39.6	40	3.3	2.5	
Sodium carbonate	31.2	36.6	31	20	

**Mathematica code for data fitting**

```
data = {{0, 0}, {30, 0.769}, {60, 2.995}, {90, 4.986}
, {120, 6.592}, {150, 8.35}, {180, 10.1}, {210, 12},
  {240, 14.06}, {270, 16.35}, {300, 18.8}, {330, 21.44},
  {360, 24.3}, {390, 27.5}, {420, 30.8}, {450, 34.36},
  {480, 38.3}, {510, 42.5}, {540, 46.9}, {570, 51.77},
  {600, 56.86}, {630, 61.9}, {660, 66.7}, {690, 71.4},
  {720, 75.66}, {750, 79.27}, {780, 82.6}, {810, 85.99},
  {840, 88.95}, {870, 91.3}, {900, 93.13}, {930, 94.6},
  {960, 95.7}, {990, 96.7}, {1020, 97.6}, {1050, 98.3},
  {1080, 98.9}, {1110, 99.26}, {1140, 99.45}, {1170, 99.53},
  {1200, 99.54}, {1230, 99.6}, {1260, 99.6}, {1290, 99.6},
  {1320, 99.66}, {1350, 99.7}, {1380, 99.8}, {1410, 99.83},
  {1440, 100}, {1470, 100}, {1500, 100}};
nlm = NonlinearModelFit[data, 100 (1 - Exp[-Abs[x/xc]^m]),
  {{xc, 10}, m}, x];
nlm["BestFitParameters"]
{xc -> 626.261, m -> 2.40041}
```